Chair of Materials Science and Testing of Polymers

Doctoral Thesis

A systematic investigation of fracture in polyamide 12

Dipl.-Ing. Mario Messiha, BSc.

February 2022

MONTANUNIVERSITÄT LEOBEN
www.unileoben.ac.at

AFFIDAVIT

I declare on oath that I wrote this thesis independently, did not use other than the specified sources and aids, and did not otherwise use any unauthorized aids.

I declare that I have read, understood, and complied with the guidelines of the senate of the Montanuniversitaet Leoben for "Good Scientific Practice".

Furthermore, I declare that the electronic and printed version of the submitted thesis are identical, both, formally and with regard to content.

Date 04.02.2022

Signature Author
Mario Messiha

DISSERTATION

A systematic investigation of fracture in polyamide 12

February 2022

This cumulative dissertation was authored by:

Dipl.-Ing. Mario Messiha, BSc.
born 17th May 1993
in Graz (Styria, Austria)

Materials Science and Testing of Polymers
Department of Polymer Engineering and Science, Montanuniversitaet Leoben

Trust in the LORD with all your heart and lean not on your own understanding;
in all your ways submit to Him, and He will make your paths straight.

– Proverbs 3:5-6

PREAMBLE

ACKNOWLEDGEMENTS

The research work of this thesis was performed at the Polymer Competence Center Leoben GmbH (PCCL, Austria) within the framework of the K1 COMET-program (Grant Nr.: 879785), which is funded by the Federal Ministry for Transport, Innovation and Technology (Austria) and Federal Ministry for Economy, Family and Youth (Austria) with contributions by Evonik Operations GmbH (Germany) and the Montanuniversitaet Leoben (Austria). The PCCL is funded by the Austrian Government and the State Governments of Styria and Upper Austria.

I would like to express my deepest gratitude to all people who helped and guided me during the progression of this thesis.

First and foremost, I take pride in acknowledging my special thanks to Univ.-Prof. Dr. mont. Gerald Pinter (Chair of Materials Science and Testing of Polymers, Montanuniversitaet Leoben) for his professional contributions and insightful guidance to improve the outcome of this work and for helping me to understand difficult topics, especially in the fields of fracture mechanics. Moreover, I am thankful for providing me unlimited access to testing devices at the Chair.

I also want to thank my mentor Prof. Patricia Frontini (Instituto de Investigaciones en Ciencia y Tecnología de Materiales, INTEMA, Universidad Nacional de Mar del Plata) and her team for their support during my thesis and the opportunity to visit Mar del Plata, ARG to investigate the rate-sensitivity of polyamides in-depth. Personally, I am also really thankful to Dr. Patrick Leevers for all the time and efforts he has invested in order to give me a clearer picture of rapid fracture behavior and possible underlying fracture mechanisms.

During last years, I also found a great teacher and supervisor, Dr. mont. Andreas Frank (Polymer Competence Center Leoben GmbH, PCCL) to whom I would like to offer my sincere gratitude for the interesting task, the trust and the professional expertise, as well as for his willingness to discuss and share his knowledge in all kind of different areas that were decisive in terms of this research.

Certainly, I also consider myself lucky to have had the opportunity of working and learning from Dr. Jan Heimink (Evonik Operations GmbH), who was a motivating power behind all research steps of this project and who supported the scientific outcome of the thesis by all means, personally and professionally.

Furthermore, I am grateful to all my colleagues at the Montanuniversitaet Leoben and the PCCL, who have always offered their help and support. In particular, I would like to thank Priv.-Doz. Dr. mont. Florian Arbeiter for his support and patience, especially within long-lasting scientific discussions on the subject of relevant structure-property relations and fracture mechanisms in polymers. At this point, I would also like to thank DI Jutta Geier, DI Jessica Hinczica, DI Christoph Waly, and Linda Schatz, BSc. for their technical support and assistance in the experimental part of this study.

Last but not least, I am indebted to deepest thanks for the undeniable moral and energetic support of my family, my parents Magdy and Alis, my sister Marina and my brother Marten, throughout the course of this thesis.

My acknowledgement would also be incomplete without personally thanking the source of my strength, my wonderful wife Maria Messiha-Awad, who bore me even in tense situations and whose support, friendship and unconditional love always gave me comfort and encouragement.

Finally, I just want to express my deepest gratitude to God Almighty for being there for me all this time and giving me the ability and opportunity to undertake this research.

ABSTRACT

Plastic pipelines used for gas and water transportation exhibit a notable record as long-term operating applications. However, failure does happen. In that manner, slow crack growth (SCG) under certain conditions is considered to be the most critical failure mode. As steel pipe systems operating at high pressure levels are increasingly replaced by modern pipe grade materials, such as polyethylene (PE) and polyamide (PA), the understanding of fundamental fracture mechanisms in order to effectively evaluate the resistance against SCG, has become of indispensable value. Yet, when it comes to materials other than PE, only few studies regarding the relevant long-term failure mechanisms have been performed. Hence, a key element within this study was to examine possible fracture and micro-deformation mechanisms as well as structure-property relationships that promote slowly extending cracks in PA, particularly PA12. This was done with the aid of an accelerated tool to characterize SCG performance of a material – the cyclic cracked round bar (CRB) test. In contrast to its non-polar paradigm PE, PA is additionally influenced by the ability to build hydrogen (H) bonds. Therefore, influences of H-bonds on SCG were examined using a sequential debonding fracture model. It was demonstrated that the additional energy needed to dissociate effective H-bonds becomes the dominating source of energy which has to be overcome. This is the case, if at least 45 % of all H-bonds crossing the crack plane engage in the fracture process and are actively resisting SCG in contrast to a theoretically non-physically cross-linked PA. Special focus was also put on the formation of crazes as predecessors to cracks as well as crack initiation and propagation resistances. PA12 grades of increasing molecular weight (M_W) showed an increasing disentanglement resistance due to hydrogen bond effects leading to higher initiation and propagation resistances, whereas plastic zone sizes do not change considerably. An impact modification, on the other hand, promotes the development of notably larger plastic zones and higher SCG resistance, whereas pigmented grades exhibit a reduced plastic zone size, rendering a lower amount of dissipated energy before physical crack initiation and during SCG.

Though, SCG may initiate only a small leak, it has also the potential to trigger rapid crack propagation (RCP) under certain conditions, which is much rarer but can be more catastrophic and destructive. Characteristic feature of RCP in critical applications, such as pressurized pipes or vessels, is recognized by a dynamic crack propagating at high-speeds of up to several hundred meters per second. The external loading situation as well as the

molecular and morphological structure of the material are known to affect the crack behavior. Thus, safe installation and operation during service lifetime of components prone to RCP, cannot be assured without sound knowledge about the resistance against RCP, particularly when considering the use of new materials, such as time- and temperature-dependent plastics. In this context, the RCP resistance of different PA12 grades was investigated using the ISO 13477 Small-Scale Steady State (S4) test. Since these grades differed not only in molecular weight but also in their use of additives (impact modifiers and pigments), structure-property relationships could be established. A new S4 evaluation concept was further proposed to increase the data yield while reducing the necessary number of tests. Yet, even a modified S4 test becomes too uneconomic and time-consuming to check for changes in RCP behavior, in order to advance material development. Based upon mathematical formulations of the adiabatic decohesion model proposed by Leevers and elasto-dynamic fracture mechanics theory, an analytical ranking parameter R^{**} was introduced which showed strong correlation to S4 test results. This was possible due to observed evidence of adiabatic decohesion mechanisms in PA12 during RCP, such as highly fibrillated regions and recorded temperature peaks of up to +80 °C relative to test temperatures during rapid fracture of pressurized pipe samples.

KURZFASSUNG

Kunststoffrohrleitungen für den Gas- und Wassertransport haben sich im Langzeitbetrieb bestens bewährt. Dennoch kann es unter bestimmten Umständen (z.B. hohe Drücke) zum Versagen kommen. Das langsame Risswachstum (Slow Crack Growth, SCG) gilt dabei als die kritischste Versagensart. Da Stahlrohrsysteme, die unter hohem Druck betrieben werden, zunehmend durch moderne Kunststoffe wie Polyethylen (PE) und Polyamid (PA) ersetzt werden, ist das Verständnis grundlegender Bruchmechanismen von hohem Wert, um die Widerstandsfähigkeit gegen SCG effektiv bewerten zu können. Im Gegensatz zu PE, gibt es allerdings für PA nur wenige Studien zum Langzeitverhalten. Ein Ziel dieser Studie war daher die Untersuchung möglicher Bruch- und Mikroverformungsmechanismen sowie Struktur-Eigenschaftsbeziehungen, die langsam wachsende Risse in PA begünstigen. Dafür wurde eine beschleunigte Prüfmethode zur Charakterisierung des SCG-Verhaltens eines Werkstoffs verwendet, der sogenannte zyklische „Cracked Round Bar“ (CRB) Test. Im Gegensatz zum unpolaren PE wird PA zusätzlich durch die Fähigkeit zur Bildung von Wasserstoffbrücken (H-Bindungen) beeinflusst. Daher wurde in einem weiteren Schritt der Einfluss von H-Bindungen auf das Risswachstumsverhalten mit Hilfe eines „Sequential Debonding Fracture“ Modell untersucht. Es wurde gezeigt, dass die zusätzliche Energie, die zum Aufbrechen effektiver H-Bindungen benötigt wird, zur dominierenden Energiequelle wird, die es zu überwinden gilt. Dies ist dann der Fall, wenn mindestens 45 % aller H-Bindungen, die die Rissebene durchqueren, in den Bruchprozess eingreifen und aktiv Widerstand gegen Ketten-Entschlaufungsprozesse leisten. Besonderes Augenmerk wurde auch auf die Bildung von plastischen Deformationszonen (sog. „Crazes“) als Vorläufer von Rissen, sowie auf den Widerstand gegen Rissinitiierung und -ausbreitung gelegt. PA12-Typen mit steigendem Molekulargewicht (M_W) zeigten einen zunehmenden Entschlaufungswiderstand aufgrund von Wasserstoffbrückenbindungseffekten, was zu höheren Initiierungs- und Ausbreitungswiderständen führt, während sich die Größe der plastischen Zone nicht wesentlich ändert. Eine Schlagzähmodifikation hingegen fördert die Entwicklung deutlich größerer plastischer Zonen und eine höhere Risswachstums-Beständigkeit. Pigmentierte Typen hingegen weisen eine geringere Größe der plastischen Zonen auf, was zu einem geringeren Anteil an dissipierter Energie vor der physikalischen Rissinitiierung und während des langsamen Risswachstums führt.

Obwohl SCG im Regelfall zu kleineren Bruchstellen und Lecks führt, besteht dennoch die Gefahr, unter bestimmten Bedingungen in ein schlagartiges, schnelles Risswachstum (Rapid Crack Propagation, RCP) überzugehen. Obwohl RCP deutlich seltener auftritt, ist der angerichtete Schaden im Vergleich zum SCG wesentlich höher. Charakteristisch für RCP in kritischen Anwendungen, wie z. B. in unter Druck stehenden Rohren oder Behältern, ist ein dynamischer Riss, der sich mit hohen Geschwindigkeiten von bis zu mehreren hundert Metern pro Sekunde ausbreitet. Dabei spielt die äußere Belastungssituation als auch die molekulare und morphologische Struktur des Materials eine große Rolle. Der sichere Einbau und Betrieb von RCP-gefährdeten Bauteilen während ihres Einsatzes kann daher ohne fundierte Kenntnisse über die RCP-Beständigkeit und das Risswachstumsverhalten der verwendeten Werkstoffe nicht gewährleistet werden. Insbesondere, wenn man den Einsatz neuer Werkstoffe und vor allem zeit- und temperaturabhängige Kunststoffe in Betracht zieht. In diesem Zusammenhang wurde die RCP-Beständigkeit verschiedener PA12-Typen mit Hilfe des ISO 13477 „Small-Scale Steady State“ (S4) Tests untersucht. Da sich diese Typen nicht nur im Molekulargewicht, sondern auch in der Verwendung von Additiven (Schlagzähmodifikatoren und Pigmenten) unterschieden, konnten Struktur-Eigenschafts-Beziehungen hergeleitet werden. Zusätzlich konnte ein neues S4-Bewertungskonzept entwickelt werden, um die Datenausbeute zu erhöhen und gleichzeitig die Anzahl der erforderlichen Tests zu verringern. Doch selbst ein modifizierter S4-Test ist zu unwirtschaftlich und zeitaufwändig, um Veränderungen im RCP-Verhalten qualitativ zu überprüfen, um die Materialentwicklung stets voranzutreiben. Auf Basis der von Leevers vorgeschlagenen mathematischen Formulierungen des adiabatischen Dekohäsionsmodells und der Anwendung der elasto-dynamischen Bruchmechanik wurde aus diesem Grund ein analytischer Rankingparameter R^{**} entwickelt, der eine hohe Korrelation mit den S4-Testergebnissen aufwies. Dies war aufgrund der beobachteten Hinweise auf adiabatische Dekohäsionsmechanismen in PA12 während RCP möglich. Beispiele dafür sind stark fibrillierte Bereiche und Temperaturspitzen von bis zu +80 °C relativ zu den Prüftemperaturen während der schnellen Rissausbreitung.

SYMBOLS & ABBREVIATIONS

Designation	Unit	Description
α	[m²/s]	Thermal diffusivity
a	[m]	Crack length
$\dot{a}$	[m/s]	Crack propagation rate
a_{ini}	[m]	Initial crack length
β	[-]	Heat fraction within active layers of a critical thickness s_c
c_0	[m/s]	Material dependent reference speed
c_p	[J/(kg·K)]	Specific heat capacity
δ_c	[m]	Critical crack tip opening displacement
ΔH_f	[J/kg]	Latent heat of fusion
d	[m]	End-to-end distance between effective entanglements
D	[m]	Pipe diameter
$\dot{\varepsilon}_{pz}$	[s^{-1}]	Mean plastic strain rate within a Dugdale craze
E^*	[MPa]	Effective tensile modulus
E_d	[MPa]	Dynamic Young's modulus
γ	[J/m²]	Weak, non-bonded interaction energy between molecules
Γ	[J/m²]	Fibrillation energy
G_f	[J/m²]	Total fracture energy during SCG
$G_{dis,f}$	[J/m²]	Dissipated energy during SCG by chain disentanglement processes
$G_{H,f}$	[J/m²]	Energy to break active H-bonds during SCG
G_I	[J/m²]	Energy release rate (mode I)
G_{Ic}	[J/m²]	Critical fracture toughness (mode I)
$G_I(t)$	[J/m²]	Time-dependent crack driving force
$G_{Ic}(t)$	[J/m²]	Time-dependent crack initiation resistance
$G_{Id}(\dot{a})$	[J/m²]	Crack speed dependent dynamic fracture toughness
$G_{Id,min}$	[J/m²]	Minimum dynamic fracture toughness
κ	[W/(m·K)]	Thermal conductivity
l_{pz}	[m]	Length of a plastic zone during SCG
μ	[-]	Poisson's number
M_W	[kg/mol]	Molecular weight

v_e	[mol/m³]	Density of effective entanglements
p	[bar]	Pressure
$p_{c,S4}$	[bar]	Critical S4 pressure
ρ	[kg/m³]	Mass density
R^{**}	[$N^{2.5}/m^3$]	Elasto-dynamic ranking parameter with regard to resistance against rapid fracture
σ_c	[MPa]	Craze strength
σ_{ys}	[MPa]	Yield stress
s_c	[m]	Critical extended chain length
$\tilde{s}_w$	[m]	Extended weight average chain length
T	[°C]	Temperature
$T_{c,S4}$	[°C]	Critical S4 temperature
T_g	[°C]	Glass transition temperature
T_m	[°C]	Melting temperature
T_{TB}	[°C]	Tough-brittle transition temperature
U_{cov}	[J/mol]	Covalent bond fracture energy
Y	[-]	Thermal conduction efficiency function
Z_p	[-]	Graetz number

CCG	Creep Crack Growth
CRB	Cracked Round Bar
ESC	Environmental Stress Cracking
FCG	Fatigue Crack Growth
FM	Fracture Mechanics
FNCT	Full-Notch Creep Test
H	Hydrogen
i-PP	Isotactic Polypropylene
IM	Impact Modifier
NPT	Notched Pipe Test
PA	Polyamide
PA12	Polyamide 12
PE	Polyethylene
PENT	Pennsylvania Edge Notch Tensile
PGM	Pigment
POM	Polyoxymethylene
RCI	Rapid Crack Initiation
RCP	Rapid Crack Propagation

S4	Small-Scale Steady-State
SCG	Slow Crack Growth
SDF	Sequential Debonding Fracture
SEM	Scanning Electron Microscopy
SH	Strain Hardening
SMART	Small-scale Accelerated Reliable Test

TABLE OF CONTENTS

PREAMBLE

OUTLINE & SUMMARY

APPENDIX

OUTLINE

&

SUMMARY

1 MOTIVATION & BACKGROUND

Unexpected failure of engineering structures is a problem that society has faced for centuries. Though an increasing understanding about the processes governing structural failures has been attained in the last decades, still a great deal of confusion is associated with causes of various failure kinds, especially when it comes to viscoelastic-viscoplastic polymers. A division into two wide-ranging categories is generally made: (i) irreversible plastic deformation and (ii) fracture. Former can be viewed as the mechanical behavior of materials when stressed beyond the yielding point, while fracture equals the physical separation of a solid material into a minimum of two fractured pieces. Basically, there are two types of fracture – brittle and ductile – which are common for specific materials. Yet, some materials such as time- and temperature-dependent plastics, are capable of fracturing in both ways depending on internal (e.g. crystal defects, contaminations, voids, etc.) and external (e.g. applied load level, load rate, temperature, surrounding media, etc.) factors. Ductile fracture is characterized by a notable amount of plastic deformation (e.g. "necking" or "ductile rupture"). This usually occurs prior to ultimate failure, as materials pull apart instead of cracking. Brittle fracture, on the contrary, is recognized by a sudden cracking with almost no evidence of ductility. However, brittle fracture processes can be additionally accompanied by "pre-damaged" zones which might occur due to irreversible plastic deformation processes, as local stresses in front of inherent crack-like flaws exceed the yield stress of the material. This type of failure is often called "quasi-brittle" failure, as the macroscopic fracture appearance is of a brittle nature, but high-level plasticity is evident on microscopic scale.

Often-cited examples to demonstrate the importance of understanding the ability of a material to transition its fracturing behavior from a ductile to a brittle manner or vice versa are the Liberty cargo ships built during World War II, where over 230 ships suffered from sudden unexpected cracks, resulting in a catastrophic failure [1–3]. According to literature, a huge number of brittle fractures also occurred in major structures of very different applications (mostly due to dynamic or pressure loads), such as the one-year old bridge across the Albert Canal in Belgium, the King's Bridge in Melbourne, the standpipe in Long Island, the hydrogen pressure tank in Schenectady, or the British de Havilland jet-propelled aircrafts in the Mediterranean [4–6]. Since those historic events, researchers recognized that defects, which might be introduced to structures during manufacturing or maintenance

processes, are capable of causing premature failure, even if applied stresses are far below the given strength of the material. Thus, *fracture mechanics* (FM) concepts were developed to prevent from undesired and unexpected failures. Contrarily to classical structural design approaches, in FM theories components are not assumed to be flawless and feasibility is not provided when the given strength is greater than the expected applied stresses [7–20]. In that context, FM can be viewed as an engineering tool that deals with all kind of failures caused by crack initiation and subsequent propagation. There are different types and definitions used when referring to crack propagation. One calls a crack growth "stable", for example, if an increase in the external load is required to maintain the propagation process. In contrast, crack growth is "unstable" if a crack propagates spontaneously from a certain point on without further increase of the remote load submitted to the cracked body. The state of stability/instability during crack growth is not only a matter of material properties but also of the geometry, type and rate of load as well as environmental conditions. Furthermore, a crack propagating under static, quasi-static or dynamic cyclic loading at very low crack speeds is often described as subcritical Slow Crack Growth (SCG). The scheme of SCG can be further denoted according to the loading type, that is, Creep Crack Growth (CCG) under static loads or Fatigue Crack Growth (FCG) under transient cyclic loads. A special case of SCG is Environmental Stress Cracking (ESC), where stress-based crack extension is additionally promoted by the invasion of fluid particles of an active medium into the open structure of a material close to the crack tip. A combination of a crack opening force alongside the access of foreign particles inside the material, can lead to a synergistic acceleration of failure promoting processes involved in plastic zone formation and decohesion [21,22]. Although, SCG is in its essence a dynamic, time-dependent failure mode, cracks are propagating so "slowly" that it becomes possible to neglect inertial forces as well as stress wave propagations during crack extension [23], resembling the failure nature of SCG as *quasi-static*. A structure exposed to a sudden explosive impact load, on the other extreme, is significantly influenced in its fracture behavior by inertial forces, applied deformation rates and reflected stress waves [23], resulting in an unstable crack initiation and propagation. If thereby crack propagation speeds reach the order of the speed of sound (approx. 300 m/s or more), it is usually termed Rapid Crack Propagation (RCP) [21,24–27].

Though sufficient fracture resistance is relevant for a huge number of plastic components, pressurized pipe lines have become famous for the high interest in resisting (quasi-) brittle fracture caused by the initiation and propagation of slowly and/or rapidly extending cracks

[28–36]. Demographic changes and rapid urbanization throughout the world have demonstrated big challenges for gas and water utility companies over the last decades, outlining the importance of pressurized piping systems for public and industrial gas and water supply. Transportation processes of fluids from wellheads to the end consumers involve a series of pipelines, such as flowlines, gathering, transmission and distribution lines as well as service lines. Depending on their field of work, those pipelines might be subjected to low- and high-pressure levels of up to 10 bar and above [1,2]. In that context, polymer pipes have been on a rise for several decades, representing an attractive alternative to traditional pipe materials like steel, grey cast iron or cement. Compared to them, polymer pipes exhibit many significant advantages in their technical performance regarding manufacturing, installation techniques, weldability, flexibility and long-term failure resistance [3–5]. However, buried pipes are submitted to more or less severe and unexpected influences, such as third-party loads and the interaction with the surrounding soil that can cause premature failures. To prevent damage to infrastructural constructions and environmental pollution (e.g. by the release of hazardous and flammable fluids of broken or leaking water and gas supply systems) the characterization of basic long-term performance (i.e. resistance against SCG) and material design against catastrophic, rapid fracture are of essential importance, especially when considering the utilization of new pipe grade materials. In over 50 years of field experience, polyethylene (PE) has been well established as pressure pipe material. Underlying failure mechanisms have been investigated comprehensively and are therefore well understood when speaking of PE [4,15–20]. Modern PE grades, though, are reaching the limits of their possible operating conditions when talking about high-pressure gas applications above 10 bar. In that manner, polyamide 12 (PA12) extended the practical applicability of polymer pipes and has proven itself as a safe, economical replacement for steel pipes [1,2,6]. Since 2005, several SDR11 gas pipes with operating pressures from 12 to 18 bar have been realized successfully with PA12 [1]. However, relatively little is known of the short- and long-term fracture behavior of PA12 in pressure pipe applications in comparison to PE. Hence, this thesis aims for an advanced understanding of the general applicability, the fracture behavior and governing mechanisms, the use of suitable testing parameters as well as relevant structure-property relations in PA12.

2 STRUCTURE OF THE THESIS

This thesis had two main objectives: First, a thorough assessment of the fracture behavior of morphologically and micro-structurally different PA12 materials. Second, the development and/or the application of accelerated tools to rank PA12 grades according their fracture resistance. To investigate the fracture performance of PA12, the outline of this thesis was divided into two major sections – (i) slow crack growth and (ii) rapid crack propagation of PA12 grades. Both parts strive for a better understanding of the governing physical fracture mechanisms (e.g. chain disentanglement and slippage, adiabatic decohesion, etc.), the structure of obtained fracture surfaces (e.g. fibrillation, defects, smooth mirror zones, etc.) as well as the effect of hydrogen (H) bonds, the molecular weight (M_W) and the use of certain additives relevant for pipe applications on the cracking behavior and resistance of PA12 materials. Considering SCG behavior two different sets of PA12 formulations were selected for this purpose:

- a homologous series of three neat low- to middle-viscous PA12 grades, which only vary in terms of average M_W maintaining very similar molecular and morphological structures;
- and a systematic series of essentially constant M_W consisting of a base PA12 grade, as well as modified derivates, which additionally incorporate an impact modifier (IM), a pigment (PGM) or the combination.

Regarding RCP properties, studies were conducted on a series of high-viscous, compounded pipe grades that differ primarily in their M_W and/or the use of IM and PGM. Since material development for non-pressurized and pressurized pipe networks is continuously seeking to improve specific properties by modifying generated material formulations, it has further become of particular interest to quickly check for changes in the fracture performance. Plastic pipe industries long for relatively simple batch tests or an accessible analytical or numerical model for SCG and RCP testing. In that manner, the second aim of this thesis was dedicated to investigate and optimize the applicability of available standard and accelerated testing methods (e.g. Small-Scale Steady-State, S4, test; Cracked Round Bar, CRB, test; strain hardening, SH, test; etc.), which have been initially developed for PE, to sufficiently characterize the SCG and RCP performance of PA12.

Key findings to extend the state of art regarding the fracture behavior of PA12 grades were based upon five publications of Messiha et al. (attached in the APPENDIX):

Publication 1

Slow crack growth resistance of modern PA-U12 grades measured by cyclic cracked round bar tests and strain hardening tests **[37]**:

In the first paper focus was put on the applicability of two well-known accelerated ranking tools to measure the resistance against slow crack extension in PA12. It was also demonstrated with the aid of the cyclic CRB test and the SH test that PA12 grades happen to fail in a similar manner as PE grades, namely by dominating chain disentanglement mechanisms.

Publication 2

How hydrogen bonds influence the slow crack growth resistance of polyamide 12 **[38]**:

The second paper aimed for a thorough analysis of governing fracture mechanisms in PA12 grades on a molecular scale during SCG. In particular, influences of hydrogen bonds, which are assumed to actively resist chain disentanglements, were studied. A theory of sequential debonding fracture was used to explain how chains react to forces that pull them out of a main crack plane.

Publication 3

On the slow crack growth process and associated structure-property relationships in polyamide 12 grades **[39]**:

Based on results of both previous publications, key element of this paper was to study structure-property relationships that affect the plastic deformation behavior ahead of crack tips prior to crack initiation as well as the ultimate SCG resistance of selected PA12 grades. In particular, the increase of the weight-average molecular chain length, as well as the incorporation of color pigments and impact modifiers were considered.

Publication 4

Structure-Property Relationships of Polyamide 12 Grades Exposed to Rapid Crack Extension **[40]**:

Analogous to the SCG regime, the RCP performance of various PA12 grades was examined in detail. Materials were selected in a way to highlight important structure-property relations affecting RCP resistance. Furthermore, a new evaluation concept was proposed to optimize the standard S4 test for rapid fracture characterization.

Publication 5

Mechanisms of rapid fracture in PA12 grades **[41]**:

Building on recent literature and on observed structural effects during conducted S4 tests (e.g. significant increase of temperature, fibrillated spots on fractured pipe surfaces, etc.) it was suggested that PA12 grades may fail by chain disentanglements guided by adiabatic decohesion mechanisms, rather than by chain scission. Following this idea, a new accelerated, semi-analytical parameter R^{**} was defined to sufficiently rank PA12 grades with regard to their RCP resistance.

3 SLOW CRACK GROWTH IN PA12

3.1 Introduction

Natural gases and fluids (e.g. methane, hydrogen, petroleum, water, etc.) have become indispensable in modern-day societies and infrastructures. Since their occurrences are commonly located at remote regions far away from areas of high gas demand, adequate transportation is important. One of the most critical applications, in this regard, is pressurized piping. Pipelines might be subjected to pressure rates up to 10 bar and above [28,29]. In that context, PA12 pipes have been favorably used as an attractive substitute for steel pipes, realizing operating pressures from 12 to 18 bar successfully [28]. Unfortunately, even though long-term properties have been improved through continuing advances on a molecular scale in the case of modern pipe grades, instances of premature failures of pressurized piping systems are still possible [30,42,43]. This can become problematic, as undetected leaks can lead to accidents and explosions due to the high flammability of natural gases. In addition, natural gas consists mainly of methane, a potent greenhouse gas. If released, it could contribute to severe climate change. There are also concerns about pipelines running through environmentally sensitive areas, such as natural habitats, populated communities, or close to water aquifers. Thus, it is of utmost importance to define the quality of plastic pipes used for pressurized pipelines by properly evaluating their long-term relevant properties, including the resistance to SCG.

A standard test method to investigate the different failure mechanisms of pressurized plastic pipe grades is supplied by the internal pressure pipe test, which is standardized in ISO 1167. Representing most thermoplastics, Fig. 1 illustrates three distinctive stages where different mechanisms govern the failure of pressurized pipes [44,45].

“Stage I” is a plasticity-controlled ductile failure, provoked by stresses exceeding the yield stress (σ_{ys}) of polymers, leading to early large-scale plastic deformations, usually shaped like fish-mouths. Noting that physical ageing processes, such as changes in a material’s crystallization (i.e. re- or post-crystallization), material’s free volume (i.e. amorphous phases), or diffusion of low-molecular-weight substances can affect σ_{ys} levels of polymers, they should be considered as influencing parameters in “Stage I” failure [46–49].

With decreasing loadings failure curves change to “Stage II”, which is clearly visible by a transfer knee, leading to failure lines of steeper slopes. In this stage, which is also known as

crack-growth-controlled "quasi-brittle" failure, the origin of failure is directly related to the presence of intrinsic initial defects at micro-scale. These defects result in a macroscopic sharp and brittle failure generated by crack initiation and SCG. Quasi-brittle failure occurs at loads significantly below materials' yield stresses. Hence, SCG is generally accepted to be the critical failure mechanisms for long-term applications. The total failure time in "Stage II" consists of the time until a crack is initiated and the time where the initiated crack is traversing the pipe wall [43,50–52]. Referring to Lang et al. [49] and Pinter et al. [53,54], the SCG regime is not only susceptible to physical ageing processes, but also to chemical ageing, for instance, thermo-oxidative degradation mechanisms, as there is sufficient time for local crack tip oxidation processes to occur.

After decades of service time "Stage III" – a degradation-controlled failure – becomes the dominant failure mechanism, as polymers have already experienced massive aging processes. In that case, failure occurs almost independently of applied stresses, but is certainly dependent on the quality of integrated stabilizer systems. The better the stabilizer effectivity against thermo-oxidative aging the longer the achievable lifetime.

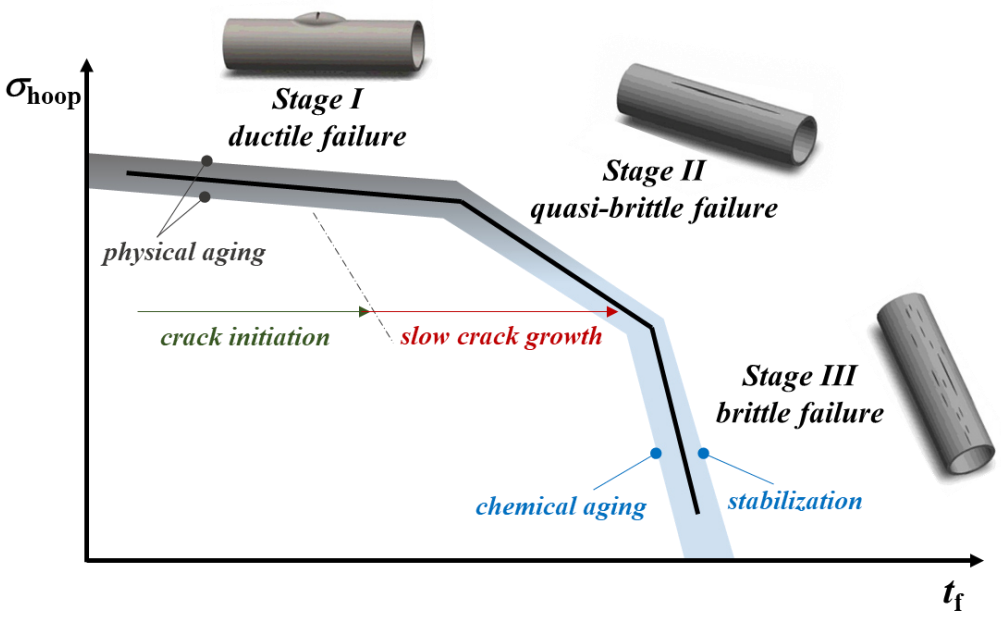

Fig. 1: Characteristic failure regions of PE pipes under internal pressure (with reference to [30,47]).

With regard to the SCG resistance of plastics, the internal pipe pressure test delivers reference values for the long-term hydrostatic strength to reach a minimum service lifetime of 50 years. Alternatively, the Full-Notch Creep Test (FNCT) according to ISO 16770, the

Pennsylvania Edge Notch Tensile test (PENT) according to ISO 16241 or the Notched Pipe Test (NPT) according to ISO 13479 can also be used for SCG characterizations. Unfortunately, these standard methods are becoming too time-consuming (testing times >10.000 h) and ineffective in terms of quasi-brittle failure through real SCG when it comes to modern pipe grades [55,56]. In Fig. 2, for example, only failure of a ductile nature ("stage I" failure) was realized for a modern PA12 pipe grade using an internal pressure pipe test at varying temperatures [57].

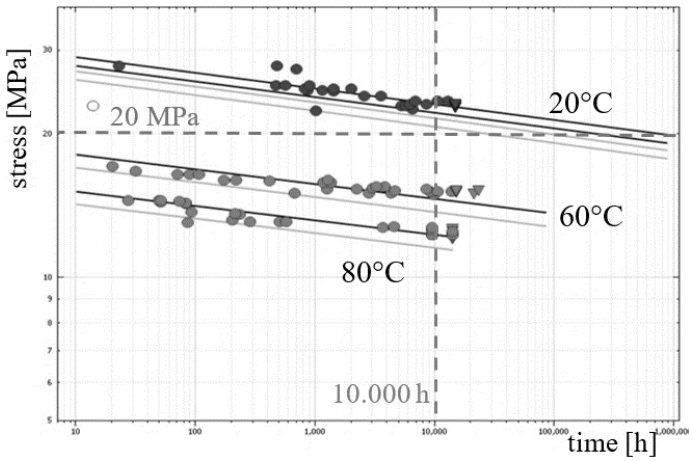

Fig. 2: Long-term hydrostatic strength curves of PA12 at different temperatures according to ISO 9080. Only ductile failure modes were achievable [57].

Yet, in 2009 a quasi-brittle failure of a modern PA12 pipe grade was reported by Hessel [55,56]. It was concluded that the creep rupture strength of current high viscous PA12 resins has reached a state of development, where a quasi-brittle failure mode as known for PE, driven by the nucleation and growth of cracks under ordinary service conditions, is hard to reach but not impossible. Currently, several studies are conducted aiming on a decrease of testing times of standardized test methods by using more aggressive surfactants [58]. Apart from modifying standard test methods, the demand for new time-efficient testing tools led to the establishment of SMall scale Accelerated Reliable Test (SMART) [59] techniques, which were initially developed for PE-HD and extended to PA12 pipe grades **[37]**, such as the cyclic Cracked Round Bar (CRB) test (ISO 18489) and the Strain Hardening (SH) test (ISO 18488).

3.2 SCG Failure Mechanism in PA12

Considering **Messiha et al. [37]**, it was demonstrated, that neat PA12 grades clearly fail by crack initiation and subsequent SCG in the cyclic CRB test at ambient testing temperature

and a load frequency of $f = 5$ Hz. This was verified by the good correlation between CRB and SH test results. For the applicability of SH tests in order to rank materials regarding their SCG behavior two prerequisites have to be fulfilled. On the one hand, materials to be tested must exhibit the formation, growth and final failure of fibrillated structures [24]. On the other hand, quantitative comparisons are only valid for materials of similar molecular and morphologic structure, which lead to similar underlying failure behavior (e.g. dominating chain disentanglement mechanism). This was backed up by a thorough investigation of occurring failure mechanisms via Scanning Electron Microscopy (SEM) measurements of fractured CRB specimens. Clear fibrillation was evident for analysed PA12 grades **[37]**, which is also commonly reported for PE-HD grades [45,60–63].

Similar results were also reported by Zhang and Zhi [64], who investigated the fracture toughness of PA66, PA1010 as well as PA610 and divided the stable crack growth steps in polyamides as follows: first, the sharp crack tip blunts, followed by craze development and craze-crack transitioning. The last two steps can be summarized as void initiation, coalescence of formed voids and the extension of crazed zones, by rupturing and pulling craze fibrils. Finally, the formation of dimples on the fracture surface gets observable as the fibril structure of the void walls separates and contracts. Moreover, Mourglia-Seignobo et al. [65] studied the microscopic damage mechanism of PA66 during SCG under fatigue conditions at different stress levels. It was found that the dynamic modulus E_{dyn} decreased linearly as a function of the logarithmic cycle numbers during fatigue tests. Hence, progressive, accumulating damage can be assumed inside the material. Analyses show that the nucleation of uncorrelated spherical domains of low density and sizes distributed between 10 and 100 nm are formed between lamellae at nanometric scale at the early stages of fatigue (Fig. 3a). With increasing fatigue cycles the number of voids increases successively until a critical number of neighbored voids is reached leading to fusions of several nano-voids to larger voids up to micro-scale (Fig. 3b). With on-going craze evolution as proposed by Friedrich [66], the void size and anisotropy grows significantly during the formation of fibrillar networks, which are gradually stretched in load direction by inter- and intralamellar deformation mechanisms (Fig. 3c). Thus, quasi-brittle fracture by craze development and breakdown in PA12 grades seems reasonable, as was concluded by **Messiha et al. [37]**.

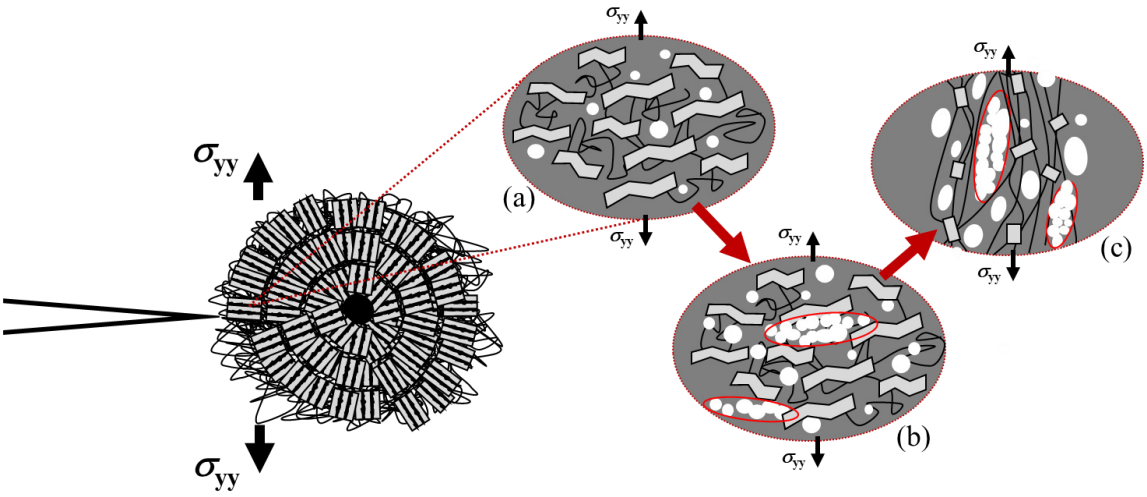

Fig. 3: Growth of submicroscopic cavities in the amorphous phase between lamellae during advancing load stages: random nucleation of uncorrelated micro-voids (a); coalescence of voids after [65] at advanced load stage (b) and increase of anisotropy during fibrillation after [66] at stage (c).

3.3 Influence of Molecular Weight

Extensive research has already been done in this field, particularly on polyolefins [61,63,67–71]. Basically speaking, a low M_W has three immediate consequences [72]:

i. high concentration of chain ends, which might act as structural defects;

ii. when chains are short relative to the interlamellar amorphous region, the probability of forming tie-molecules between lamellae becomes small;

iii. even if tie chains are formed, they become highly unstable with regard to chain disentanglements compared to long tie chains at a high M_W.

Consequently, an increase of M_W results in a lower degree of crystallinity, thus increasing the number of amorphous interlayers in which craze nucleation preferably occurs first. Moreover, the formed fibrils after craze initiation become longer the higher M_W, explaining the observed increase of fracture resistance [66]. Brown [62] further demonstrated that a long lifetime of a linear PE component is mostly influenced by the M_W distribution, primarily the high M_W end of the distribution, as well as the branch density. Yet, the low M_W end must balance in order to allow for suitable processing. The addition of 4 - 6 branches per 1000 carbon atoms increased the lifetime by a factor of 10^4. Egan and Delatycki [73] validated Brown's observations by demonstrating an increasing resistance to crack propagation under

static loads with increasing M_W and short branch concentration, as well as decreasing lamellar thickness for PE-HD. Especially a higher M_W plays a dominant role in the fracture process, as longer polymer chains are more probable to act as connecting tie molecules between lamellae, delaying disentanglement mechanisms during SCG. The positive influence of a raised short branch content can also be explained by an increased resistance against disentanglement reactions aiming to pull out new chains from the bulk into the plastic deformation zone. A raised amount of chain branches also promotes the development of trapped entanglements within the crazed zone. Subsequently, a high entanglement density participates in the load transfer processes and hence favors plastic deformation, assuming an effective anchoring of the chains by the lamellae [72]. However, the implementation of short chain branches is only positive, as long as corresponding variations in M_W are rather small. It was further suggested that the use of higher 1-olefin comonomers provides more effective means of inhibiting SCG (e.g. pentyl or hexyl instead of ethyl [74]), although Brown reported the short side chain length to be insignificant with respect to the lifetime.

In case of PA12, however, only low degrees of random chain branching is perceived – therefore, M_W is regarded to be the defining parameter with respect to SCG performance [75]. In recent studies by **Messiha et al. [37,39]**, focus was put on the question of how plastic zones and fracture resistance of PA12 change with varying M_W. An increase of crack initiation resistance and SCG resistance was generally observed in PA12 with increasing M_W. However, while Kausch et al. [76–78] reported a tendency of growing craze zones with increasing M_W in POM and i-PP, no increase of the plastic zone size (l_{pz}) was observed with increasing chain length of tested PA12 formulations (cf. Fig. 4). Instead, l_{pz} stayed almost at same levels at a given cycle number during fatigue testing **[39]**. It was concluded, therefore, that the plastic zone size is not predominantly influenced by the weight-average polymer chain length in PA12. However, since an increase of the average chain length by 80 % enhanced the resulting lifetime by approx. 1850 % **[37]**, the general disentanglement resistance seems to be considerably improved by (cf. Fig. 4):

- an increasing entanglement density of chains surrounding the plastic zone;
- increasing amount of secondary attraction forces actively resisting chain deformation processes (i.e. disentanglement);
- as well as longer remaining chain segments, which have to be pulled inside the plastic zone before physical crack initiation or extension occurs.

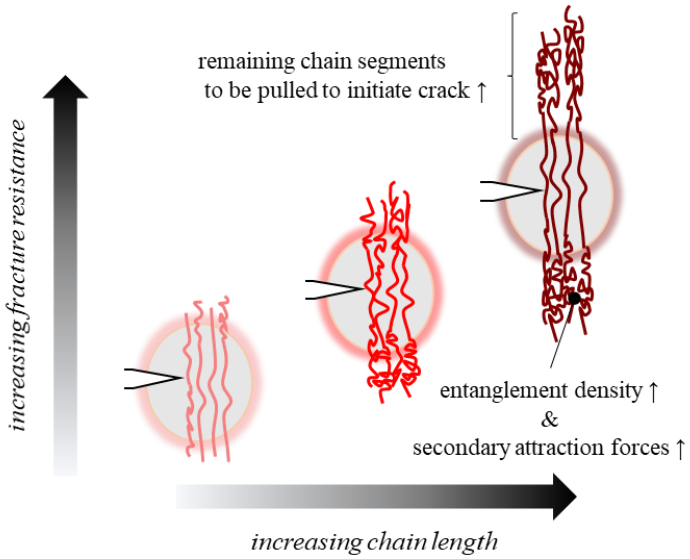

Fig. 4: Schematic illustration of fracture resistance as a function of weight-average chain length, whereas plastic zone size remains unchanged. Reproduced from Messiha et al., "On the slow crack growth process and associated structure-property relationships in polyamide 12 grades", manuscript submitted for publication, 2022.

Yet, a significant decrease of the fibrillation density was also recognized on the fractured CRB specimen of PA12 grades with increasing M_W (see Fig. 5). Obviously, this result supports the idea that it is more difficult to disentangle macro-molecules the longer they are (→lower content of fibrillation). But it also questions for how long SCG is primarily governed by chain disentanglement mechanisms with respect to an increasing chain length. Perhaps, there exists a critical chain length above which the underlying fracture mechanism changes.

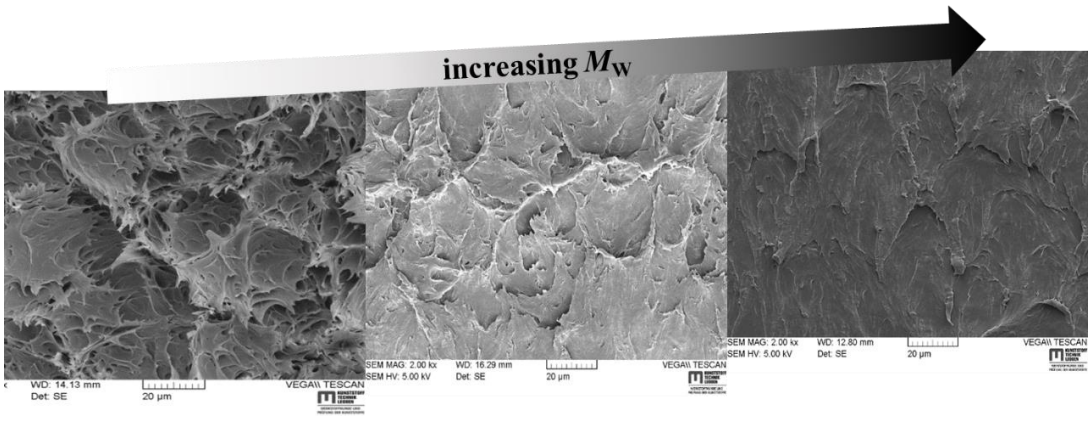

Fig. 5: Influence of increasing M_W on fibrillation density of PA12 grades tested via cyclic CRB test **[37]**. Reproduced from Messiha et al., "Slow crack growth resistance of modern PA-U12 grades measured by cyclic cracked round bar tests and strain hardening tests", *Polymer Testing*, vol. 86, 2020, with permission from Elsevier.

3.4 Influence of Hydrogen Bonds

In an attempt to answer that question, a *hydrogen bond hypothesis* was postulated by **Messiha et al. [37]** to account for this smoothening fracture appearance trend. Polyamides are generally characterized by methylene groups of various lengths that are bonded together through amide linkages (-CO-NH-) [79]. Their amide density, which equals the frequency of occurrence of amide groups in the polymer chain, is responsible for their unique property profile. The presence of high amounts of amide groups results in high degrees of polarity and subsequent inter-chain and intra-chain hydrogen bonds, which are likely to create different polymer physical effects that do not exist in polyolefin materials. Thinking of molecular chains, it then seems easier for disentanglement processes to occur for shorter chains with fewer amounts of hydrogen bonds. As soon as the weight-average chain length increases, subsequently the number of hydrogen bonds also increases, leading to more difficult disentanglement conditions as polymer chains have to overcome more "H-cross-linked" locations where they "stick" tighter together. Presumably, if PA12 chains exceed a critical molecular mass or a corresponding critical number of hydrogen bonds, chain disentanglements within the process zone are successively inhibited and a change of the classical crazing failure mechanism to shear yielding may occur (cf. Fig. 5). Similar observations were also made by Kausch et al. [76–78]. It was demonstrated that craze formation prior to craze-crack transition is highly influenced by the average chain length of a given material. A tendency of growing craze zones with increasing M_W in a series of polyoxymethylene (POM) and isotactic polypropylene (i-PP) was observed, while the ultimate number of crazes decreased. At very high M_W, however, crazing was increasingly suppressed in favor of shear deformation.

Whether crazing or shear yielding predominates, depends on several external factors, such as load rate and temperature as well as inherent material parameters (e.g. crystalline structure, entanglement density, characteristic temperatures, relaxation time, etc.). Friedrich [66,80] deduced that crazes and shear bands coexist in semi-crystalline polymers. At high temperatures relative to the melting point T_m, (or correspondingly low deformation rates), for example, homogenous shear flow is mostly recognized to be the governing mechanism in semi-crystalline plastics. Otherwise, craze formation occurs, which is mostly associated with quasi-brittle fracture. In terms of crack growth resistance, shearing is far more effective than crazing, since the entire material volume within the plastic zone participates in the

energy dissipation (no voids). From a polymer-physical perspective, it can be stated that at conditions where the fibrillation energy (Γ) to create a new surface within a plastic zone is relatively high, the material tries to avoid crazing [81,82]. Thus, Γ seems to be the determining factor in terms of craze or shear domination and can be expressed as [46,83]:

$$\Gamma = \gamma + \frac{1}{4} v_e U_{cov} d \tag{1}$$

where γ is the weak, non-bonded interaction energy between molecules, which is collectively referred to as van der Waals cohesive energy [84], v_e the density of effective entanglements that participate in load convection, d the end-to-end distance between effective entanglements and U_{cov} the energy needed to fracture a covalent bond. The factor ¼ considers two surfaces to be created and the fact that during load transfer a single effective entanglement involves two molecular stems. In that context, the second term describes the contribution of covalent bonds crossing the created surface, which are able to bear load and thus contribute to cohesion [46,83]. Following Kramer and Berger [85] the craze stress σ_c is proportional to $\sqrt{(\sigma_{ys}\Gamma)}$ for polymers that exhibit a power-law behavior in drawing fibrils from non-crazed surfaces into the craze zone (usually observed in semi-crystalline thermoplastics). As soon as σ_{ys} of the material becomes higher than σ_c, i.e. at high triaxial stress states (plane strain condition), the prevailing micro-deformation mechanism favorably shifts from shearing to crazing and vice versa [46]. Thinking of PA chains, additional hydrogen bond interactions would significantly increase the van der Waals energy term γ in Eq. (1). Consequently, the fibrillation energy Γ is expected to rise, so that $\sigma_c > \sigma_{ys}$ and shear yielding mechanism instead of crazing is preferred.

The hydrogen bond hypothesis **[37]** further correlates well with early predictions on the influence of H-bonds on SCG resistance drawn from studies of Lu et al. [69], Lee and Phillips [86], Kausch [87], as well as Zimmerman [88,89]. A minimum M_W value was determined, below which studied materials showed zero to very poor resistances against crack propagation. By comparing polymers with no physical cross-links, such as PE and POM, to polymers with H-bonds (i.e. PA), it was concluded, for example, that PE exhibits zero resistance at M_W < 18 kg/mol and poor resistance up to 150 kg/mol. The transition from an overall brittle to a ductile behavior occurred in PE above a value of M_W = 150 kg/mol and for POM above M_W = 100 kg/mol, whereas PA grades showed significant fracture toughness

improvement already at some 15 kg/mol, apparently owing to the strong hydrogen bonding influence [72].

In that context, **Messiha et al. [38]** aimed for a quantitative estimate of the additional resistance against crack propagation associated with H-bonded PA12 chains compared to theoretically non-bonded PA12 chains. A reversed engineering approach was adapted to determine the energy ($G_{dis,f}$), which is dissipated during SCG by chain disentanglement and effects associated with it (e.g. deformation processes and destruction of crystalline structure) of a theoretically non-cross-linked chain in PA12. This was achieved by subtracting an analytically estimated energy necessary to break all active hydrogen bond cross-links ($G_{H,f}$) during subcritical crack growth from the experimentally measured total SCG fracture energy (G_f) obtained from the cyclic CRB test. The latter was calculated by means of the time-temperature superposition principle according Arrhenius on the pure SCG fracture process, regardless of the crack initiation stage. To approximate $G_{H,f}$ a modified Sequential Debonding Fracture (SDF) model [38,90] was applied which takes into considerations the consecutive and sequential dissociation of H-bonded physical cross-links during crack propagation. The main idea is strongly related to the fracture energy theory of Lake and Thomas [91], who recognized that the energy to be overcome in order to propagate a crack across a failing interface of stretched material (i.e. craze zone) is not only the bond scission energy. Rather, the fracture energy must reflect the energy that goes into entropically stretching and enthalpically deforming each strand that bridges the crack plane, as shown in Fig. 6.

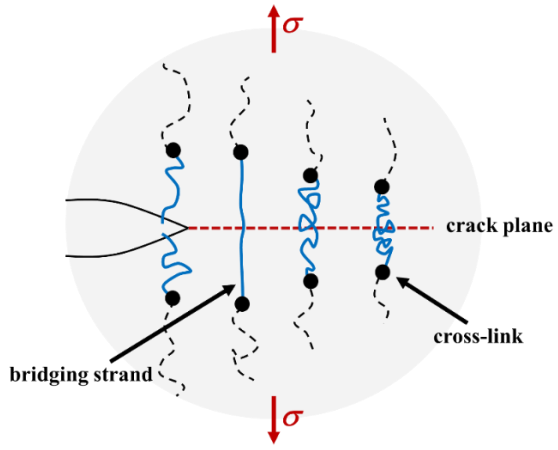

Fig. 6: Schematic illustration of crack propagation according to the Lake-Thomas fracture model [91,92]. Reprinted from Messiha et al., "How hydrogen bonds influence the slow crack growth resistance of polyamide 12", *Polymer*, 2021, with permission from Elsevier.

According to the Lake-Thomas model, the bridging strand defines the cross-link to cross-link portion of a polymer strand that spans the plane of the crack propagation. Thereby, Lake and Thomas referred to chemical cross-links, which are found in elastomers, or thermosets [91]. By slightly modifying the assumptions of the Lake-Thomas theory, these chemical cross-links can be replaced by physical cross-links (i.e. H-bonds in hydrogels or polyamides), as can be found in the sequential debonding fracture model according to Xin et al. [90]. The main assumption backing up this model is that the deformed bridging strands undergo repeated partial stress release as physical cross-links, which connect the stretched strand to neighboring chains by H-bonds, dissociate. In contrast to polymers without the capability of forming H-bonds, polymers exhibiting H-bonds, which act as cross-linking points distributed along their chains, may experience additional toughening effects with respect to that model. Each black dot shown in Fig. 7 marks such an effective cross-link location in a PA chain. When the crack propagates, the PA strands conquering the crack plane in front of the crack tip get strained and stressed (strand "b" to "c") until one of the H-bonds on each side of the crack breaks. Up to that point, deformations also follow the assumptions proposed by Lake & Thomas. However, as soon as the first physical cross-link fails (point "c") the elastic energy stored on the network strand will be partially released. In turn, the bridging strand does not fail, as no backbone bond scission has taken place. Instead, the chain relaxes until the load is transferred to the next-in-line H-bond (i.e. point "d"). This process repeats, leading to a sequence of multiple H-bond breakages **[38]**.

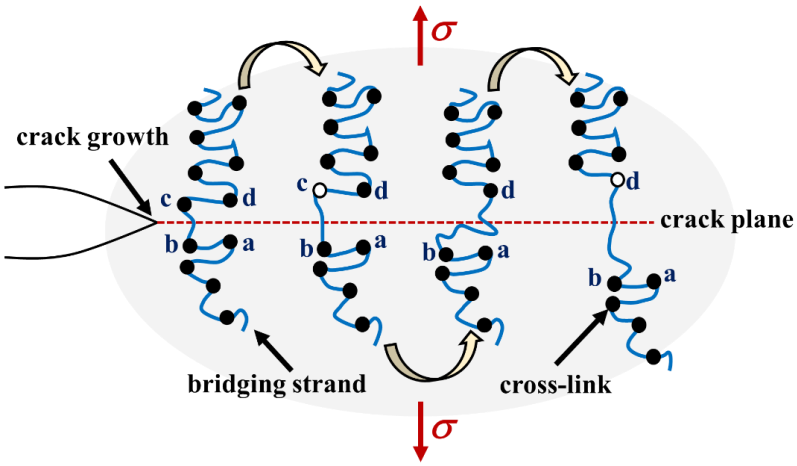

Fig. 7: Schematic illustration of a sequential hydrogen debonding fracture mechanism according to the model of Xin et al. [90]. Reprinted from Messiha et al., "How hydrogen bonds influence the slow crack growth resistance of polyamide 12", *Polymer*, 2021, with permission from Elsevier.

A total fracture energy G_f of 1.74 kJ/m² was eventually calculated for the selected PA12 grade. Interestingly, for a hypothetical amount of 50 % of active H-bond per chain that participate in resisting crack propagation, $G_{H,f}$ and $G_{dis,f}$ make up 54 % and 46 % of G_f, respectively. In that context, $G_{H,f}$ becomes the major source of energy that has to be overcome, if at least 45 % of all H-bonds participate in the SCG fracture process **[38]**. The SDF model, though, does not consider reformation processes of dissociated H-bonds, as well as any time-dependency of energy dissipations during strand loading and unloading [90]. Both processes may further increase the toughening behaviour of H-bonds, which may explain the remarkably high SCG resistance of PA12 grades compared to other polyolefins, such as PE [93]. Because of this, the SDF model is not intended to be used as a predictive tool to give accurate calculations about the effective energetical terms. It is primarily proposed as a way to explain how and why the observed and confirmed increase of SCG resistance in PA might be explained in comparison to its non-physically-crosslinked paradigm PE [86].

3.5 Influence of Impact Modifiers and Color Pigments

Bearing that in mind, it becomes inevitably important to consider the influences of H-bonds during SCG, when developing new PA formulations for certain applications. However, the ability of a material to resist the initiation and propagation of a crack is additionally influenced by a variety of parameters. Intrinsic factors on a molecular scale (e.g. molecular weight and its distribution; entanglement density; etc.), as well as morphological structures (e.g. lamellae: size, shape, distribution and orientation; inter-crystalline amorphous regions and tie molecules; short and long chain branching; impact modification via rubber particles; addition of pigments; residual stresses; etc.) determine the fracture toughness [94].

In a current study **[39], Messiha et al.** systematically examined the plastic zone development and fracture resistance of PA12 formulations when adding impact modifiers and/or pigments. Implementing IM and PGM showed significant effects on the plastic zone size, as schematically highlighted in Fig. 8. It appears that l_{pz} of pigmented grades is much smaller than of non-pigmented counterparts. Perhaps a higher local stress triaxiality level is accompanied by the presence of pigments during fatigue loading, which would lead to remarkably higher local critical stresses (e.g. σ_c or σ_{ys}) and thus limited plastic deformation. Also, the resistance to crack initiation and slow crack growth was observed to reduce due to

pigments. Fractographic analysis of CRB specimens showed that the addition of pigments reveals an increasing number of locations at which cracks can be more easily initiated or grow **[39]**. From a fracture mechanics viewpoint, introducing pigments equals the introduction of additional rigid stress concentration spots, which might promote the formation of micro-cracks alongside the interface between polymer matrix and pigment. As a consequence, the single dominant crack is accelerated as it coalesces with the smaller micro-cracks within the leading crack plane.

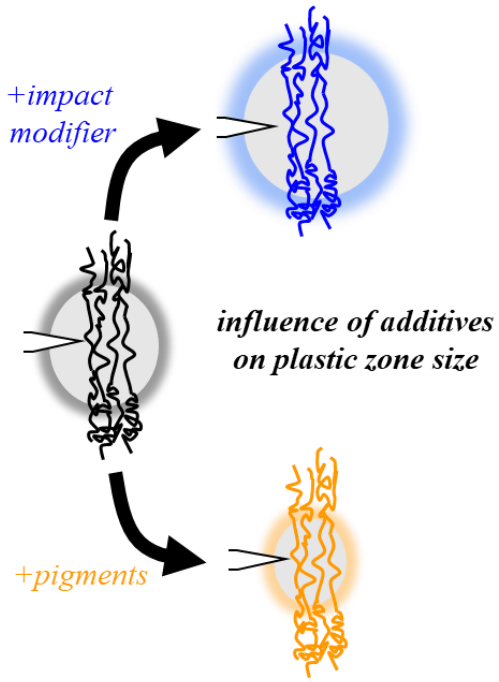

Fig. 8: Schematic diagram of plastic zones as a function of different additives implemented in PA12 grades of the same M_W (with reference to **[39]**).

In case of impact modified grades, the generation of notably large plastic deformation zones is promoted (cf. Fig. 8) and resistance to initiation and SCG is remarkably improved **[39]**. Incorporated soft rubber particles lead to a very fine fibrillation and significantly increasing plasticity at a microscopic level of investigated PA12 grades. It can, therefore, be assumed that rubber particles have enough time during fatigue to plastically deform and cavitate [40]. Different theories were proposed to explain the toughening mechanisms due to impact modification:

- the rubber is stretched during the fracture process and absorbs a large amount of energy [95] within the plastic zone;

- rubber particles are crack terminators that create a large number of stress concentration points, promoting multiple crazing and subsequent propagation of smaller cracks, which require more energy than a single main crack due to the formation of numerous new surfaces [96];
- a rubbery phase results in cavitation mechanisms that dissipate hydrostatic strain energy and increase shear flow of the matrix [97].

Independent of the actual toughening mechanism, the dispersion of soft rubber particles in the polymer matrix seems to dissipate a large amount of energy, shifting the total failure time in the CRB test to relatively long testing times **[39]**.

Considering obtained structure-property relationships with regard to SCG in PA12, a strong case can be made for improving the long-term behavior of newly developed PA12 grades, particularly used in pressure pipe applications. However, SCG failure is not the only failure mode for which a pressure pipe system must be designed against. SCG may initiate only a small leak, but it has also the potential to trigger RCP, which is much rarer but more catastrophic and destructive. In that context, it is necessary to emphasize that SCG and RCP are entirely different dynamic problems, with different underlying failure mechanisms [46,98].

4 RAPID CRACK PROPAGATION IN PA12

4.1 Introduction

Generally speaking, the key factor that determines whether SCG or RCP will dominate after crack initiation, is how abruptly a transition from non-loaded to loaded conditions is achieved. If the applied load on a tough material is static or very slowly increased (quasi-static), an existing crack might either go blunt or trigger SCG until structural failure occurs. On the other extreme, if a component is submitted to an explosive increase of applied loads the initiated crack will rapidly accelerate throughout the SCG regime to enter a state of RCP (e.g. RCP failure in pressurized applications) [21]. RCP itself can be maintained under static, or quasi-static loads – what is difficult, though, is to initiate RCP without the aid of dynamic high-speed loading [99]. Characteristic for RCP failures are long, straight or meandering axial crack paths at speeds of up to hundreds of meters per second. It is driven by internal (residual) and external (pressure) loads and resisted by molecular and morphological characteristics of the polymer. The safe installation and operation of a pipe throughout its service lifetime, therefore, requires additional knowledge of its resistance to RCP, particularly when using new materials.

For gas- and water-pressurized pipe systems, resistance to RCP is measured using the *Full-Scale* pipe test method – standardized as ISO 13478 [100], which has become the gold standard for product qualification. It measures a critical pressure value ($p_{c,FS}$) above which RCP can occur under operating conditions for pressurized pipes in service. It requires a 25 m long pipe section of up to 500 mm diameter, which is buried in gravel to at least 100 mm above the upper surface, simulating real operating conditions. Temperature is regulated via circulating water systems, maintaining a uniform and controlled test environment. Attached to both ends of the pipe specimen are steel pipes of a specific length in order to simulate an infinitely long pipe, which is then pressurized with air or nitrogen gas. Dynamic crack initiation is provoked by impact loading close to one end of the plastic pipe by means of a 400 mm long steel blade. The crack initiation zone itself can be locally cooled down to -60 °C and internally notched, to ensure high-speed fracture at the instance of impact. Valid RCP is considered if the crack length exceeds more than 90 % of the specimen length, otherwise it is perceived as an arrested crack. Since several FS tests are needed to evaluate the RCP behavior of a given material, this method is expensive and time-consuming.

Because of that a lab-scale *Small-Scale Steady-State* (S4) test was developed and standardized as ISO 13477 [101] by which a rapid crack is initiated in a small pipe sample (~7 to 8 pipe diameters, D, long). As in the FS test, pipes are tested at a specific temperature (e.g. 0 °C) and pressurized with air. Fast crack extension is provoked by the impact of a chisel-ended striker close to one end of the pipe. To prevent excess flaring of the pipe walls, as compressed air escapes, a steel cage surrounds the sample, while internal baffles prevent the axial decompression of the pipe and ensure a steady pressure in each compartment between the baffles. Critical pressure ($p_{c,S4}$) and temperature ($T_{c,S4}$) values are then determined, quantifying for how long a tested material can sustain RCP.

A novel evaluation concept of the S4 test results was proposed to improve the determination of $p_{c,S4}$ and $T_{c,S4}$ on the basis of a significantly reduced amount of S4 tests by **Messiha et al. [40]**. To precisely identify the critical RCP/crack arrest transition point according to ISO 13477 at a constant temperature, for example, at least one crack arrest point at a lower applied pressure must be followed by a valid RCP fracture point at a slightly higher applied pressure (cf. Fig. 9). Similarly, transition at a constant pressure level necessitates the existence of an RCP point following crack arrest with successively decreasing temperatures. However, these premises are not always achievable in practice without significantly extending the experimental and subsequent financial effort.

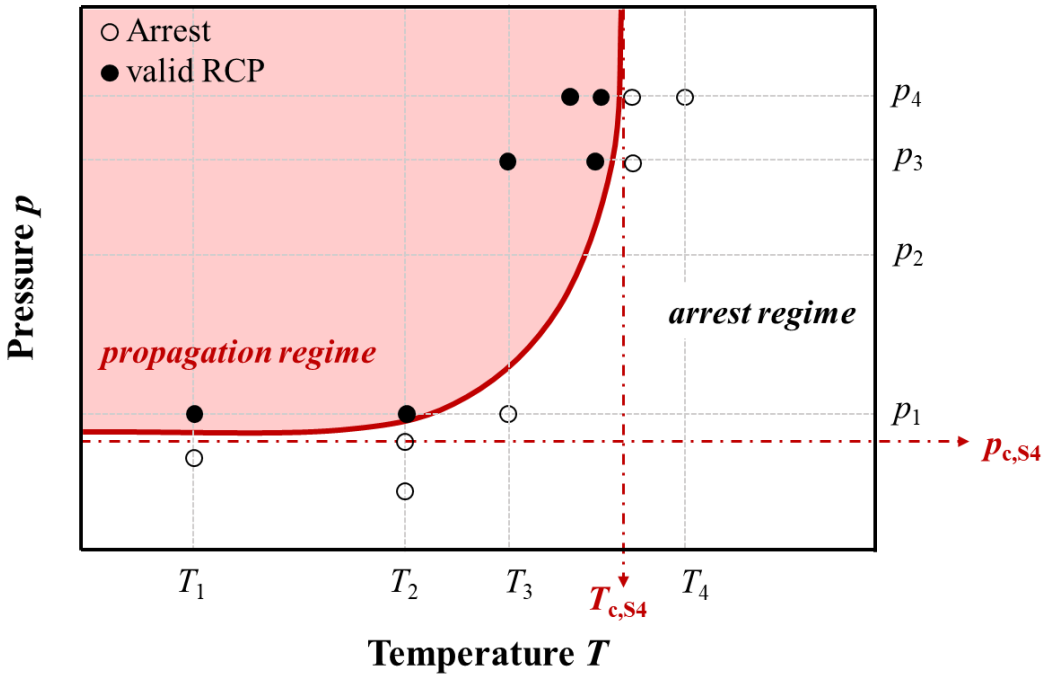

Fig. 9: Illustration of rapid crack propagation and arrest regimes during S4 testing according to [102].

Therefore, a modified S4 evaluation was used, aiming for maximization of the data yield from each test. Measured arrest lengths of cracked pipe samples were processed numerically, as well as being classified as arrest/propagation. A linear correlation was then found when plotting at least three crack lengths as a function of test pressure at a given temperature or as a function of temperature at constant pressure. In doing so, critical pressure and temperature values could be predicted **[40]**. For example, instead of starting at extreme pressures and successively decreasing the applied p at a constant T to obtain the point of transition from RCP to crack arrest, it is proposed to test first at very low p and then at very high p. The critical S4 pressure point can then be estimated by (extra-/) intrapolation and refined successively by additional intermediate tests.

4.2 Structure-Property Relationships

Using the modified S4 test, **Messiha et al. [40]** systematically investigated the influence of M_W, as well as the implementation of pigments and impact modifiers on RCP performance of different PA12 formulations. Findings showed a remarkable benefit of RCP resistance with increasing M_W in PA12 grades. Krishnaswamy et al. [103] and Argyrakis [102] reported similar observations for PE-HD: high molecular weight and narrow molecular weight distributions appear to be important elements for superior RCP resistances.

Pigmentation, on the contrary, reduced RCP resistances of PA12 grades significantly. The addition of rigid pigments corresponds to the addition of inherent defects and localities of stress concentrations at which cracks are preferentially launched. Several studies confirm that the improvement of esthetical properties of different materials by coloration is often accompanied by significant reductions of their fracture toughness [104–107]. This was also observed in terms of SCG behavior of PA12 grades **[39]**.

Surprisingly, an impact modification of PA12 grades caused a negative effect on RCP resistance. Rubbers are widely used to toughen polymers in critical applications that might expose them to impact loads. In theory, the soft particles absorb much of the input impact energy, either by stretching the rubbery material, or by promoting multiple crazing, shear yielding or the combination of both [95]. The contribution of each mechanism to toughen the rubber-matrix system depends on a number of variables, such as the rubber particle size, distribution and concentration [108]. However:

1) Impact modifiers generally increase the *crack initiation resistance* $G_{Ic}(t)$ against rapid loading but do not influence the resistance to its propagation [109–112], and
2) Impact modifiers are themselves time-dependent elastomers undergoing significant strain-rate hardening [95,113].

It can, therefore, be assumed that rubber particles have enough time during static and quasi-static load conditions (i.e. low and moderate local strain rates) to plastically deform and cavitate, enhancing the resistance to crack initiation and subsequent SCG. Once a crack starts to extend at low crack speeds $\dot{a}$, low crack opening strain rates prevail at areas surrounding the crack tip, so that incorporated elastomers get easily strained and continue to absorb large amounts of energy even during slow crack extension [95]. In contrast, a structure exposed to highly dynamic, time-dependent load conditions experiences local deformations at extremely high rates. If the applied time-dependent crack driving force $G(t)$ is sufficiently high, a rapid crack initiates. In that case, soft rubber parts at the vicinity of the fast running crack tip have no time to follow the governing local crack opening deformations. Even worse, bearing the time-temperature principle in mind, it was suggested that elastomeric parts could pass through the glass transition when a critical local strain rate is exceeded, which is equivalent to the rubber's T_g or tough-brittle transition temperature (T_{TB}). Consequently, the hardened rubber particles might act as additional stress concentrators, at which rapid cracks initiate and propagate more easily (similar to rigid pigments). Therefore, incorporation of toughers may feature a significant reduction of the RCP resistance during S4 testing [40,112].

The use of abovementioned accelerating ranking tools and obtained structure-property relationships with regard to RCP in PA12 grades is essential for future material design at molecular and micro-structural levels. However, in order to keep up with increasingly demanding criteria and the competitive development of new material formulations, even an S4 test with modified evaluation is too uneconomical and time-consuming to check for RCP properties. Material developers need either a relatively simple batch test, or an accessible and reliable model for *virtual* RCP testing. In this context, atomistic models have been on a rise in last decades trying to describe fracture behavior and mechanisms of different materials. One classic approach regards a body as a crystal with single atoms that interact with each other i.e. by a Lennard-Jones potential. The calculation is then done by molecular dynamic computer simulation [114–116] to analyze the dynamic crack behavior at atomic

scale. A plasticization of the material at the crack tip is not possible in these models and the crack is therefore ideally brittle, which of course is not entirely true for semi-crystalline thermoplastics. Other models, such as the widely used mass-spring model, where individual atoms are connected by elastic springs, determine the dynamic crack behavior without considering the actual microstructure of the body. At a certain elongation the springs break and a crack is formed [117–119]. The huge advantage of these models is that the propagation dynamics of a crack can be modelled quite well on atomic scales, which are in good accordance with experimental results within a very specific section of the full fracturing body: computer-assisted calculations were even able to explain and simulate the crack branching behavior [120] and the rough fracture appearance [116,121] in some cases. However, the course of the crack velocity on large scales cannot usually be understood by such models, even if, like Abraham [114], millions of atoms are used for calculations. Furthermore, it is only possible to model regularly structured solids with reasonable effort, whereas cracks in viscoelastic polymers with additional considerations of molecular and morphological dynamics, would be too complex.

4.3 RCP Fracture Mechanism in PA12

For an improved RCP characterization, the underlying physical processes during rapid fracture must be fundamentally understood first. Two mechanisms have been proposed so far with respect to RCP in polymers. The first regards chain scission as the dominant failure mechanism [46,72,122,123], given that the time scale of RCP does not allow creep or chain disentanglement. The second considers chain disentanglement to be the dominant mechanism but, unlike SCG [45,67,122–125], accelerated by adiabatic heating [98,126–128] and not only by mechanical creep and chain slipping against secondary forces (e.g. London forces, dipole-dipole attractions, hydrogen bonds, etc.) of neighboring chains.

In frame of this, Leevers developed a relatively simple analytical model – the adiabatic decohesion model (ADM) – in order to assess RCP phenomena in plastics, while accounting for their semi-crystalline microstructure. Different to aforementioned numerical models, ADM is solely based on the question of how dynamic fracture occurs in polymeric materials and arose from concerns of gas and water distribution industries to avoid RCP in pressure-pipelines, particularly made from PE-HD [126–129]. The ADM is based on Dugdale's strip yield model, where the size of the craze is dictated by the applied crack driving force G_I. At the point of fracture, that is $G_I = G_{Ic}$, the cohesive zone starts to fail by

whatever separation criterion limits the length l_{pl} or the height δ of the plastic zone to a critical value. Hence, the craze must survive an applied load or grow in order to resist fracture. Two limiting cases in which craze zones are rapidly developed under adiabatic conditions are known:

i. Rapid Crack Initiation (RCI) – under abrupt loads at high deformation rates, the plastic zone length and thickness grow, but the crack does not extend;

ii. RCP – at high propagation speeds of running cracks, the plastic zone geometry at the crack front remains essentially constant under adiabatic conditions.

In both cases, short-time decohesion is described by the introduction of a melt fracture mechanism grounded on adiabatic heating effects [127] that is capable of predicting the fracture initiation resistance against high-speed impact loads $G_{Ic}(t)$, as well as the fracture resistance against RCP $G_{Id}(\dot{a})$. During RCI and subsequent RCP energy is ultimately converted into heat. If the crack propagates at low speeds, the surrounding bulk material has sufficient time to conduct the generated heat away from the crack tip and the temperature stays almost constant. Due to the low thermal conductivity of polymers, however, a comparatively low crack propagation velocity is sufficient to obtain adiabatic conditions in front of the crack tip. The limiting velocity v_{lim} [130] above which the adiabatic state at the crack tip applies is approximated by Eq. (2):

$$v_{lim} \approx \frac{4\kappa}{\rho c_p \delta_c} \tag{2}$$

where κ is the thermal conductivity, c_p the specific heat capacity, ρ the density and δ_c the critical crack tip opening displacement according to the Dugdale model [12,126]. For example, PMMA shows a v_{lim} in the range of 0.1 m/s [131] – that means that low speeds are already sufficient to provoke adiabatic conditions at ambient temperatures. With falling temperature, c_p and κ also decrease; yet, their ratio stays nearly the same, so that in case of unstable crack extension, adiabatic conditions in front of the crack tip are certain to prevail, even at low temperatures.

Considering the issue of poor thermal conduction of semi-crystalline polymers, Leevers [128] asserted the creation of a localized melt zone as a consequence of the heat, which is irreversibly generated at each cohesive zone surface by plastic work (cf. Fig. 10). The craze fibril extension is thereby assumed to follow a “cold drawing” mechanism as proposed by

Lauterwasser and Kramer [132]. Bridging polymer chains from the surrounding bulk material are pulled into the craze zone through a thin active layer at the craze-bulk interface. This active layer can be regarded as a hot spot, where local temperatures rise to melt point T_m due to adiabatic heating. It contains a mixture of polymer chains, which must be fully extended to give the craze strength, and others which are neither stretched, nor anchored. Once a chain transits the active layer, it pulls new bulk material along with it. Significant work is done to stretch, orient and fuse chains, that cross the active layer, into strong fibrillar structures. In doing so, more heat dissipates, which cannot be conducted away fast enough, heating up neighboring surfaces to the active layer. Eventually a successively growing melt zone of specific depth is left behind over a short time range (cf. Fig. 11). At the point where the melt layer thickness reaches a critical value s_c, at which the weight-average polymer chain becomes too short to bridge the growing gap between the bulk/active layer interface and the onset of the craze fibrils, it becomes mechanically unstable and the cohesive strength σ_c collapses instantaneously. In that manner, the energy needed to separate fibrils through the melt layer is much smaller than that needed to further expand the melt zone. This is why the separation mechanism is regarded to be a low-energy disentanglement of polymer chains, promoted by adiabatic heating, which prevails over competing conduction processes.

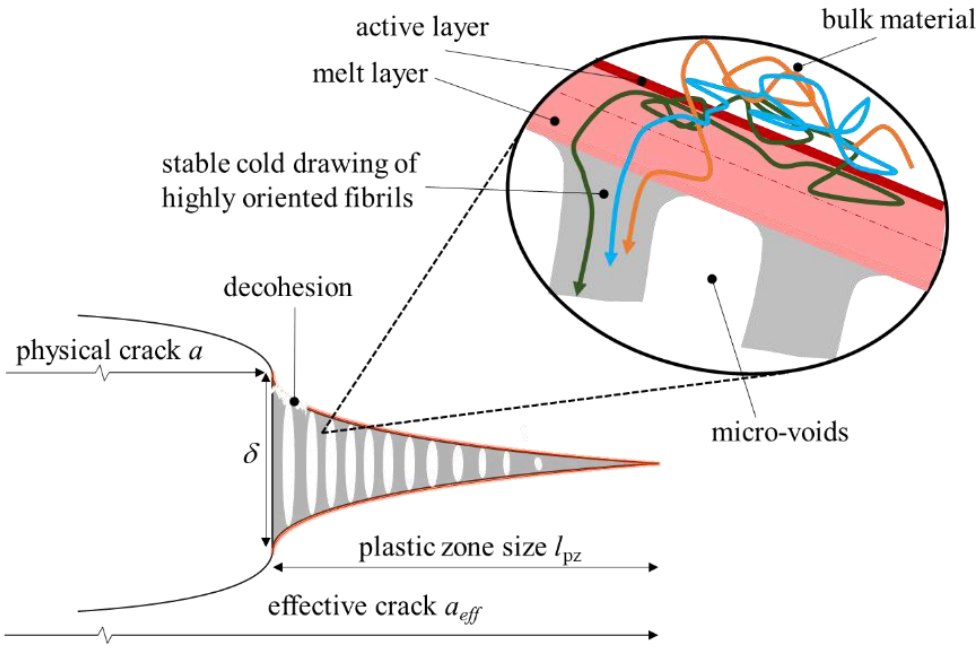

Fig. 10: The crack-tip craze in a polymer, modelled as a Dugdale cohesive zone [128]. Reprinted from Messiha et al., "Mechanisms of rapid fracture in PA12 grades", *Theoretical and Applied Fracture Mechanics*, 2021, with permission from Elsevier.

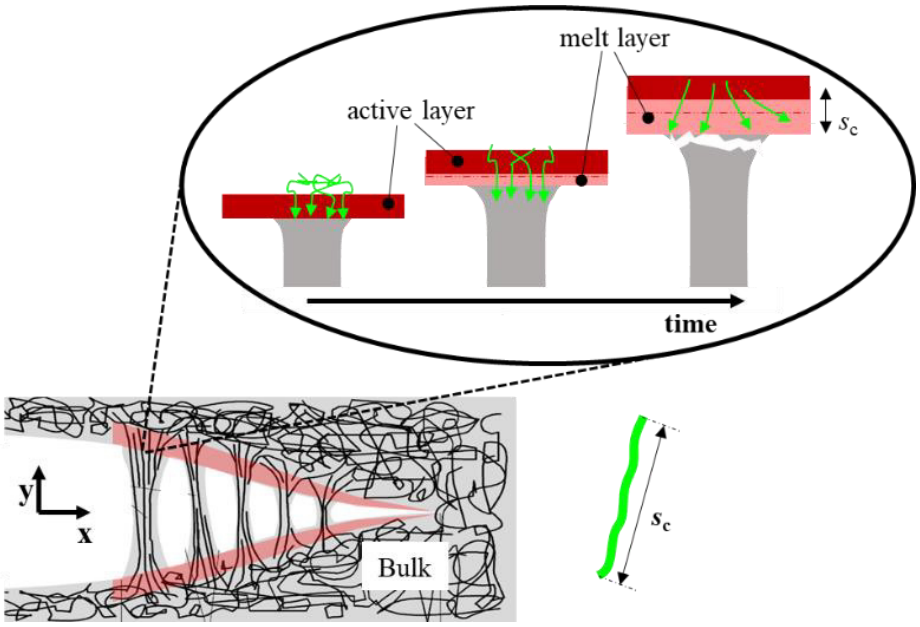

Fig. 11: Successive stages of decohesion at a craze-fibril root [127,133]. Reprinted from Messiha et al., "Mechanisms of rapid fracture in PA12 grades", *Theoretical and Applied Fracture Mechanics*, 2021, with permission from Elsevier.

A running crack at nearly constant high speeds (steady-state RCP), where $G_I(t) = G_{Id}(\dot{a})$, can be used to determine the mean plastic strain rate $\dot{\varepsilon}_{pz}$ within a Dugdale craze as:

$$\dot{\varepsilon}_{pz} = \frac{\dot{a}}{l_{pz}} = \frac{8}{\pi}\frac{\sigma_{ys}^2 \dot{a}}{E_d G_{Id}} \tag{3}$$

where E_d is the dynamic Young's modulus, which can be determined via ultrasonic techniques. In case of PE and other semi-crystalline thermoplastics, it was also found that $\dot{\varepsilon}_{pz}$ conforms to an Eyring process, that can be experimentally examined (e.g. using a Split Hopkinson Pressure Bar method [126]) to further allow for an estimate of σ_{ys} and $\dot{\varepsilon}_{pz}$ as a function of $\dot{a}$. Leevers [126] also emphasized that both heated melt layer depths must be small enough in comparison to the craze thickness and that they cannot significantly influence either the bulk properties, or each other. Therefore, cohesive surfaces can be visualized as independent, internally heated regions from which chains are drawn from the bulk, which itself remains relatively cold. Considering aforementioned points and by applying the thermal separation criterion, which requires cohesive surfaces to reach the fusion point T_m and melt to a depth sufficient to liberate every crossing polymer chain, Leevers [126] formulated a mathematical relation to express $G_{Id}(\dot{a})$ as:

$$G_{\mathrm{Id}} = 2\tilde{s}_{\mathrm{w}}\rho\left[\frac{1}{Y(Z_{\mathrm{p}})}c_{\mathrm{p}}(T_{\mathrm{m}} - T) + \Delta H_{\mathrm{f}}\right] \tag{4}$$

with

$$Y(Z_{\mathrm{p}}) \equiv 4\left[\left(\frac{Z_{\mathrm{p}}}{\pi}\right)^{1/2} \mathrm{e}^{-Z_{\mathrm{p}}} - Z_{\mathrm{p}}\left(1 - \mathrm{erf}\left({Z_{\mathrm{p}}}^{1/2}\right)\right)\right] \tag{5}$$

and

$$Z_{\mathrm{p}} \equiv \frac{{\tilde{s}_{\mathrm{w}}}^2 \dot{a}}{16\alpha l_{\mathrm{pz}}} \tag{6}$$

where α is thermal diffusivity, $\tilde{s}_{\mathrm{w}}$ the contour length of a weight average chain, Z_{p} the Graetz number that defines the passage of the craze over the active layer and $Y(Z_{\mathrm{p}})$ a corresponding thermal conduction efficiency function. By means of numerical calculations, it was demonstrated that $Y(Z_{\mathrm{p}})$ passes through a global maximum at $Z_{\mathrm{p}} \sim 0.187$ of about 0.405, at a crack speed of nearly 30 % of the material dependent reference speed c_0, which is defined as [127]:

$$c_0 \equiv 4.43\frac{E^{*}\rho\alpha c_{\mathrm{p}}}{\beta\sigma_{\mathrm{c}}^2 s_{\mathrm{c}}}(T_{\mathrm{m}} - T) \tag{7}$$

where E^{*} is the effective tensile modulus, β is a material dependent fraction (approx. 80 – 90 % for most semi-crystalline polymers [134]) of the whole plastic work that dissipate as heat within the active layers of a critical thickness s_{c}. The craze stress (or cohesive strength) σ_{c} is properly approximated by σ_{ys}. A schematic plot of G_{Id} as a function of $\dot{a}$, resulting from abovementioned mathematical formulations, is shown in Fig. 12a. Although, the curvature in Fig. 12a is very similar to experimental measurements of G_{Id} over $\dot{a}$ for rate-sensitive materials (Fig. 12b) as proposed by some investigators, such as Burns, Hahn, Kanninen and Broek [135–139]. The adiabatic decohesion theory actually does not address rate-sensitivity of the material at all. It instead suggests that the rate-dependence of fracture toughness arises mainly from a time-dependent thermal diffusion process, and is especially important in thermoplastics, because of their poor thermal diffusivity with respect to relatively large structural dimensions of the component [140].

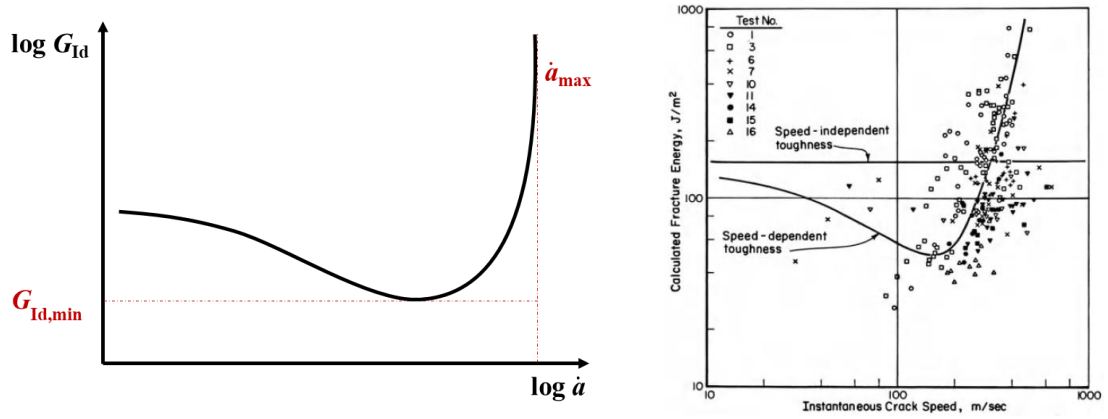

(a) (b)

Fig. 12: Schematic (a) and experimentally validated [139,141] (b) relationship of fracture toughness G_{Id} as a function of crack speed $\dot{a}$ with global minimum $G_{Id,min}$.

It follows from Fig. 12 and by modifying Eq. (4), an approximation of the minimum resistance against RCP ($G_{Id,min}$) through which $G_{Id}(\dot{a})$ has to pass at ~$0.3 \cdot c_0$ for any kind of semi-crystalline polymer [126]:

$$G_{Id,min} = \tilde{s}_w \rho \left[5 c_p (T_m - T) + 2 \Delta H_f \right] \tag{8}$$

This equation can be interpreted as follows:

- The longer the extended weight average chain, $\tilde{s}_w$, the thicker the melt zone can become before separation at one side of the cohesive surfaces occurs due to an insufficiency of oriented chains to span the gap and to provide any strength;
- an increase of the specific heat capacity ($c_p\uparrow$) means that the material can absorb more energy to increase its local temperature by 1 K, which subsequently results in more necessary energy to reach T_m at the active layer;
- a higher heat fusion enthalpy ($\Delta H_f\uparrow$) subsequently requires more energy to transform solid crystallites into melt state, where chains can move freely through the active layer into the craze zone.

Building upon this model, **Messiha et al. [40,41]** reflected on novel perspectives to explain different rapid fracture appearances on S4 tested PA12 samples (e.g. river lines, fibrillated zones, craze flakes, etc.). While the common opinion states that *river lines* (see Fig. 13a), for example, originate from the interconnection of micro-cracks at different fracture surface levels of cleavage planes with different orientations with the main fracture plane [142].

Referring to ADM, river lines in PA12 are believed to be regions of rapidly extending crack fronts, which stopped at an instance of time, before jumping into a neighbouring crack plane (cf. Fig. 13b). Reason therefore could be the superposition of different reflected stress waves (e.g. p-waves, s-waves, Rayleigh waves, etc.) at the crack tip, varying stress triaxiality levels along the thickness of the pipe, as well as inhomogenously distributed weak points (e.g. crystal defects, contaminations, pigments or hardened impact modifiers). Only if adiabatic decohesion is governing RCP on a molecular level, the abrupt change of the main crack plane would leave behind a ridge of fibrillar structures, that is not able to continue participating in the physical crack extension by thermal decohesion [98,126,128]. With a new hot craze-crack front passing by in a "new" main crack plane, fibrils beneath river lines solidify, freezing in the observed structures in Fig. 13b **[40]**.

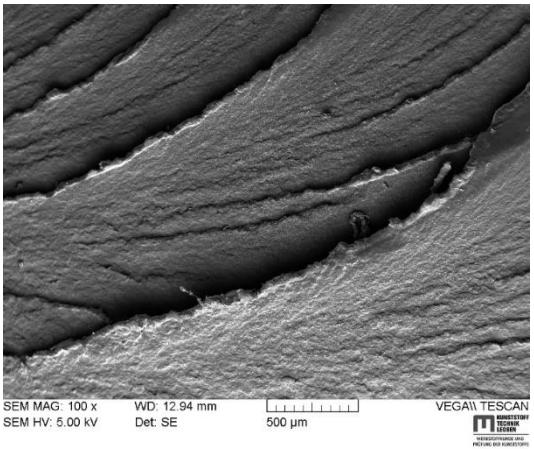

(a)

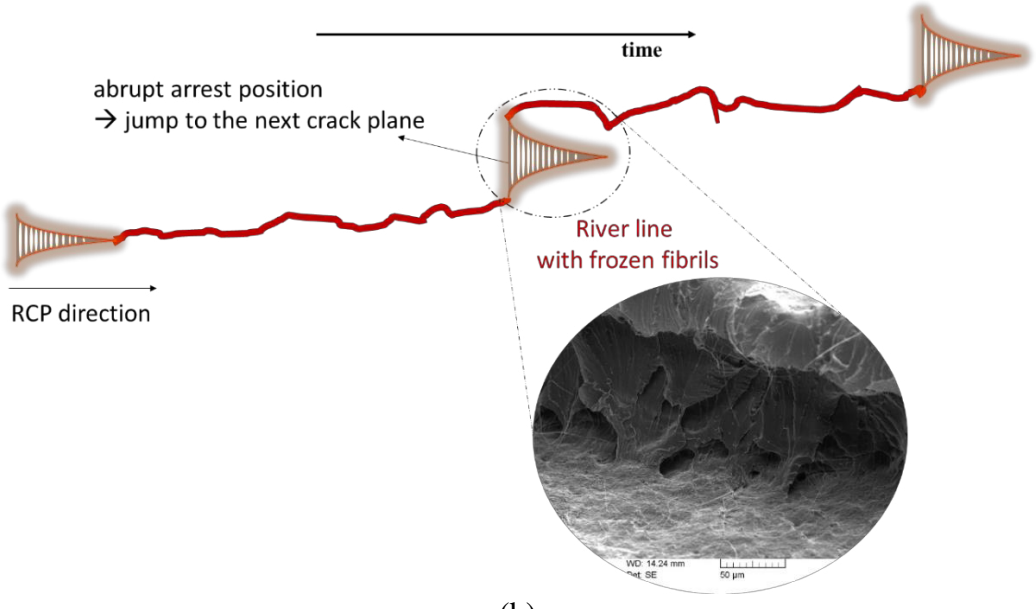

(b)

Fig. 13: River lines bottom view (a) and representation of how these structures could have evolved (b) in accordance to **[40]**.

Furthermore, fibrillar micro-structures as reported by Hazra [143] and Leevers [98] were observed within S4 fractured PA12 pipe samples **[41]**. Although fibrils are not extended over the entire fractured surfaces, it does not necessarily follow that thermal decohesion must be only restricted to small local regions. Instead, the theory would rather predict very small amounts to no visible fibrils at all, as it would be more likely for them to contract back into the molten ground (compare to Fig. 13b) after decohesion before solidifying as observable highly-stretched structures. Another indication for a governing adiabatic decohesion mechanism in PA12 grades was delivered by an in-situ thermographic analysis of rapid fracture processes using an infra-red (IR) camera during S4 testing **[41]**. Although there was no chance to capture the instantaneous crack tip temperature, peaks of approx. 60 °C to 80 °C compared to the actual bulk temperature were recorded. Even if no hot spots with temperatures around the melting point of the materials could be measured, thermographic results hint at a possible adiabatic heating process and support the idea of a thermal decohesion mechanism for PA12 pipe grades. In comparison, during SCG of PA12 pipe grades only minor temperature variations of up to a maximum of 5 °C were recorded.

4.4 Accelerated Ranking Parameter

Finally, the gained knowledge about the governing failure mechanism of PA12 grades exposed to rapid fracture **[40,41]** led to a recent development of R^{**} – an accelerated ranking parameter based on elasto-dynamic fracture mechanics concepts that characterizes RCP performance of materials with dominating adiabatic decohesion **[41]**. The main idea behind this parameter is represented in Fig. 14: To investigate RCP resistance of different pipe grades, structural and/or (fracture) mechanical tests (e.g. S4 test, strip band test, high-speed double torsion test, etc. [102,112]) may be conducted. Thereby, focus is put on the evaluation of dynamic fracture toughness at different crack speeds (step 1: G_{Id}, orange curves). For the given materials A, B and C, the latter would exhibit the highest RCP resistance. However, this assumption is not entirely true – different materials may experience different local loadings, although the applied loading situation is the same. Hence, the relation between crack driving force and fracture resistance of a material must be considered (step 2: G_{Id} & G_I, black curves). In that case, material B would show the highest resistance against RCP, as G_I does not exceed G_{Id} at given conditions. Appealing to the minimum fracture toughness $G_{Id,min}$ deduced from ADM (step 3) as well as the maximum dynamic crack driving force $G_{I,max}$ from the mathematical model of Kanninen and O'Donoghue [144,145] (step 4),

Messiha suggested that it can be sufficient to use the ratio of $G_{I,max}/G_{Id,min}$ instead of determining the whole curves experimentally. Eventually, R^{**} for plane strain state was proposed as:

$$R^{**} = \frac{G_{Id,min} E_d^{1.5}}{1-\mu^2} \tag{9}$$

with μ as the Poisson number. In so doing, results of R^{**} were found to be in high accordance ($R^2 = 0.98$) with the critical pressure values $p_{c,S4}$ obtained from S4 tests of different PA12 pipe grades. While in the past O'Donoghue and Zhuang et al. [144,146–149], as well as Ivankovic et al. [150,151] developed different numerical models (i.e. Pipeline Fracture Analysis Code, PFRAC by O'Donoghue and Zhuang) to account for the dynamic deformation and fracture of pressurized pipes, the gas dynamics of the pressurizing fluid and corresponding interactions, as well as the presence of soil backfill during RCP in a pipeline. Accounting for all kinds of different factors lead to successively increasing complexity. In this context, proposed semi-analytical solution of R^{**} is viewed as satisfactory for a quick estimate of RCP properties of newly developed grades, while simultaneously decreasing experimental efforts and numerical complexity significantly.

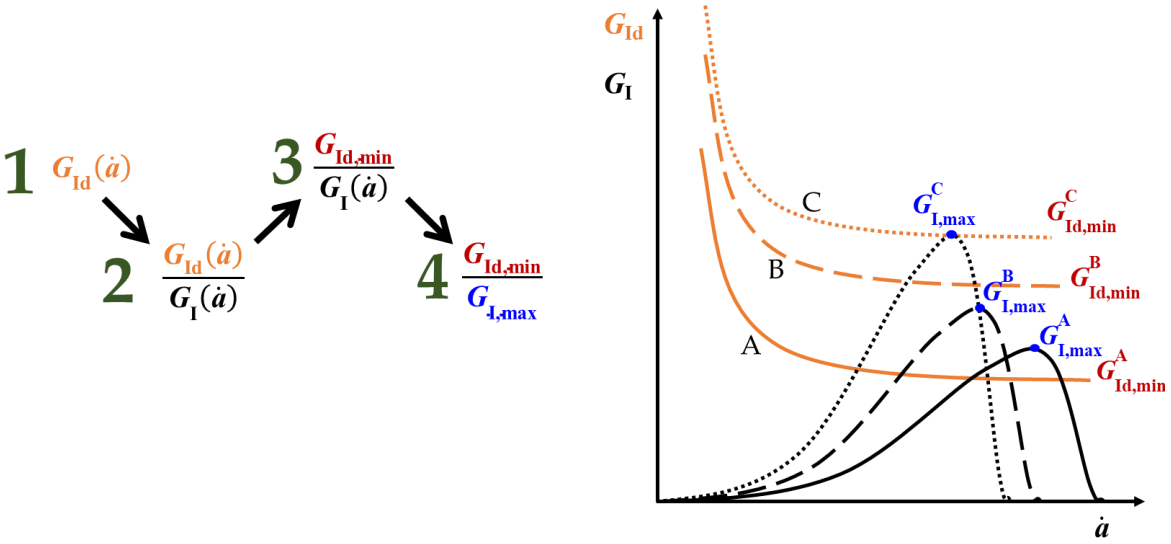

Fig. 14: Schematic illustration of development steps for R^{**} according Messiha et al. **[41]**.

5 SUMMARY & CONCLUSION

This thesis has highlighted the complex relationship between the overall fracture performance and fracture mechanisms occurring from molecular perspective up to macro-scale deformations in semi-crystalline polyamide 12 (PA12) grades. Various, often highly interdependent intrinsic and extrinsic parameters were reported to have significant impact on a material's fracture toughness, especially by affecting the craze and void formation as well as the craze-crack transition during slow crack growth (SCG) and rapid crack propagation (RCP).

Considering SCG, the applicability of the cyclic cracked round bar (CRB) test and the strain hardening (SH) test as suitable tools to characterize quasi-brittle fracture resistance was demonstrated. PA12 was found to fail by a governing chain disentanglement mechanism, which was verified by fibrillated fracture surfaces of CRB specimens. Fibrils are built during the evolution and breakdown of crazed zones, which are also found in other polyolefins. Contrarily, however, the SCG behavior of PA12 is additionally influenced by its capability to build hydrogen bonds. In that context, a sequential debonding fracture model was carefully examined and applied to PA12, estimating the amount of fracture energy which has to be additionally supplied to break physical cross-links between PA chains compared to a theoretically non-cross-linked PA chain. In so doing, the remarkable SCG performance of PA12, in which hydrogen bonds are believed to inhibit chain disentanglements, can be explained. Moreover, focus was put on the question of how plastic zones and fracture mechanisms in PA12 change when the molecular weight (M_W) is increased, or impact modifiers and/or pigments are added. An increase of crack initiation resistance and SCG resistance was generally observed in PA12 with increasing M_W and by the implementation of an impact modifier. A positive influence of higher M_W is attributed to the *hydrogen bond effect* – an increasing disentanglement resistance arises when a critical number of active hydrogen bonds is exceeded. Consequently, the craze breakdown process is significantly delayed due to additional inter- and intra-molecular attraction forces, which have to be overcome. Impact modification, on the other hand, generates remarkably large plastic zones which absorbs large amounts of energy and significantly increases the material's micro-plasticity during SCG. Adding pigments, on the opposite, reduces the plastic zone size presumably due to a higher local stress triaxiality, resulting in a reduction of the crack initiation and SCG resistance. Fractographic analysis confirms an increasing

number of flaw-like locations at which cracks can be initiated or accelerated alongside the interfaces between polymer matrix and pigments.

The dynamic rapid fracture behavior in PA12 was also studied in frame of this project. Whether a crack will initiate, rapidly grow or eventually arrest, however, is no simple matter and depends not only on the amplitude of the loading, but also on the complete history of load application as well as on the time- and temperature-dependent material response. Relevant structure-property relationships regarding the resistance against RCP in morphologically different PA12 grades were established via the small-scale steady-state (S4) test according ISO 13477. A novel evaluation concept of the S4 test was further applied to improve the determination of critical temperature and pressure values on the basis of a significantly reduced amount of S4 tests. Results highlighted an obvious improvement of the RCP resistance with increasing M_W, while the incorporation of inorganic pigments reduced the rapid fracture toughness of PA12. Furthermore, rubber-toughening of PA12 grades was also found to decrease the RCP resistance, due to underlying strain-rate effects. During RCP elastomeric parts are exposed to remarkably high local strain rates. Considering the time-temperature equivalence principle, rubber particles may pass through a tough-brittle transition temperature when a critical local strain rate is exceeded. In that case, the hardened rubber particles might act as additional stress concentrators, at which rapid cracks initiate and propagate more easily.

In contrast to the general believe that chain scission mechanism is governing physical processes on a molecular scale during rapid crack extension, an *in-situ* thermographic analysis during S4 tests backed up the existence of high temperatures, most likely due to adiabatic heating. Moreover, a postmortem fractographic investigation revealed highly fibrillated structures on PA12 fracture surfaces indicating thermo-mechanical disentanglement processes on a molecular level. Finally, a novel accelerated ranking parameter (R^{**}) based on elasto-dynamic fracture mechanics concepts and the presupposition of a thermal decohesion as prime fracture mechanism during RCP of semi-crystalline plastics was proposed. Semi-analytical results of R^{**} were found to be in high accordance with the critical pressure values $p_{c,S4}$ obtained from S4 tests of different PA12 pipe grades.

6 OUTLOOK

There are already quite a number of works regarding slow and rapid crack propagation in polymers, particularly polyolefins. This thesis, on the contrary, aimed for a comprehensive overview of fracture behavior in PA12 grades. Though, numerous new insights were generated in the scope of this thesis, still more research would be beneficial to account for given uncertainties. Regarding SCG, for example, it should be investigated for how long chain disentanglement fracture mechanism predominates with increasing M_W, before shear yielding takes over. This, of course, is important and should be implemented in future calculations based on the sequential debonding fracture model. With regard to RCP, current findings suggest that RCP is governed by adiabatic decohesion and not by chain scission mechanisms in PA12 grades. However, this is challenged by structural effects of the used S4 test. Though this test allows to get as close as possible to the critical RCP conditions in service and seems very satisfactory to compare grades and obtain a critical pressure. It presents some "shortcomings" when concluding on the dynamic fracture behavior of a material. In that sense, a running crack might arrest, re-initiate and re-propagate in an S4 test due to structural effects (e.g. stress wave reflections). Observed fibril structures could then be possibly assigned to the SCG regime through which a re-initiated crack has to pass before accelerating again to RCP. Although this conclusion seems reasonable, it would neither explain the remarkable increase of temperature observed in PA12, nor the highly correlating results based solely on thermal decohesion assumptions. Future work could, therefore, be dedicated to investigate RCP fracture mechanisms in different fracture mechanical tests that guarantee a steady-state RCP (e.g. strip band test or high-speed double torsion test).

Moreover, there have been many interesting results in the field of simulation in recent years. Several models have in common that it is not possible to deal with the different molecular and micro-structure of the materials. Within the continuum mechanical models, only very general parameters such as the Young's modulus (E) can be used as material-specific quantities. However, based on obtained structure-property relations as well as accelerated ranking parameter, existing models (e.g. adiabatic decohesion model, etc.) could be adapted and modified in order to assess fracture behavior of PA12 without the need of time-consuming and costly experiments. In this sense, on-going work is dedicated to develop a semi-numerical model which ranks PA12 formulation according their RCP resistance by appealing to standard characterization parameters, such as M_W, E or the zero-viscosity η_0.

7 REFERENCES

[1] H. P. Rossmanith, "The struggle for recognition of engineering fracture mechanics," in *Fracture research in retrospect*: *An anniversary volume in honour of George R. Irwin's 90th birthday*, Balkema, Rotterdam, 1997.

[2] T. L. Anderson, *Fracture Mechanics*: *Fundamentals and Applications, Fourth Edition*, Chapman and Hall/CRC, Boca Raton, 2017.

[3] C. T. Sun and Z.-H. Jin, "Introduction," in *Fracture Mechanics*, pp. 1–10, Elsevier, 2012.

[4] G. M. Boyd, *Brittle fracture in steel structures*, Published by Butterworth for the Navy Department Advisory Committee on Structural Steel, London, 1970.

[5] J. Knott, "Brittle fracture in structural steels: perspectives at different size-scales," *Philosophical transactions. Series A, Mathematical, physical, and engineering sciences*, vol. 373, no. 2038, 2015.

[6] M. E. Shank, "Brittle failure of steel structures - a brief history," *Metal Progress*, vol. 66, pp. 83–88, 1954.

[7] E. Orowan, "Fracture and strength of solids," *Journal of Applied Mechanics-Transactions of the Asme*, vol. 12, no. 1, pp. 185–232, 1949.

[8] G. R. Irwin, "Fracture dynamics: Fracturing of Metals," pp. 147–166.

[9] J. D. Eshelby, "The Continuum Theory of Lattice Defects," *Solid State Physics*, Vol. 3, pp. 79–144.

[10] G. R. Irwin, "Analysis of Stresses and Strains Near the End of a Crack Traversing a Plate," *Journal of Applied Mechanics*, vol. 24, pp. 361–364, 1957.

[11] G. R. Irwin, J. A. Kies, and H. L. Smith, "Fracture strength relative to onset and arrest of crack propagation," *Proceedings of the American Society for Testing Materials,* Vol 58, pp. 640–657, 1958.

[12] D. S. Dugdale, "Yielding of steel sheets containing slits," *Journal of the Mechanics and Physics of Solids*, vol. 8, no. 2, pp. 100–104, 1960.

[13] G. R. Irwin, "Plastic zone near a crack and fracture toughness," *Sagamaore Conference Research Proceedings,* Vol. 4, pp. 63–78, 1961.

[14] A. A. Wells, "Unstable crack propagation in metals: Cleavage and fast fracture," *Proceedings of the Crack Propagation Symposium,* Paper 84, 1961.

[15] G. I. Barenblatt, "The Mathematical Theory of Equilibrium Cracks in Brittle Fracture," in *Advances in Applied Mechanics Volume 7*, vol. 7, pp. 55–129, Elsevier, 1962.

[16] J. W. Hutchinson, "Singular behaviour at the end of a tensile crack in a hardening material," *Journal of the Mechanics and Physics of Solids*, vol. 16, no. 1, pp. 13–31, 1968.

[17] J. R. Rice, “A Path Independent Integral and the Approximate Analysis of Strain Concentration by Notches and Cracks,” *Journal of Applied Mechanics-Transactions of the Asme*, vol. 35, no. 2, pp. 379–386, 1968.

[18] J. R. Rice and G. F. Rosengren, “Plane strain deformation near a crack tip in a power-law hardening material,” *Journal of the Mechanics and Physics of Solids*, vol. 16, no. 1, pp. 1–12, 1968.

[19] P. C. Gehlen and M. F. Kanninen, “An atomic model for cleavage crack propagation in iron,” *Inelastic Behavior of Solids*, pp. 587–603, 1970.

[20] J. A. Begley and J. D. Landes, “The J-Integral as a Fracture Criterion,” ASTM STP 514, 1-23, 1972.

[21] P. S. Leevers, “Fracture of Polymeric Materials,” in *Encyclopedia of materials*: *Science and technology,* K. H. J. Buschow, Ed., pp. 3322–3329, Elsevier, Amsterdam, 2001.

[22] W. Kreher, “H. Blumenauer, G. Pusch. Technische Bruchmechanik. Deutscher Verlag für Grundstoffindustrie, Leipzig, 1993, ISBN 3-342-00659-5. 244 Seiten, 209 Abbildungen, 48 Tabellen, DM 90.–,” *Crystal Research and Technology*, vol. 28, no. 7, p. 952, 1993.

[23] D. Gross and T. Seelig, *Bruchmechanik*: *Mit einer Einführung in die Mikromechanik*, Springer Vieweg, Berlin, Heidelberg, 2016.

[24] G. Pinter, A. Frank, A. Redhead, and R. W. Lang, “Cyclic CRB Tests - A Quick and Reliable Tool for Ranking of PE Pipe Grades,” in *Proceedings PPXV*, 2010.

[25] M. S. Parsons, E. V. Stepanov, A. Hiltner, and E. Baer, “Effect of strain rate on stepwise fatigue and creep slow crack growth in high density polyethylene,” *Journal of Material Science Letters*, vol. 35, no. 8, pp. 1857–1866, 2000.

[26] M. S. Parsons, E. V. Stepanov, A. Hiltner, and E. Baer, “Correlation of fatigue and creep slow crack growth in a medium density polyethylene pipe material,” *Journal of Materials Science*, vol. 35, no. 11, pp. 2659–2674, 2000.

[27] M. S. Parsons, E. V. Stepanov, A. Hiltner, and E. Baer, “Correlation of stepwise fatigue and creep slow crack growth in high density polyethylene,” *Journal of Materials Science*, vol. 34, pp. 3315–3326, 1999.

[28] M. Hartmann, “Polyamid 12-Rohre im Gas-Hochdruckbereich,” *KRV Nachrichten*, 15-17, 2014.

[29] M. Hartmann and K. Kuhmann, “Von der Kraftstoffleitung zum Gasrohr: Rohre aus PA12 zur Führung kohlenwasserstoffhaltiger Medien,” *Kunststoffe,* no. 6, pp. 76–79, 2014.

[30] H. Brömstrup, *PE 100 Pipe Systems*, Oldenbourg Industrieverlag, Essen, 2012.

[31] M. B. Barker, J. Bowman, and M. Bevis, “The Performance and causes of failure of polyethylene pipes subjected to constant and fluctuating internal pressure loadings,” *Journal of Material Science Letters,* no. 18, pp. 1095–1118, 1983.

[32] A. Gray, J. N. Mallinson, and J. B. Price, “Fracture behavior of polyethylene pipes,” *Plastics and Rubber Processing and Applications*, vol. 1, pp. 51–53, 1981.

[33] S. J.F. Gould, P. Davis, D. J. Beale, and D. R. Marlow, “Failure analysis of a PVC sewer pipeline by fractography and materials characterization,” *Engineering Failure Analysis*, vol. 34, pp. 41–50, 2013.

[34] Y. Hu, J. Summers, A. Hiltner, and E. Baer, “Kinetics of fatigue and creep crack propagation in PVC pipe,” *Journal of Vinyl and Additive Technology*, vol. 8, no. 4, pp. 251–258, 2002.

[35] F. Arbeiter, G. Pinter, and A. Frank, “Characterisation of quasi-brittle fatigue crack growth in pipe grade polypropylene block copolymer,” *Polymer Testing*, vol. 37, pp. 186–192, 2014.

[36] R. Steenbakkers, L. Havermans, P. Voets, J. Rabiei, and R. Deblieck, “Strain Hardening Modulus: A Measure for Ranking Time to Failure of Random Polypropylene Pipe Materials,” in *Proceedings PPXVIII*, 2016.

[37] M. Messiha, B. Gerets, J. Heimink, A. Frank, F. Arbeiter, and K. Engelsing, “Slow crack growth resistance of modern PA-U12 grades measured by cyclic cracked round bar tests and strain hardening tests,” *Polymer Testing*, vol. 86, p. 106468, 2020.

[38] M. Messiha, A. Frank, F. Arbeiter, and G. Pinter, “How hydrogen bonds influence the slow crack growth resistance of polyamide 12,” *Polymer*, p. 124437, 2021.

[39] M. Messiha, F. Andreas, F. Arbeiter, and G. Pinter, “On the slow crack growth process and associated structure-property relationships in polyamide 12 grades,” manuscript submitted for publication, 2022.

[40] M. Messiha, A. Frank, J. Heimink, F. Arbeiter, and G. Pinter, “Structure-Property Relationships of Polyamide 12 Grades Exposed to Rapid Crack Extension,” *Materials (Basel, Switzerland)*, vol. 14, no. 19, p. 5899, 2021.

[41] M. Messiha, A. Frank, J. Heimink, F. Arbeiter, and G. Pinter, “Mechanisms of rapid fracture in PA12 grades,” *Theoretical and Applied Fracture Mechanics*, p. 103145, 2021.

[42] A. Shamiri, M. H. Chakrabarti, S. Jahan, M. A. Hussain, W. Kaminsky, P. V. Aravind, and W. A. Yehye, “The Influence of Ziegler-Natta and Metallocene Catalysts on Polyolefin Structure, Properties, and Processing Ability,” *Materials (Basel, Switzerland)*, vol. 7, no. 7, pp. 5069–5108, 2014.

[43] A. Frank and G. Pinter, “Evaluation of the applicability of the cracked round bar test as standardized PE-pipe ranking tool,” *Polymer Testing*, vol. 33, pp. 161–171, 2014.

[44] L. Janson, *Plastics Pipes for Water Supply and Sewage Disposal*, Majornas CopyPrint AB, Stockholm, 2003.

[45] F. Arbeiter, B. Schrittesser, A. Frank, M. Berer, and G. Pinter, “Cyclic tests on cracked round bars as a quick tool to assess the long-term behaviour of thermoplastics and elastomers,” *Polymer Testing*, vol. 45, pp. 83–92, 2015.

[46] R. A.C. Deblieck, D.J.M. van Beek, K. Remerie, and I. M. Ward, "Failure mechanisms in polyolefines: The role of crazing, shear yielding and the entanglement network," *Polymer*, vol. 52, no. 14, pp. 2979–2990, 2011.

[47] K. Richard, E. Gaube, and G. Diedrich, "Trinkwasserrohre aus Niederdruckpolyäthylen," *Kunststoffe*, vol. 49, no. 10, pp. 516–525, 1959.

[48] R. W. Lang, G. Pinter, and W. Balika, "Qualification concept for lifetime assessment of PE pressure pipes for arbitrary installation conditions: Konzept zur Nachweisführung für Nutzungsdauer und Sicherheit von PE-Druckrohren bei beliebiger Einbausituation," *3R International*, vol. 44, 1-2, pp. 33–41, 2005.

[49] R. W. Lang, A. Stern, and G. F. Dörner, "Applicability and limitations of current lifetime prediction models for thermoplastics pipes under internal pressure," *Angewandte Makromolekulare Chemie*, vol. 247, no. 1, pp. 131–145, 1997.

[50] F. Arbeiter, *Evaluation of long-term properties of polymeric pipe grade materials using fatigue tests and fracture mechanics,* Dissertation, Montanuniversity, 2015.

[51] A. Benhamena, B. Bachir Bouiadjra, A. Amrouche, G. Mesmacque, N. Benseddiq, and M. Benguediab, "Three finite element analysis of semi-elliptical crack in high density polyethylene pipe subjected to internal pressure," *Materials & Design*, vol. 31, no. 6, pp. 3038–3043, 2010.

[52] A. Frank, *Fracture Mechanics Based Lifetime Assessment and Long-term Failure Behavior of Polyethylene Pressure Pipes,* Doctoral Dissertation, University of Leoben, 2010.

[53] G. Pinter and R. W. Lang, "Effect of stabilization on creep crack growth in high-density polyethylene," *Journal of Applied Polymer Science*, vol. 90, no. 12, pp. 3191–3207, 2003.

[54] G. Pinter, M. Haager, C. Wolf, and R. W. Lang, "Thermo-Oxidative Degradation during Creep Crack Growth of PE-HD Grades as Assessed by FT-IR Spectroscopy," *Macromolecular Symposia*, vol. 217, no. 1, pp. 307–316, 2004.

[55] J. Hessel, "Buried PA 12 pipes for then transport of gas & water; No sand embedding necessary?," in *Proceedings PPXIV*, 2008.

[56] J. Hessel, "Punktlastversuche an PA12-Rohren (110x10) im Hinblick auf die Anwendung nichtkonventioneller Verlegemethoden," Hessel Ingenieurtechnik GmbH, 2009.

[57] Plastic Pipe Institute, "Unpublished Report: LTHS of PA12.," 2011.

[58] T. R. Kratochvilla, R. Eremiasch, and C. Bruckner, "Accelerated pipe test methods to evaluate PE100-RC materials - possibilities for ISO standardisation," in *Proceedings PPXIX*, Las Vegas, Nevada, USA, 2018.

[59] D. J. M. Havermans van Beek, R. Deblieck, M. McCarthy, R. Kloth, and L. Kurelec, "An elegant and fast method to predict the slow crack growth behavior of High-Density Polyethylene (HDPE) pipe materials," in *3R international*, vol. 49, 548 551, 2011.

[60] G. Pinter, M. Haager, W. Balika, and R. W. Lang, “Cyclic crack growth tests with CRB specimens for the evaluation of the long-term performance of PE pipe grades,” *Polymer Testing*, vol. 26, no. 2, pp. 180–188, 2007.

[61] N. Brown, X. Lu, Y. Huang, and R. Qian, “Slow crack growth in polyethylene - a review,” *Makromolekulare Chemie. Macromolecular Symposia*, vol. 41, no. 1, pp. 55–67, 1991.

[62] N. Brown, I. P. Harrison, and N. Ishikawa, “The fundamental material parameters that govern slow crack growth in linear polyethylenes,” *Plastics and Rubber Processing and Applications*, vol. 17, no. 4, pp. 255–258, 1992.

[63] Y.-L. Huang and N. Brown, “Dependence of slow crack growth in polyethylene on butyl branch density: Morphology and theory,” *Journal of Polymer Science: Part B: Polymer Physics*, vol. 29, no. 1, pp. 129–137, 1991.

[64] M. J. Zhang and F. X. Zhi, “Crack growth mechanism in some polyamides,” *Polymer*, vol. 29, no. 12, pp. 2152–2158, 1988.

[65] E. Mourglia-Seignobos, D. R. Long, L. Odoni, L. Vanel, P. Sotta, and C. Rochas, “Physical Mechanisms of Fatigue in Neat Polyamide 6,6,” *Macromolecules*, vol. 47, no. 12, pp. 3880–3894, 2014.

[66] K. Friedrich, “Crazes and shear bands in semi-crystalline thermoplastics,” in *Crazing in Polymers,* H. H. Kausch, Ed., 52-53, pp. 225–274, Springer-Verlag, Berlin/Heidelberg, 1983.

[67] N. Brown, “A fundamental theory for slow crack growth in polyethylene,” *Polymer*, vol. 36, no. 3, pp. 543–548, 1995.

[68] H. R. Brown, “A molecular interpretation of the toughness of glassy polymers,” *Macromolecules*, vol. 24, no. 10, pp. 2752–2756, 1991.

[69] X. Lu, N. Ishikawa, and N. Brown, “The critical molecular weight for resisting slow crack growth in a polyethylene,” *Journal of Polymer Science: Part B: Polymer Physics*, vol. 34, no. 10, pp. 1809–1815, 1996.

[70] P. J. DesLauriers and D. C. Rohlfing, “Estimating Slow Crack Growth Performance of Polyethylene Resins from Primary Structures such as Molecular Weight and Short Chain Branching,” *Macromolecular Symposia*, vol. 282, no. 1, pp. 136–149, 2009.

[71] A. Frank, G. Pinter, and A. Redhead, “Accelerated Cyclic Fracture Mechanics Tests to Analyze Molecular and Morphological Effects on Slow Crack Growth in Modern PE Pipe Grades,” in *Proceedings ANTEC*, 2010.

[72] C.J.G. Plummer and H. H. Kausch, “Semicrystalline Polymers: Fracture Properties,” in *Reference Module in Materials Science and Materials Engineering*, Elsevier, 2016.

[73] B. J. Egan and O. Delatycki, “The morphology, chain structure and fracture behaviour of high-density polyethylene: Part II Static fatigue fracture testing,” *Journal of Materials Science*, vol. 30, no. 13, pp. 3351–3357, 1995.

[74] D. B. Barry and O. Delatycki, “The effect of molecular structure and polymer morphology on the fracture resistance of high-density polyethylene,” *Polymer*, vol. 33, no. 6, pp. 1261–1265, 1992.

[75] P. Steeman and A. Nijenhuis, “The effect of random branching on the balance between flow and mechanical properties of polyamide-6,” *Polymer*, vol. 51, no. 12, pp. 2700–2707, 2010.

[76] H.-H. Kausch, ed., *Crazing in Polymers Vol. 2*, Springer, Berlin, Heidelberg, 1990.

[77] H.-H. Kausch, ed., *Intrinsic Molecular Mobility and Toughness of Polymers I*, Springer-Verlag GmbH, Berlin Heidelberg, 2005.

[78] C. J. G. Plummer and H.-H. Kausch, “Micronecking in thin films of isotactic polypropylene,” *Macromolecular Chemistry and Physics*, vol. 197, no. 6, pp. 2047–2063, 1996.

[79] H. Domininghaus, P. Elsner, P. Eyerer, et al., eds., *Kunststoffe*: *Eigenschaften und Anwendungen*, Springer, Berlin, Heidelberg, 2008.

[80] K. Friedrich, “Scherbänder und Bruch in amorphen und teilkristallinen Polymeren,” *Colloid and Polymer Science*, vol. 259, no. 2, pp. 190–201, 1981.

[81] E. Paredes and E. W. Fischer, “Röntgenkleinwinkel-Untersuchungen zur Struktur der Crazes (Fließzonen) in Polycarbonat und Polymethlmethacrylat,” in *Mechanisches Verhalten von Polymeren Wechselwirkung in Polymeren bzw. kolloiden Systemen*: *Vorträge der Hauptversammlung der Kolloid-Gesellschaft e.V. in Regensburg, 2. bis 5. Oktober 1979,* H. Rupprecht, R. Bonart, F. H. Müller et al., Eds., vol. 67, p. 149, Steinkopff, Darmstadt, 1980.

[82] E. J. Kramer, “Microscopic and molecular fundamentals of crazing,” in *Crazing in Polymers,* H. H. Kausch, Ed., 52-53, pp. 1–56, Springer-Verlag, Berlin/Heidelberg, 1983.

[83] H.-H. Kausch and G. H. Michler, “The Effect of Time on Crazing and Fracture,” in *Intrinsic Molecular Mobility and Toughness of Polymers I,* H.-H. Kausch, Ed., vol. 187, pp. 1–33, Springer-Verlag GmbH, Berlin Heidelberg, 2005.

[84] G. S. Tschumper, “Reliable Electronic Structure Computations for Weak Noncovalent Interactions in Clusters,” in *Reviews in Computational Chemistry,* K. B. Lipkowitz and T. R. Cundari, Eds., pp. 39–90, publisher not identified, Place of publication not identified, 2008.

[85] E. J. Kramer and L. L. Berger, “Fundamental processes of craze growth and fracture,” in *Crazing in Polymers Vol. 2,* H.-H. Kausch, Ed., 91/92, pp. 1–68, Springer, Berlin, Heidelberg, 1990.

[86] S. S. Lee and P. J. Phillips, “Melt crystallized polyamide 6.6 and its copolymers, Part I. Melting point – Lamellar thickness relations in the homopolymer,” *European Polymer Journal*, vol. 43, no. 5, pp. 1933–1951, 2007.

[87] H.-H. Kausch-Blecken von Schmeling, *Polymer Fracture*, Springer, Berlin, Heidelberg, 1978.

[88] J. Zimmerman and M. I. Kohan, “Nylon-selected topics,” *Journal of Polymer Science Part A: Polymer Chemistry*, vol. 39, no. 15, pp. 2565–2570, 2001.

[89] W. Brostow and R. D. Corneliussen, *Failure of plastics*, Hanser Pub.; Distributed in the United States of America by Macmillan Pub, Munich, New York, 1986.

[90] H. Xin, F. Oveissi, S. Naficy, and G. M. Spinks, “A Sequential Debonding Fracture Model for Hydrogen-Bonded Hydrogels,” *Journal of Polymer Science: Part B: Polymer Physics*, vol. 56, no. 19, pp. 1287–1293, 2018.

[91] G. J. Lake and A. G. Thomas, “The strength of highly elastic materials,” *Proceedings of the Royal Society of London. Series A. Mathematical and Physical Sciences*, vol. 300, no. 1460, pp. 108–119, 1967.

[92] S. Wang, S. Panyukov, M. Rubinstein, and S. L. Craig, “Quantitative Adjustment to the Molecular Energy Parameter in the Lake–Thomas Theory of Polymer Fracture Energy,” *Macromolecules*, vol. 52, no. 7, pp. 2772–2777, 2019.

[93] M. Messiha, A. Frank, I. Berger, G. Pinter, F. Arbeiter, J. Heimink, and H. van Laak, “Differences and similarities in fatigue failure mechanisms of PA12 pipe grades compared to modern PE pipe grades,” in *Proceedings ANTEC*, 2019.

[94] H. H. Kausch, R. Gensler, C. Grein, Plummer, C. J. G., and P. Scaramuzzino, “Crazing in semicrystalline thermoplastics,” *Journal of Macromolecular Science, Part B*, vol. 38, 5-6, pp. 803–815, 2006.

[95] W. G. Perkins, “Polymer toughness and impact resistance,” *Polymer Engineering & Science*, vol. 39, no. 12, pp. 2445–2460, 1999.

[96] C. B. Bucknall, “Fracture and failure of multiphase polymers and polymer composites,” in *Failure in Polymers*: *Molecular and Phenomenological Aspects,* H.-J. Cantow, G. Dall'Asta, K. Dušek et al., Eds., vol. 27, pp. 121–148, Springer, Berlin, Heidelberg, 1978.

[97] C. Cheng, A. Hiltner, E. Baer, P. R. Soskey, and S. G. Mylonakis, “Deformation of rubber-toughened polycarbonate: Macroscale analysis of the damage zone,” *Journal of Applied Polymer Science*, vol. 52, no. 2, pp. 177–193, 1994.

[98] P. S. Leevers and M.-A. Godart, “Adiabatic decohesion in a thermoplastic craze thickening at constant or increasing rate,” *Journal of the Mechanics and Physics of Solids*, vol. 56, no. 6, pp. 2149–2170, 2008.

[99] L. B. Freund, *Dynamic fracture mechanics*, Cambridge University Press, Cambridge, 1990.

[100] International Standards Organisation (ISO), "Thermoplastics pipes for the conveyance of fluids — Determination of resistance to rapid crack propagation (RCP) — Full-scale test (FST)," 2007, ISO 13478.

[101] International Standards Organisation (ISO), "Thermoplastics pipes for the conveyance of fluids - Determination of resistance to rapid crack propagation (RCP) - Small-scale steady-state test (S4 test)," 2008, ISO 13477.

[102] C. Argyrakis, *Models for designing pipe-grade polyethylenes to resist rapid crack propagation,* Dissertation, Imperial College London, 2010.

[103] R. K. Krishnaswamy, P. S. Leevers, M. J. Lamborn, D. F. Register, A. M. Sukhadia, and P. L. Maeger, "Rapid Crack Propagation (RCP) Failures in HDPE Pipes: Structure-Property Investigations," in *Proceedings*, pp. 3152–3156, 2005.

[104] M. N. Aboushelib, N. de Jager, C. J. Kleverlaan, and A. J. Feilzer, "The influence of pigments on the slow crack growth in dental zirconia," *Dental materials: official publication of the Academy of Dental Materials*, vol. 28, no. 4, pp. 410–415, 2012.

[105] M. J. Lodeiro, P. E. Tomlins, and A. Pearce, "The influence of pigments on the mechanical properties of High Density Polythylene (HDPE)," NPL Report, CMMT(A)258, 2000.

[106] V. Janostik and V. Senkerik, "Effect of Pigment Concentration on Mechanical Properties of Polycarbonate," *MATEC Web of Conferences*, vol. 125, p. 2052, 2017.

[107] R. Kanu, M. Chesebrough, and T. Spotts, "The effects of some organic and inorganic pigments on the tensile and impact properties of injection-molded polypropylene," *Journal of Modern Engineering*, vol. 2, no. 1, 2001.

[108] I. Walker and A. A. Collyer, "Rubber toughening mechanisms in polymeric materials," in *Rubber Toughened Engineering Plastics,* A. A. Collyer, Ed., pp. 29–56, Springer Netherlands, Dordrecht, 2012.

[109] C. Fond and R. Schirrer, "Influence of crack speed on fracture energy in amorphous and rubber toughened amorphous polymers," *Plastics, Rubber and Composites*, vol. 30, no. 3, pp. 116–124, 2001.

[110] C. Fond and R. Schirrer, "Dynamic fracture surface energy values and branching instabilities during rapid crack propagation in rubber toughened PMMA," *Comptes Rendus de l'Académie des Sciences - Series IIB - Mechanics*, vol. 329, no. 3, pp. 195–200, 2001.

[111] J.-B. Kopp, J. Schmittbuhl, O. Noel, J. Lin, and C. Fond, "Fluctuations of the dynamic fracture energy values related to the amount of created fracture surface," *Engineering Fracture Mechanics*, vol. 126, pp. 178–189, 2014.

[112] J.-B. Kopp, C. Fond, and G. Hochstetter, "Rapid crack propagation in PA11: An application to pipe structure," *Engineering Fracture Mechanics*, vol. 202, pp. 445–457, 2018.

[113] C. R. Siviour and J. L. Jordan, "High Strain Rate Mechanics of Polymers: A Review," *Journal of Dynamic Behavior of Materials*, vol. 2, no. 1, pp. 15–32, 2016.

[114] Abraham, Brodbeck, Rafey, and Rudge, "Instability dynamics of fracture: A computer simulation investigation," *Physical Review Letters*, vol. 73, no. 2, pp. 272–275, 1994.

[115] B. L. Holian and R. Thomson, "Crack limiting velocity," *Physical Review E*, vol. 56, no. 1, pp. 1071–1079, 1997.

[116] Y. W. Zhang and T. C. Wang, "Lattice instability at a fast-moving crack tip," *Journal of Applied Physics*, vol. 80, no. 8, pp. 4332–4336, 1996.

[117] W. T. Ashurst and W. G. Hoover, "Microscopic fracture studies in the two-dimensional triangular lattice," *Physical Review B*, vol. 14, no. 4, pp. 1465–1473, 1976.

[118] Marder and Liu, "Instability in lattice fracture," *Physical Review Letters*, vol. 71, no. 15, pp. 2417–2420, 1993.

[119] J. G. Williams, "The analysis of dynamic fracture using lumped mass-spring models," *International Journal of Fracture*, vol. 33, no. 1, pp. 47–59, 1987.

[120] Sharon, Gross, and Fineberg, "Local crack branching as a mechanism for instability in dynamic fracture," *Physical Review Letters*, vol. 74, no. 25, pp. 5096–5099, 1995.

[121] M. J. Doyle, "A mechanism of crack branching in polymethyl methacrylate and the origin of the bands on the surfaces of fracture," *Journal of Materials Science*, vol. 18, no. 3, pp. 687–702, 1983.

[122] A. M. Donald, "The effect of temperature on crazing mechanisms in polystyrene," *Journal of Materials Science*, vol. 20, no. 7, pp. 2630–2638, 1985.

[123] A. M. Donald and E. J. Kramer, "The competition between shear deformation and crazing in glassy polymers," *Journal of Materials Science*, vol. 17, no. 7, pp. 1871–1879, 1982.

[124] G. Pinter, *Rißwachstumsverhalten von PE-HD unter statischer Belastung,* Doctoral Dissertation, University of Leoben, 1999.

[125] A. Frank, F. J. Arbeiter, I. J. Berger, P. Hutař, L. Náhlík, and G. Pinter, "Fracture Mechanics Lifetime Prediction of Polyethylene Pipes," *Journal of Pipeline Systems Engineering and Practice*, vol. 10, no. 1, p. 4018030, 2019.

[126] P. S. Leevers, "Impact and dynamic fracture of tough polymers by thermal decohesion in a Dugdale zone," *International Journal of Fracture*, vol. 73, no. 2, pp. 109–127, 1995.

[127] P. Leevers, "Modelling Impact Fracture and RCP Resistance of Thermoplastics from Cohesive Properties," in *Proceedings ANTEC*, 2004.

[128] P. S. Leevers and R. E. Morgan, "Impact fracture of polyethylene: A non-linear-elastic thermal decohesion model," *Engineering Fracture Mechanics*, vol. 52, no. 6, pp. 999–1014, 1995.

[129] C. J. Greenshields and P. S. Leevers, "Rapid crack propagation in plastic water pipes: measurement of dynamic fracture resistance," *International Journal of Fracture*, vol. 79, no. 1, pp. 85–95, 1996.

[130] R. Weichert and K. Schönert, "On the temperature rise at the tip of a fast running crack†," *Journal of the Mechanics and Physics of Solids*, vol. 22, no. 2, pp. 127–133, 1974.

[131] F. E. Wittig, "Landolt-Börnstein: Zahlenwerte und Funktionen aus Physik, Chemie, Astronomie, Geophysik und Technik. 6. Auflage. Herausgegeben von J. Bartels, H. Borchers, P. ten Bruggencate, H. Hausen, K. H. Hellwege, Kl. Schäfer, E. Schmidt. 2. Band: Eigenschaften der," *Berichte der Bunsengesellschaft für physikalische Chemie*, vol. 67, no. 2, pp. 240–241, 1963.

[132] B. D. Lauterwasser and E. J. Kramer, "Microscopic mechanisms and mechanics of craze growth and fracture," *Philosophical Magazine A*, vol. 39, no. 4, pp. 469–495, 1979.

[133] J. Hertling, "Ausbreitungsgeschwindigkeit von instabilen Rissen in Polymeren bei tiefen Temperaturen," 1999.

[134] Y. K. Godovsky, *Thermophysical Properties of Polymers*, Springer Berlin Heidelberg, Berlin, Heidelberg, 1992.

[135] M. F. Kanninen, "An Analysis of Dynamic Crack Propagation and Arrest for a Material Having a Crack Speed Dependent Fracture Toughness," in *Prospects of Fracture Mechanics,* G. C. Sih, H. C. van Elst, and D. Broek, Eds., pp. 251–266, Springer Netherlands, Dordrecht, 1974.

[136] G. T. Hahn, R. G. Hoagland, M. F. Kanninen, and A. R. Rosenfield, "A preliminary study of fast fracture and arrest in the DCB test specimen," in *Proceedings of an international conference on Dynamic Crack Propagation,* G. C. Sih, Ed., pp. 649–662, Springer Netherlands, Dordrecht, 1973.

[137] D. Broek, *Elementary engineering fracture mechanics*, Nijhoff, Boston, The Hague, 1982.

[138] S. J. Burns and Z. J. Bilek, "The dependence of the fracture toughness of mi steel on temperature and crack velocity," *Metallurgical Transactions*, vol. 4, no. 4, pp. 975–984, 1973.

[139] M. F. Kanninen, "Dynamic Fracture Mechanics and its Applications to Material Behavior Under High Stress and Loading Rates," in *Material Behavior Under High Stress and Ultrahigh Loading Rates,* J. Mescall and V. Weiss, Eds., pp. 197–210, Springer, Boston, MA, 1983.

[140] P. S. Leevers, personal communication, 2020.

[141] J. Mescall and V. Weiss, eds., *Material Behavior Under High Stress and Ultrahigh Loading Rates*, Springer, Boston, MA, 1983.

[142] J. L. González-Velázquez, *Fractography and Failure Analysis*, Springer International Publishing, Cham, 2018.

[143] S. Hazra, *Crazing and yielding of polyethylene under impact.,* PhD Thesis, University of London, 2000.

[144] P. E. O'Donoghue, M. F. Kanninen, C. P. Leung, G. Demofonti, and S. Venzi, "The development and validation of a dynamic fracture propagation model for gas transmission pipelines," *International Journal of Pressure Vessels and Piping*, vol. 70, no. 1, pp. 11–25, 1997.

[145] C. Lawrence, "A proposed model for the periodic behaviour observed in the fast fracture failures seen in routine and full-scale tests on plastic pipes," *Polymer Testing*, vol. 15, no. 2, pp. 129–151, 1996.

[146] Z. Zhuo and P. E. O'Donoghue, "Analysis model to simulate the cracked pipe buried in soil," *Acta Mechanica Sinica*, vol. 14, no. 2, pp. 147–156, 1998.

[147] Z. Zhuang and P. E. O'Donoghue, "Determination of material fracture toughness by a computational/experimental approach for rapid crack propagation in PE pipe," *International Journal of Fracture*, vol. 101, no. 3, pp. 251–268, 2000.

[148] Z. Zhuang and P. E. O'Donoghue, "The recent development of analysis methodology for rapid crack propagation and arrest in gas pipelines," *International Journal of Fracture*, vol. 101, no. 3, pp. 269–290, 2000.

[149] P. E. O'Donoghue, S. T. Green, M. F. Kanninen, and P. K. Bowles, "The development of a fluid/structure interaction model for flawed fluid containment boundaries with applications to gas transmission and distribution piping," *Computers & Structures*, vol. 38, 5-6, pp. 501–513, 1991.

[150] A. Ivankovic and G. P. Venizelos, "Rapid crack propagation in plastic pipe: predicting full-scale critical pressure from S4 test results," *Engineering Fracture Mechanics*, vol. 59, no. 5, pp. 607–622, 1998.

[151] C. J. Greenshields, G. P. Venizelos, and A. Ivankovic, "A fluid–structure model for fast brittle fracture in plastic pipes," *Journal of Fluids and Structures*, vol. 14, no. 2, pp. 221–234, 2000.

APPENDIX

8 LIST OF PUBLICATIONS

8.1 Within the framework of this thesis

8.1.1 Publication 1

Bibliographic information:

Title:	**Slow crack growth resistance of modern PA-U12 grades measured by cyclic cracked round bar tests and strain hardening tests**
Authors:	Mario Messiha[a], Britta Gerets[b], Jan Heimink[c], Andreas Frank[a], Florian Arbeiter[d], Kurt Engelsing[b]
Affiliation:	[a] PCCL GmbH, Leoben, Austria [b] SKZ - German Plastics Center (a member of Zuse-Gemeinschaft), Wuerzburg, Germany [c] Evonik Operations GmbH, Marl, Germany [d] Montanuniversitaet, Leoben, Austria
Processing status:	published
DOI:	https://doi.org/10.1016/j.polymertesting.2020.106468

Relevant contributions to this publication:

Conceptualization:	Mario Messiha (70 %), Britta Gerets (30 %)
Methodology:	Mario Messiha (70 %), Britta Gerets (30 %)
Validation:	Mario Messiha (20 %), Britta Gerets (20 %), Jan Heimink (15 %), Andreas Frank (15 %), Florian Arbeiter (15 %), Kurt Engelsing (15 %)
Investigation:	Mario Messiha (60 %), Britta Gerets (40 %)
Writing – Original Draft:	Mario Messiha (70 %), Britta Gerets (30 %)
Writing – Review & Editing:	Mario Messiha (20 %), Britta Gerets (20 %), Jan Heimink (15 %), Andreas Frank (15 %), Florian Arbeiter (15 %), Kurt Engelsing (15 %)
Supervision:	Andreas Frank (35 %), Florian Arbeiter (35 %), Kurt Engelsing (30 %)

Polymer Testing 86 (2020) 106468

Contents lists available at ScienceDirect

Polymer Testing

journal homepage: http://www.elsevier.com/locate/polytest

Test Procedure

Slow crack growth resistance of modern PA-U12 grades measured by cyclic cracked round bar tests and strain hardening tests

Mario Messiha [a,**], Britta Gerets [b], Jan Heimink [c], Andreas Frank [a], Florian Arbeiter [d], Kurt Engelsing [b]

[a] PCCL GmbH, Leoben, Austria
[b] SKZ - German Plastics Center (a member of Zuse-Gemeinschaft), Wuerzburg, Germany
[c] Evonik Resource Efficiency GmbH, Marl, Germany
[d] Montanuniversitaet, Leoben, Austria

ARTICLE INFO

Keywords:
SCG resistance
Cracked round bar test
Strain hardening test
Polyamide 12
Piping systems

ABSTRACT

A critical failure mechanism in long-term applications of plastic structures, such as piping systems, is considered to be crack initiation and subsequent Slow Crack Growth (SCG). Thus, safe installation and operation during service lifetime of such structures are not conceivable without the knowledge of the resistance against SCG for any new material, like Unplasticized PolyAmide 12 (PA-U12). Unfortunately, long-term static tests at elevated temperatures lead to unreasonably long test times and measurements may also be affected by thermal aging and hydrolysis. Against this backdrop, the current study examines two accelerated test methods, namely the cyclic Cracked Round Bar (CRB) test as well as the Strain Hardening (SH) test, in order to characterize the SCG behavior. Both were originally developed for PolyEthylene (PE) and successfully implemented in recent years. While the cyclic CRB test measures SCG directly, accelerated through cyclic loading, the SH test quantifies the molecular disentanglement resistance, which determines craze formation and breakdown. The focus of this work was initially put on the extension of the CRB test towards PA-U12 grades, checking the occurrence of actual crack initiation and propagation. Afterwards a correlation to SH test results was done in terms of SCG resistance. Thereby, adequate test conditions were developed and the influence of the Molecular Weight (*MW*), expressed by the Viscosity Number (*VN*) of the PA-U12 grades, was considered. Results confirm the suitability of each method to rank SCG resistance and show a good correlation of the abovementioned SMall scale Accelerated Reliable Test (SMART) methods, highlighting their sensitivity to long-term relevant molecular parameters.

1. Introduction

In terms of pressurized pipe applications, PolyEthylene (PE) is leading the market up to an operating pressure of 10 bar. For high-pressure applications above 10 bar, however, commodity plastics are insufficient [1–3]. In that context, PolyAmide (PA), particularly Unplasticized PolyAmide 12 (PA-U12), was found to be a possible substitute to steel in gas pipe applications, which are subjected to pressure levels up to 18 bar [4,5]. However, plastic pipes in operation are usually submitted to more or less severe and sometimes unexpected influences (i.e. third-party attacks or external surface damages, etc.) that can shorten their service lifetime. Hence, the characterization of basic long-term failure mechanisms of polymer pipes is of essential importance. In the field of buried PE pressure pipe grades for gas and water supply, failure induced by crack initiation and subsequent Slow Crack Growth (SCG) is found to be a critical failure mechanism [6]. In order to define and determine the quality of plastic pipes, their service lifetime relevant properties, including resistance to SCG, have to be evaluated properly. In general, the Internal Pipe Pressure Test according to ISO 9080:2012 delivers reference values for the long-term hydrostatic strength to reach minimum service lifetimes of 50 years. In addition, for commercial PE pipe grades the influence of SCG is determined by the Full-Notch Creep Test (FNCT) according to ISO 16770:2019, the Pennsylvania Edge Notch Tensile test (PENT) according to ISO 16241:2005 or the Notched Pipe Test (NPT) according to ISO 13479:2009. Last generation PE pipe grades are characterized by an extraordinary SCG resistance, which leads to the fact that aforementioned standard test methods exceed acceptable timeframes and are therefore incapable of

* Corresponding author.
E-mail address: mario.messiha@pccl.at (M. Messiha).

https://doi.org/10.1016/j.polymertesting.2020.106468
Received 12 December 2019; Received in revised form 24 January 2020; Accepted 1 March 2020
Available online 3 March 2020

gaining a reliable material ranking. Currently, several studies are conducted, aiming on a decrease of testing times of standardized test methods by using more aggressive surfactants [7].

Apart from modified standard test methods, the demand for new time-efficient testing tools led to the establishment of SMall scale Accelerated Reliable Test (SMART) [8] techniques for High-Density PE (PE-HD) pipe grades, such as the cyclic Cracked Round Bar (CRB) test (ISO 18489:2015) and the Strain Hardening (SH) test (ISO 18488:2015). Both methods have been developed to allow for a fast material ranking based on SCG resistance. Cyclic CRB tests initiate a crack, which is slowly evolving throughout the material, while SH tests evaluate SCG resistances by observing the disentanglement resistance of polymer chains.

When it comes to other materials than PE, only few studies regarding the applicability, suitable test parameters and sensitivity for a correct interpretation of the relevant long-term failure mechanisms have been performed [9–11]. Hence, a key element within this study was to examine the fundamental applicability of the cyclic CRB test and the SH test as methodical approaches to rank modern PA-U12 grades based on their SCG resistance as well as to depict the overall scheme and objectives of both methods.

2. Background

2.1. Cyclic cracked round bar test

The cyclic CRB test has been initially developed for an accelerated determination of SCG resistance of thermoplastic pipe grades by Frank et al. [12–15] and has been further standardized for PE-HD in ISO 18489:2015. As shown in Fig. 1a, a pre-notched cylindrical bar is subjected to cyclic loading at an ambient temperature of $T = 23$ °C until fracture [16]. Thereby, accelerated SCG is promoted just by fatigue, without the aid of any surface-active agents. Currently, the method has been improved via the use of extensometers in order to detect crack initiation and crack growth kinetics [12]. This procedure allows a direct fracture mechanical measurement of the total failure cycle number N_f of different materials at different stress ranges $\Delta\sigma_0$, see Fig. 1b. Contrarily to most tests (i.e. FNCT, PENT or NPT) results are gained within relatively short timeframes, giving a valid basis for a sufficient material ranking with respect to long-term properties, expressed by the SCG resistance.

As the cyclic CRB test was optimized for PE-HD, two important factors have to be elucidated before extending its applicability towards PA-U12, as has been the case for PolyPropylene (PP) [10,18] and PolyVinylChloride (PVC) [9,19]: In contrast to monotonic and static tests, fatigue tests rely on the load ratio R, which defines the relation between minimum stress σ_{min} and maximum stress σ_{max}. Thinking of a sinusoidal cyclic load, which is usually applied during the cyclic CRB test, it can be derived that a large difference between maximum and minimum load (low value for R) results in faster failure appearances due to fatigue. The higher the R ratio is, the weaker the applied stress differences $\Delta\sigma_0$ are. Thus, materials reach longer lifetimes till total failure occurs as crack initiation and propagation are delayed. An R ratio of 1 implies the same values for minimum and maximum load and corresponds to a long-term static load, which can be regarded as weakest possible form of fatigue loading. As the main intention for fatigue tests is an accelerated failure, tests for PA-U12 may also be reasonably executed at $R = 0.1$ as recommended for PE-HD grades according to ISO 18489:2015. The second essential parameter for cyclic tests is the load frequency f. At high frequencies, materials tend to fail within very short test times. However, frequency values should be chosen carefully with regard to the tested materials, especially in terms of plastics. The problem thereby is attributed to the hysteretic heating phenomenon, which leads to a temperature increase of the material, especially at the vicinity of the crack tip. Those aggravated conditions ahead of crack tips support thermally induced disentanglement processes of tie molecules, encouraging faster crack initiation and SCG. Hence, materials prone to hysteretic heating (i.e. PP, PA etc.) should be tested at low frequency levels (e.g. $f \leq 5$ Hz) [9,18], while PE-HD pipe grades, less susceptible to hysteretic heating, can be tested at higher frequencies up to a maximum of 20 Hz as recorded by Frank et al. [15].

2.2. Strain hardening test

The SH test is a method to classify the resistance to SCG of various PE-HD pipe grades and has been standardized in ISO 18488:2015. Based mainly on the work of Brown et al. [20] and Kramer [21], who considered crack evolution and extension in polymers, Kurelec et al. [22], Havermans et al. [8] and Deblieck et al. [23] developed a technique to assess the SCG performance by an uniaxial tensile test. The idea behind this concept is that the processes during SCG, especially the formation, growth and final failure of the fibrillated structure, could be understood as microscale tensile creep behavior, which can be evaluated at macroscale through examination of the SH region [24]. This is valid as the same molecular parameters determine materials' behavior, namely the resistance against disentanglement, on both scales.

For PE-HD the SH test is conducted at a constant temperature of $T = 80$ °C, which is above the alpha transition temperature T_α to enable the required molecular mobility (relaxation processes in the crystalline regions [25]), and a constant test speed of $v_T = 20$ mm/min. As a result, the technical stress σ – technical strain ε response of the material is recorded (Fig. 2a). Under the assumption of volume constancy, those technical values can be transferred by Eq. (1) and Eq.(2) into a true stress σ_{true} vs. draw ratio λ representation (Fig. 2b). To gain a representative single point value, the SH modulus $<G_p>$, defined as the slope in the SH region, is evaluated. In practical determination a Neo-Hookean fit according Eq. (3) is applied first, wherein C is a mathematical parameter describing the yield stress extrapolated to $\lambda = 0$ and G_p is the average

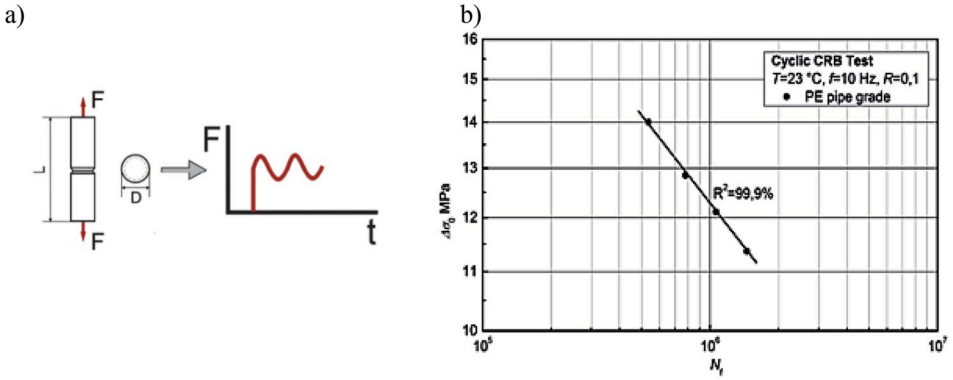

Fig. 1. Crack Round Bar (CRB) specimen and fatigue loading mode (a) [16] and example of a $\Delta\sigma_0$–N_f diagram [17] (b).

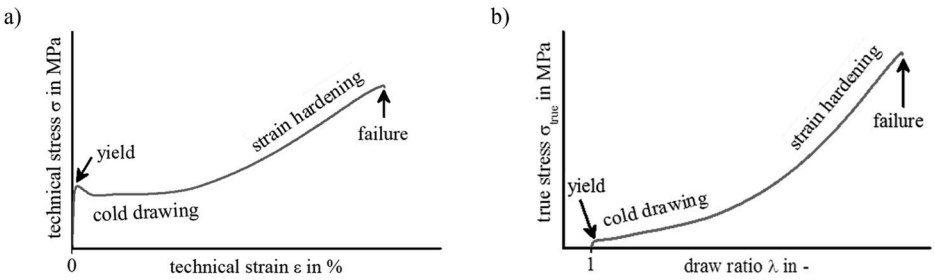

Fig. 2. Schematic representation of the material response in a Strain Hardening test as technical diagram (a) and true stress σ_{true} vs. draw ratio λ representation (b) [26].

slope in the fit interval (for PE-HD $\lambda = 8$ to 12, which was shown to be useful in the case of pipe grades covered by the ISO 18488:2015 standard). Afterwards, the SH modulus $<G_p>$ is calculated by using Eq. (4) according to ISO 18488:2015 [8,22].

$$\lambda = 1 + \varepsilon \tag{1}$$

$$\sigma_{true} = \sigma \cdot (1 + \varepsilon) \tag{2}$$

$$\sigma_{true} = C + G_p\left(\lambda^2 + \frac{1}{\lambda}\right) \tag{3}$$

$$\langle G_p \rangle = \frac{\Delta\sigma_{true}}{\Delta\lambda} \approx 20 \cdot G_p \tag{4}$$

Specimen employed in SH tests have to ensure a rapid and homogenous heating as well as save clamping up to high deformations. This is achieved by a thin dogbone geometry with a large width ratio of shoulder and parallel section. In previous studies a smaller dogbone geometry, which was derived from the type 5B geometry according ISO 527-2 by increasing the shoulder width, was demonstrated to lead to the same quantitative results, when tested at the same strain rate (corresponding to an adjusted testing speed of $v_T = 15$ mm/min) [27]. This special geometry was developed to allow SH tests on samples directly prepared from plastic components and became part of EN 17096:2018.

Furthermore, different authors demonstrated that SH experiments on PE can also be run with parameters different to those of ISO 18488:2015 as stated e.g. by Cheng et al. [28] and Robledo et al. [29]. In that context, a change in temperature normally requests an adjustment of the test speed and leads to quantitatively different results, while the material ranking remains unchanged [30]. However, the prerequisite is an adaption of the draw ratio range used for evaluation. In previous works Gerets et al. [30] provided a procedure using the draw ratio at maximum stress $\lambda_{\sigma,max}$ as upper limit and the draw ratio at the global Natural Draw Ratio (NDR) λ_{NDR} as lower limit for the Neo-Hookean fit, supporting a sufficient assessment of G_p independent of material type and test parameters [26,27]. Nevertheless, the SH modulus was calculated according to Eq. (4) with a constant factor of 20, which is a kind of normalization. This approach was applied to other materials than PE such as PP [31], PA-U12, 1-PolyButene (PB-1) and Unplasticized PVC (PVC–U), recently [11].

3. Experimental

In order to evaluate the general applicability of the cyclic CRB test and the SH test to the characterization of PA-U12 as well as to investigate the suitability to rank materials with both SMART methods, three different grades (PA-U12-a, PA-U12-b, PA-U12-c) were selected. All materials were provided by Evonik Resource Efficiency GmbH, Essen (Germany) and are part of a homologous series of pure PA-U12, only varying in terms of average Molecular Weight (*MW*), maintaining very similar molecular and morphologic structures. The Viscosity Number (*VN*), which is a measure for the average *MW* was determined on a Micro-Ubbelohde viscosimeter (AVSPro Schott-Geräte GmbH, Hofheim am Taunus, Germany) according to ISO 307:2019 showing that PA-U12-a has the lowest average *MW* (*VN* = 120 ml/g), while PA-U12-b and -c exhibit higher MW, expressed by *VN* = 175 ml/g and *VN* = 210 ml/g.

3.1. Cyclic cracked round bar test

All PA-U12 grades were characterized via cyclic CRB tests in reference to ISO 18489:2015 to rank PA-U12 grades regarding their SCG resistance. For specimen manufacturing, the PA-U12 grades were extruded to cylindrical rods with a diameter of 25 mm. Afterwards, CRB specimen with a diameter of 14 mm and a length of 100 mm were milled out and circumferentially pre-notched with a razor-blade to an initial crack length of $a_{ini} = 1.5$ mm at the center of each specimen. All cyclic CRB tests were carried out at an ambient temperature of $T = 23$ °C on a servo-hydraulic test device of the type MTS 858.02 Table Top System (MTS Systems GmbH, Berlin, Germany). To prevent effects of hysteretic heating, the force controlled sinusoidal cyclic load was applied with a frequency of $f = 5$ Hz as recommended by Arbeiter [9]. In contrast to ISO 18489:2015, which recommends testing within a stress range of $\Delta\sigma_0 =$ 10.5to 13.5 MPa for PE, for PA-U12 higher loads were necessary to gain acceptable test times, resulting in stress values of $\Delta\sigma_0 > 20$ MPa. The cycle number until total failure N_f was counted from beginning of the test till breakage of the CRB specimen. Furthermore, crack initiation was measured with the aid of three extensometers with an initial gauge length $l_0 = 10$ mm (±1.5 mm, ISO 9513 Class 0.5) produced by MTS Systems GmbH (Berlin, Germany), which were evenly mounted around the pre-notched CRB specimens (positions: 0°, 120° and 240° around the crack) in order to precisely capture the Crack Opening Displacement *COD* during the test. The extensometer signals were evaluated as the difference of maximum and minimum crack opening displacement *ΔCOD* over cycle numbers *N* as an indicator of crack initiation. When total failure was achieved, the fracture surfaces of the CRB specimens were studied via a Scanning Electron Microscope (SEM) of the type Tescan Vega II (Tescan Brno, Brno, Czech Republic). Therefore, surfaces were sputter coated with gold. Examinations of initial pre-notch dimensions and actual crack propagations were done according to ISO 18489:2015 via incident light microscopy, using an Olympus SZX12 (Olympus Europa Holding GmbH, Hamburg, Germany).

3.2. Strain hardening test

SH tests of all PA-U12 grades were performed with regard to their SCG resistance and ranking thereof. Experiments were executed on a universal testing machine Zwick/Roell Z010 (Zwick/Roell GmbH & Co. KG, Ulm, Germany) equipped with an OptiXtens optical extensometer and a temperature chamber. A test speed of $v_T = 15$ mm/min was chosen to gain strain rate conditions equivalent to ISO 18488:2015 as the smaller dogbone specimen, according to EN 17096:2018, was used. Previous to the tensile test, each specimen was conditioned for at least 30 minutes at test temperature *T*. For each grade the draw ratio range for evaluation was chosen λ_{NDR} to $\lambda_{\sigma,max}$ to determine the SH modulus as

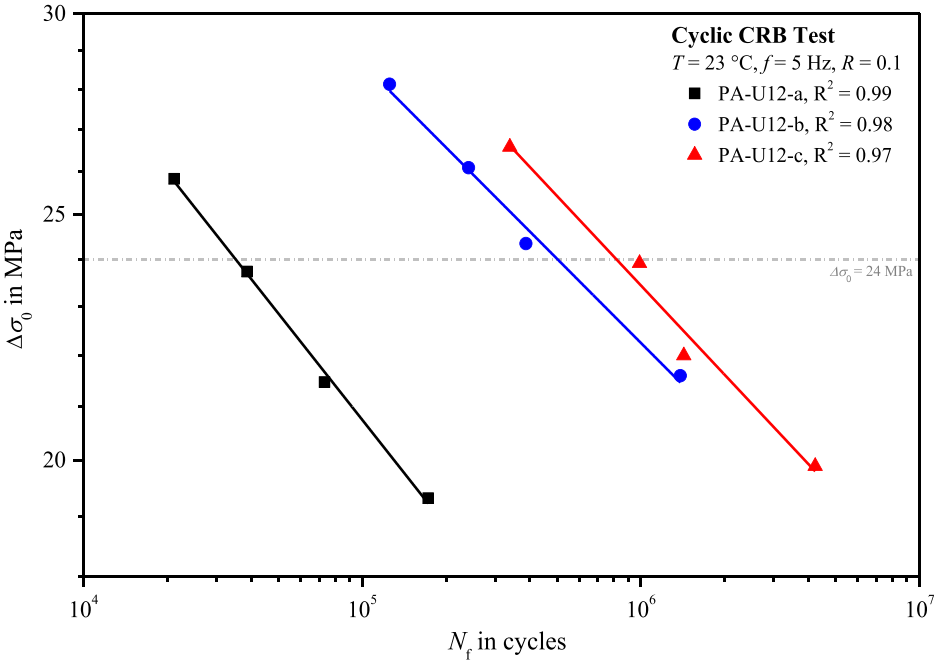

Fig. 3. Failure cycle numbers N_f as a function of the applied stress ranges $\Delta\sigma_0$ in the cyclic Cracked Round Bar tests of PA-U12-a to PA-U12-c. Full lines are pointing to the linear regression.

described before. To investigate the temperature influence on the SH test results of the homologous series PA-U12-a to PA-U12-c, the test temperature was varied between $T = 23$ °C and $T = 120$ °C. Samples were prepared from 4 mm thin slices of all PA-U12 grades, which were cut from the extruded 25 mm bars used for CRB sample preparation. Subsequently, they were held for 5 minutes at $T = 200$ °C in a Dr. Collin P/300 platen press (Dr. Collin GmbH, Ebersberg, Germany) and were then pressed to 1 mm thickness, before cooling down to 30 °C with an average cooling rate of $\Delta T/\Delta t$ of 15 K/min.

4. Results and discussion

4.1. Cyclic cracked round bar test

For the homologous series PA-U12-a to PA-U12-c the failure curves determined by the cyclic CRB tests are displayed in Fig. 3. A linear trend with very similar slopes is recognizable for each material in the double-logarithmic diagram, which indicates the high similarity of the tested materials at molecular and morphologic levels. Comparing PA-U12-b and PA-U12-c to PA-U12-a as reference material with the lowest *VN*, a growing failure resistance is observable as failure cycle numbers N_f are significantly increasing. Benchmarking the three PA-U12 grades, a single-point evaluation was done at a stress level of $\Delta\sigma_0 = 24$ MPa. Therefore, values were interpolated using a linear regression. In this context, PA-U12-a fails after approx. 42,000 cycles, PA-U12-b after 500,000 cycles, whilst PA-U12-c resists more than 800,000 cycles at $\Delta\sigma_0 = 24$ MPa (see Table 1). Considering an applied test frequency of $f = 5$ Hz, the failure times correspond to approx. 2 h of testing for PA-U12-a, 28 h for PA-U12-b and about 45 h for PA-U12-c.

Furthermore, crack initiation N_{ini} was determined by detecting the first clear deviation of ΔCOD over N from the base line of constant ΔCOD, as shown in Fig. 4. As soon as the first bundle of the fibrillar network within evolving crazing zones fades and gets pulled out of the crazes or breaks down, the crack initiates and starts to propagate. This was already observed for PE-HD [32] and now found also for the homologous PA-U12 series as an increase of extensometer signals, confirming the existence of real SCG in PA-U12 grades, expressed by the failure cycle number of pure SCG N_{SCG}.

According to literature [33–35], an increased average molecular weight would benefit the creation of tie molecules, which is of high importance for a good resistance to SCG as usually found in modern PE-HD pipe grades (i.e. PE100 or PE100-RC). This trend is considerably highlighted in Fig. 5 when speaking of PA-U12 grades. An increasing *VN* results in improved resistance against SCG. In that manner, *VN* values of PA-U12 grades as well as their total failure cycle numbers N_f at a reference stress of 24 MPa, as presented in Table 1, were normalized with respect to values of PA-U12-a, providing the lowest molecular mass and chain length. This was done to assess the influence of the relative increase of the molecular weight on the SCG resistance of all materials as depicted in Fig. 6. The graph also displays a more profound improvement of long-term properties considering the lower relative rise of *VN* of PA-U12-b towards PA-U12-c with approx. 35 ml/g (see red dashed line) compared to PA-U12-a towards PA-U12-b with about 55 ml/g (see grey dashed line). That would infer, that the relative increase of *MW* is dependent on the actual average *MW* of the material itself. Thus, a relative increase of *MW* by a certain content would affect a

Table 1
Viscosity number *VN*, total failure cycle number N_f at 24 MPa, relativized values based upon PA-U12-a for the homologous series, as well as average SH modulus $<G_p>$ at $T = 120$ °C.

Material	*VN* ml/g	VN_{rel} –	Relative increase of *VN* considering PA-U12-a %	N_f at 24 MPa cycles	$N_{f,rel}$ at 24 MPa –	$<G_p>$ MPa
PA-U12-a	120	1.0	0	41,799	1.0	151.0 ± 1.5
PA-U12-b	175	1.5	50	501,944	12.0	202.2 ± 8.5
PA-U12-c	210	1.8	80	814,929	19.5	235.6 ± 4.5

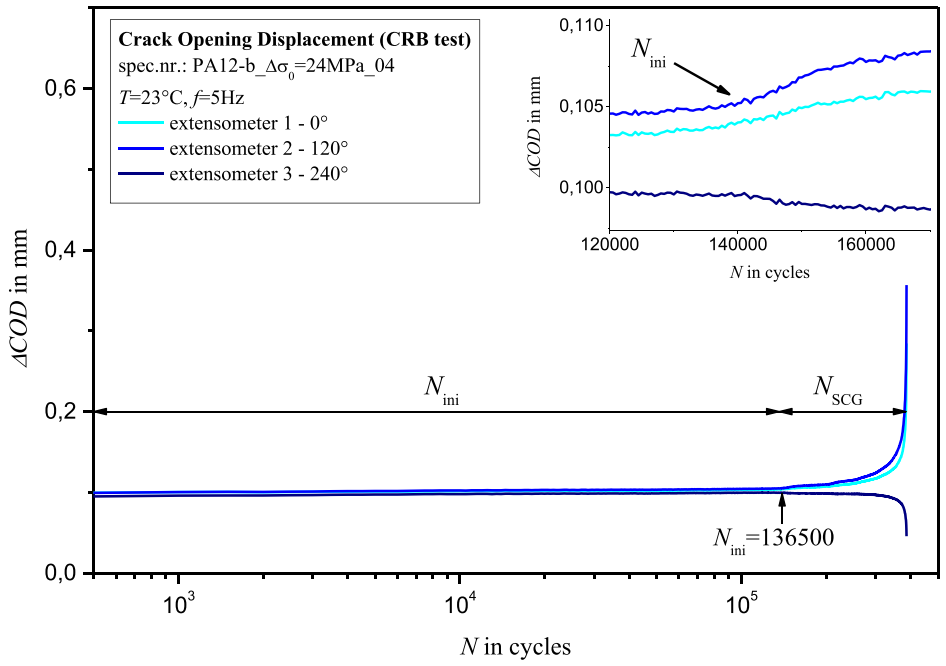

Fig. 4. Crack Opening Displacement ΔCOD curves as a function of cycle numbers N at a reference stress of $\Delta\sigma_0 = 24$ MPa for PA-U12-b as representative of the homologous series.

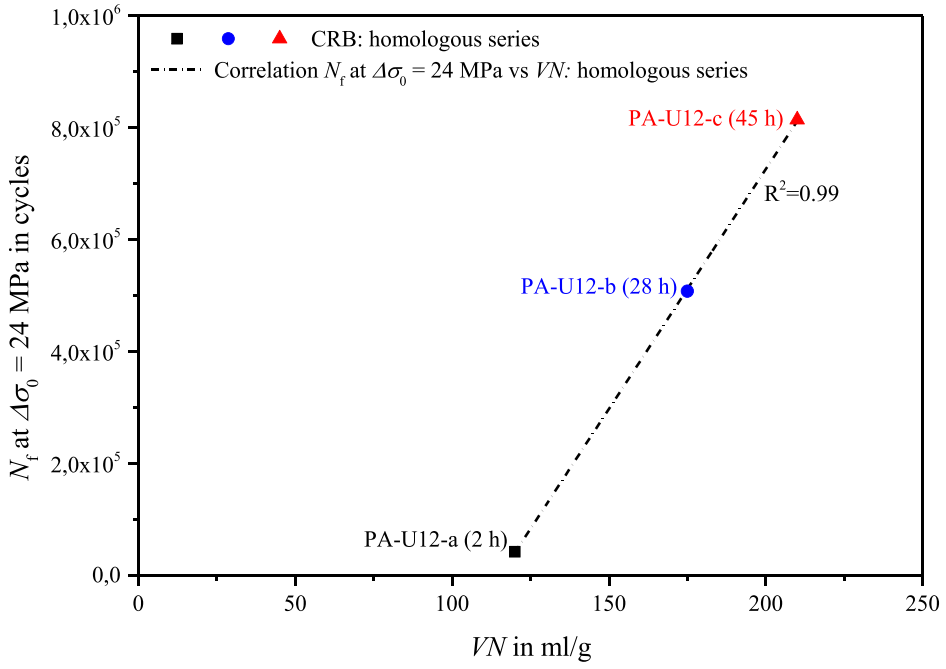

Fig. 5. Comparison of the cycle number N_f until fatigue failure at a reference stress of $\Delta\sigma_0 = 24$ MPa in the cyclic CRB test as a function of the average molecular weight expressed by the viscosity number VN for PA-U12 grades.

PA-U12 material of a higher average *MW* more effectively with respect to its SCG resistance than one of a lower average *MW*.

This behavior could be explained by thinking of the principle structure of PA-U12. Polyamides are generally characterized by methylene groups of various lengths that are bonded together through amide linkages (-CO-NH-) [36]. Their amide density, which equals the frequency of occurrence of amide groups in the polymer chain, is responsible for their unique property profile. The presence of high amounts of amide groups results in high degrees of polarity and subsequent inter-chain and intra-chain hydrogen bonds. A major influence on the fracture mechanical failure behavior of PA-U12 is expected to be based on these hydrogen bonds, which create different polymer physical effects that do not exist in polyolefin materials. Thinking of molecular chains, it seems easier for disentanglement processes to occur for shorter chains with fewer amounts of hydrogen bonds. As soon as the average chain length (average *MW*) increases, subsequently the number of hydrogen bonds also increase, which leads to more difficult disentanglement conditions as polymer chains have to overcome more "H-cross-linked" locations where they stick tighter together.

Fracture surface analysis in fatigue tests allows a distinction between

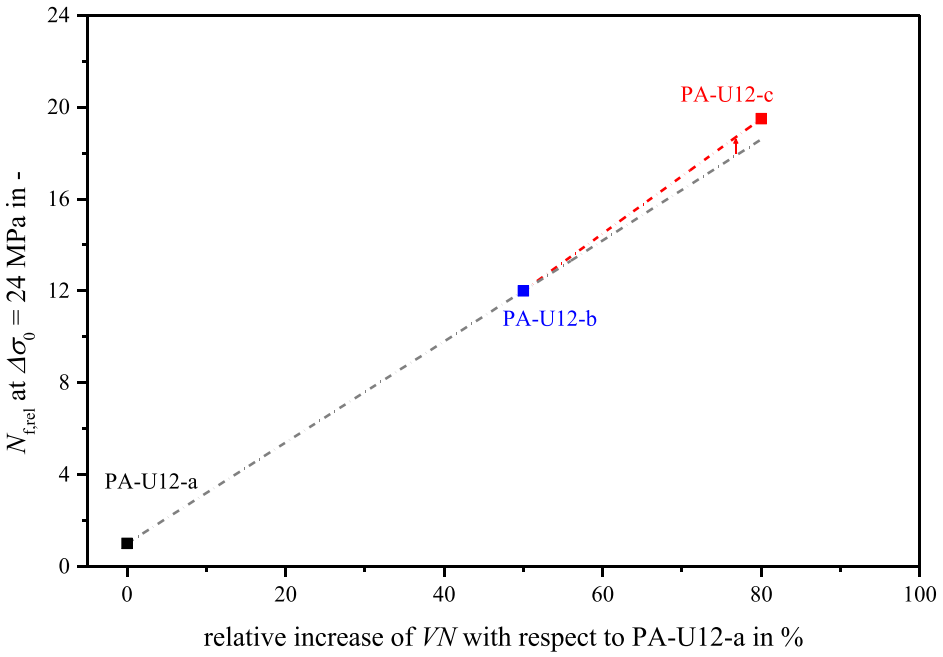

Fig. 6. Relative increase of the cycle number ($N_{f,rel}$) until quasi-brittle failure at $\Delta\sigma_0 = 24$ MPa as a function of the relative increase of the average molecular weight expressed by *VN* for PA-U12 grades.

different failure mechanisms, which are typical for some thermoplastic materials, such as PE-HD [9,37]. First, a quasi-brittle region adjacent to the pre-notch is visible, where SCG failure mechanisms like small scale yielding and crazing dominate. Second, a brittle-ductile-transition region can be seen. Third, a ductile failure zone appears, due to stress levels considerably above the yielding point leading to large-scale deformations and ductile failure [38]. For the investigated PA-U12 grades fracture surface images of CRB specimens tested at a nominal stress $\Delta\sigma_0 \approx 24$ MPa are shown in Fig. 7a. Therein, the three aforementioned zones can be observed. A typical characteristic of SCG in PE-HD is an evident fibrillation of the fracture surface, which is created during the polymer physical mechanisms of craze development and breakdown. The fracture surfaces of the analyzed PA-U12 materials clearly show evidence for fibrillation (Fig. 7b). Taking a deeper look on SEM images of PA-U12-a to PA-U12-c a change in structure from larger distinctive fibrils to fibrils of a lower micro-plasticity gets observable. With increasing *VN* fracture surfaces become smoother exhibiting flattened fibrils. This observation supports the aforementioned hydrogen bond hypothesis. As the average *MW* increases (i.e. PA-U12-c) a proportionate change in the general failure mechanism from craze formation and craze breakdown to shear yielding or even chain scission could take place. That might be due to effects of hydrogen bonds, which can be regarded as additional secondary forces between two PA-U12 chains. Hence, PA-U12 chains exceeding a critical molecular mass result in a critical number of hydrogen bonds with stronger interactions that inhibit disentanglement processes of fibrils in crazing zones. Thus, a change of the classical failure mechanism to shear yielding or chain scission (known for PE grades) seems to be realistic considering the SEM images.

4.2. Strain hardening test

For the applicability of SH tests in order to rank materials regarding their SCG behavior respectively stress crack resistance two prerequisites have to be fulfilled: On the one hand materials to be tested must exhibit the formation, growth and final failure of fibrillated structures [24], as shown before for PA-U12 (Fig. 7). On the other hand, quantitative comparisons are only valid for materials of similar molecular and morphologic structure, which lead to similar failure behavior respectively identical failure mechanisms.

In Fig. 8 the resulting SH moduli $<G_p>$ are plotted as a function of test temperature for the homologous series PA-U12-a to PA-U12-c. At a temperature of 23 °C no smooth transition from cold drawing to strain hardening was observed, preventing meaningful results as exemplarily shown for PA-U12-b in Fig. 9. This can be explained by an insufficient molecular mobility at the applied combination of test temperature *T* and test speed v_T. At temperatures well above 120 °C the PA-U12 materials began to soften, not allowing for SH tests. Analogous to results known from PE [30], the SH modulus $<G_p>$ of all PA-U12 grades linearly decreases with an increasing test temperature *T*. Since the mobility of chains rises with temperature in thermoplastics, especially in the amorphous region, disentanglement processes are simplified and therefore the resistance against disentanglement expressed by $<G_p>$ decreases. All PA-U12 materials show a linear trend for the temperature dependency with similar slopes (Fig. 8), indicating a high molecular and morphological similarity as found in the CRB tests before, signifying the ability of SH tests to rank PA-U12-a to PA-U12-c.

Benchmarking the three PA-U12 grades, a single-point evaluation was done at a temperature level of $T = 120$ °C, due to a good testability, reproducibility and material differentiability as depicted in Fig. 10. All PA-U12 materials of the homologous series were tested threefold, each showing a smooth transition from cold drawing to the SH region. While the transition seems to happen at a nearly material independent draw ratio range, afterwards a clear differentiation with regard to their entire slopes was observed, indicating again the structural similarity despite their differences in disentanglement resistance respectively SCG behavior.

The average SH modulus $<G_p>$ of PA-U12-a to PA-U12-c is plotted as a function of the viscosity number *VN* in Fig. 11. As demonstrated before in the context of the CRB test results, an increase in viscosity correlates with a higher molecular weight respectively longer polymer chains increasing the probability of entanglements [33–35]. Therefore the SH modulus $<G_p>$, being a measure for the resistance against disentanglement [8,22,23], has to rise the higher the number of entanglements becomes. That is exactly what was observed for the investigated PA-U12 materials in the present study: A good correlation for the homologous series PA-U12-a to PA-U12-c is found, signifying the

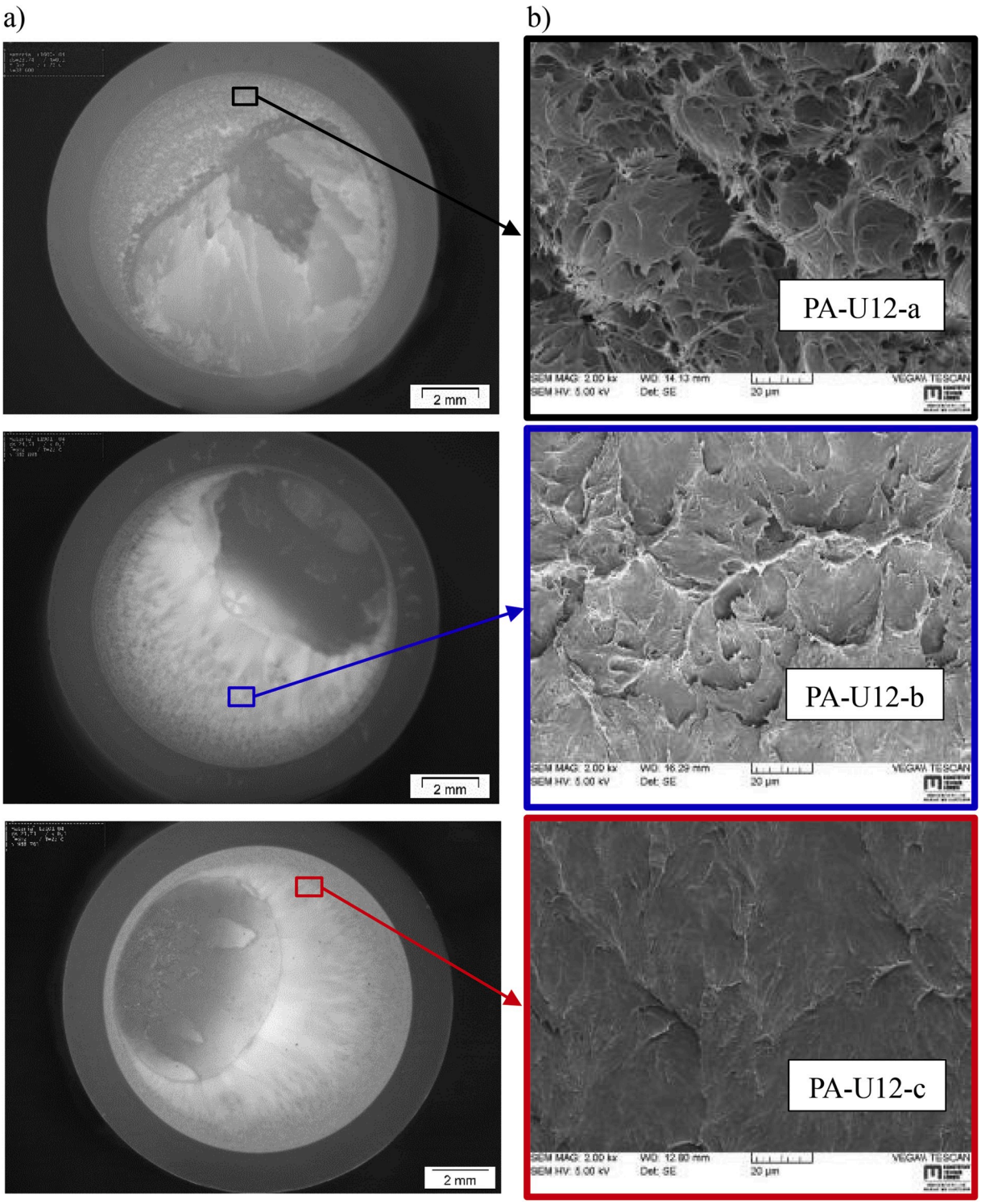

Fig. 7. Appearance of Cracked Round Bar fracture surfaces of PA-U12-a to PA-U12-c at $\Delta\sigma_0 \approx 24$ MPa: a) light microscopy; b) SEM image, 2000x magnification.

dominance of the *MW* on the resistance against the disentanglement processes associated with the stress crack resistance. The higher the *MW*, the higher the resistance against SCG, expressed by a linearly growing average SH modulus $<G_p>$ from approx. 150 MPa for PA-U12-a to approx. 235 MPa for PA-U12-c (see Table 1).

4.3. Correlation of strain hardening test and cyclic cracked round bar test

The cyclic CRB test and SH test show similar results: A profound improvement of crack resistance of PA-U12 is clearly displayed with elevated *VN* values. Of course, this is only valid if the molecular weight is assumed to be the only changing parameter, whereas remaining parameters, such as Molecular Weight Distribution *MWD*, modality, comonomers, manufacturing parameters etc., are constant. However, even if that is not the case, results still represent a clear and strong relationship between *MW* and SCG resistance for the investigated PA-U12 grades. This good agreement of both test methods, which are based on completely different approaches in determining the resistance

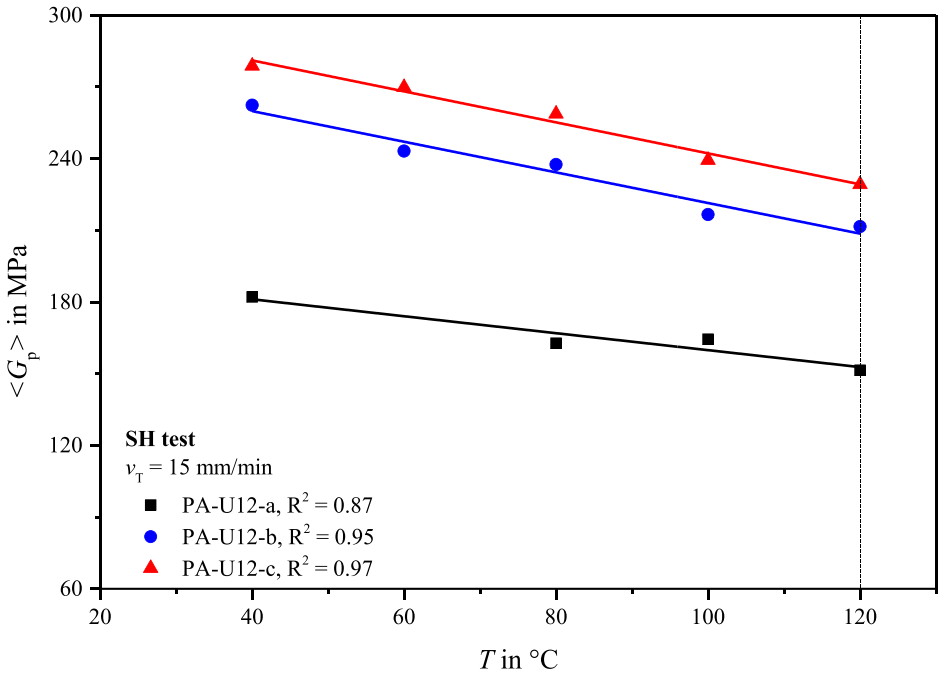

Fig. 8. Strain Hardening modulus $<G_p>$ as a function of the applied test temperature T in Strain Hardening tests of PA-U12-a to PA-U12-c. Full lines are pointing to the linear regression.

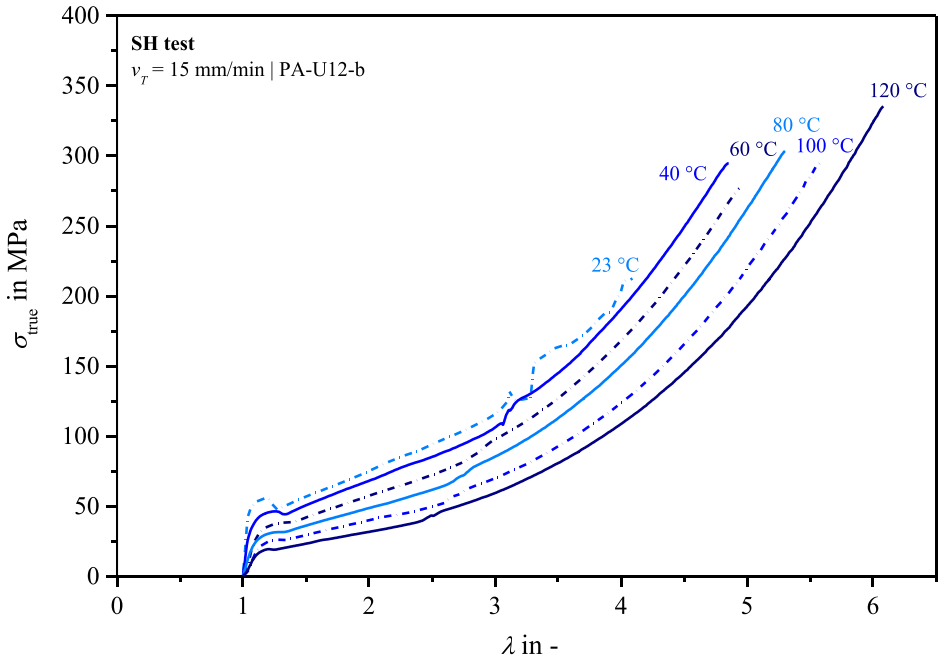

Fig. 9. Temperature dependent true stress σ_{true} - draw ratio λ - curves of PA-U12-b.

against SCG, is mirrored in Fig. 12. This allows for an expansion of the application of both SMART methods, which have been already proven to work for ranking purposes of several thermoplastics [11,16,22,28,30,31,39,40], towards PA-U12 grades.

5. Conclusion

The current paper demonstrates the ability of the cyclic Cracked Round Bar (CRB) test and the Strain Hardening (SH) test to characterize the Slow Crack Growth (SCG) failure resistance of unplasticized polyamide 12 (PA-U12). Additional emphasis was put on an analysis of the failure mechanism as well as on the influences of molecular weight (*MW*) variations with regard to the SCG resistance of PA-U12 grades. Cyclic CRB test results clearly show that the homologous series fails by crack initiation followed by SCG. A thorough investigation of occurring failure mechanisms via SEM measurements showed a clear fibrillation of the fracture surfaces of each material. However, an increase of the *MW* of PA-U12-a towards PA-U12-c was accompanied by a decrease in the fibrillation density. This could be explained by an increasing content of shear yielding or chain scission failure mechanisms provoked by higher numbers of hydrogen bonds, next to the well-known craze deformation and breakdown failure mechanism. The latter one is typical for the SCG

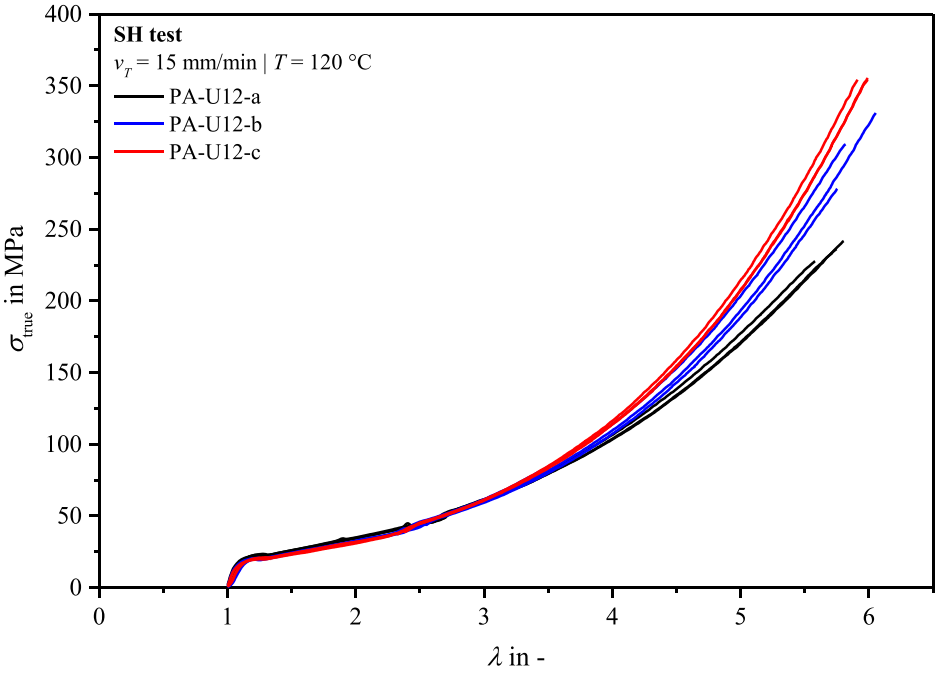

Fig. 10. Comparison of the true stress σ_{true} - draw ratio λ - curves of PA-U12-a to PA-U12-c.

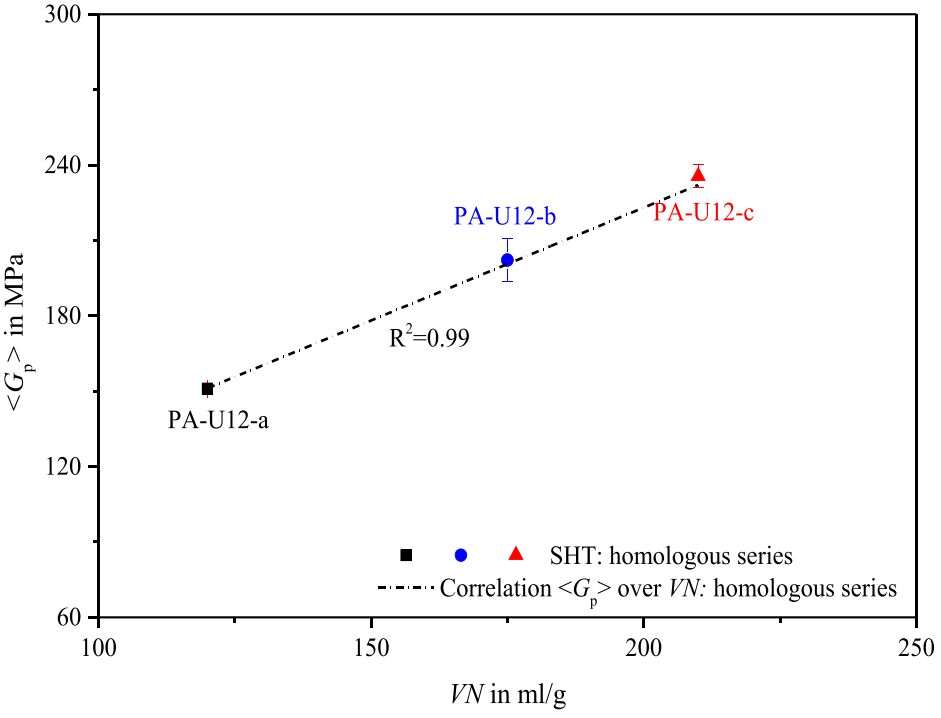

Fig. 11. Comparison of the Strain hardening modulus <G_p> at a reference temperature T = 120 °C as a function of the average molecular weight expressed by the viscosity number *VN* for PA-U12 grades.

driven quasi-brittle failure of high-density polyethylene (PE-HD), which does not have any hydrogen bonds [32]. A linear correlation of the failure cycle number N_f and applied load $\Delta\sigma_0$ on double-logarithmic scale was obtained with PA-U12-a to PA-U12-c. On the one hand, results confirm that with increasing Viscosity Number (*VN*), respectively *MW*, the SCG resistance as measured by cyclic CRB tests increases significantly. On the other hand, failure curves exhibiting comparable slopes signify the high similarity regarding the molecular basis. This behavior was likewise proven by SH tests, which showed a similar influence of test temperature for all investigated PA-U12 materials, pointing to a molecular and morphological likeness. SH test results also demonstrate a direct correlation of SH modulus <G_p> and *VN* for PA-U12-a to PA-U12-c, confirming the SCG resistance dependency to *MW*. Finally, a good correlation of both SMART methods was found, showing a sufficient material ranking of PA-U12 grades for the homologous series regarding the SCG resistance.

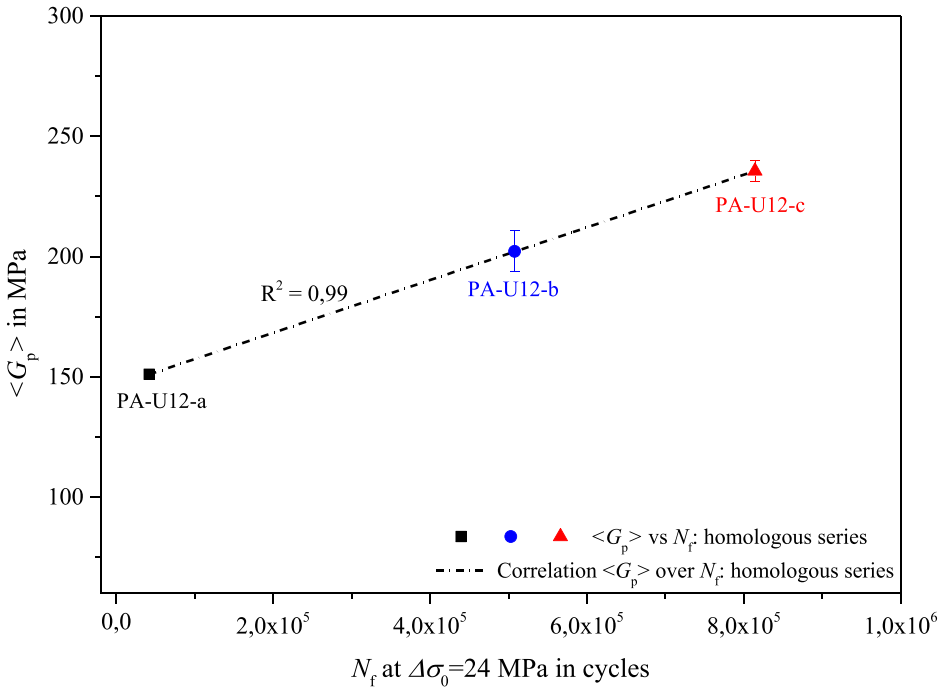

Fig. 12. Direct correlation between the total failure cycle number N_f at a reference stress of $\Delta\sigma_0$ = 24 MPa in the cyclic Cracked Round Bar test and the strain hardening modulus $<G_p>$ at T = 120 °C in the Strain Hardening test for various PA-U12 grades.

Declaration of competing interest

The authors declare that they have no known competing financial interests or personal relationships that could have appeared to influence the work reported in this paper.

CRediT authorship contribution statement

Mario Messiha: Conceptualization, Methodology, Investigation, Data curation, Writing - original draft, Validation. **Britta Gerets:** Conceptualization, Methodology, Investigation, Data curation, Writing - review & editing, Validation. **Jan Heimink:** Resources, Funding acquisition, Writing - review & editing. **Andreas Frank:** Supervision, Writing - review & editing, Project administration. **Florian Arbeiter:** Supervision, Writing - review & editing. **Kurt Engelsing:** Supervision, Writing - review & editing.

Acknowledgement

The cyclic CRB test research work of this paper was performed at the Polymer Competence Center Leoben GmbH (PCCL, Austria) within the framework of the COMET-program of the Federal Ministry for Transport, Innovation and Technology (Austria) and Federal Ministry for Economy, Family and Youth (Austria) with contributions by Evonik Resource Efficiency GmbH (Germany) and the Montanuniversitaet Leoben (Austria). The PCCL is funded by the Austrian Government and the State Governments of Styria and Upper Austria. The SH test research work was performed at SKZ – German Plastics Center (Germany) in the context of the Industrial Collective Research (IGF) project no. 18649 N. The financial support by the Federal Ministry for Economic Affairs and Energy (BMWi, Germany) based on a decision of German Bundestag through the German Federation of Industrial Research Associations (AiF, Germany) is gratefully acknowledged. Special thanks are attributed to Mr. Hermann van Laak (Evonik Resource Efficiency GmbH, Germany), Prof. Gerald Pinter (Montanuniversitaet Leoben, Austria) as well as Dr. Mirko Wenzel, Dr. Thomas Hochrein and Prof. Martin Bastian (SKZ – German Plastics Center, Germany) for their critical review, in depth discussions and challenging our ideas, providing insights and guidance. The lab staff and students at SKZ – German Plastics Center (Germany) are acknowledged for performing the SH tests.

References

[1] H. Brömstrup, PE 100 Pipe Systems, Oldenbourg Industrieverlag, Essen, 2012.
[2] L. Janson, Plastics Pipes for Water Supply and Sewage Disposal, Majornas CopyPrint AB, Stockholm, 2003.
[3] "HDPE performance pipes: leading the pipe market," INEOS olefin & polymers europe. https://www.ineos.com/globalassets/ineos-group/businesses/ineos-olefins-and-polymers-europe/brochures/ineos_flyer_hdpe_pipes.pdf.
[4] M. Hartmann, Polyamid 12-Rohre im Gas-Hochdruckbereich, KRV Nachrichten 15–17 (2014).
[5] M. Hartmann, K. Kuhmann, Von der Kraftstoffleitung zum Gasrohr: Rohre aus PA12 zur Führung kohlenwasserstoffhaltiger Medien, Kunststoffe 6 (2014) 76–79.
[6] R.W. Hertzberg, Deformation and Fracture Mechanics of Engineering Materials, J. Wiley & Sons, New York, 1996.
[7] T.R. Kratochvilla, R. Eremiasch, C. Bruckner, Accelerated pipe test methods to evaluate PE100-RC materials - possibilities for ISO standardisation, in: Proceedings PPXIX, Las Vegas, Nevada, USA, 2018.
[8] D. J. M. Havermans van Beek, R. Deblieck, M. McCarthy et al., "An elegant and fast method to predict the slow crack growth behavior of High Density Polyethylene (HDPE) pipe materials," in 3R International, vol. 49, 548 551.
[9] F. Arbeiter, B. Schrittesser, A. Frank, et al., Cyclic tests on cracked round bars as a quick tool to assess the long term behaviour of thermoplastics and elastomers, Polym. Test. 45 (2015) 83–92.
[10] F. Arbeiter, A. Frank, G. Pinter, Influence of molecular structure and reinforcement on fatigue behavior of tough polypropylene materials, J. Appl. Polym. Sci. 133 (38) (2016) 1237.
[11] B. Gerets, K. Engelsing, T. Hochrein, et al., Charakterisierung der Spannungsrissbeständigkeit von Thermoplasten: Entwicklung eines schnellen Prüfverfahrens, Shaker Verlag, Düren, 2019.
[12] A. Frank, W. Freimann, G. Pinter, et al., A fracture mechanics concept for the accelerated characterization of creep crack growth in PE-HD pipe grades, Eng. Fract. Mech. 76 (18) (2009) 2780–2787.
[13] A. Frank, G. Pinter, Evaluation of the applicability of the cracked round bar test as standardized PE-pipe ranking tool, Polym. Test. 33 (2014) 161–171.
[14] A. Frank, A. Redhead, M. Kapur, et al., Characterization of crack initiation and slow crack growth in polyethylene with cyclic cracked round bar tests, in: Proceedings ANTEC, 2011, pp. 2214–2219.
[15] A. Frank, G. Pinter, A. Redhead, The influence of test frequency and eccentric crack growth on cyclic CRB tests, Proceedings ANTEC (2012), https://doi.org/10.13140/RG.2.1.2407.4640.
[16] G. Pinter, A. Frank, A. Redhead, et al., Cyclic CRB tests - a quick and reliable tool for ranking of PE pipe grades, Proceedings PPXV (2010), https://doi.org/10.13140/RG.2.1.2997.2882.

[17] International Standards Organisation (ISO), Polyethylene (PE) Materials for Piping Systems — Determination of Resistance to Slow Crack Growth under Cyclic Loading — Cracked Round Bar Test Method, 2015, p. 18489.
[18] F. Arbeiter, G. Pinter, A. Frank, Characterisation of quasi-brittle fatigue crack growth in pipe grade polypropylene block copolymer, Polym. Test. 37 (2014) 186–192.
[19] G. Pinter, F. Arbeiter, A. Frank, Fast Comparison of Different Polymeric Pipe Materials: Extending the Use of the Cyclic CRB-Test (ISO 18489), 2016.
[20] H.R. Brown, A molecular interpretation of the toughness of glassy polymers, Macromolecules 24 (10) (1991) 2752–2756.
[21] E.J. Kramer, Microscopic and Molecular Fundamentals of Crazing, 1983.
[22] L. Kurelec, M. Teeuwen, H. Schoffeleers, et al., Strain hardening modulus as a measure of environmental stress crack resistance of high density polyethylene, Polymer 46 (17) (2005) 6369–6379.
[23] R.A.C. Deblieck, D.J.M. van Beek, K. Remerie, et al., Failure mechanisms in polyolefines: the role of crazing, shear yielding and the entanglement network, Polymer 52 (14) (2011) 2979–2990.
[24] P.A. O'Connell, M.J. Bonner, R.A. Duckett, et al., The relationship between slow crack propagation and tensile creep behaviour in polyethylene, Polymer 36 (12) (1995) 2355–2362.
[25] T.R. Crompton, Polymer Reference Book, Rapra Technology Limited, Shrewsbury, 2006.
[26] B. Gerets, M. Wenzel, "Current developments in ESCR testing of Polyethylene – an overview, in: Proceedings 6th International Conference „Plastic Materials in Plant Engineering, GER, Munich, 2018.
[27] B. Gerets, Schnelltest-Methode zur Charakterisierung der Spannungsrissbeständigkeit von Polyethylen, Final report IGF-No. 18324 N, SKZ Würzburg, GER, 2016.
[28] J.J. Cheng, M.A. Polak, A. Penlidis, A tensile strain hardening test indicator of environmental stress cracking resistance, J. Macromol. Sci., Part A 45 (8) (2008) 599–611.
[29] N. Robledo, C. Domínguez, R.A. García-Muñoz, Alternative accelerated and short-term methods for evaluating slow crack growth in polyethylene resins with high crack resistance, Polym. Test. 62 (2017) 366–372.
[30] B. Gerets, K. Engelsing, Strain hardening behavior of polyethylene: influence of temperature and time, in: Proceedings DYFP Conference, Kerkrade, NL, 2018.
[31] B. Gerets, Fast testing of stress crack resistance of polypropylene, in: Proceedings PolyMerTec 18 Conference, Merseburg, GER, 2018.
[32] A. Frank, F.J. Arbeiter, I.J. Berger, et al., Fracture mechanics lifetime prediction of polyethylene pipes, J. Pipeline Syst. Eng. Pract. 10 (1) (2019) 4018030.
[33] G.H. Michler, Kunststoff-Mikromechanik: Morphologie, Deformations- und Bruchmechanismen, C. Hanser, München, 1992.
[34] G.R. Strobl, The Physics of Polymers: Concepts for Understanding Their Structures and Behavior, Springer, Berlin, New York, 2007.
[35] A. Redhead, G. Pinter, A. Frank, Analysis of molecular and morphological effects on slow crack growth in modern PE pipe grades by cyclic fracture mechanics tests, Macromol. Symp. 311 (1) (2012) 41–48.
[36] H. Domininghaus, P. Elsner, P. Eyerer, et al. (Eds.), Kunststoffe: Eigenschaften und Anwendungen, Springer, Berlin, Heidelberg, 2008.
[37] G. Pinter, M. Haager, W. Balika, et al., Cyclic crack growth tests with CRB specimens for the evaluation of the long-term performance of PE pipe grades, Polym. Test. 26 (2) (2007) 180–188.
[38] M. Messiha, A. Frank, I. Berger, et al., Determination of the slow crack growth resistance of PA12 pipe grades, in: Proceedings PPXIX, Las Vegas, Nevada, USA, 2018.
[39] A. Redhead, Zyklische Risswachstumsversuche an CRB-Proben als Qualitätssicherungstest zur Abschätzung des Langzeitverhaltens von PE-Rohrwerkstoffen, Masterarbeit, Montanuniversität, 2009.
[40] R. Steenbakkers, L. Havermans, P. Voets, J. Rabiei, R. Deblieck, Strain hardening modulus: a measure for ranking time to failure of random polypropylene pipe materials, in: Proceedings PPXVIII, 2016.

8.1.2 Publication 2

Bibliographic information:

Title:	**How hydrogen bonds influence the slow crack growth resistance of polyamide 12**
Authors:	Mario Messiha[a], Andreas Frank[a], Florian Arbeiter[b], Gerald Pinter[b]
Affiliation:	[a] PCCL GmbH, Leoben, Austria [b] Montanuniversitaet, Leoben, Austria
Processing status:	published
DOI:	https://doi.org/10.1016/j.polymer.2021.124437

Relevant contributions to this publication:

Conceptualization:	Mario Messiha (100 %)
Methodology:	Mario Messiha (100 %)
Validation:	Mario Messiha (40 %), Andreas Frank (20 %), Florian Arbeiter (20 %), Gerald Pinter (20 %)
Investigation:	Mario Messiha (100 %)
Writing – Original Draft:	Mario Messiha (100 %)
Writing – Review & Editing:	Mario Messiha (40 %), Andreas Frank (20 %), Florian Arbeiter (20 %), Gerald Pinter (20 %)
Supervision:	Andreas Frank (30 %), Florian Arbeiter (35 %), Gerald Pinter (35 %)

Polymer 239 (2022) 124437

Contents lists available at ScienceDirect

Polymer

journal homepage: www.elsevier.com/locate/polymer

How hydrogen bonds influence the slow crack growth resistance of polyamide 12

Mario Messiha [a], Andreas Frank [a], Florian Arbeiter [b,*], Gerald Pinter [b]

[a] Polymer Competence Center Leoben GmbH, Leoben, Austria
[b] Materials Science and Testing of Polymers, Montanuniversitaet Leoben, Leoben, Austria

ARTICLE INFO

Keywords:
Slow crack growth
Micro-deformation mechanisms
Polyamides
Hydrogen bonds
Cyclic cracked round bar test

ABSTRACT

Slow Crack Growth (SCG) is considered to be the most critical failure mode for a variety of long-term applications. A key element within this research was to examine the SCG behaviour of polyamide 12 (PA12). Because hydrogen (H) bonds are well-known to affect the mechanical properties of plastics, such as PA12, special focus was put on their influences during quasi-brittle fracture. Therefore, the total fracture energy G_f of PA12 was divided into a pure chain disentanglement fracture energy, driven by creep processes during SCG ($G_{dis,f}$), and the additional energy needed to dissociate effective H-bonds that are actively resisting SCG ($G_{H,f}$) within PA12. In that context, G_f was calculated from the experimentally measured activation energy for SCG via *Cracked Round Bar* (CRB) tests at different temperatures and the subsequent use of a time-temperature superposition. Subsequently, $G_{H,f}$, was estimated with the aid of a modified *Sequential Debonding Fracture* (SDF) model. Subtracting $G_{H,f}$ from G_f, the remaining energy could be classified as $G_{dis,f}$ and was calculated for different amounts of effective H-bonds. It was demonstrated for the selected material, that $G_{H,f}$ would become the dominating source of energy which has to be overcome, if at least 45% of all H-bonds crossing the crack plane engage in the fracture process and follow a sequential debonding mechanism.

1. Introduction

Polyamides (PA) are generally characterized by methylene groups of various lengths that are bonded together through amide linkages (-CO-NH-) [1]. Their amide density, which equals the frequency of occurrence of amide groups in the polymer chain, is responsible for their unique property profile. The presence of high amounts of amide groups results in high degrees of polarity and subsequent interchain and intrachain hydrogen (H) bonding. Therefore, H-bonds shape the strength and stiffness, but also the fracture resistance and governing mechanisms of materials, such as PA12, as they create different polymer-physical conditions during Slow Crack Growth (SCG) that are not existing in polyolefins and other thermoplastics, such as polyethylene (PE), polypropylene (PP), or polyvinylchloride (PVC).

A first impression of the influence of H-bonds can be drawn from studies of Lu et al. [2], Lee and Phillips [3], Kausch [4], as well as Zimmerman [5,6]. A critical M_W value was determined, below which studied materials showed zero to very poor resistances against crack propagation. By comparing polymers with no physical cross-links, such as PE and polyoxymethylene (POM), to polymers with H-bonds (i.e. PA), it was concluded, that, for example, PE exhibits almost no resistance at $M_W < 18$ kg/mol and poor resistance up to 150 kg/mol. The transition from an overall brittle manner to more ductile behaviour occurred in PE above a value of $M_W = 150$ kg/mol and for POM above $M_W = 100$ kg/mol. Polyamides, on the other hand, exhibited a significant fracture toughness improvement already at 15 kg/mol, presumably owing to the strong hydrogen bonding influence [7].

From a chemo-physical viewpoint, a H-bond is an electrostatic attraction force between a positively charged atom due to its covalent binding to an electronegative atom (e.g. H-bond donor) and a partially negatively charged atom (e.g. H-bond acceptor) [8]. Different to other secondary attraction forces, H-bonds may undergo variations of their energetic and geometrical parameters even when formed by the same couple of donor and acceptor atoms. This is observed in $R_1{-}O{-}H{\cdots}O{-}R_2$ bonds for example, that according to the choice of R_1 and R_2 can display bonding energies from less than 4 kJ/mol (weak electrostatic H-bonds), to more than 125 kJ/mol (strong H-bonds classifiable as covalent nature). The corresponding O···O and H···O contact distances changes thereby from 3.00 to 2.38 Å and 2.00 to 1.20 Å, respectively [9]. Driving factors that determine the strength of H-bonds

* Corresponding author.
E-mail address: florian.arbeiter@unileoben.ac.at (F. Arbeiter).

https://doi.org/10.1016/j.polymer.2021.124437
Received 15 September 2021; Received in revised form 3 November 2021; Accepted 5 December 2021
Available online 7 December 2021

within a material are primarily the number of bonds involved as well as secondary interactions (van der Waal forces, dipole-dipole attractions, etc.), organisational and tautomeric effects, environmental effects, state of aggregate (e.g. H-bonds in gas phase, solids or aqueous solutions), morphological effects (e.g. in crystals, or amorphous phases, etc.) and others (for detailed investigations see Refs. [9,10]).

In case of polyamide, the presence of H-bonds is essentially important, particularly with respect to the crystalline structure and consequential (fracture-) mechanical, thermal, optical or electrical performances. Due to H-bonds, crystals involved in PAs exhibit a form of physical cross-linking, leading to enhanced intra-lamellar deformation resistances [11,12]. Furthermore, crystal strength is significantly higher than crystals without further H-bond attraction [10,11]. When thinking of SCG failure by disentanglement or scission crazing [13], one has to additionally account for higher energetical barriers prohibiting disentanglement processes, as the chain mobility is constrained not only by van der Waal forces, but also by H-bonds. Based on that, Xin et al. [14] developed a *Sequential Debonding Fracture* (SDF) model which considers the consecutive and sequential dissociation of H-bonded physical cross-links during crack propagation for tough polyurethane hydrogels. The main idea is strongly related to the fracture energy theory of Lake and Thomas [15] for rubbery materials, who recognized that the energy to be overcome in order to propagate a crack across a failing interface of stretched material (i.e. craze zone) does not only consist of the bond scission energy. Rather, the fracture energy must reflect the energy that goes into entropically stretching and enthalpically deforming each strand that bridges the crack plane within a plastic zone, as shown in Fig. 1. Because PA also exhibits local plastic zones at sites of stress concentration points prior to crack growth and hence acquires a higher level of mobility, it is argued that the SDF model can be principally used for PA.

According to the Lake-Thomas model, the bridging strand defines the cross-link to cross-link portion of a polymer strand that spans the plane of the crack propagation. However, Lake and Thomas only referred to chemical cross-links, which are found in elastomers, or thermosets [15]. By slightly modifying the assumptions of the Lake-Thomas theory, these chemical cross-links can be replaced by physical cross-links (i.e. H-bonds in hydrogels or polyamides), as shown in the SDF model [14]. The main idea of the model is, that the deformed bridging strands undergo repeated partial stress release as physical cross-links, which connect the stretched strand to neighbouring chains by H-bonds, dissociate. In contrast to polymers without the capability of forming H-bonds, polymers exhibiting H-bonds, which act as cross-linking points alongside their chains, may experience additional toughening effects. Each black dot shown in Fig. 2 marks such an effective cross-link location in a PA chain. When the crack propagates, the PA strands occupying the crack plane in front of the crack tip get strained and stressed (strand "b" to "c") until one of the H-bonds on each side of the crack plane dissociates. Up to that point, deformations also follow the assumptions proposed by Lake & Thomas. However, as soon as the first physical cross-link fails (point "c"), the elastic energy stored on the network strand will be released partially. In turn, the bridging strand does not fail, as no backbone bond scission has taken place. Instead, the chain relaxes until the load is transferred to the next-in-line H-bond (i.e. point "d"). This process repeats, leading to a sequence of multiple H-bond breakages.

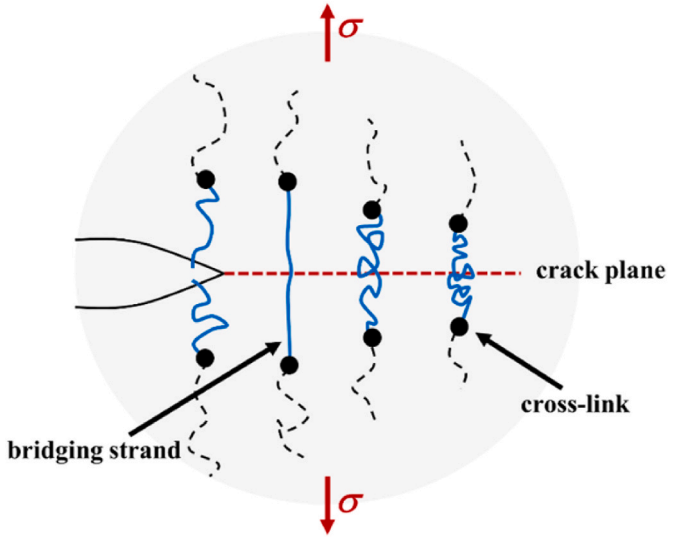

Fig. 1. Schematic illustration of crack propagation according to the Lake-Thomas fracture model [15,16].

Thinking of a low-molecular weight PA12 chain that gets strained and disentangled during SCG, it follows that the whole fracture energy G_f can be regarded as a superposition of the energy needed to disentangle the theoretically non-cross-linked chain $G_{dis,f}$ and the energy necessary to break all active hydrogen cross-links $G_{H,f}$.This assumption remains valid only as long as disentanglement remains the dominating failure mechanism. In order to derive $G_{H,f}$, Xin et al. [14] assumed an initial number n_1 of backbone carbon bonds between a strand (e.g. strand "b-c" in Fig. 2), which crosses the crack plane, as well as an average hydrogen bond scission energy of U_h (e.g. between 10 and 40 kJ/mol, depending on the particular polymer). Supposing a linear elastic behaviour by replacing the chain strands between two cross-links with springs, which are connected to each other in series (see Fig. 3), the elastically stored energy at initial conditions $E_{H,1}$ can be approximated as [14]:

$$E_{H,1} = U_h \cdot n_1 \tag{1}$$

between two cross-link positions that cross the crack plane, i.e. point "e" and "f" in Fig. 3. Furthermore, $E_{H,1}$ must also scale with the square of the strand strain, due to the linear elastic spring approximation and can be rewritten as [14]:

$$E_{H,1} = \frac{1}{2} k \Delta x_1^2 \tag{2}$$

where k is the spring constant between cross-links "e" and "f" and Δx_1 the elongation reached by the applied load.

As soon as all backbone bonds between "e" and "f" have reached the critical hydrogen bond scission energy U_h, one of both H-bond junction points will fail before the other (i.e. here point "f"). Concomitantly, the load bearing spring length doubles, resulting in a new spring constant ½·k and the stored energy after the first H-bond fracture becomes:

$$E_{H,1}^{'} = \frac{1}{2}\frac{k}{2}\Delta x_1^2 = \frac{1}{2}E_{H,1} \tag{3}$$

The energy to fracture the first H-bond is then calculated as:

$$\Delta E_{H,1} = E_{H,1} - E_{H,1}^{'} + U_h = \frac{E_{H,1}}{2} + U_h \tag{4}$$

where the additional U_h accounts for the scission of the first H-bond ("f"). The new spring continues to extend until the stored energy at each backbone bond of the new strand "e-g" again reaches the value of U_h, before another H-bond dissociation takes place. The load bearing spring length further increase (now three times of the initial length) and the overall spring constant of the new load bearing strand "e-h" becomes 1/3·k. The energy to fracture the second H-bond is then calculated as:

$$\Delta E_{H,2} = E_{H,2} - E_{H,2}^{'} + U_h = \frac{E_{H,2}}{3} + U_h \tag{5}$$

Since it can be assumed that H-bond cross-links are uniformly distributed along a polyamide chain, the backbone carbon bond number n_2 also doubles (=2·n_1) when the first cross-link fails. Hence, the overall stored energy in strand "e-g" right before the breakage of the second H-

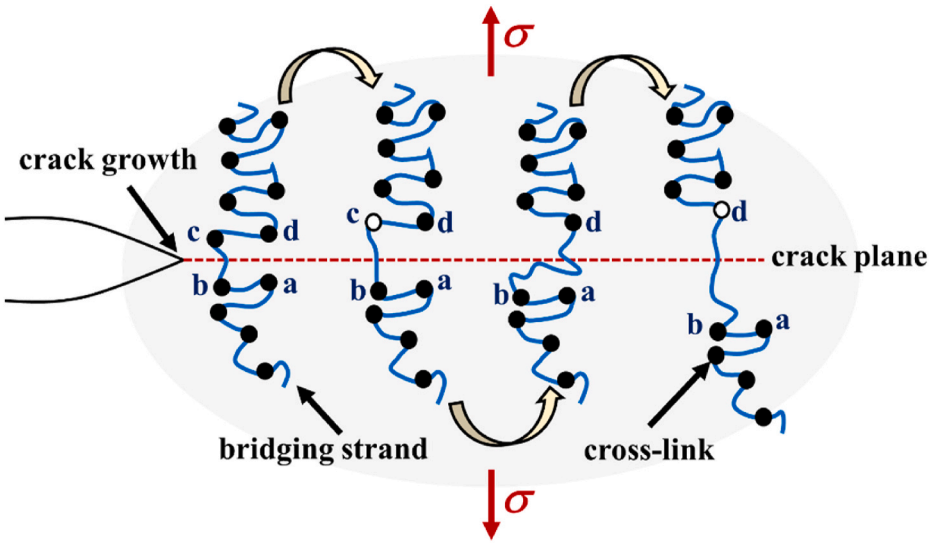

Fig. 2. Schematic illustration of a sequential hydrogen debonding fracture mechanism according to the model of Xin et al. [14].

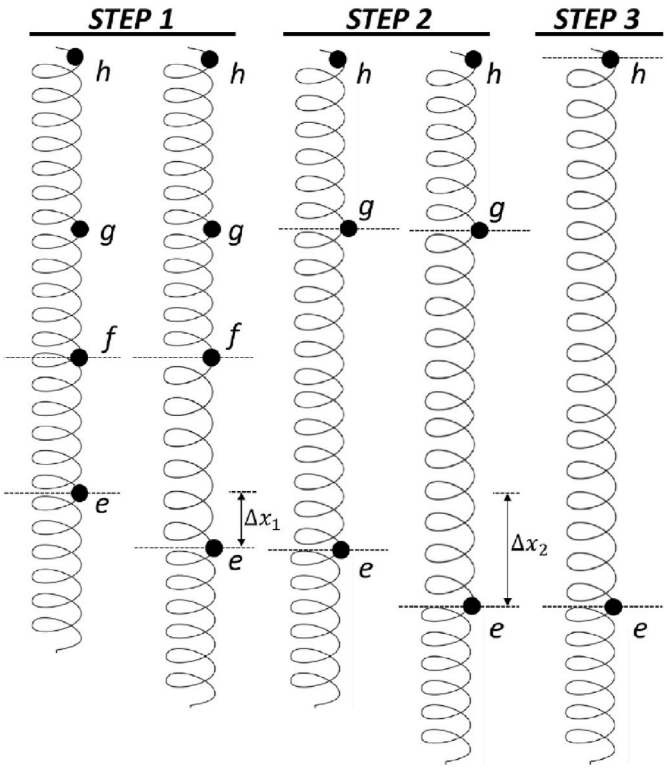

Fig. 3. Spring model representation of a H-bonded chain during crack extension (see annex of [14]).

bond is:

$$E_{H,2} = n_2 U_h = 2n_1 U_h = 2E_{H,1} \tag{6}$$

leading to a dissociation energy for the second H-bond fracture of:

$$\Delta E_{H,2} = \frac{2E_{H,1}}{3} + U_h \tag{7}$$

By continuing the calculations for each H-bond fracture, the dissociation energy for the ith step becomes [14]:

$$\Delta E_{H,i} = \frac{i}{i+1} E_{H,1} + U_h \tag{8}$$

and the total dissipated energy per each chain can be written as [14]:

$$E_{H,f} = \sum_{i=1}^{x} \Delta E_{H,i} = U_h \sum_{i=1}^{x} \frac{i}{i+1} n_1 + 1 \tag{9}$$

where i ranges from 1 to x, which is the total number of effective H-bonds per each chain. This equation highlights the importance of the dissipated energy during loading and unloading steps until all active H-bonds per chain are dissociated (→ it is not just the product of $U_h \bullet x$). The mathematical expression of the fracture energy $G_{H,f}$ to break all H-bonds of all chains crossing a specific crack area alongside the main crack plane follows as:

$$G_{H,f} = E_{H,f}\, \Gamma = U_h \left(x + n_1 \sum_{i=1}^{x} \frac{i}{i+1} \right) \Gamma \tag{10}$$

with Γ as the areal density of network strands crossing the crack plane (see Fig. 4). To estimate Γ, the Gaussian length of a strand between the first two hydrogen bonds is used as width of the crack plane. Furthermore, a random-walk model is used to estimate Γ as [14]:

$$\Gamma \approx \zeta \varepsilon d \sqrt{\frac{3}{8}} \tag{11}$$

for a material in a dry state with ζ as the density of polymer chains ($=\rho/M_W$) and ε as the total number of strands per weight-average polymer chain length and d as the width of the crack zone, that is considered to be the unstrained end-to-end distance of network strands using a Gaussian distribution of strand lengths [17]. If a polymer is in a dry state, d is further estimated to be [14]:

$$d \approx C\sqrt{bn_1} \tag{12}$$

with b as the average length of a single atomic bond within a PA12 chain (b ≈ 153 p.m.) and C as a structural rigidity parameter, that was approximated to be $C \approx 4$ for PA12 considering the rigidity constants of other similar plastics [14,18].

In the following a reversed engineering approach was adapted to determine the energy $G_{dis,f}$, which is dissipated during SCG by chain disentanglement and effects associated with it (e.g. deformation processes and destruction of crystaline structure) of a theoretically non-cross-linked chain in PA12. This was achieved by subtracting the analytically estimated energy necessary to break all active hydrogen bond cross-links $G_{H,f}$ during subcritical crack growth from the experimentally measured total SCG fracture energy G_f, obtained from the

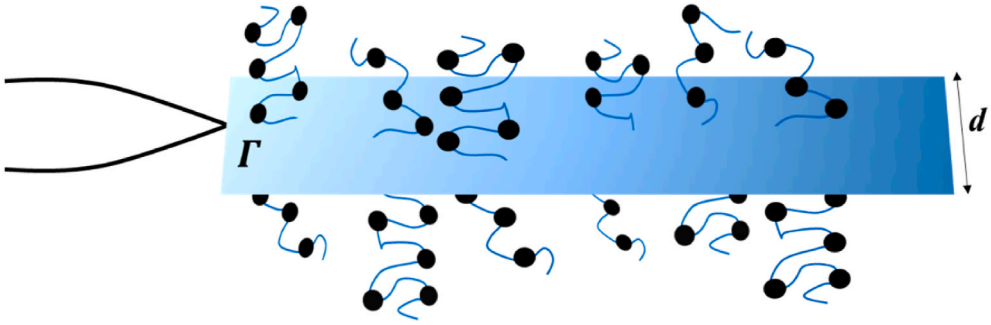

Fig. 4. Schematic illustration of the areal density of network strands Γ crossing the crack plane of width d ahead of a physical crack tip during SCG.

cyclic *Cracked Round Bar* (CRB) test.

2. Experimental

In recent studies [19,20] the general applicability of the cyclic CRB test (ISO 18489) to characterize the SCG resistance of PA12 grades was demonstrated. Hence, this method was applied to identify the total fracture energy of a PA12 with dominating chain disentanglement during slow crack propagation for the low molecular weighed PA12-H_1. For specimen manufacturing cylindrical rods with a diameter of 25 mm were extruded. Afterwards, CRB specimen with a diameter of 14 mm and a length of 100 mm were milled out and circumferentially pre-notched with a razor-blade to an initial crack length of $a_{ini} = 1.5$ mm at the center of each specimen. All cyclic CRB tests were carried out at four different temperatures ranging from $T = -20$ °C to $T = 23$ °C on a 15 kN servo-hydraulic actuator (MTS Systems GmbH, Berlin, GER). To prevent effects of hysteretic heating, the force controlled sinusoidal cyclic load was applied with a frequency of $f = 5$ Hz [19,21]. In contrast to ISO 18489, which recommends testing within a stress range of $\Delta\sigma_0 =$ 10.5–13.5 MPa for PE, for PA12-H_1 higher loads were necessary to gain acceptable testing times and brittle failure, resulting in stress values of $\Delta\sigma_0 > 16$ MPa. The cycle number until total failure N_f was counted from beginning of the test till breakage of the CRB specimen. Furthermore, the crack initiation point N_{ini} was measured with the aid of three extensometers with an initial gauge length $l_0 = 10$ mm (±1.5 mm, ISO 9513 Class 0.5, MTS Systems GmbH, Berlin, Germany). Extensometers were evenly mounted around the pre-notched CRB specimens (positions: 0°, 120° and 240° around the crack) in order to precisely capture the crack opening displacement (COD) during the active test (see also [22,23]). To determine the point of crack initiation, the difference between the maximum and minimum crack opening displacement ΔCOD was monitored during the test for each extensometer. The number of cycles at which the first deviation of the signal appeared was defined as the point of crack initiation and is subsequently called N_{ini}. In doing so, a separation of initiation stage (until N_{ini}) and crack propagation stage ($N_{SCG} = N_f - N_{ini}$) was possible. For most materials, crack initiation onset can be determined via observation of ΔCOD signals during testing. In case of a more transient initiation procedure, however, it can be beneficial to use the evaluation of the dynamic Modulus E_{dyn} (see full line in Fig. 5), which was calculated for each hysteresis at every 500th cycle during the CRB test. While E_{dyn} accounts for the material damage accumulation (Fig. 6a), the secant Modulus E_{sec} additionally considers viscoelastic creep effects [24]. Using both parameters, it is possible to distinguish between the specific contributions of creep and material damage, in a plastic material during cyclic loading. However, in this work E_{sec} is not further considered. A detailed monitoring of E_{dyn}, instead, can additionally help to indicate a clear onset of crack initiation, as soon as the hysteresis begin to tip (Fig. 6b) and a corresponding reduction of E_{dyn} becomes notable, as already portrayed in Fig. 5.

For the use of the SDF model, the weight average chain length of

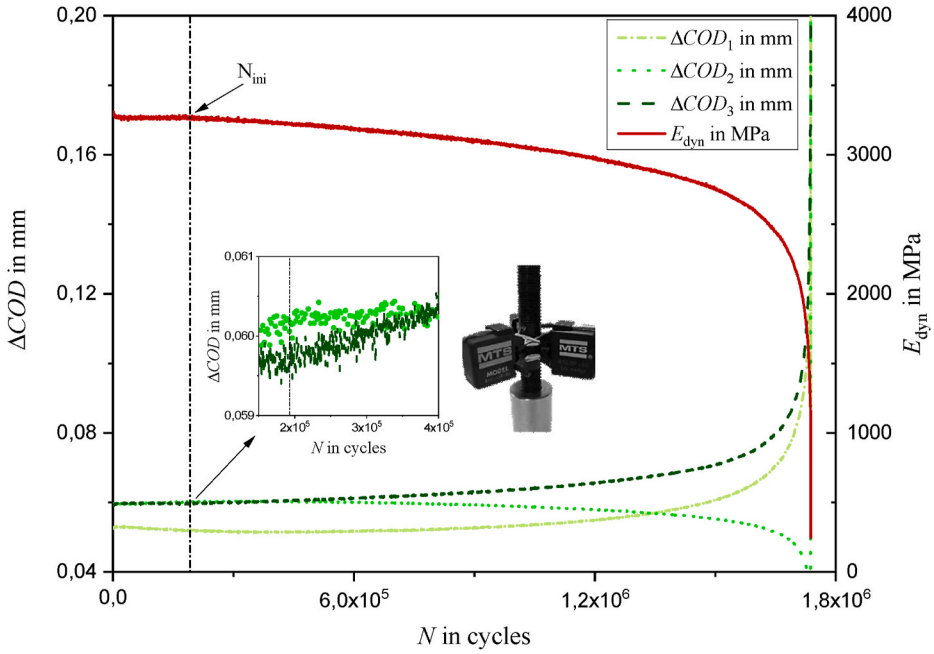

Fig. 5. Representative ΔCOD curves (dashed lines) and E_{dyn} (full line) measured via extensometer signals as a function of cycle numbers N.

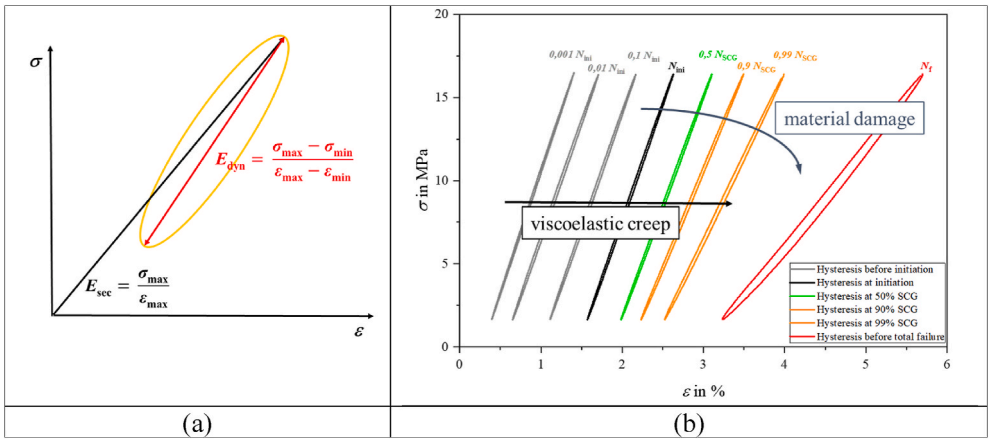

Fig. 6. Dynamic Modulus E_{dyn} and secant Modulus E_{sec} of a hysteresis during cycling loading of a material (a) and schematic hysteresis progression over increasing cycle numbers N during a CRB test of a PA12 grade until ultimate failure N_f (b).

PA12-H_1 was estimated via Size Exclusion Chromatography (SEC). Samples, taken from extruded bars of the given material were dissolved in hexafluoroisopropanol and potassium-trifluoroacetate at room temperature rendering an average chain length of 460 nm. A density (ρ) value of 1018 kg/m^3 was determined for PA12-H_1 according to ISO 1183-1 using a balance of the type Mettler-Toledo AG 204 Delta Range and the Archimedes' principle.

3. Results & discussion

In order to obtain the total SCG fracture energy G_f of PA12-H_1, the apparent activation energy of SCG mechanisms ΔU_{SCG} must be derived first. In that context, Paris and Erdogan [25] confirmed a power-law relation between the crack propagation rate da/dt and the stress intensity K at the crack tip of different materials:

$$\frac{da}{dt} = A \cdot K^m \tag{13}$$

where A and m are material constants. Applying the model of Kim and Wang [26–28] following Manson's approach [29,30] to investigate the temperature effect of polymeric materials exposed to fatigue loading, the crack propagation rate da/dN using a load frequency $f = N/t$ can be described as:

$$\frac{da}{dN} = C \cdot e^{-\frac{\Delta U_{SCG} - \gamma log(\Delta K)}{2.3 k_B T}} \tag{14}$$

where C, and γ are material constants and ΔK the stress intensity factor range during fatigue loading. The factor k_B is known as the Boltzmann constant. From Eq. (14) it can be noted, that ΔU_{SCG} is independent of the applied ΔK [31]. Subsequently, it is directly measurable from the SCG crack kinetic curve governed by the Paris-Erdogan power-law relation [25] when applying the time-temperature equivalence principle according to the Arrhenius equation [27] (compare to Fig. 7 left):

$$ln(a_T) = ln\left(\frac{\left[\frac{da}{dN}\right]_T}{\left[\frac{da}{dN}\right]_{T_0}}\right) = \frac{\Delta U_{SCG} + \gamma \Delta K}{2.3 k_B}\left(\frac{1}{T} - \frac{1}{T_0}\right) \tag{15}$$

In Eq. (15), a_T is the shift factor of a specific property (e.g. the resistance against SCG expressed by da/dN as a function of ΔK) that varies over time t (or cycle numbers N) and temperature T in comparison to a reference time (or cycle number) and temperature, t_0 (or N_0) and T_0, respectively [32]. From the above equation ΔU_{SCG} can be easily determined at $\Delta K = 1$ MPa$\sqrt{\text{m}}$.

However, instead of determining crack kinetic curves at different temperatures, it is suggested to be sufficient to impose the time-temperature superposition principle on the pure slow crack growth fracture process, regardless of the crack initiation stage. Justification for this simplified assumption is given by the comparison of Eq. (15) and the more practical form of the Arrhenius equation:

$$ln(a_T) = ln\left(\frac{t}{t_0}\right) = \frac{\Delta U_i}{2.3 k_B}\left(\frac{1}{T} - \frac{1}{T_0}\right) \tag{16}$$

where ΔU_i denotes the necessary energy to activate a specific reaction i. Instead of determining ΔU_{SCG} via vertical shifting at $\Delta K = 1$ MPa$\sqrt{\text{m}}$ (see Fig. 7 left), a horizontal shift at the same stress intensity range is applied to the pure SCG failure diagram (Fig. 7 right) by substituting t and t_0 of Eq. (12) with N and N_0 at given temperatures T and T_0.

Additionally, the time-temperature shift factor ln(a_T) can be rewritten as:

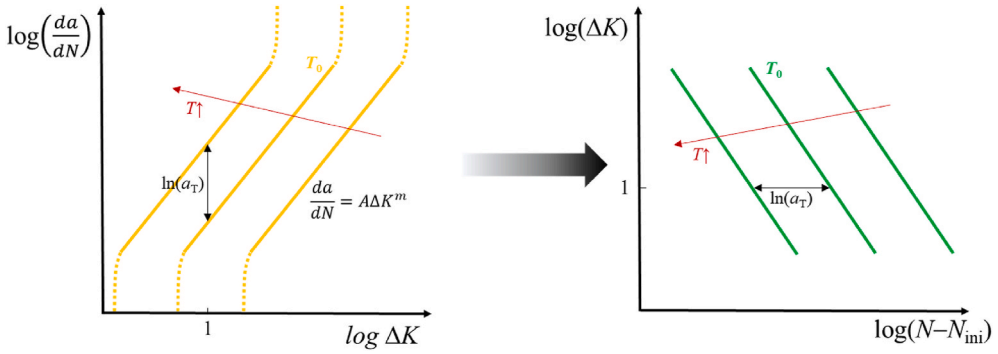

Fig. 7. Transformation of sub-critical crack kinetic law of a material (left) into time-dependent failure behaviour at different load conditions (right).

$$ln(a_T) = ln\left(\frac{\left[\frac{da}{dN}\right]_T}{\left[\frac{da}{dN}\right]_{T_0}}\right) = ln\left(\frac{\left[\frac{dN}{da}\right]_{T_0}}{\left[\frac{dN}{da}\right]_T}\right) = ln\left(\frac{[dN]_{T_0}}{[dN]_T}\frac{[da]_T}{[da]_{T_0}}\right) \quad (17)$$

It must be noted at this point, that crack propagation da is primarily determined by ΔK and the geometry of the CRB specimen during SCG. The crack starts at an initial notch length of a_0 and extends to a maximum crack length a_{max} at given test conditions (see Fig. 8). At elevated T, a_{max} does not change significantly, whereas dN is strongly influenced by T in comparison, as illustrated in Fig. 8. Therefore, it is suggested that ln(a_T) can be approximated as:

$$ln(a_T) \cong ln\left(\frac{[dN]_{T_0}}{[dN]_T}\right) \quad (18)$$

Furthermore, a post-mortem fracture surface analysis of CRB specimens of PA12-H_1 exposed to different temperatures at identical loading conditions (i.e. $a_{ini} = 1.5$ mm, $\Delta\sigma_0 = 16$ MPa, $f = 5$ Hz, $R = 0.1$), reveals very similar crack propagation patterns during fracture process (see Fig. 9). A distinction between three failure regions, which are typical for some thermoplastic materials, such as PE-HD [21,33] can also be made for PA12-H_1 at each temperature. First, a quasi-brittle region adjacent to the pre-notch is visible, where SCG failure mechanisms such as small scale yielding and crazing dominate. Second, a brittle-ductile-transition region can be seen. Finally, a ductile failure zone appears, due to stress levels considerably above the yielding point leading to large-scale deformations and ductile tearing [34]. Comparing all CRB fracture surfaces, it can be seen that the ratio of abovementioned failure regions stays almost constant, confirming the idea of negligible T influence with regard to da.

Based on the identification of the crack initiation onset according to ΔCOD and E_{dyn} evaluations, Fig. 10a reflects an increasing amount of crack initiation with regard to the ultimate failure time during fatigue testing with increasing ΔK_I (index I stands for crack-opening mode I [35]). In the frame of linear elastic fracture mechanics (LEFM) based tests, such as the cyclic CRB test, it is assumed that the plastic zone size of a material is relatively small and solely dependent on the applied ΔK_I, as well as the material's yield stress. An increasing applied ΔK_I, therefore, inevitably leads to larger plastic zones; that is, larger regions of highly deformed materials ahead of the crack tip. Consequently, the time until crack initiation expressed by N_{ini}/N_f increases. Simultaneously, higher applied loads lead to faster crack propagation speeds, which perfectly explains the reduction of N_{SCG}/N_f. A similar effect is apparent with increasing temperature. Again, the increase of N_{ini}/N_f can be ascribed to larger plastic zones at a given applied ΔK_I. This time, however, the key factor is the yield stress of the material, which decreases significantly at elevated T. A decrease of N_{SCG}/N_f, on the other hand, is explainable by a higher chain mobility at higher T, which allows for faster chain disentanglement processes during the SCG stage.

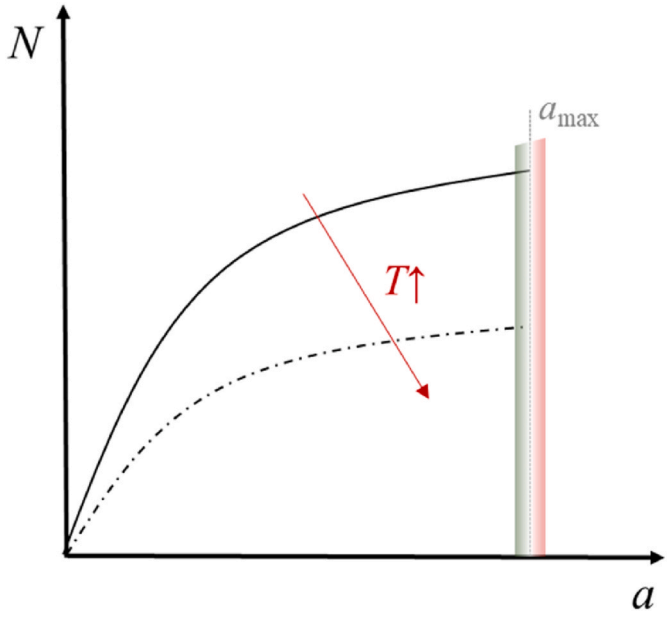

Fig. 8. Temperature effect on a material's resistance to SCG in a cyclic CRB test.

These findings are also reflected in the pure SCG failure diagram of PA12-H_1 in Fig. 10b. A linear trend with slightly changing slopes is recognizable for each test condition in the double-logarithmic diagram. This indicates the thermal sensitivity of PA12-H_1, but also the general consistency of the underlying fracture mechanism during SCG. Growing fracture resistance is observable with decreasing temperatures, as failure cycle numbers N_f are significantly increasing. This can be explained by a declining mobility of polymer chains at lower temperatures, which is necessary for chain disentanglement processes as the governing failure mechanism during SCG in neat PA12 [19]. Another cause for the increased toughness can be accounted to the T-dependent strength of active hydrogen bonds within the material. At low T, polymers exhibit higher densities, and thus, lower contact distances between H-bond donators and acceptors, which is a driving factor that determines the strength of H-bonds [9].

Furthermore, fracture surface analysis via SEM reveals fibrillated structures at identical load conditions and different temperatures for PA12-H_1 (Fig. 11). This is important for two reasons: First, it confirms the idea of the physical fracture mechanism to be dominated by craze development and breakdown through chain disentanglement processes [19,36]. In theory, a plastic deformation zone (e.g. craze) of highly oriented fibrils is developed for a number of plastics during SCG [19,23,37–39]. As long as the material is exposed to a sufficiently high load, a thermo-mechanically activated localized molecular flow occurs (=forced reptation) by pulling polymer chains out of initially non-crazed material regions adjacent to the craze's boundary surfaces. As soon as the first bundle of the fibrillar network within this evolving craze zone breaks, the crack initiates and extends as more and more chains are disentangled [19,40–42]. Fibrillar structures observed in Fig. 11 confirm this fracture mechanism. Secondly, to determine the activation energy of a process, in general, using the concept of the Arrhenius equation, it is required to have an unchanging nature of that process at different temperatures. In that context, Fig. 11 demonstrates a steady-state of the governing failure mechanism at the molecular level across the chosen temperature range, $-20\ °C < T < 23\ °C$, which is sufficiently below the glass transition point at $T_g = 45\ °C$. Hence, a time-temperature superposition is justifiable.

To calculate the SCG activation energy ΔU_{SCG}, the time-temperature shift factor a_T is determined from Fig. 10b according to Eq. (18). The application of the time-temperature superposition according to the Arrhenius concept of Eq. (15) results in Fig. 12. Due to the highly correlating linear regression with a corrected R^2 value of 98.6%, the activation energy ΔU_{SCG} can be viewed as the only factor, by which all changes of a_T, at a given T, are entirely explained. Using the slope in Fig. 12, a ΔU_{SCG} of 58 ± 3.9 kJ/mol can be identified for PA12-H_1. This value is in a reasonable range compared to typical SCG activation energies for PE-HD around 50 kJ/mol for a wide range of temperatures beneath 60 °C [43–45]. Since recent studies [20] showed remarkably higher SCG resistances for PA12 grades compared to modern PE-HD grades at identical test conditions (by at least a factor of 10), even higher ΔU_{SCG} values were expected for PA12-H_1. However, it is important to emphasize that the 50 kJ/mol value for PE-HD according to Baer et al. and Cerpentier [43–45] was determined from fatigue tests that were extrapolated to static creep conditions at $R = 1$, whereas ΔU_{SCG} of PA12-H_1 was extracted from results of $R = 0.1$ fatigue tests. If the activation energy of SCG is dependent on the R ratio, it would be expectable to gain higher ΔU_{SCG} values at $R = 1$, as the overall fracture

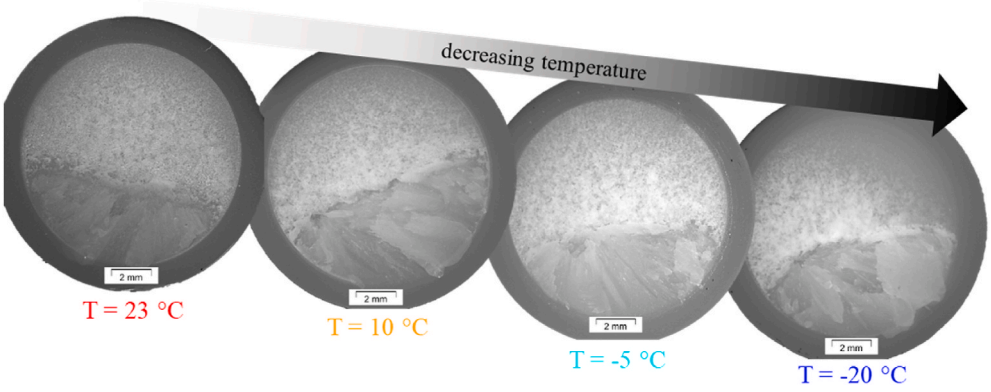

Fig. 9. Fracture appearance of PA12-H_1 at varying temperatures and constant load conditions.

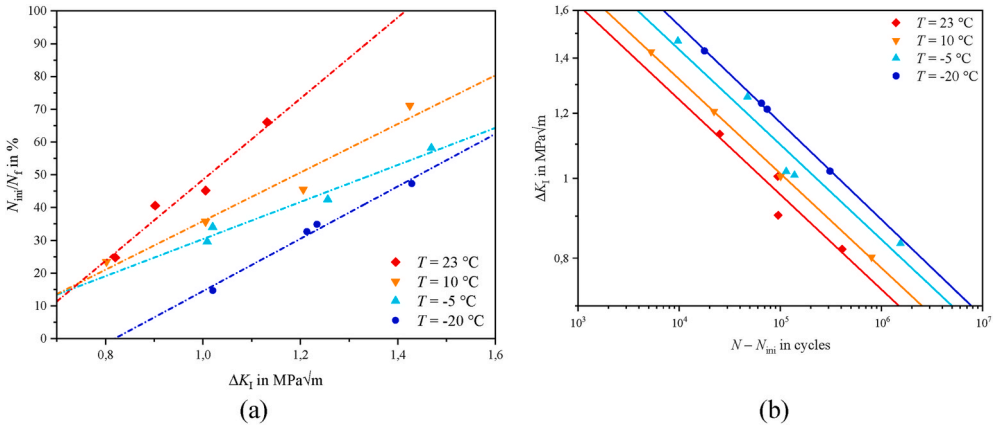

Fig. 10. Ratio of N_{ini}/N_f (a), as well as pure SCG failure curves regardless of the crack initiation stage (b) as a function of ΔK_I and T for PA12-H_1.

toughness is also increasing.

In order to calculate the total fracture energy G_f and to distinguish between the H-bond fracture energy part $G_{H,f}$ as well as the pure disentanglement energy part $G_{dis,f}$ the following assumptions and data are used:

- an average hydrogen bond dissociation energy of $U_h \approx 30$ kJ/mol in PA12 [12,17,46];
- an average SCG activation energy ΔU_{SCG} of 58 kJ/mol;
- the specific amount of H-bonds per chain crossing the crack-plane that are actively engaging in the SCG fracture process is unknown and strongly depends on the location of strands, as well as the direction to which chain disentanglement is going to happen;
- the SDF model (Eq. (1) to Eq. (12)) with a maximum number of effective H-bonds per each weight-average chain of $x = 230$, an initial number of backbone bonds within the first strand of $n_1 = 11$, a polymer chain density of $\zeta = 20.36$ mol/m^3, as well as an areal density of strands crossing the crack plane of $\Gamma = 5.896 \bullet 10^{-6}$ mol/m^2.

Summing up all the data, a total fracture energy G_f of 1.74 kJ/m^2 was calculated for PA12-H_1 on basis of experimental results and the SDF model (e.g. ΔU_{SCG} and the adapted use of Eq. (10) using ζ). This value is reasonable and in good comparison with reported values obtained from monotonic and cyclic fatigue tests of PA12 with a critical fracture toughness G_{Ic} ranging from 0.98 kJ/m^2 (water saturated state) to 5.95 kJ/m^2 (dry state) and fatigue threshold fracture toughness ΔG_{th} ranging from 0.14 kJ/m^2 (water saturated state) to 1.70 kJ/m^2 (dry state) [47]. The used PA12 grade was not dried or water saturated and therefore lies in between both condition extremes. In Fig. 13, the contributions of H-bond fracture energy $G_{H,f}$ with respect to G_f was estimated as a function of different amounts of effective H-bonds. The remaining energy, $G_{dis,f}$, can be regarded as pure disentanglement fracture energy of a theoretically non-cross-linked PA12, which is purely driven by creep processes. Interestingly, for a hypothetical amount of 50% of active H-bond per chain that resist crack propagation, $G_{H,f}$ and $G_{dis,f}$ make up 54% and 46%, respectively. In that context, $G_{H,f}$ becomes the majority source of energy that has to be overcome, if at least 45% of all H-bonds in PA12-H_1 participate in the SCG fracture process. Finally, it should be noted that the SDF model does not consider reformation processes of dissociated H-bonds, as well as any time-dependency of energy dissipations during strand loading and unloading [14]. Both processes may further increase the toughening behaviour of H-bonds, which may explain the remarkably high SCG resistance of PA12 grades. Because of this, the SDF model is not intended to be used as a predictive tool to give accurate calculations about the effective energetical terms. It is primarily proposed as a way to explain how and why the observed and confirmed increase of SCG resistance in PA might be explained in comparison to it's paradigm PE [3].

4. Conclusion

The complex relationship between hydrogen (H) bonds and the quasi-brittle fracture performance of polyamide 12 (PA12) was highlighted in this study. A *Sequential Debonding Fracture* (SDF) model was applied to estimate the amount of fracture energy, which must be additionally supplied to break physical cross-links between PA12 chains compared to a non-cross-linked material, such as polyethylene. By means of *Cracked Round Bar* (CRB) tests at different temperatures and the time-temperature superposition using the Arrhenius' equation, the

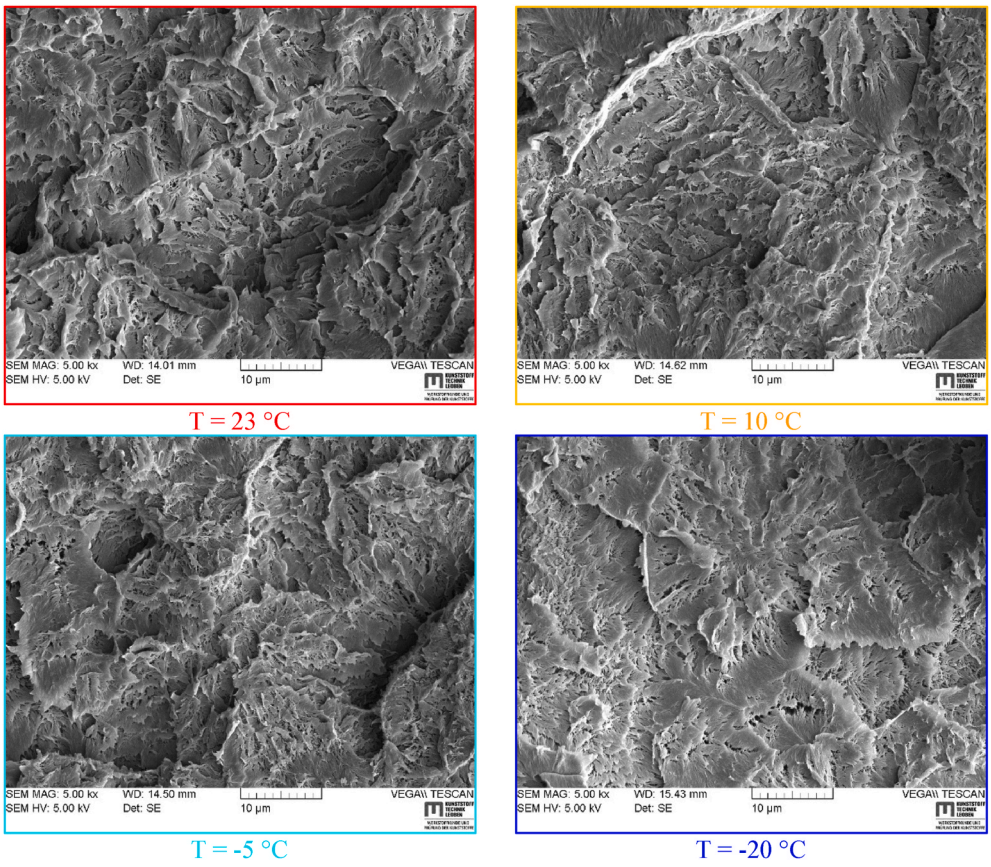

Fig. 11. Post-mortem fracture surface analysis of PA12-H_1 via SEM exposed to identical load conditions at different temperatures.

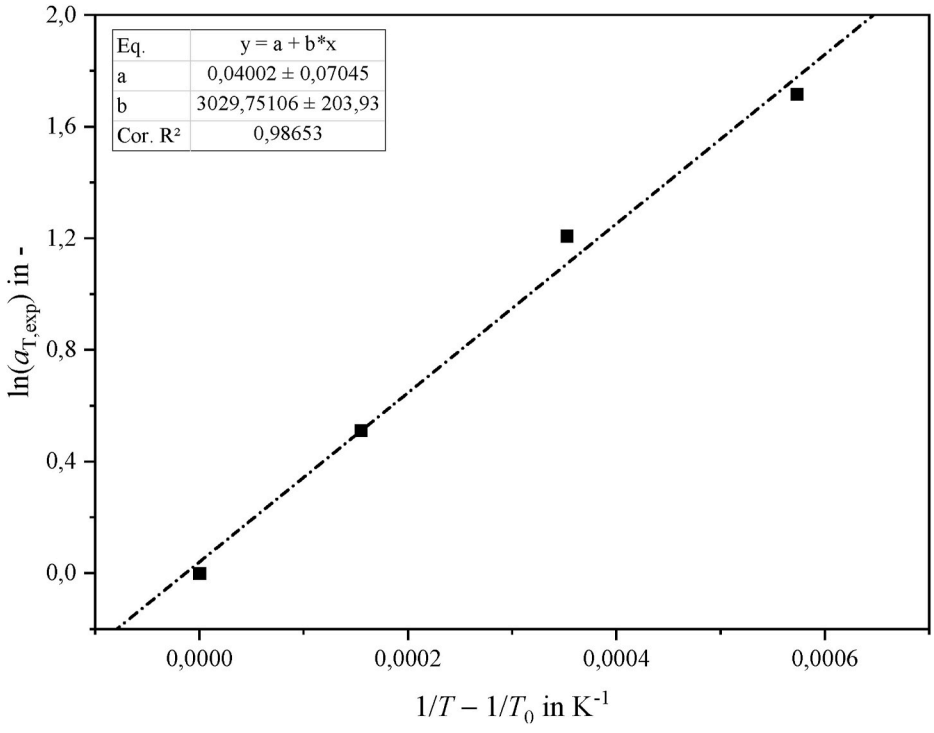

Fig. 12. Arrhenius equation fitted to the natural logarithm of shift factors used during time-temperature superposition of PA12-H_1 exposed to SCG.

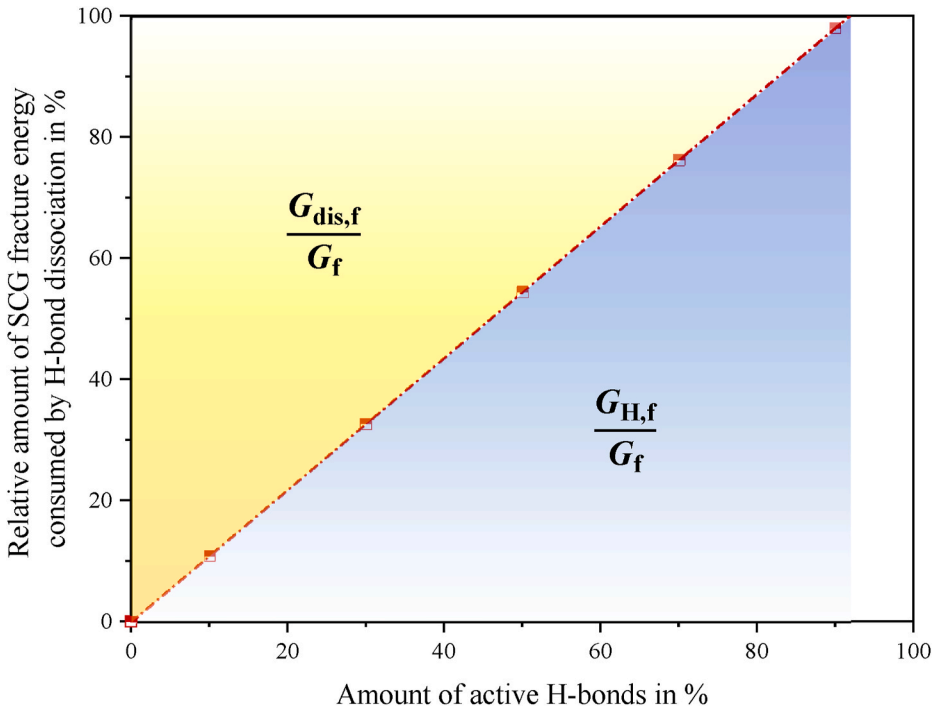

Fig. 13. Ratio of H-bond fracture energy as a function of the number of active H-bonds participating in the SCG fracture process.

activation energy for *Slow Crack Growth* (SCG) was approximated. Based on that, a division into a pure chain disentanglement fracture energy of a theoretically non-cross-linked PA12 material ($G_{dis,f}$) and the pure energy needed to dissociate effective H-bonds that are actively resisting SCG ($G_{H,f}$) within PA12 was possible. Results reflected a total fracture energy G_f of 1.74 kJ/m^2 from which $G_{H,f}$ becomes the dominating source of energy that has to be overcome, if at least 45% of all H-bonds in the selected PA12 grade engage in the fracture process and follow a sequential debonding behaviour.

CRediT authorship contribution statement

Mario Messiha: Conceptualization, Methodology, Validation, Formal analysis, Investigation, Data curation, Writing – original draft, Writing – review & editing, Visualization. **Andreas Frank:** Conceptualization, Validation, Formal analysis, Resources, Writing – review & editing, Supervision, Project administration, Funding acquisition. **Florian Arbeiter:** Conceptualization, Methodology, Validation, Formal analysis, Investigation, Writing – review & editing, Supervision. **Gerald Pinter:** Conceptualization, Validation, Formal analysis, Resources, Writing – review & editing, Supervision, Project administration.

Declaration of competing interest

The authors declare that they have no known competing financial interests or personal relationships that could have appeared to influence the work reported in this paper.

Acknowledgement

The research work of this paper was performed at the Polymer Competence Center Leoben GmbH (PCCL, Austria) within the framework of the K1 COMET-program (Grant Nr.: 879785), which is funded by the Federal Ministry for Transport, Innovation and Technology (Austria) and Federal Ministry for Economy, Family and Youth (Austria) with contributions by Evonik Operations GmbH (Germany) and the Montanuniversitaet Leoben (Austria). The PCCL is funded by the Austrian Government and the State Governments of Styria and Upper Austria.

References

[1] H. Domininghaus, P. Elsner, P. Eyerer, et al. (Eds.), Kunststoffe: Eigenschaften und Anwendungen, Springer, Berlin, Heidelberg, 2008.
[2] X. Lu, N. Ishikawa, N. Brown, The critical molecular weight for resisting slow crack growth in a polyethylene, J. Polym. Sci. B Polym. Phys. 34 (10) (1996) 1809–1815.
[3] S.S. Lee, P.J. Phillips, Melt crystallized polyamide 6.6 and its copolymers, Part I. Melting point – lamellar thickness relations in the homopolymer, Eur. Polym. J. 43 (5) (2007) 1933–1951.
[4] H.-H. Kausch-Blecken von Schmeling, Polymer Fracture, Springer, Berlin, Heidelberg, 1978.
[5] J. Zimmerman, M.I. Kohan, Nylon-selected topics, J. Polym. Sci. Polym. Chem. 39 (15) (2001) 2565–2570.
[6] W. Brostow, R.D. Corneliussen, Failure of Plastics, Hanser Pub.; Distributed in the United States of America by Macmillan Pub, Munich, New York, 1986.
[7] C.J.G. Plummer, H.H. Kausch, "Semicrystalline Polymers: Fracture Properties," in *Reference Module In Materials Science And Materials Engineering*, Elsevier, 2016.
[8] M. Kleman, O.D. Lavrentovich, Soft Matter Physics: an Introduction, Springer-Verlag New York Inc, New York, NY, 2004.
[9] G. Gilli, P. Gilli, The Nature of the Hydrogen Bond: Outline of a Comprehensive Hydrogen Bond Theory, Oxford Univ. Press, Oxford, 2013.
[10] S.-W. Kuo, Hydrogen Bonding in Polymeric Materials, John Wiley and Sons Inc, Weinheim, Germany, 2018.
[11] E. Vinken, Polyamides:hydrogen Bonding, the Brill Transition, and Superheated Water, PhD Thesis, Eindhoven University of Technology, 2008.
[12] C.L. Lewis, K. Stewart, M. Anthamatten, The influence of hydrogen bonding side-groups on viscoelastic behavior of linear and network polymers, Macromolecules 47 (2) (2014) 729–740.
[13] R.A.C. Deblieck, D.J.M. van Beek, K. Remerie, et al., Failure mechanisms in polyolefines: the role of crazing, shear yielding and the entanglement network, Polymer 52 (14) (2011) 2979–2990.
[14] H. Xin, F. Oveissi, S. Naficy, et al., A sequential debonding fracture model for hydrogen-bonded hydrogels, J. Polym. Sci. B Polym. Phys. 56 (19) (2018) 1287–1293.
[15] G.J. Lake, A.G. Thomas, The strength of highly elastic materials, Proc. Roy. Soc. Lond. Math. Phys. Sci. 300 (1460) (1967) 108–119.
[16] S. Wang, S. Panyukov, M. Rubinstein, et al., Quantitative adjustment to the molecular energy parameter in the Lake–Thomas theory of polymer fracture energy, Macromolecules 52 (7) (2019) 2772–2777.
[17] H. Xin, S.Z. Saricilar, H.R. Brown, et al., Effect of first network topology on the toughness of double network hydrogels, Macromolecules 46 (16) (2013) 6613–6620.
[18] R.d.J.P. Casanova, W.E.S. González, J.d.C.Z. Loría, et al., Structure and kinetic rigidity of polymers as related to chain relaxations, J. Thermoplast. Compos. Mater. 34 (5) (2021) 596–613.

[19] M. Messiha, B. Gerets, J. Heimink, et al., Slow crack growth resistance of modern PA-U12 grades measured by cyclic cracked round bar tests and strain hardening tests, Polym. Test. 86 (2020), 106468.
[20] M. Messiha, A. Frank, I. Berger, et al., Differences and similarities in fatigue failure mechanisms of PA12 pipe grades compared to modern PE pipe grades, in: Proceedings ANTEC, 2019.
[21] F. Arbeiter, B. Schrittesser, A. Frank, et al., Cyclic tests on cracked round bars as a quick tool to assess the long term behaviour of thermoplastics and elastomers, Polym. Test. 45 (2015) 83–92.
[22] A. Frank, W. Freimann, G. Pinter, et al., A fracture mechanics concept for the accelerated characterization of creep crack growth in PE-HD pipe grades, Eng. Fract. Mech. 76 (18) (2009) 2780–2787.
[23] M. Messiha, A. Frank, T. Koch, et al., Effect of polyethylene and polypropylene cross-contamination on slow crack growth resistance, Int. J. Polym. Anal. Char. (2020) 1–18.
[24] E. Mourglia-Seignobos, D.R. Long, L. Odoni, et al., Physical mechanisms of fatigue in neat polyamide 6,6, Macromolecules 47 (12) (2014) 3880–3894.
[25] P.C. Paris, F. Erdogan, A critical analysis of crack propagation laws, J. Basic Eng. 85 (1963) 528–533.
[26] H.-S. Kim, Y.-W. Mai, Effect of temperature on fatigue crack growth in unplasticized polyvinyl chloride, J. Mater. Sci. 28 (20) (1993) 5479–5485.
[27] H.S. Kim, X.M. Wang, N.A.H.N. Abdullah, Effect of temperature on fatigue crack growth in the polymer ABS, Fatig. Fract. Eng. Mater. Struct. 17 (3) (1994) 361–367.
[28] H.S. Kim, X.M. Wang, Temperature and frequency effects on fatigue crack growth in acrylonitrile–butadiene–styrene (ABS), J. Appl. Polym. Sci. 57 (7) (1995) 811–817.
[29] W.M. Cheng, G.A. Miller, J.A. Manson, et al., Mechanical behaviour of poly (methyl methacrylate), J. Mater. Sci. 25 (4) (1990) 1924–1930.
[30] J.A. Manson, L.H. Sperling, Polymer Blends and Composites, Springer US, Boston, MA, 1976 s.l.
[31] F. Saghir, N. Merah, Z. Khan, et al., Modeling the combined effects of temperature and frequency on fatigue crack growth of chlorinated polyvinyl chloride (CPVC), J. Mater. Process. Technol. 164–165 (2005) 1550–1553.
[32] W. Grellmann, S. Seidler, Kunststoffprüfung, Carl Hanser Verlag GmbH & Co. KG, München, 2011.
[33] G. Pinter, M. Haager, W. Balika, et al., Cyclic crack growth tests with CRB specimens for the evaluation of the long-term performance of PE pipe grades, Polym. Test. 26 (2) (2007) 180–188.
[34] M. Messiha, A. Frank, I. Berger, et al., Determination of the slow crack growth resistance of PA12 pipe grades, in: Proceedings PPXIX, Las Vegas, Nevada, USA, 2018.
[35] T.L. Anderson, Fracture Mechanics: Fundamentals and Applications, fourth ed., Chapman and Hall/CRC, Boca Raton, 2017.
[36] S.C. Bellemare, M.N. Bureau, J. Denault, et al., Fatigue crack initiation and propagation in polyamide-6 and in polyamide-6 nanocomposites, Polym. Compos. 25 (4) (2004) 433–441.
[37] A. Frank, M. Messiha, T. Koch, et al., Correlation of the cyclic cracked round bar test and hydrostatic pressure test for unplasticized polyvinylchloride, Polym. Test. 95 (2021), 107125.
[38] G. Pinter, F. Arbeiter, A. Frank, Fast Comparison of Different Polymeric Pipe Materials: Extending the Use of the Cyclic CRB-Test (ISO 18489), 2016.
[39] F. Arbeiter, G. Pinter, A. Frank, Characterisation of quasi-brittle fatigue crack growth in pipe grade polypropylene block copolymer, Polym. Test. 37 (2014) 186–192.
[40] N. Brown, A fundamental theory for slow crack growth in polyethylene, Polymer 36 (3) (1995) 543–548.
[41] A. Frank, F.J. Arbeiter, I.J. Berger, et al., Fracture mechanics lifetime prediction of polyethylene pipes, J. Pipeline Syst. Eng. Pract. 10 (1) (2019), 4018030.
[42] N. Brown, X. Lu, Y. Huang, et al., Slow crack growth in polyethylene - a review, Makromol. Chem. Macromol. Symp. 41 (1) (1991) 55–67.
[43] R.R.J. Cerpentier, Influence Of Molecular and Morphological Parameters on the Long-Term Performance of High-Density Polyethylene, Dissertation, Technische Universiteit Eindhoven, 2020.
[44] M.S. Parsons, E.V. Stepanov, A. Hiltner, et al., Correlation of fatigue and creep slow crack growth in a medium density polyethylene pipe material, J. Mater. Sci. 35 (11) (2000) 2659–2674.
[45] Z. Zhou, A. Hiltner, E. Baer, Predicting long-term creep failure of bimodal polyethylene pipe from short-term fatigue tests, J. Mater. Sci. 46 (1) (2011) 174–182.
[46] L.R. Schroeder, S.L. Cooper, Hydrogen bonding in polyamides, J. Appl. Phys. 47 (10) (1976) 4310–4317.
[47] A. Salazar, A. Rico, J. Rodríguez, et al., Monotonic loading and fatigue response of a bio-based polyamide PA11 and a petrol-based polyamide PA12 manufactured by selective laser sintering, Eur. Polym. J. 59 (2014) 36–45.

8.1.3 Publication 3

Bibliographic information:

Title:	**On the slow crack growth process and associated structure-property relationships in polyamide 12 grades**
Authors:	Mario Messiha[a], Andreas Frank[a], Florian Arbeiter[b], Gerald Pinter[b]
Affiliation:	[a] PCCL GmbH, Leoben, Austria [b] Montanuniversitaet, Leoben, Austria
Processing status:	*under peer-review*; submitted on 13th of December 2021
DOI:	

Relevant contributions to this publication:

Conceptualization:	Mario Messiha (100 %)
Methodology:	Mario Messiha (100 %)
Validation:	Mario Messiha (40 %), Andreas Frank (20 %), Florian Arbeiter (20 %), Gerald Pinter (20 %)
Investigation:	Mario Messiha (100 %)
Writing – Original Draft:	Mario Messiha (100 %)
Writing – Review & Editing:	Mario Messiha (40 %), Florian Arbeiter (30 %), Gerald Pinter (30 %)
Supervision:	Andreas Frank (20 %), Florian Arbeiter (40 %), Gerald Pinter (40 %)

On the slow crack growth process and associated structure-property relationships in polyamide 12 grades

Mario Messiha, PCCL GmbH, Leoben, AT
Andreas Frank, PCCL GmbH, Leoben, AT
Florian Arbeiter, Montanuniversitaet, Leoben, AT*
Gerald Pinter, Montanuniversitaet, Leoben, AT

**corresponding author: florian.arbeiter@unileoben.ac.at*

Keywords: slow crack growth, crack initiation, micro-deformation mechanisms, polyamides, hydrogen bonds, cyclic cracked round bar test,

1. Abstract

The influence of micro-structural changes within polyamide 12 (PA12) grades on their resistance against crack initiation and subsequent *Slow Crack Growth* (SCG) was examined. Possible micro-deformation mechanisms and processes guiding slow crack extensions in PA12 are discussed. Special focus was put on the formation of plastic zones as predecessors to microscopic cracks prior to crack initiation via *crack freezing* analysis. Simultaneously, variations in the pure SCG resistance after a recorded craze-crack transition were determined via cyclic Cracked Round Bar (CRB) tests. In that context, a homologous series of PA12 grades of increasing molecular weight (M_W), as well as a systematically developed series of PA12 grades incorporating a pigment and/or an impact modifier, were selected for this study. Results show a good correlation between the crack initiation resistance and the disentanglement resistance of PA12 chains as well as the size of the plastic zone. In that context, an increasing average M_W, leads to increasing disentanglement resistances due to hydrogen bond effects. An impact modification promotes the development of notably larger plastic zones. Contrarily, colored grades exhibit a reduced plastic zone size, rendering a lower amount of dissipated energy before physical crack initiation. Pure SCG resistance follows a similar trend and is improved by high average M_W as well as the use of impact modifier. Crack growth acceleration, however, is assumed to occur alongside the relatively weak interfaces between polymer matrix and pigments.

2. Introduction

Crazing is primarily associated with quasi-brittle fractures in semi-crystalline thermoplastics[1–3] and preferentially occurs around pre-existing crack-like flaws in the micro-structure (e.g. voids, foreign particles, agglomerates of additives resulting from poor

mixing, or crystal defects). When crystalline polymers are subjected to a remote stress σ_{appl}, it is at localities of enhanced stress concentration, where the local, tensile stress σ_{yy} in y-direction approaches a theoretical singularity (cf. **Figure 1**-I), striving to open up spherulites and drive a crack throughout the material (i.e. mode I). A sequence of events is triggered at this point, to form a craze and eventually transfer it into a physical crack, as represented by Figure 1-II and Figure 1-III. Although there is no unified, generally accepted theory, the evolutionary stages of crazing can be appropriately explained by findings of Friedrich[4] and Yarysheva et al.[5]:

i. At an initial stage of stretching (σ_{yy} << yield stress of the material, σ_{ys}), the stress–strain response is approximately linear, allowing for reversible interlamellar deformations (i.e. interlamellar shear, rotations, etc.) in the more compliant amorphous phase, owing to the rubberlike properties of the polymer chains. With increasing strains in front of localities of stress concentrations intralamellar reactions additionally take place.

ii. Once a local critical tensile stress which equals σ_{ys} is reached, individual lamellar blocks are then pulled out from the crystal ribbons to form micro-fibrils by lamellar unfolding and fragmentation into smaller parts (Figure 1-II at instants of increasing strain). It is at this stage, where further stress relaxation is achieved by the nucleation of submicroscopic voids between lamellae.[4,6,7]

iii. In a last stage the local strain is directly transferred onto the crazed zone, leading to a perfect stretching of fibrils. Once the fibrils stabilize the void volume between them, which is often formed by a coalescence of several submicroscopic voids, the macroscopically deformed zone is denoted “craze”.

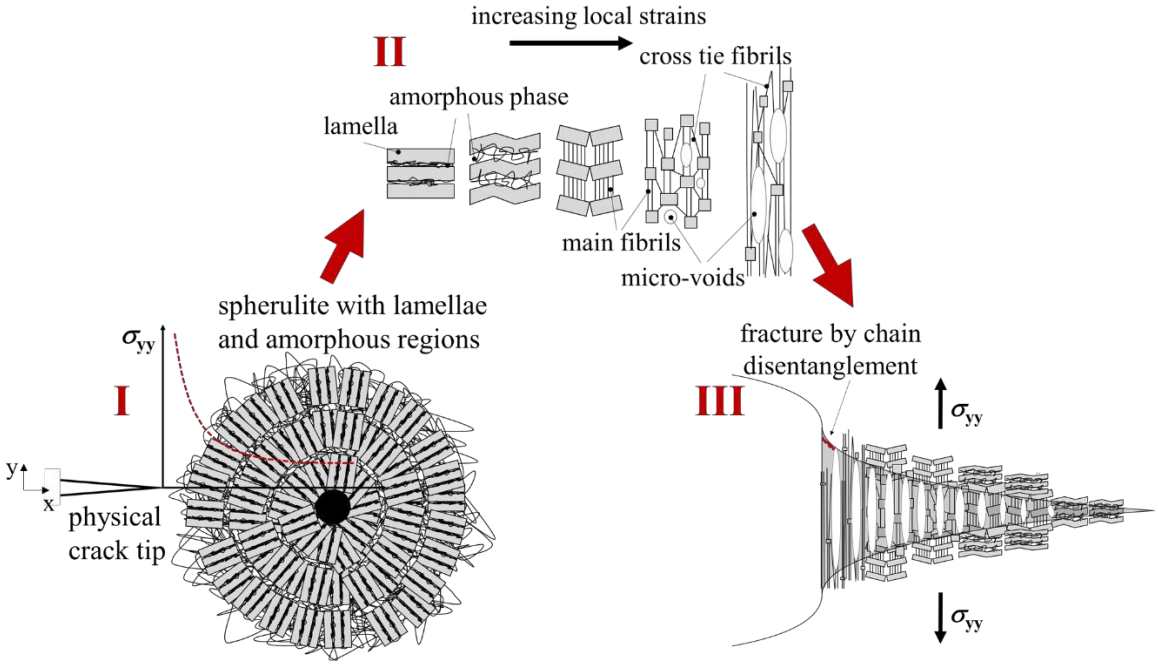

Figure 1: Sketch of craze formation stages in semi-crystalline polymers after Friedrich and Hornbogen's model.[4]

There are two possible mechanisms[8] leading to a craze break down and consequent initiation or extension of a physical crack: *scission crazing*[8–10] where a covalent bond between two carbon atoms of a polymer chain is broken and *disentanglement crazing*[9–14] where molecules separate from one another and remain intact. Chain scission is aided by the fact that molecules in front of crack-like flaws are not stressed uniformly. Certain chain segments may carry a disproportionate amount of load, which can be sufficient to exceed the strength of the covalent bond. At very high strain rates (even at temperatures above T_g) chains may not have enough time to rearrange and redistribute applied loads resulting in chain scission. Analogously, at very low temperatures (even at low strain rates) polymer chains are "frozen" and craze fibrils remain in their highly stretched condition until failure by covalent bond rupture. Chain disentanglement, on the other hand, is promoted by local chain sliding and creep deformations, overcoming van der Waals attraction forces between polymer chains.[15] Thereby, a thermo-mechanically activated localized molecular flow occurs (=forced reptation) by pulling polymer chains out of initially non-crazed material regions adjacent to a craze's boundary surfaces. Since the energy needed to allow for chain disentanglement at moderate temperatures and strain rates is much lower than that to break covalent bonds, the latter failure mechanism is of minor importance in quasi-brittle failures of thermoplastics. This is why Huang and Brown[16] were able to sufficiently predict the rate

of Slow Crack Growth (SCG) in high-density polyethylene (PE-HD) only by focusing on disentanglement processes, although Kausch[17] proved an increased radical concentration within PE-HD crack tips, indicating partial chain scission occurrences.

As soon as the first fibrillar bundles of the craze zone fail as a conclusion of damage accumulation, the physical crack length increases. Since craze fibrils are stretched almost to the maximum possible extension of the entanglement network, no significant change in elongation is observed during overstressing and rupture of fibrils (→ strain hardening). Thus, an extending quasi-brittle crack within the craze shows negligible to no tendency of crack tip re-blunting. Key elements influencing the crack propagation behavior in that case, are regarded to be the thicker main fibrils, as well as thinner connecting cross-tie fibrils. Based on that and on the general micro-structure of the material, crazes may show a higher void content (lower density) in midst of the craze or more frequently larger voids adjacent to the craze/bulk interface. As a matter of fact, the crack preferably propagates at sites of least resistance, partly jumping from one site to another.[18] Crack growth continues as newly developed micro-voids coalesce as a result of successively failing fibrils until ultimate failure occurs by SCG or by a transition to unstable brittle or ductile failure. Depending on given extrinsic (i.e. surrounding media, kind and rate of load, temperature, notch, etc.) and intrinsic (i.e. morphology, molecular structure, inherent defects etc.) conditions, the duration until a crack initiates varies between 20 % to 80% of the total lifetime of a plastic component.[19]

As crack initiation and SCG are regarded to be the most critical failure mechanisms for long-term applications (e.g. pressurized pipe lines, vessels, etc.) the knowledge about resistance behavior of plastics is fundamental. For polyethylene (PE), these failure mechanisms have been extensively studied over a long period of time. In contrast, the crack initiation and SCG behavior of polyamide 12 (PA12) are still under investigation. Although it is known that PA12 can fail by crack initiation and SCG in a similar way to PE, a lack of knowledge about underlying crack growth mechanisms prevails. Therefore, the aim of this study is to systematically investigate the development of plastic zones prior to crack initiation of PA12 grades of varying molecular and morphological structures to assess the crack initiation resistance. Resistance against pure SCG after crack initiation is also analysed. Moreover, the influence of additives relevant for plastics used in long-term

applications (i.e. impact modifier and color pigments) on crack initiation and propagation resistances is studied.

3. Experimental

Seven different grades provided by Evonik Operations GmbH, Essen (GER) were selected for this research (**Figure 2**). A division into two sets of materials can be made:

- a homologous series of three neat PA12 grades (H1, H2 and H3), which only vary in terms of average M_W maintaining very similar molecular and morphologic structures.[20] A relative increase in M_W of 46% from H1 to H2 and 75% from H1 to H3;
- a systematic series of essentially constant M_W consisting of a base PA12 grade termed S_{Base}, as well as modified derivates, which additionally incorporate an impact modifier (IM), a pigment (PGM) or the combination: S_{IM}, S_{PGM} and S_{IM_PGM}.

Based on this material selection, clear structure-property relationships can be drawn between micro-structural changes and corresponding resistances against crack initiation and SCG.

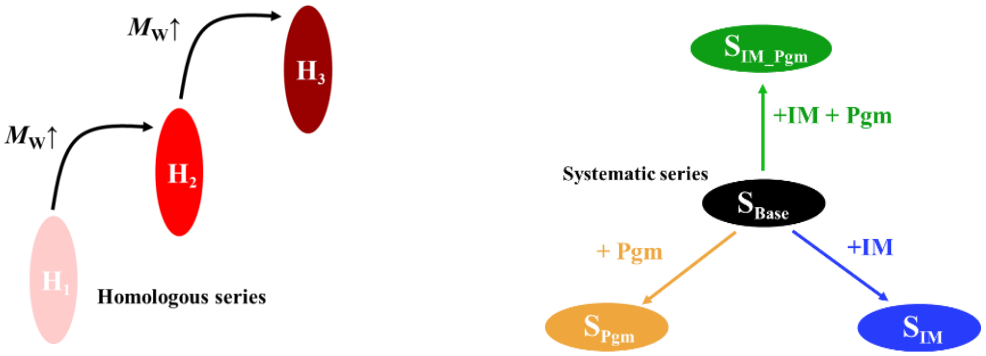

(a) (b)

Figure 2: Systematically developed series (a) and homologous series[20] (b) of unplasticized PA12 grades.

Weight average molecular mass was investigated by Size Exclusion Chromatography (SEC). Samples, taken from extruded pipes of the given materials were dissolved in hexafluoroisopropanol and potassium-trifluoroacetate at room temperature. Tensile properties, such as Young's modulus (E), yield stress (σ_{ys}) and strain at break (ε_b) of the

materials are determined according to ISO 527.[21] Five specimens of each grade were measured and evaluated. The measurements were performed on a tensile/compression-universal testing machine type Z010 (ZWICK GmbH & Co. KG, Ulm, Germany) with a 10 kN load cell at T = 23 °C. Determination of the tensile modulus E is carried out at a test speed of 1 mm/min. Subsequently, measurements are performed until failure at a test speed of 50 mm/min. **Table 1** and **Table 2** summarise relevant properties of the selected materials; for clarity, M_W values are normalized against that of H1 for the homologous series and S_{Base} for the systematic series (see columns of $M_{W,rel}$).

Table 1: Basic characterization of selected PA12 pipe grades, homologous series.

Material	IM	PGM	$M_{W,rel}$ (-)	E (MPa)	σ_{ys} (MPa)	ε_b (%)
H1	–	–	1.00	1538 ± 3	47.2 ± 0.1	238 ± 87
H2	–	–	1.46	1501 ± 7	45.6 ± 0.1	273 ± 38
H3	–	–	1.75	1483 ± 12	44.2 ± 0.1	245 ± 13

Table 2: Basic characterization of selected PA12 pipe grades, systematic series.

Material	IM	PGM	$M_{W,rel}$ (-)	E (MPa)	σ_{ys} (MPa)
S_{Base}	–	–	1.00	1352 ± 18	40.4 ± 0.3
S_{IM}	+	–	1.04	1350 ± 13	39.0 ± 0.1
S_{PGM}	–	+	1.01	1413 ± 6	42.5 ± 0.1
S_{IM_PGM}	+	+	1.03	1369 ± 14	39.4 ± 0.1

Characterization of SCG performance was done via cyclic CRB tests in reference to ISO 18489.[22] All grades were extruded to cylindrical rods with a diameter of 25 mm. Afterwards, CRB specimens with a diameter of 14 mm and a length of 100 mm were milled out and circumferentially pre-notched with a razor-blade to an initial crack length of a_{ini} = 1.5 mm at the center of each specimen. Cyclic CRB tests were carried out at an ambient temperature of T = 23 °C on a servo-hydraulic test device of the type MTS 858.02 Table Top System (MTS Systems GmbH, Berlin, GER). To prevent effects of hysteretic heating, the force controlled sinusoidal cyclic load was applied with a frequency of f = 5 Hz.[13,20] In contrast to ISO 18489[22], which recommends testing within a stress range of $\Delta\sigma_0$ = 10.5 to 13.5 MPa for PE, for PA12 higher loads were necessary to gain acceptable testing times, resulting in stress values of 16 MPa ≤ $\Delta\sigma_0$ ≤ 26 MPa and an equivalent applied stress

intensity factor of $K \geq 0.9$. According to Linear Elastic Fracture Mechanics (LEFM), K can be determined as[23]:

$$K = Y\left(\frac{b}{R}\right) \cdot \frac{P}{\pi b^2} \cdot \sqrt{\frac{\pi a b}{R}} \tag{1}$$

with

$$Y(x) = \frac{1}{2}\left[1 + \frac{1}{2}x + \frac{3}{8}x^2 - 0.363x^3 + 0731x^4\right] \tag{2}$$

where P is the applied crack-opening force, a the crack length, b the ligament length and R the radius of the CRB specimen. The geometry factor Y is obtained by Eq. (1) according to Benthem and Koiter.[23] The cycle number until total failure N_f was counted from beginning of the test till breakage of the CRB specimen. Furthermore, crack initiation was measured with the aid of three extensometers with an initial gauge length l_0 = 10 mm (± 1.5 mm, ISO 9513[24] Class 0.5) produced by MTS Systems GmbH (Berlin, Germany), which were evenly mounted around the pre-notched CRB specimens (positions: 0 °, 120 ° and 240 ° around the crack) in order to precisely capture the crack opening displacement (COD) during the active test. The extensometer signals were evaluated as the difference of maximum and minimum crack opening displacement ΔCOD over cycle numbers N as an indicator of crack initiation.[20,25] When total failure was achieved, the fracture surfaces of the CRB specimens were studied via a Scanning Electron Microscope (SEM) of the type Tescan Vega II (Tescan Brno, Brno, CZ). Therefore, surfaces were sputter coated with gold.

Examination of initial pre-notch dimensions as well as the evolution of plastic zones were done via incident and transmitted polar light microscopy, using an Olympus SZX12 and an Olympus BX51 light microscope. Microscopic inspections of the fractured CRB specimens were done by mounting them on microscope glass slides, while the inspection of plastic zone at the crack tip necessitated the use of 15 µm to 20 µm thin slices, which were cut off from the center of the CRB samples using a microtome (Rotary Microtome Leica RM2255). Changes in the formation of plastic regions in front of crack tips were obtained in so-called *crack freezing* experiments[25]. Therefore, CRB fatigue tests were undertaken for all grades at a stress level of $\Delta\sigma_0$ = 20 MPa and a loading ratio of R = 0.1. Knowing the approximate total failure time as well as crack initiation and SCG times from previously completed CRB tests, the tests were stopped before crack initiation at different cycle numbers (e.g. 10^1, 10^2, 10^3, 10^4 and 90 % of N_{ini}). Subsequently, a hot adhesive was inserted into the cracks in order

to “freeze” them, enabling further sample preparation for microscopic analysis. Measured quantities of *crack freezings* (e.g. length, height and area of plastic zones) are schematically presented in **Figure 3**. The length of the razor-blade pre-notch was measured separately at a smaller magnification of 50x. Furthermore, the models of Irwin and Dugdale [26–28] are used to estimate plastic zone sizes and compared to actual results obtained from crack freezing experiments. Presupposing the validity of LEFM, the plastic zone size can be estimated according to Eq. (3) for Irwin’s approach and Eq. (4) using Dugdale’s estimation [29].

$$r_{\mathrm{pz,\,Irwin}} = \frac{1}{\pi} \cdot \left(\frac{K_{\mathrm{I}}}{m_{\mathrm{pl}} \sigma_{\mathrm{ys}}(t)} \right)^2 \tag{3}$$

$$r_{\mathrm{pz,\,Dugdale}} = \frac{\pi}{8} \cdot \left(\frac{K_{\mathrm{I}}}{\sigma_{\mathrm{ys}}(t)} \right)^2 \tag{4}$$

In Eq. (3) m_{pl} stands for the plastic constraint factor, which is accounting for the governing triaxial stress state ($m_{\mathrm{pl}} = \sqrt{3}$ for plane strain state and $m_{\mathrm{pl}} = 1$ for plane stress state) and $\sigma_{\mathrm{ys}}(t)$ is the time-dependent yield stress of a material.

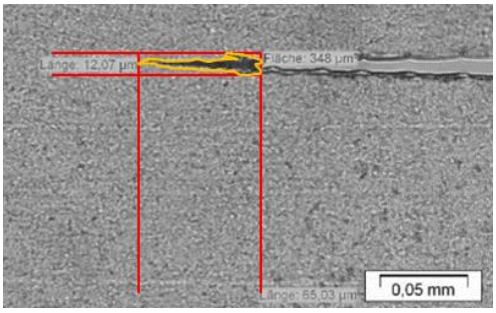

Figure 3: Schematic evaluation of plastic zones; magnification 400x.

4. Results

4.1 Homologous series

Quasi-brittle failure behavior at different loads is depicted for the homologous series in **Figure 4**. An increase of the molecular weight leads to an increase of the total failure time of the three PA12 grades.[2,20] Given the fact that M_{W} is increased by approx. 50 % from H1 to H2 and around 20 % from H2 to H3 one might expect a more significant improvement of the quasi-brittle fracture resistance from H1 to H2 than from H2 to H3. However, considering the logarithmic scale in Figure 4 it should be outlined that especially at low load levels (< 14 MPa) the relative increase of fracture resistance from H2 to H3 exceeds that of

H1 to H2. It must also be noted that the slope of selected grades is slightly levelling off with increasing M_W. A possible explanation to this observation was given by the so-called *hydrogen bond hypothesis* [20], where hydrogen (H) bonds inhibit disentanglement processes of PA chains to a certain extent when exceeding a critical molecular mass or equivalent number of physical cross-links [30]. In that sense, chain disentanglement resistance increases, whereas fibrillation density within the plastic zone of PA12 grades reduce with increasing M_W. Instead, a partial transition from classical crazing to a more energy-consuming shear yielding is reported, as portrayed in SEM analysis of the homologous series in **Figure 5**.[20] Bearing this in mind, the increase of cycles to failure can be explained by the strong delay of chain disentanglement mechanisms due to intervening H-bonds, particularly at lower stresses and increasing M_W.

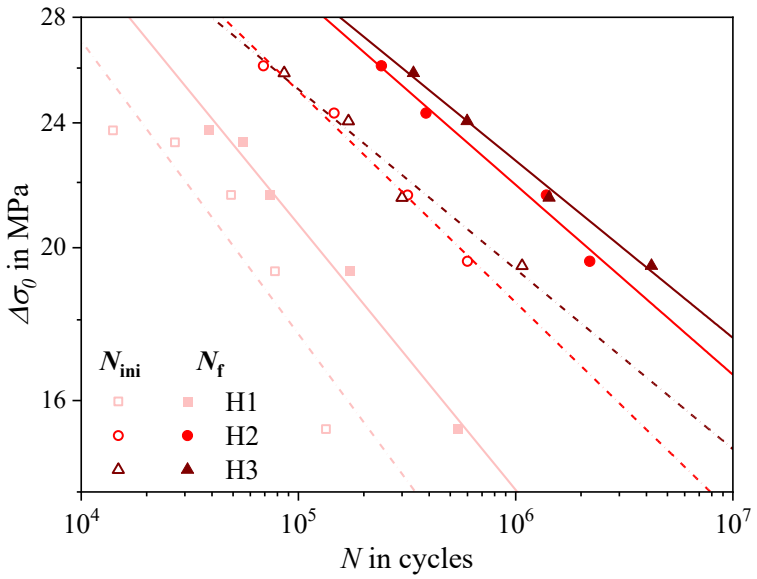

Figure 4: Crack initiation (dashed) and total failure (full) lines of the homologous series obtained from cyclic CRB test.

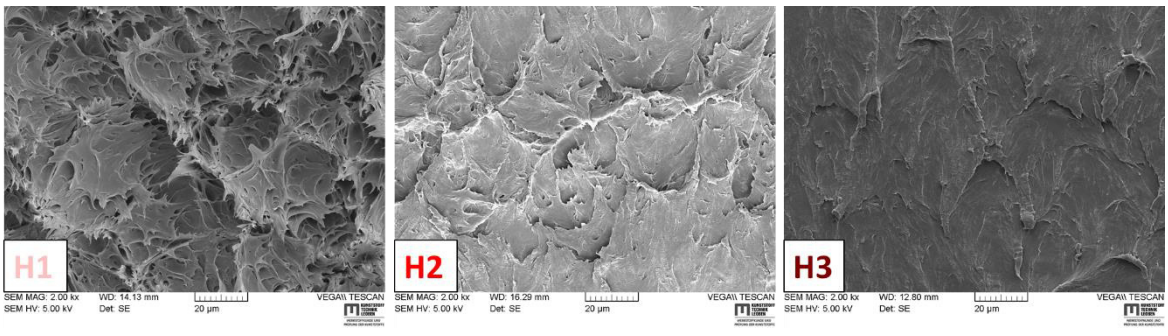

Figure 5: SEM analysis of homologous series, 2000x. Decreasing fibrillation indicates an increase of chain slippage mechanisms associated with shear-yielding processes. Reproduced with permission[20] 2020, Elsevier.

By the use of extensometer signals the total failure curves can be additionally divided into a crack initiation stage and a pure SCG stage (cf. Figure 4). At this point it is obvious that an increase of M_W results in a better performance during the cyclic CRB test. The more interesting question, though, is whether the crack initiation resistance or the pure SCG resistance is more significantly affected by longer chains. **Figure 6** provides a response to that question using a single-point data evaluation at 20 MPa: In absolute cycle numbers a strong increase of pure N_{ini} and pure N_{SCG} can be observed for H1 towards H3 (Figure 6a). If crack initiation resistance as well as SCG resistance are equally influenced by a higher M_W, the N_{ini}/N_f and N_{SCG}/N_f ratio should be independent of an increasing $M_{W,rel}$ (e.g. straight line at 40 % N_{ini}/N_f). However, since N_{ini}/N_f is decreasing with increasing $M_{W,rel}$ it seems that the SCG resistance is becoming the dominating factor that determines the overall material toughness (Figure 6b). This effect is even stronger pronounced at lower applied loads, as the difference between crack initiation and total failure lines is significantly increasing.

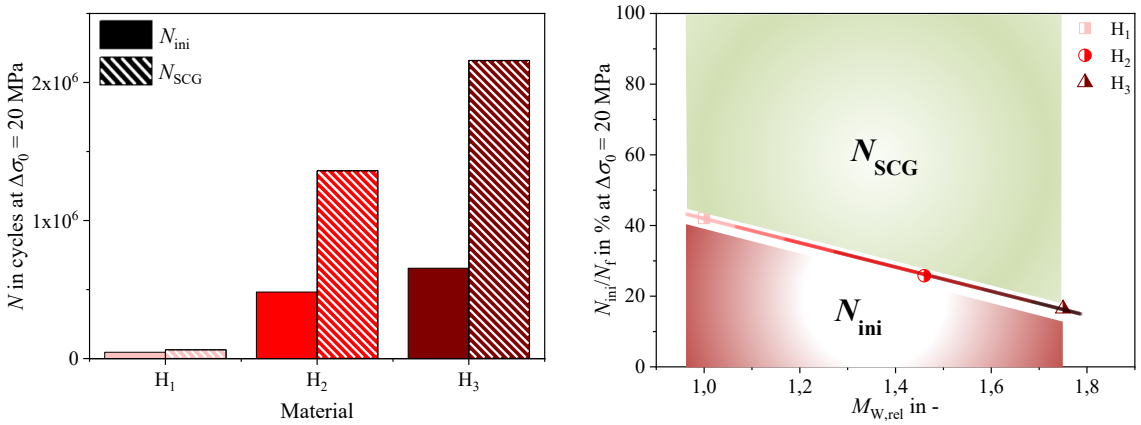

Figure 6: Absolute (a) and relative (b) changes in crack initiation and SCG behavior at $\Delta\sigma_0$ = 20 MPa with regard to varying $M_{W,rel}$.

Obtained results agree well with conclusions drawn from the hydrogen bond hypothesis [20]. Longer PA chains exhibit higher disentanglement resistances, which is one of the driving mechanisms for SCG in PA12. Crack initiation, on the other hand, is not only dependent on mechanisms that drive the collapse of a plastic zone, but additionally on the volume and size of the plastically deformed material ahead of a sharp crack tip or an inherent crack-like defect and the time dependency of visco-elastic/visco-plastic materials. In **Figure 7**, a general increase of the measured plastic zone length l_{pz} over time (Figure 7a), as well as representative images of "wedge-shaped" craze zones of PA12 grades are shown (Figure 7b). The progression of l_{pz} indicates a change of σ_{ys} over accumulating cycle numbers due

to time dependent effects in the plastic zone [31–33]. Interestingly, l_{pz} follows a very similar path for all homologous grades and reaches a niveau around 80 to 90 µm after approx. 10^3 cycles, even though, a slight decrease of σ_{ys} from 47.2 MPa to 44.2 MPa from H1 to H3 is accompanied by the increase of M_W. It can be concluded, therefore, that the plastic zone size is not predominantly influenced by the weight-average polymer chain length (cf. **Figure 8**). Whereas, the general disentanglement resistance is improved by (cf. Figure 8):

- an increasing entanglement density of chains surrounding the plastic zone;
- a higher number of inter- and intra-molecular H-bonds actively resisting chain deformation processes (i.e. disentanglement);
- as well as longer remaining chain segments, which have to be pulled inside the plastic zone before physical crack initiation begins.

This explains well the decrease of the relative amount of crack initiation resistance with increasing M_W (i.e. stagnating plastic zone size), while the absolute crack initiation resistance is still increasing (i.e. H-bond influence on disentanglement mechanism).

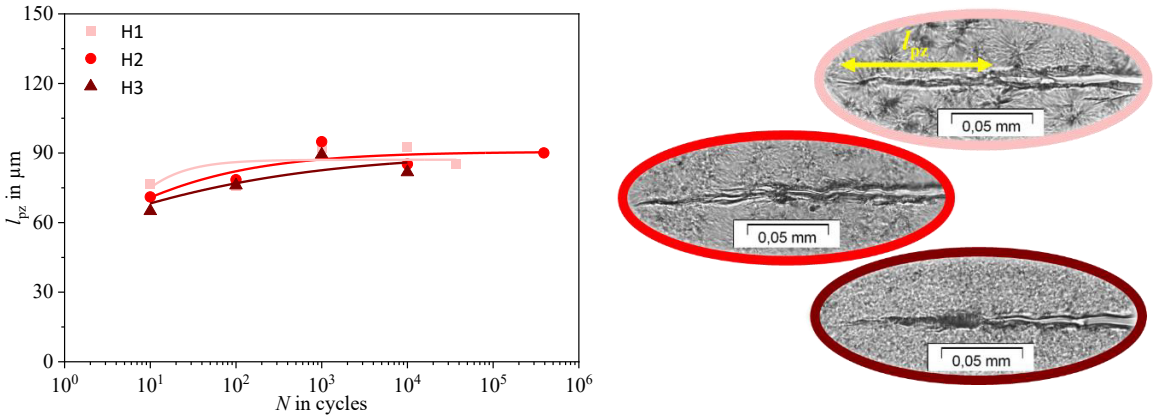

(a) (b)

Figure 7: Measured plastic zone length l_{pz} (a) and representative crack freezing images at $N = 10^3$ cycles (b) of the homologous series at $\Delta\sigma_0 = 20$ MPa.

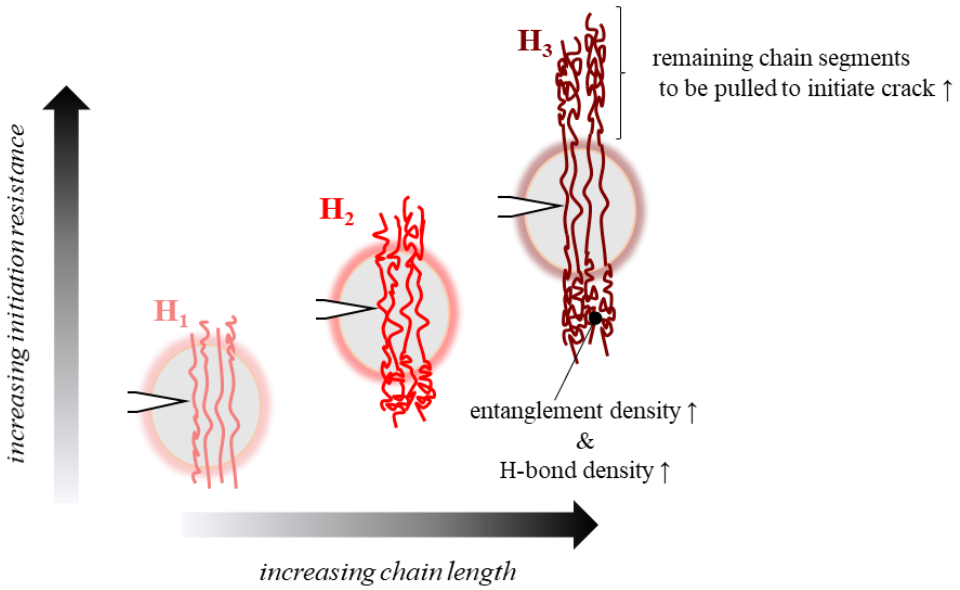

Figure 8: Schematic diagram of crack initiation resistance as a function of weight-average chain length.

A comparison of the actual l_{pz} and predicted r_{pz} using Irwin's and Dugdale's model is presented in **Figure 9**. Full lines represent the measured plastic zone length, whereas dashed and dotted lines represent Irwin's model for plane stress and strain state and Dugdale's model, respectively. Actual plastic zone sizes were found to be in good accordance with Irwin's estimation at a governing plane strain state for the homologous series, whereas Dugdale's model, which is originally deduced for a governing plane stress state, overestimated the actual plastic zone size. This is also in correspondence with expectations drawn from the use of the CRB test. As demonstrated by Arbeiter et al. [34] the CRB specimen leads to a governing plane strain state alongside the circumferential notch, since there is no free surface perpendicular to the notch. This, inevitably constrains the ability of a material to plastically deform, reducing l_{pz} to a minimum value. Another reason for the small sizes of measured plastic zones is the glass transition temperature (T_g) of PA12. Selected materials exhibit a T_g around 40 °C, whereas testing was conducted at room temperature. Hence, the molecular mobility of PA12 grades is expected to be low.

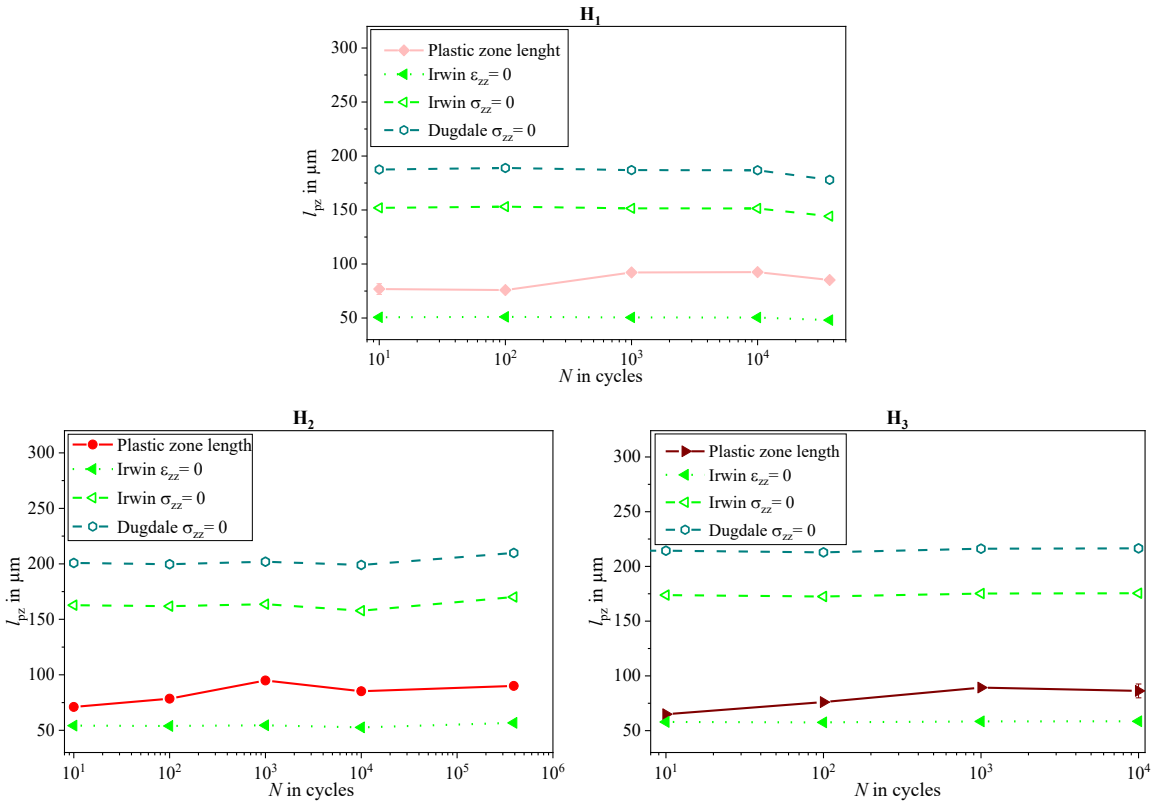

Figure 9: Measured and estimated plastic zone lengths of the homologous series.

4.2 Systematic series

Quasi-brittle failure behavior of the systematic series is depicted in **Figure 10** at different loads. Results show that the addition of a pigment leads to a general decrease of the total failure time of a PA12 grade (compare S_{Base} to S_{PGM}, or S_{IM} to S_{IM_PGM}), whereas the addition of an impact modifier causes a higher fracture toughness (compare S_{Base} to S_{IM}, or S_{PGM} to S_{IM_PGM}). Interestingly, the addition of PGM not only shifts the entire failure curve to shorter lifetimes, but it also changes the slope of the failure line. On the contrary, the addition of IM or a combination of IM and PGM does not affect the slope as much. Crack initiation curves also follow a similar slope and trend as the total failure curves.

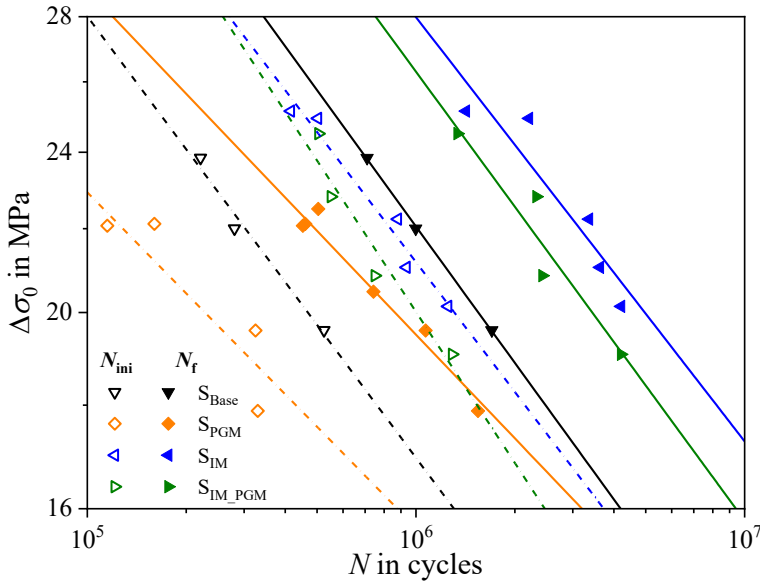

Figure 10: Crack initiation (dashed) and total failure (full) lines of the systematic series obtained from cyclic CRB test.

Fractographic analysis of CRB specimens give a good explanation to the obtained failure lines: the addition of pigments reveals an increasing number of locations at which cracks can be more easily initiated or grow (compare S_{PGM} and S_{IM_PGM} to non-pigmented counterparts in **Figure 11**). From a fracture mechanics viewpoint, introducing pigments equals the introduction of additional rigid stress concentration spots, which might promote the formation of micro-cracks alongside the interface between polymer matrix and pigment. As a consequence, the single dominant crack is accelerated as it coalesces with the smaller micro-cracks within the leading crack plane.

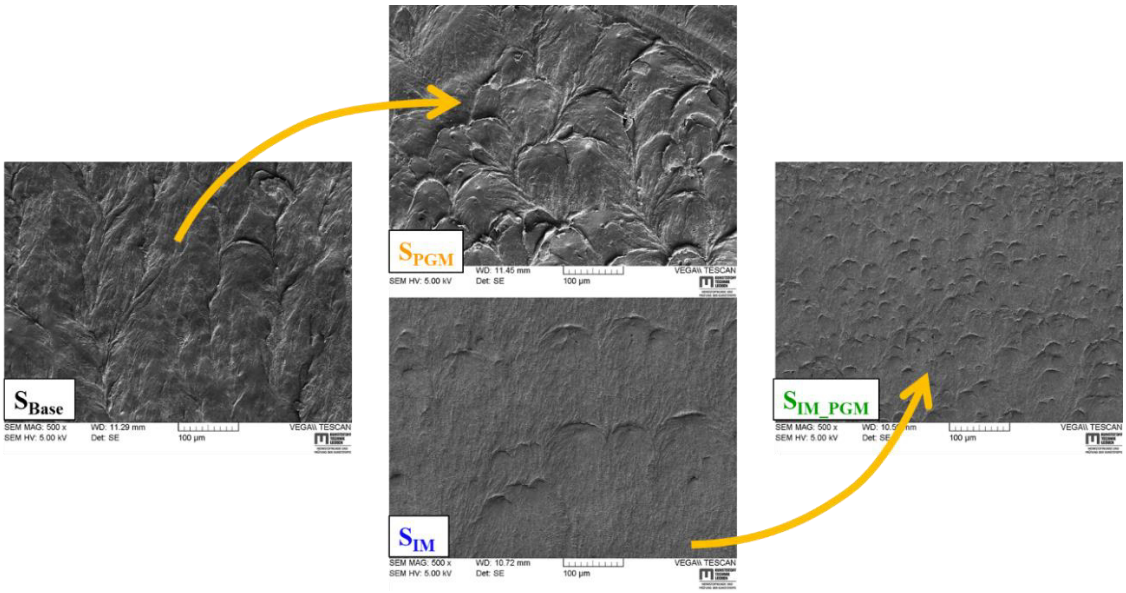

Figure 11: Effect of color pigments in PA12 – SEM images taken close to initial pre-notch.

In contrast, an impact modification surely leads to a very fine fibrillation and a significantly increasing plasticity at a microscopic level of the materials S_{IM} and S_{IM_PGM} compared to S_{Base} and S_{PGM}, respectively (see **Figure 12**). It can, therefore, be assumed that rubber particles have enough time during quasi-static fatigue to plastically deform and cavitate, enhancing the resistance against crack initiation and SCG [35]. Different theories were proposed to explain the toughening mechanisms due to impact modification:

- the rubber is stretched during the fracture process and absorbs a large amount of energy [36] within the plastic zone;
- rubber particles are crack terminators that create a large number of stress concentration points, promoting multiple crazing and subsequent propagation of smaller cracks, which require more energy than a single main crack due to the formation of numerous new surfaces [37];
- a rubbery phase results in cavitation mechanisms that dissipate hydrostatic strain energy and increase shear flow of the matrix [38].

Independent of the actual toughening mechanism, the dispersion of soft rubber particles in the polymer matrix seems to dissipate a large amount of energy, shifting the total failure time in the CRB test to relatively long testing times.

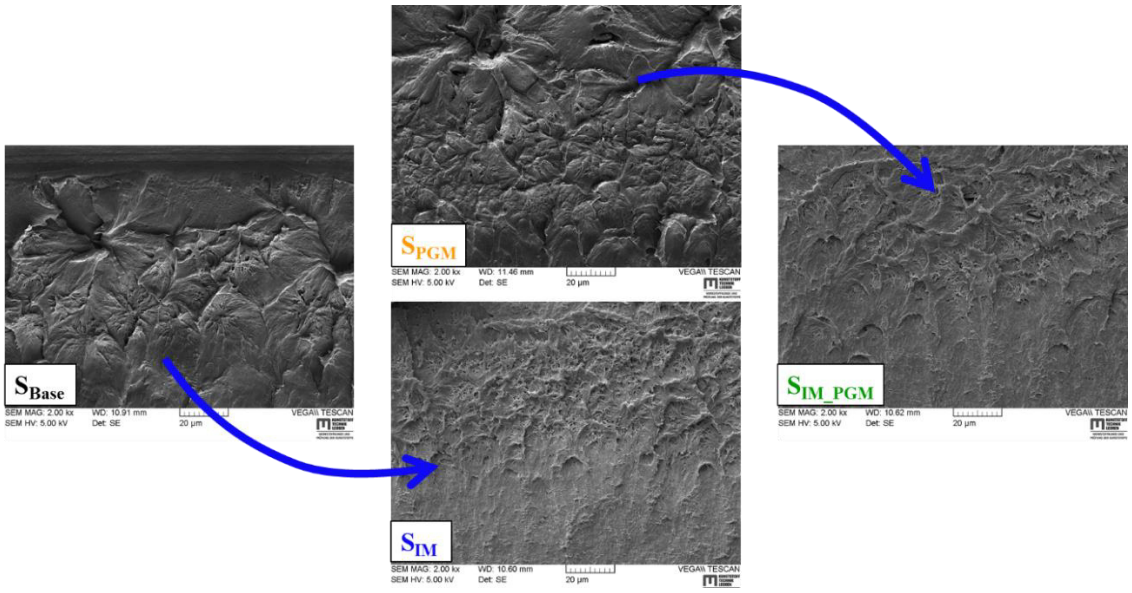

Figure 12: Effect of impact modifier in PA12 – SEM images taken close to initial pre-notch.

Analogously to the homologous series, it is to be asked whether the implementation of certain additives is affecting either the crack initiation or the SCG resistance equally or differently. To answer that question, a single-point data evaluation at a stress level range of

20 MPa was conducted (**Figure 13**a) using the linear regression lines of the double-logarithmic failure diagram in Figure 10. In absolute cycle numbers a decrease of the pure crack initiation resistance as well as the SCG resistance is observed with the addition of pigments. On the other hand, an increase of crack initiation and SCG resistance is obtained when adding an impact modifier. A combination of both additives follows a classical "rule of mixture". Since the relative amount of N_{ini}/N_f and N_{SCG}/N_f stays almost constant at around 30 % for each systematic grade (Figure 13b), it can be assumed that additivation has equal influences on both failure regimes.

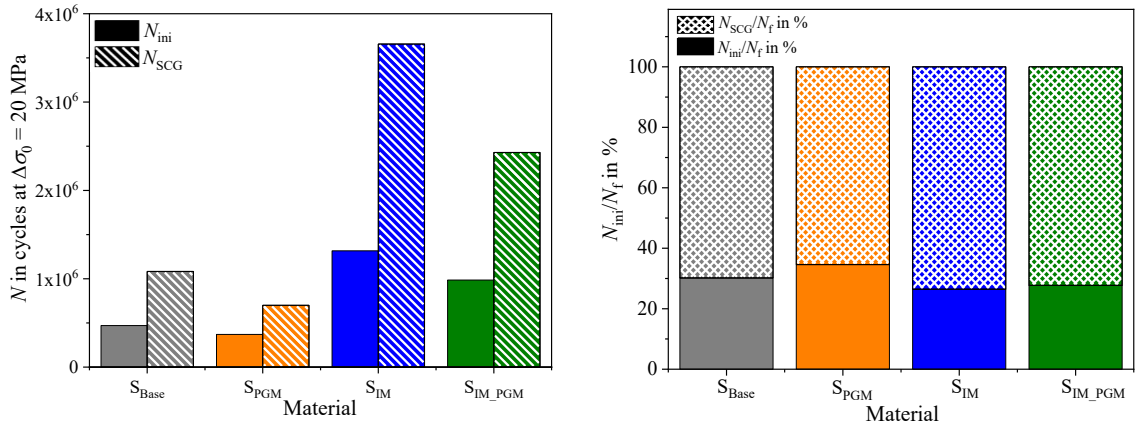

Figure 13: Absolute (a) and relative (b) changes in crack initiation and SCG behavior at $\Delta\sigma_0 = 20$ MPa with regard to the implementation of additives.

Crack freezing experiments of the systematic PA12 grades at an applied stress of 20 MPa were also performed. Representative images obtained by the transmission light microscope of crack frozen CRB specimens at $N = 10^4$ cycles are given in **Figure 14**a. Experimentally measured plastic zone length l_{pz} was determined and plotted against the corresponding cycle number at which the CRB test was stopped (Figure 14b). Similar to prior observations of H1 to H3, systematic grades exhibit an increase of the plastic zone length at earlier cycle numbers before entering a plateau region prior to crack initiation at approx. 10^3 cycles. This, again indicates a reduction of $\sigma_{ys}(t)$ over time due to time-dependency effects [33]. In contrast to observed l_{pz} results of the homologous series, however, the plastic zone size of systematic grades varies significantly with the implementation of pigments and impact modifiers, as highlighted in Figure 14a and -b. Remarkably, σ_{ys} values obtained from tensile tests scatter in a similar range as in the homologous series, which did not show strong variations in plastic zone size. It appears, that l_{pz} of S_{PGM} or S_{IM_PGM}, however, is much smaller than of S_{Base} and S_{IM}, respectively. Perhaps a higher local stress triaxiality level is

accompanied by the presence of pigments during fatigue loading, which would lead to remarkably higher local yield stresses and thus limited plastic deformation. In case of impact modified grades, the generation of notably large plastic deformation zones as schematically illustrated in **Figure 15** is promoted – l_{pz} yields higher values from beginning of the test towards the point of crack initiation. For S_{IM_PGM} a superposition of both effects, provoked by IM and PGM, occur – the plastic zone size follows again a rule of mixture, resulting in a l_{pz} between that of S_{PGM} and S_{IM} (see Figure 14 and Figure 15).

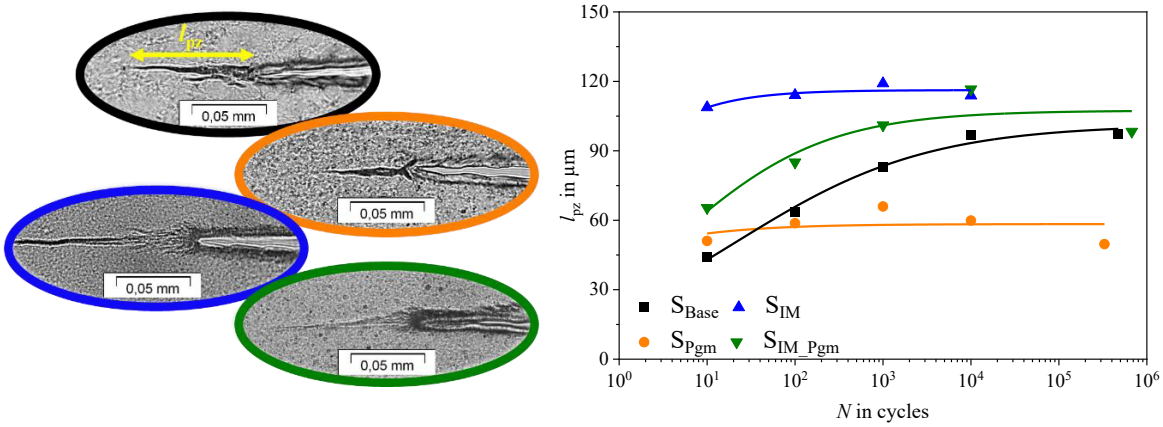

(a) (b)

Figure 14: Representative crack freezing images at $N = 10^3$ cycles (a) and measured plastic zone length l_{pz} (a) of the systematic series at $\Delta\sigma_0 = 20$ MPa.

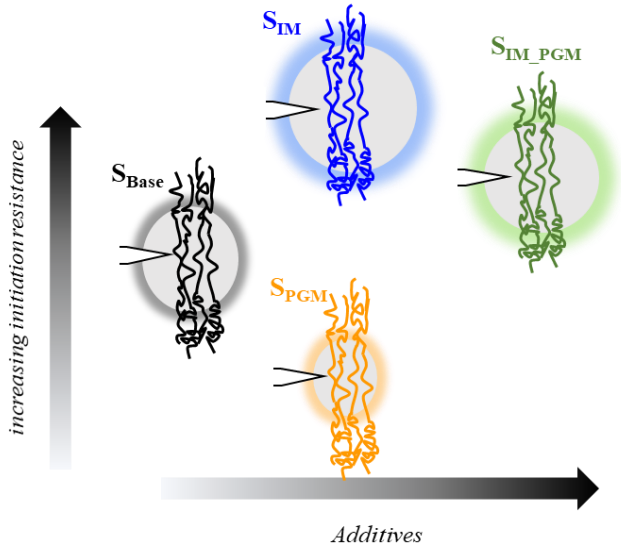

Figure 15: Schematic diagram of crack initiation resistance as a function of different additives implemented in PA12 grades of the same M_W.

As for the homologous series, different estimations of the plastic zone lengths for a governing plane strain (ε_{zz}=0) and plane stress (σ_{zz}=0) state were calculated and plotted

against N in **Figure 16**. All systematic grades show high accordance to predictions made by Irwin´s model of the plastic zone length at plane strain conditions. Based on that, the validity of LEFM approaches may be assumed for selected PA12 grades.

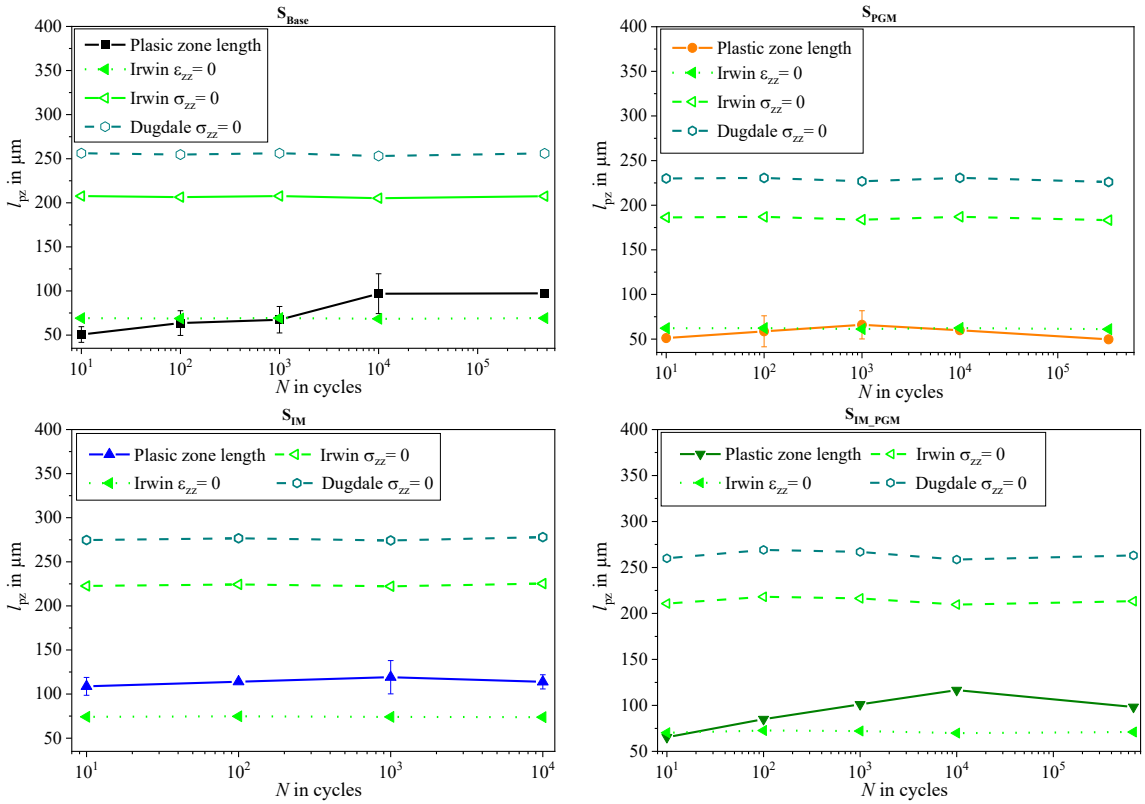

Figure 16: Measured and estimated plastic zone lengths according Irwin and Dugdale for S_{Base}, S_{PGM}, S_{IM}, and S_{IM_PGM}.

5. Conclusion

The present work focuses on the question of how plastic zones and fracture mechanisms in polyamide 12 (PA12) change when the molecular weight (M_W) is increased, or impact modifiers and/or pigments are added. An increase of crack initiation resistance and SCG resistance was generally observed in PA12 with increasing M_W and by the implementation of an impact modifier. A positive influence of higher M_W is attributed to the *hydrogen bond effect* – an increasing disentanglement resistance arises when a critical number of active hydrogen bonds is exceeded. Consequently, the craze breakdown process is significantly delayed due to additional inter- and intra-molecular attraction forces, which have to be overcome. Impact modification, on the other hand, generates remarkably large plastic zones which absorbs large amounts of energy and significantly increases the material's micro-plasticity during SCG. In contrast, the addition of pigments reduces the plastic zone size presumably due to a higher local stress triaxiality level, resulting in a reduction of the

crack initiation resistance. In that context, SCG resistance is also found to decline for pigmented PA12 grades. Fractographic analysis reveal an increasing number of locations at which cracks can be initiated or accelerated alongside the interfaces between polymer matrix and pigments. Finally, it was also demonstrated that Linear Elastic Fracture Mechanics (LEFM) is applicable for the selected PA12 grades. Experimentally measured plastic zone sizes are in good accordance with predicted values of Dugdale's model under a plane strain constraint.

6. Acknowledgement

The research work of this paper was performed at the Polymer Competence Center Leoben GmbH (PCCL, Austria) within the framework of the K1 COMET-program (Grant Nr.: 879785), which is funded by the Federal Ministry for Transport, Innovation and Technology (Austria) and Federal Ministry for Economy, Family and Youth (Austria) with contributions by Evonik Operations GmbH (Germany) and the Montanuniversitaet Leoben (Austria). The PCCL is funded by the Austrian Government and the State Governments of Styria and Upper Austria. Special thanks go to Linda Schatz for the performance of crack freezing experiments and Jutta Geier for fractographic analysis via SEM.

7. References

[1] G. Pinter, F. Arbeiter, and A. Frank, “Fast comparison of different polymeric pipe materials: extending the use of the cyclic CRB-test (ISO 18489),” 2016.

[2] M. Messiha, B. Gerets, J. Heimink et al., “Investigating the influence of changes in molecular structure of polyamide 12 grades on the resistance against Slow Crack Growth,” in *Proceedings PPXX*, 2021.

[3] A. Frank, I. Berger, M. Messiha et al., “Slow crack growth resistance of non-virgin polymers,” in *Proceedings PPXIX,* Plastic Pipe Conference Association, Ed., 2018.

[4] K. Friedrich, “Crazes and shear bands in semi-crystalline thermoplastics,” in *Crazing in Polymers,* H. H. Kausch, Ed., 52-53, pp. 225–274, Springer-Verlag, Berlin/Heidelberg, 1983.

[5] A. Y. Yarysheva, E. G. Rukhlya, L. M. Yarysheva et al., “The structural evolution of high-density polyethylene during crazing in liquid medium,” *European Polymer Journal*, vol. 66, pp. 458–469, 2015.

[6] A. Pawlak and A. Galeski, “Plastic Deformation of Crystalline Polymers: The Role of Cavitation and Crystal Plasticity,” *Macromolecules*, vol. 38, no. 23, pp. 9688–9697, 2005.

[7] A. Pawlak, “Plastic deformation and cavitation in semicrystalline polymers studied by X-ray methods,” *Polimery*, vol. 59, 7/8, pp. 533–541, 2014.

[8] R. A.C. Deblieck, D.J.M. van Beek, K. Remerie et al., “Failure mechanisms in polyolefines: The role of crazing, shear yielding and the entanglement network,” *Polymer*, vol. 52, no. 14, pp. 2979–2990, 2011.

[9] A. M. Donald and E. J. Kramer, “The competition between shear deformation and crazing in glassy polymers,” *Journal of Materials Science*, vol. 17, no. 7, pp. 1871–1879, 1982.

[10] A. M. Donald, “The effect of temperature on crazing mechanisms in polystyrene,” *Journal of Materials Science*, vol. 20, no. 7, pp. 2630–2638, 1985.

[11] N. Brown, “A fundamental theory for slow crack growth in polyethylene,” *Polymer*, vol. 36, no. 3, pp. 543–548, 1995.

[12] G. Pinter, *Rißwachstumsverhalten von PE-HD unter statischer Belastung,* Doctoral Dissertation, University of Leoben, 1999.

[13] F. Arbeiter, B. Schrittesser, A. Frank et al., “Cyclic tests on cracked round bars as a quick tool to assess the long-term behaviour of thermoplastics and elastomers,” *Polymer Testing*, vol. 45, pp. 83–92, 2015.

[14] A. Frank, F. J. Arbeiter, I. J. Berger et al., “Fracture Mechanics Lifetime Prediction of Polyethylene Pipes,” *Journal of Pipeline Systems Engineering and Practice*, vol. 10, no. 1, p. 4018030, 2019.

[15] H. H. Kausch, R. Gensler, C. Grein et al., “Crazing in semicrystalline thermoplastics,” *Journal of Macromolecular Science, Part B*, vol. 38, 5-6, pp. 803–815, 2006.

[16] Y.-L. Huang and N. Brown, “Dependence of slow crack growth in polyethylene on butyl branch density: Morphology and theory,” *Journal of Polymer Science: Part B: Polymer Physics*, vol. 29, no. 1, pp. 129–137, 1991.

[17] H. H. Kausch and R. Bonart, “Polymer physics in germany,” *Journal of Polymer Science: Polymer Letters Edition*, vol. 14, no. 9, pp. 565–568, 1976.

[18] G. H. Michler and F. J. Baltá Calleja, *Nano- and micromechanics of polymers*: *Structure modification and improvement of properties*, Hanser, München, 2012.

[19] A. Chudnovsky, Z. Zhou, H. Zhang et al., “Lifetime assessment of engineering thermoplastics,” *International Journal of Engineering Science*, vol. 59, pp. 108–139, 2012.

[20] M. Messiha, B. Gerets, J. Heimink et al., “Slow crack growth resistance of modern PA-U12 grades measured by cyclic cracked round bar tests and strain hardening tests,” *Polymer Testing*, vol. 86, p. 106468, 2020.

[21] International Standards Organisation (ISO), “Plastics — Determination of tensile properties — Part 2: Test conditions for moulding and extrusion plastics,” 2012, ISO 527-2.

[22] International Standards Organisation (ISO), “Polyethylene (PE) materials for piping systems — Determination of resistance to slow crack growth under cyclic loading — Cracked Round Bar test method,” 2015, no. 18489.

[23] M. Scibetta, R. Chaouadi, and E. van Walle, “Fracture toughness analysis of circumferentially-cracked round bars,” *International Journal of Fracture*, vol. 104, no. 2, pp. 145–168, 2000.

[24] International Standards Organisation (ISO), “Metallic materials — Calibration of extensometer systems used in uniaxial testing,” 2012, ISO 9513.

[25] M. Messiha, A. Frank, T. Koch et al., “Effect of polyethylene and polypropylene cross-contamination on slow crack growth resistance,” *International Journal of Polymer Analysis and Characterization*, pp. 1–18, 2020.

[26] T. L. Anderson, *Fracture Mechanics*: *Fundamentals and Applications, Fourth Edition*, Chapman and Hall/CRC, Boca Raton, 2017.

[27] G. R. Irwin, “Plastic zone near a crack and fracture toughness,” *Sagamaore Conference Research Proceedings,* Vol. 4, pp. 63–78, 1961.

[28] D. S. Dugdale, “Yielding of steel sheets containing slits,” *Journal of the Mechanics and Physics of Solids*, vol. 8, no. 2, pp. 100–104, 1960.

[29] M.Scibetta, R. Chaouadi, E. Van Walle, “Fracture toughness analysis of circumferentially-cracked round bars,” *International Journal of Fracture*, vol. 2000, no. 104, pp. 145–168, 2000.

[30] M. Messiha, A. Frank, F. Arbeiter et al., “How hydrogen bonds influence the slow crack growth resistance of polyamide 12,” *Polymer*, p. 124437, 2021.

[31] D. S. Dugdale, “Yielding of Steel Sheets Containing Slits,” *Journal of the Mechanics and Physics of Solids,* no. 8, 1960.

[32] G. R. Irwin, “Analysis of Stresses and Strains Near the End of a Crack Traversing a Plate,” *Journal of Applied Mechanics*, vol. 24, no. 3, pp. 361–364, 1957.

[33] M. J.W. Kanters, *Prediction of long-term performance of load-bearing thermoplastics,* PhD Thesis, Technische Universiteit Eindhoven, 2015.

[34] F. Arbeiter, G. Pinter, R. W. Lang et al., “Fracture Mechanics Methods to Assess the Lifetime of Thermoplastic Pipes,” in *Deformation and Fracture Behaviour of Polymer Materials,* W. Grellmann and B. Langer, Eds., vol. 247, pp. 33–54, Springer International Publishing, Cham, 2017.

[35] M. Messiha, A. Frank, J. Heimink et al., “Structure-Property Relationships of Polyamide 12 Grades Exposed to Rapid Crack Extension,” *Materials (Basel, Switzerland)*, vol. 14, no. 19, p. 5899, 2021.

[36] W. G. Perkins, “Polymer toughness and impact resistance,” *Polymer Engineering & Science*, vol. 39, no. 12, pp. 2445–2460, 1999.

[37] C. B. Bucknall, “Fracture and failure of multiphase polymers and polymer composites,” in *Failure in Polymers*: *Molecular and Phenomenological Aspects,* H.-J. Cantow, G. Dall'Asta, K. Dušek et al., Eds., vol. 27, pp. 121–148, Springer, Berlin, Heidelberg, 1978.

[38] C. Cheng, A. Hiltner, E. Baer et al., “Deformation of rubber-toughened polycarbonate: Macroscale analysis of the damage zone,” *Journal of Applied Polymer Science*, vol. 52, no. 2, pp. 177–193, 1994.

8.1.4 Publication 4

Bibliographic information:

Title:	**Structure-Property Relationships of Polyamide 12 Grades Exposed to Rapid Crack Extension**
Authors:	Mario Messiha[a], Andreas Frank[a], Jan Heimink[b], Florian Arbeiter[c], Gerald Pinter[c]
Affiliation:	[a] PCCL GmbH, Leoben, Austria [b] Evonik Operations GmbH, Marl, Germany [c] Montanuniversitaet, Leoben, Austria
Processing status:	published
DOI:	https://doi.org/10.3390/ma14195899

Relevant contributions to this publication:

Conceptualization:	Mario Messiha (70 %), Florian Arbeiter (15 %), Gerald Pinter (15 %)
Methodology:	Mario Messiha (70 %), Jan Heimink (30 %)
Validation:	Mario Messiha (40 %), Jan Heimink (15 %), Andreas Frank (15 %), Florian Arbeiter (15 %), Gerald Pinter (15 %)
Investigation:	Mario Messiha (80 %), Jan Heimink (20 %)
Writing – Original Draft:	Mario Messiha (100 %)
Writing – Review & Editing:	Mario Messiha (40 %), Jan Heimink (15 %), Andreas Frank (15 %), Florian Arbeiter (15 %), Gerald Pinter (15 %)
Supervision:	Andreas Frank (30 %), Florian Arbeiter (30 %), Gerald Pinter (40 %)

materials

MDPI

Article

Structure-Property Relationships of Polyamide 12 Grades Exposed to Rapid Crack Extension

Mario Messiha [1,*], Andreas Frank [1], Jan Heimink [2], Florian Arbeiter [3] and Gerald Pinter [3]

[1] PCCL GmbH, 8700 Leoben, Austria; andreas.frank@pccl.at
[2] Evonik Operations GmbH, 45772 Marl, Germany; jan.heimink@evonik.de
[3] Department Polymer Engineering and Science, Montanuniversitaet, 8700 Leoben, Austria; florian.arbeiter@unileoben.ac.at (F.A.); gerald.pinter@unileoben.ac.at (G.P.)
* Correspondence: mario.messiha@pccl.at

Abstract: Thermoplastic materials have established a reputation for long-term reliability in low-pressure gas and water distribution pipe systems. However, occasional *Slow Crack Growth* (SCG) and *Rapid Crack Propagation* (RCP) failures still occur. SCG may initiate only a small leak, but it has the potential to trigger RCP, which is much rarer but more catastrophic and destructive. RCP can create a long, straight or meandering axial crack path at speeds of up to hundreds of meters per second. It is driven by internal (residual) and external (pressure) loads and resisted by molecular and morphological characteristics of the polymer. The safe installation and operation of a pipe throughout its service lifetime therefore requires knowledge of its resistance to RCP, particularly when using new materials. In this context, the RCP resistance of five different polyamide (PA) 12 grades was investigated using the ISO 13477 *Small-Scale Steady State* (S4) test. Since these grades differed not only in molecular weight but also in their use of additives (impact modifiers and pigments), structure-property relationships could be deduced from S4 test results. A new method is proposed for correlating these results more efficiently to evaluate each grade using the crack arrest lengths from individual S4 test specimens.

Keywords: small-scale steady state (S4) test; rapid crack propagation (RCP); polyamide 12; structure-property relationships; strain-rate effects

Citation: Messiha, M.; Frank, A.; Heimink, J.; Arbeiter, F.; Pinter, G. Structure-Property Relationships of Polyamide 12 Grades Exposed to Rapid Crack Extension. *Materials* **2021**, *14*, 5899. https://doi.org/10.3390/ma14195899

Academic Editor: Aleksander Muc

Received: 2 September 2021
Accepted: 4 October 2021
Published: 8 October 2021

1. Introduction

To determine the resistance against *Rapid Crack Propagation* (RCP) of newly developed plastic pipe grades, the *Full-Scale* (FS) test, standardized in ISO 13478, has become the "gold standard" for product qualification. It measures a critical pressure value ($p_{c,FS}$) above which RCP can occur under operating conditions for pressurized pipes in service. However, it requires 25 m long pipe specimens of up to 500 mm diameter. Since several FS tests are needed to evaluate the RCP behavior of a given material, this method is expensive and time-consuming.

These disadvantages were mitigated by the development of an accelerated laboratory test, the so-called *Small-Scale Steady State* (S4) test standardized for thermoplastic pipes in ISO 13477 [1]. The S4 test initiates a rapid crack in a pipe sample only 7 to 8 pipe diameters (D) long. As in the FS test, pipes are tested at a specific temperature (e.g., 0 °C) and pressurized with air. RCP is initiated by the impact of a chisel-ended striker close to one end of the pipe. To prevent excess flaring of the pipe walls while allowing the compressed air to escape freely, a rigid cage surrounds the sample, while internal baffles retard axial decompression and ensure a relatively steady pressure in each compartment between them [2].

The result of each S4 test is classified as *propagation* if the crack extends to a length a within the gauge section of at least $4.7D$, or *arrest* if $0.7D < a < 4.7D$. Cracks shorter than 70% of a pipe's diameter are regarded as being too highly influenced by gauge section

end effects, e.g., insufficient internal gas volume. A series of S4 tests can determine either a *critical pressure* ($p_{c,S4}$) for pipe at a specified temperature or a *critical temperature* at a specified pressure (Figure 1). In either case, however, *false arrest* points can appear within the propagation regime (see Figure 1) resulting in a bell-shaped (*cloche*) crack-length curve and complicating the evaluation of critical pressure or temperature [2].

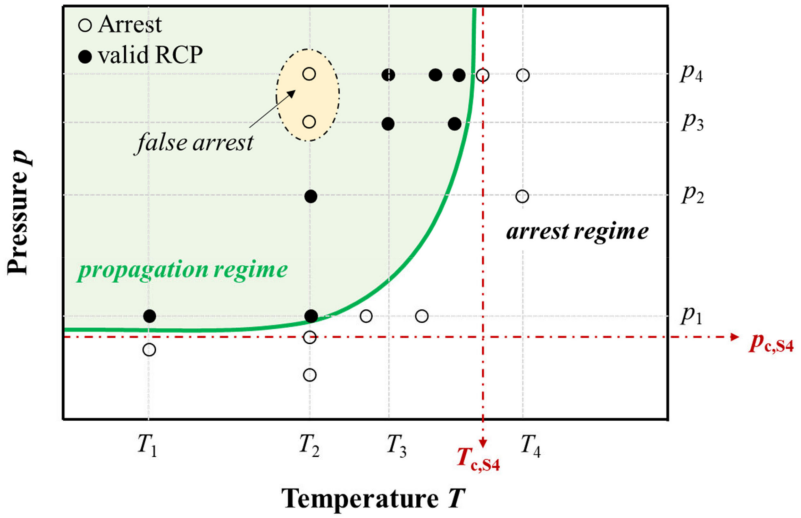

Figure 1. Schematic of crack propagation and arrest regimes for RCP during S4 testing as well as false arrest points within the propagation regime (according to [3]).

The present work developed a more efficient procedure for characterizing the RCP behavior of morphologically different PA12 grades. Various S4 tests were carried out to characterize critical RCP/crack arrest transition temperatures and pressures, and to more securely establish structure-property relationships. To better understand underlying physical processes, detailed post-mortem examination of fracture surfaces was carried out.

2. Experimental

The five PA12 grades selected for this study (Figure 2) were part of a systematic series of unplasticized grades that differed primarily in their molecular weight (M_W) and/or the use of specific additives, such as an impact modifier (IM) or an inorganic pigment (PGM). Four of the five grades, coded with the letter "C", are highly viscous compounds based on PA12-0 (Figure 2). C3-nc is a natural colored (nc) compound without impact modification. Adding an IM to it yields C4-im-nc, while additional coloration results in C2-im-pgm. Finally, C5-im-pgm can be viewed as a derivative of C2-im-pgm, modified to increase molecular weight.

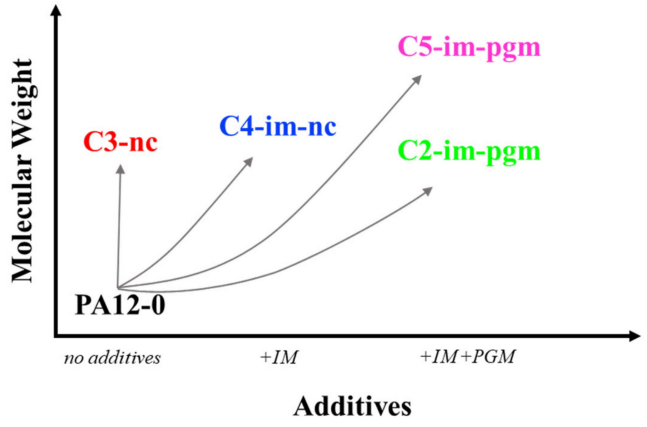

Figure 2. Systematically developed series of unplasticized PA12 grades.

Weight average molecular mass M_w was measured using Size Exclusion Chromatography (SEC). Samples taken from extruded pipes of the given materials were dissolved in hexafluoroisopropanol (HFIP) and potassium–trifluoroacetate at room temperature. Table 1 summarizes relevant properties of the selected materials; for clarity, M_w values are normalized against that of PA12-0.

Table 1. Basic characterization of selected PA12 grades.

Material	IM	PGM	$M_{W,rel}$
PA12-0	–	–	1.0
C2-im-pgm	+	+	1.2
C3-nc	–	–	1.4
C4-im-nc	+	–	1.5
C5-im-pgm	+	+	1.6

Each grade was first characterized for RCP resistance using the S4 test according ISO 13477 [1]. Extruded pipe specimens with a length of 835 mm, an outer diameter of D = 110 mm and a Standard Dimension Ratio (SDR) 11 were used. Applied pressures ranged from 1.5 bar to 8 bar at temperatures between 0 °C and 45 °C and the impact speed was 16 m/s. Furthermore, a newly modified data evaluation process, which additionally accounts for the crack length a in relation to the to the maximum possible crack length (a_{max}) of 758 mm (i.e., from the center of the impact position to the end of the gauge length), is suggested. Fracture surfaces were studied using a Tescan Vega II Scanning Electron Microscope (Tescan Brno, Brno, Czech Republic).

3. Results and Discussion

Critical pressure results for the five PA12 grades are shown in Figure 3. Solid symbols represent tests with valid RCP initiation according to ISO 13477 [1], while hollow symbols represent valid RCP arrests. At T = 0 °C, the grades can be grouped as follows:

1. Those with low critical pressures of ~3.2 bar: these include neat PA12-0 as well as C2-im-pgm;
2. Those with slightly higher $p_{c,0°C}$ values of 4.1–4.4 bar: C4-im-nc and C5-im-pgm; and
3. C3-nc, having the remarkably high $p_{c,0°C}$ of ~8 bar.

At temperatures above 20 °C the critical RCP pressure increases significantly for all materials tested. Only PA12-0 still exhibited valid RCP at T > 25 °C and pressures of up to 12 bar, with no crack arrest seen even at 45 °C—which exceeds the T_g (40 °C). This indicates a very high critical S4 temperature $T_{c,S4}$ and very poor RCP resistance. Compounded grades, on the other hand, exhibit $T_{c,S4}$ values of around ambient temperature.

The chain lines shown for each material in Figure 3 sketch boundaries between RCP arrest and propagation regions. However, there are not enough data points to identify for every material, with adequate precision, either an ISO 13477 [1] critical pressure at a given temperature (e.g., C3-nc at T = 0 °C) or a critical temperature at a given pressure (e.g., PA12-0 and C5-im-pgm at p = 12 bar). To do so, as Figure 2 illustrates schematically for just one material, a significant number of additional tests would be needed.

To maximize the data yield from each test the measured arrest length of each crack was processed numerically, as well as being classified as arrest/propagation (see Figures 4 and 5). Plotting at least three crack lengths as a function of test pressure at a given temperature (e.g., at 0 °C, Figure 4) allows the critical pressure to be extrapolated by linear regression. For example, instead of starting at extreme pressures and successively decreasing the applied p at a constant T to obtain the point of transition from RCP to crack arrest, it is proposed to test first at very low p and then at very high p. The critical S4 pressure point can then be estimated by intra- or extrapolation and refined successively by additional intermediate tests. If possible, it is recommended to base the linear regression primarily on data points between $0.7D < a < 4.7D$, in order to avoid effects from initiation as well as reflection of decompression waves and end-cap constraints.

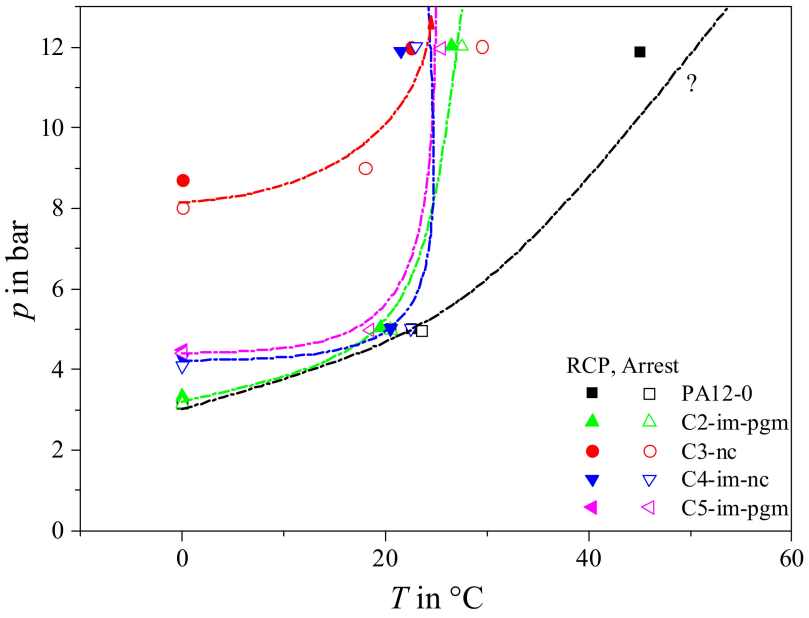

Figure 3. RCP characteristics of various PA12 grades measured via S4 tests.

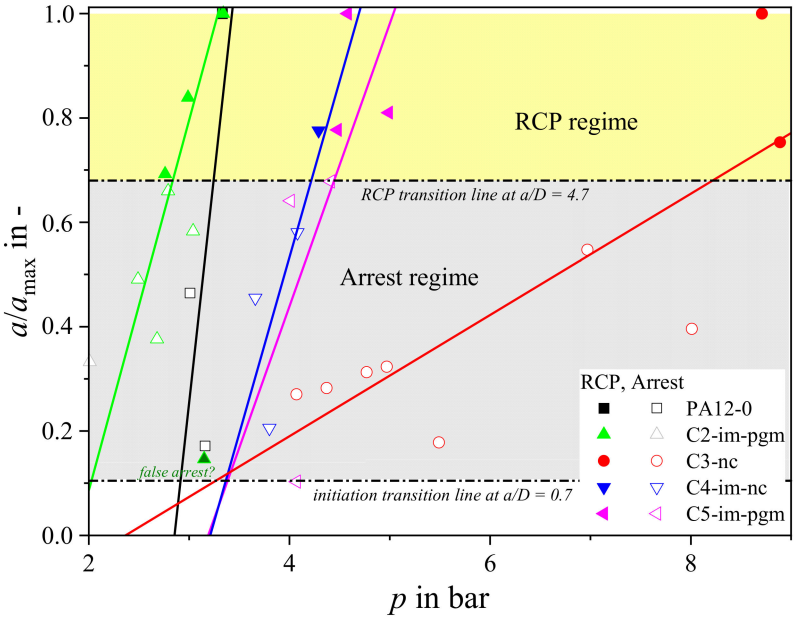

Figure 4. Modified evaluation of the critical pressure values of all grades at 0 °C.

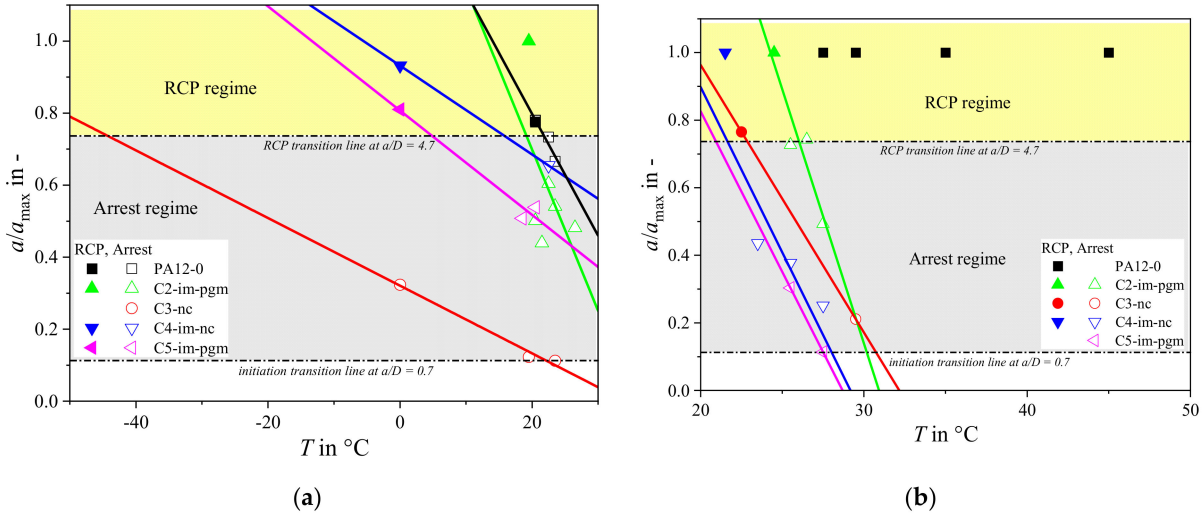

Figure 5. Modified evaluation of the critical temperature values of all grades at (**a**) 5 bar and (**b**) 12 bar.

Using this method yielded slightly different $p_{c,0°C}$, $T_{c,5bar}$, and $T_{c,12bar}$ values (Figures 5 and 6) from those using the ISO standard method. Each grade except PA12-0 could be characterized at 0 °C, 5 bar, and 12 bar (Figure 5b). The use of crack length data also makes it easier to exclude false arrest points that might significantly affect the critical pressure result (e.g., C2-im-pgm in Figure 4).

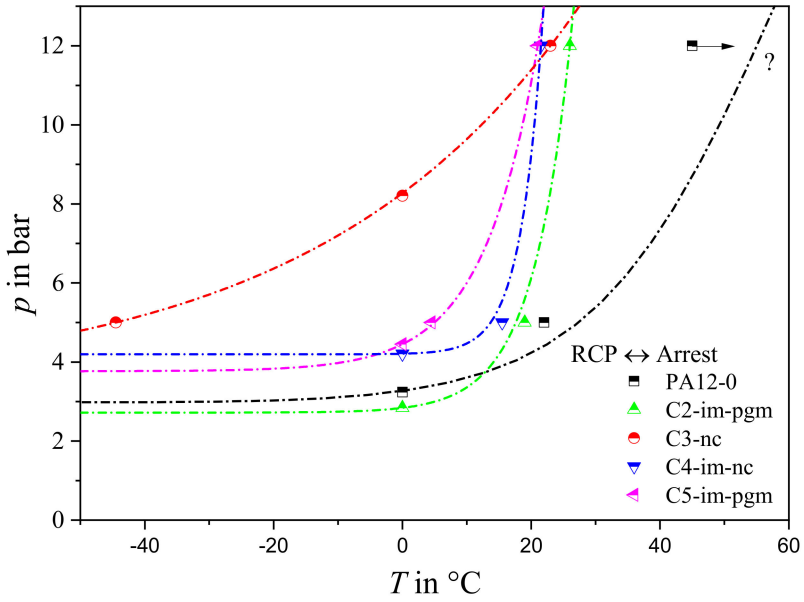

Figure 6. Rapid fracture behavior of PA12 grades as acquired from S4 tests according to the modified evaluation with predicted RCP/crack arrest transition points.

Table 2 compares transition values obtained using this method with those from the ISO standard procedure. Clearly the same amount of S4 test data can now yield more $T_{c,5bar}$ and $T_{c,12bar}$ values.

Table 2. Standard evaluation according ISO 13477 vs. modified evaluation of S4 test data.

Material	ISO 13477			Modified S4 Evaluation		
	$p_{c,0°C}$ (bar)	$T_{c,5bar}$ (°C)	$T_{c,12bar}$ (°C)	$p_{c,0°C}$ (bar)	$T_{c,5bar}$ (°C)	$T_{c,12bar}$ (°C)
PA12-0	3.16	22.5	*	3.24	22	*
C2-im-pgm	3.15	20.5	27.5	2.84	19	26
C3-nc	8.01	*	22–29.5	8.21	−44.5	23
C4-im-nc	4.08	22.5	23	4.22	15.5	21.5
C5-im-pgm	4.41	*	*	4.45	4.5	21

* No RCP/crack arrest transition detectable at given pressure or temperature levels.

Transition temperatures extrapolated using crack length measurements are plotted in Figure 6. Except for PA12-0—having only two transition point data—transition lines were determined via exponential fitting, allowing standard S4 failure lines to be extended beyond the test data envelope (e.g., $T_{c,5bar}$ of C3-nc). The two evaluation methods yield very similar results (cf. Figures 3 and 6) showing that PA12-0 and C2-im-pgm fall short of the remaining compounds, becoming susceptible to RCP at lower applied pressures. While C2-im-pgm becomes resistant to RCP above ambient temperature, PA12-0 remains susceptible over a wider temperature range. In contrast, C3-nc exhibits an extraordinary RCP resistance. At T = 0 °C, RCP only occurs at much higher pressures than in the other grades. This implies that significantly increasing M_W by compounding (e.g., from PA12-0 to C3-nc, Figure 2) benefits RCP resistance. Krishnaswamy et al. [4] and Argyrakis [3] reported similar observations for PE-HD: high molecular weight and narrow molecular weight distributions appear to be important to superior RCP resistances in PE-HD.

In contrast, comparing C3-nc and C4-im-nc indicates that impact modifier has a negative effect on RCP resistance. Rubbers are widely used to toughen polymers in critical applications that might expose them to impact loads. In theory, the soft particles absorb much of the input impact energy, either by stretching the rubbery material, or by promoting multiple crazing, shear yielding or the combination of both [5]. The contribution of each mechanism to toughen the rubber-matrix system depends on a number of variables, such as the rubber particle size, distribution and concentration [6]. However:

(1) Impact modifiers generally increase the *initiation resistance* $G_{Ic}(t)$ to rapid loading of a crack but do not influence resistance to its propagation [7–10];
(2) Impact modifiers are themselves time-dependent elastomers undergoing significant strain-rate hardening [5,10,11].

It can, therefore, be assumed that rubber particles have enough time during static and quasi-static load conditions (i.e., low and moderate local strain rates) to plastically deform and cavitate, enhancing the resistance to (quasi-) static crack initiation G_{Ic} through extensive shear yielding or multiple crazing phenomena. If the applied (quasi-) static crack driving force G reaches the critical G_{Ic} a crack starts to extend at low crack speeds $\dot{a}$. Thereby, low crack opening strain rates prevail at areas surrounding the crack tip, so that incorporated elastomers get easily strained and continue to absorb large amounts of energy even during slow crack extension [5]. In contrast, a structure exposed to highly dynamic, time-dependent load conditions $G(t)$ experiences local deformations at extremely high rates. Once $G(t)$ becomes equal to or bigger than the time-dependent initiation fracture toughness $G_{Ic}(t)$ of a rate-sensitive material, a rapid crack is initiated. In that context, time t is substitutable with the applied impact speed v during an abrupt loading. Considering Figure 7, it becomes clear why an improvement of fracture initiation properties due to rubber toughening of rate-sensitive plastics is ineffective at very high impact speeds (e.g., S4 tests). As $G_{Ic}(v)$ is possibly reduced to a minimum value [12], the fundamental rapid fracture resistance of different pipe grades during S4 testing at 16 m/s load speed can be considered to be primarily dependent on the dynamic crack propagation resistance $G_{Id}(\dot{a})$ after crack initiation.

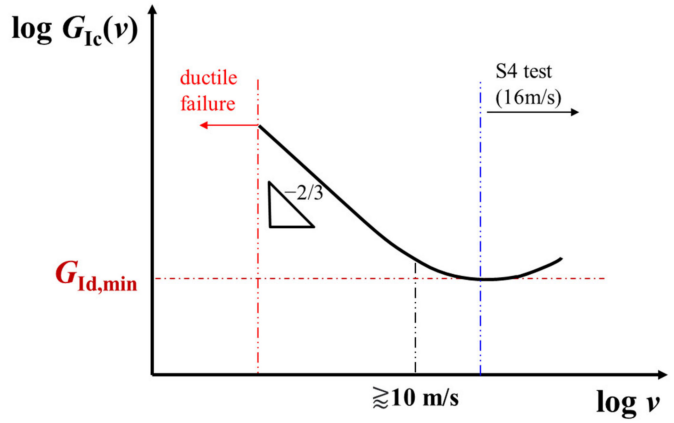

Figure 7. Schematic illustration of a time-dependent initiation energy release rate $G_{Ic}(v)$ as a function of the load rate v for rate-sensitive materials with dominating embrittlement (in accordance to [13]).

Subsequently, the soft rubber parts of the microstructure at the vicinity of the fast-running crack tip have no time to follow the governing local crack opening deformations. Even worse, bearing the time-temperature principle in mind, it may be well suggested that elastomeric parts could pass through the glass transition when a critical local strain rate is exceeded, which is equivalent to the rubber's T_g or tough-brittle transition temperature (T_{TB}). In that case, the hardened rubber particles might act as additional stress concentrators, at which rapid cracks initiate and propagate more easily. As a result, the incorporation of toughers may feature a significant reduction of the RCP resistance during S4 testing [10]. This hypothesis is validated by the S4 results of C3-nc and C4-im-nc, where the systematic addition of an IM leads to remarkably lower critical $p_{c,S4}$ values (Figure 6).

On the same basis, the pigmentation of materials exposed to crack driving forces can correspond to the addition of inherent defects and localities of stress concentrations at which cracks are preferentially launched. Several studies confirm that the improvement of esthetical properties of different materials by coloration is often accompanied by significant reductions of their fracture toughness [14–17]. In that manner, the addition of an inorganic pigment to C4-im-nc resulting in C2-im-pgm, yields to a further decrease of $p_{c,S4}$ from approximately 4.2 to 3.2 bar (or even less, if false arrests are accounted for). Simultaneously, the critical $T_{c,S4}$ is slightly shifted towards higher values—from 23 °C to 27.5 °C—which further affirms the rather negative impact of coloration on rapid fracture behavior. Finally, C5-im-pgm, which equals a high-molecular weight C2-im-pgm, achieves improved $p_{c,S4}$ values of 4.5 bar and slightly lower $T_{c,S4}$ values of 25 °C. This corresponds to the counterbalancing effect of an enhanced M_w on a material's RCP resistance.

Studying the overall shape of the S4 failure regimes presented in Figure 6 it can also be seen that both grades, which do not contain a rubber part, exhibit a successive increase of RCP resistance with rising temperatures. In contrast, the three impact modified grades hardly show any kind of improvement in terms of RCP resistance with increasing temperatures up to 0 °C. However, once a critical temperature around 10–20 °C is reached, the impact modifier seems to go through a brittle-tough transition at underlying strain rates and quickly transfers from an inherent defect to an energy absorber, explaining the rather sharp transition observed in S4 results of C2-im-pgm, C4-im-nc, and C5-im-pgm.

Fracture surfaces of S4 tested PA12 samples are presented in Table 3. Macroscopic overview images of all grades (Table 3a) reveal a major difference between the general fracture appearance of non-toughened and toughened grades. Basically, non-toughened grades PA12-0 and C3-nc exhibit a very rough surface, with structural discrepancies. Contrarily, PA12 grades with integrated soft particles present smoother fracture surfaces. Furthermore, a distinction between two noticeable microscopic structures can be made for all grades: regions of distinctive *river lines* that look like deep carvings inside the fractured surfaces (Table 3b), as well as a dominating flat failure region (often denoted as mirror zone [18]), which appears featureless at low magnification images (Table 3c). At this mirror

zone intense crack acceleration might be expected, regardless of the imposed load rate. Although river lines are commonly observed on RCP fracture surfaces [3,19], no universal theory could be found, describing how this river pattern of radiating lines is caused. Basically, river lines are believed to originate from the interconnection of micro-cracks at different fracture surface levels of cleavage plains with different orientations with the main fracture plane [20]. Hayes et al. [21] observed river markings to be more pronounced if polymers experience a mixed mode loading, in particular Mode I and Mode III. As the main crack moves across the component, micro-cracks coming from different cleavage planes have to rotate to keep the continuity of RCP. Thus, river markings are dependent on the micro-structure of the material and become significantly prominent with increasing Mode III [20,21]. From Table 3b it can be seen, that river lines also vary on a microstructural scale. Particularly, C4-im-nc and C5-im-pgm display a spherulite-like marking of different sizes around river lines, which may be provoked by either the incorporated IM or pigment. Surprisingly, the structure of C2-im-pgm is quite similar to that of C3-nc, which does not contain IM or pigments. A magnified view on the featureless fracture region (compare Table 3a–c) reveals a reversed tendency with regard to aforementioned macroscopic fracture appearances. In that context, PA12 grades that contain an impact modifier highlight a very coarse surface with many irregularities and bumps, especially in combination with color pigments (i.e., C2-im-pgm and C5-im-pgm), whereas PA12-0 and C3-nc are relatively smooth in comparison.

In order to analyze the aforementioned river lines more deeply, the scanning electron beam used during SEM measurements was angled about 45°–52° to fracture surface. In doing so, it became possible to take a closer look underneath river markings on RCP fracture surfaces. An evident fibrillation was found beneath each observed river line in almost all grades—an example of C2-im-pgm is given in Figure 8a. Principally, there are two major views, advocated in the scientific community, with regard to the actual failure mechanism during rapid fracture events. The first perspective considers chain scission of covalent backbone bonds as dominant failure mechanism as reported by Donald and Kramer [22,23], Plummer and Kausch [24], as well as Deblieck [25]. This position is based on the fact that the crack speed is too high to promote chain reptation and subsequent disentanglement. The second viewpoint, however, considers chain disentanglement to be still the dominant mechanism, as it is the case for slow crack growth (SCG) [22,23,26–29]. In contrast to SCG, however, which is guided by mechanical creep and chain slipping against secondary forces (e.g., van der Waal, hydrogen bonds, etc.) of neighboring chains, chain disentanglement is assumed to be promoted by additional adiabatic heating processes [12,30–32] during fast fractures. The idea of a thermal decohesion mechanism during RCP assumes that adiabatic conditions are certainly obtained at high crack speeds due to the low thermal conductivity of polymers. This was reported by Leevers [12] for PE-HD, but also for brittle bulk metallic glass that exhibited a maximum crack velocity of ~800 m/s [33]. Considering Figure 8a, such fibrillated structures seem to be highly improbable, if RCP is solely governed by chains scission. Yet, an adiabatic decohesion mechanism [12,30,32], would predict thermo-mechanically activated fibrillation and cavitation. In agreement with aforementioned fundamental observations of river markings, a conceivable explanation for river lines in PA12 could be that they were regions of rapidly extending crack fronts, which eventually stopped at an instance of time, before jumping into a neighboring crack plane (Figure 8b). Reason therefore could be the superposition of different reflected stress waves at the crack tip, varying stress triaxiality levels along the thickness of the pipe, as well as inhomogenously distributed weak points (e.g., crystal defects, contaminations, pigments or hardened impact modifiers). Only if adiabatic decohesion is governing RCP on a molecular level, the abrupt change of the main crack plane would leave behind a ridge of fibrillar structures, that is not able to continue participating in the physical crack extension by thermal decohesion [12,30,32]. With a new hot craze-crack front passing by in a "new" main crack plane, fibrils beneath river lines solidify, freezing in the observed structures in Figure 8a.

Table 3. Fracture surface analysis of S4 tested PA12 pipe fragments via SEM: macroscopic overview (a), river line regions (b) and brittle rapid fracture regions (c).

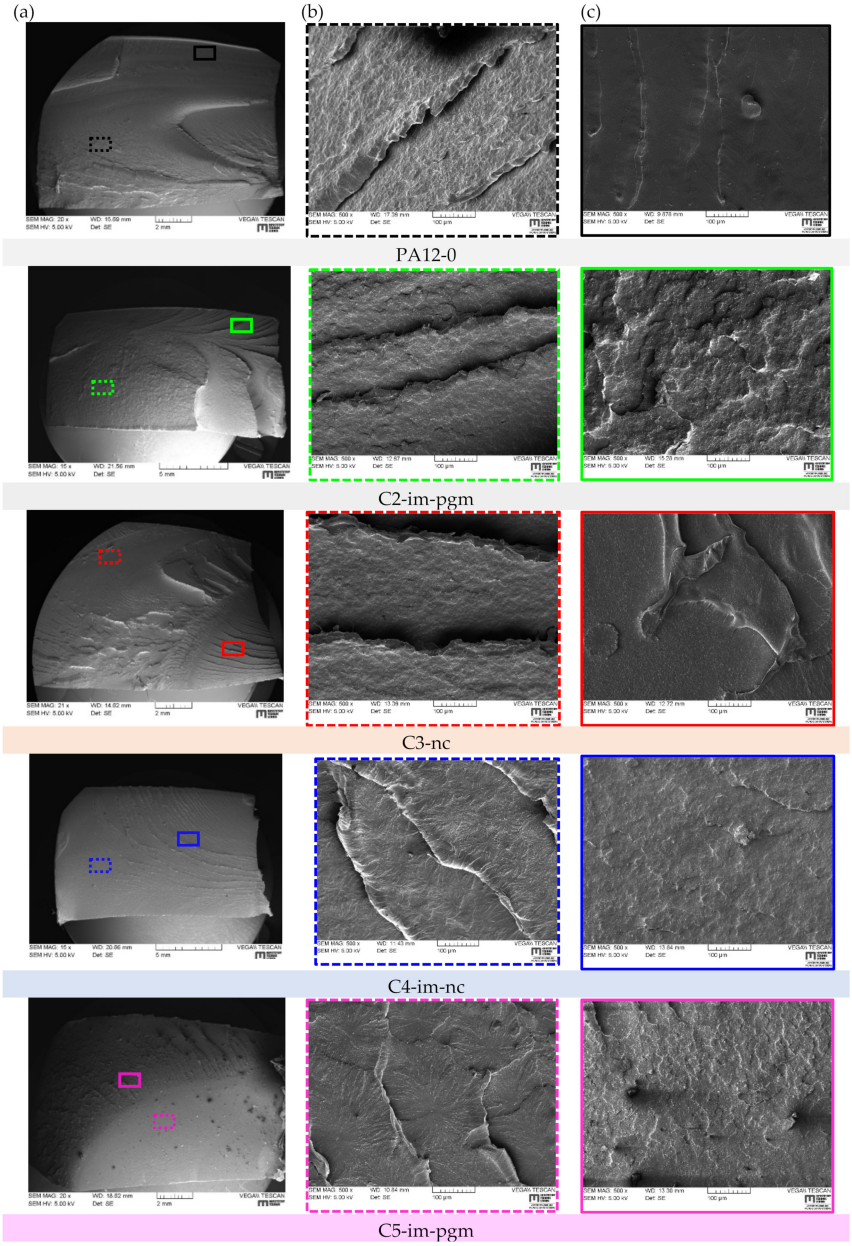

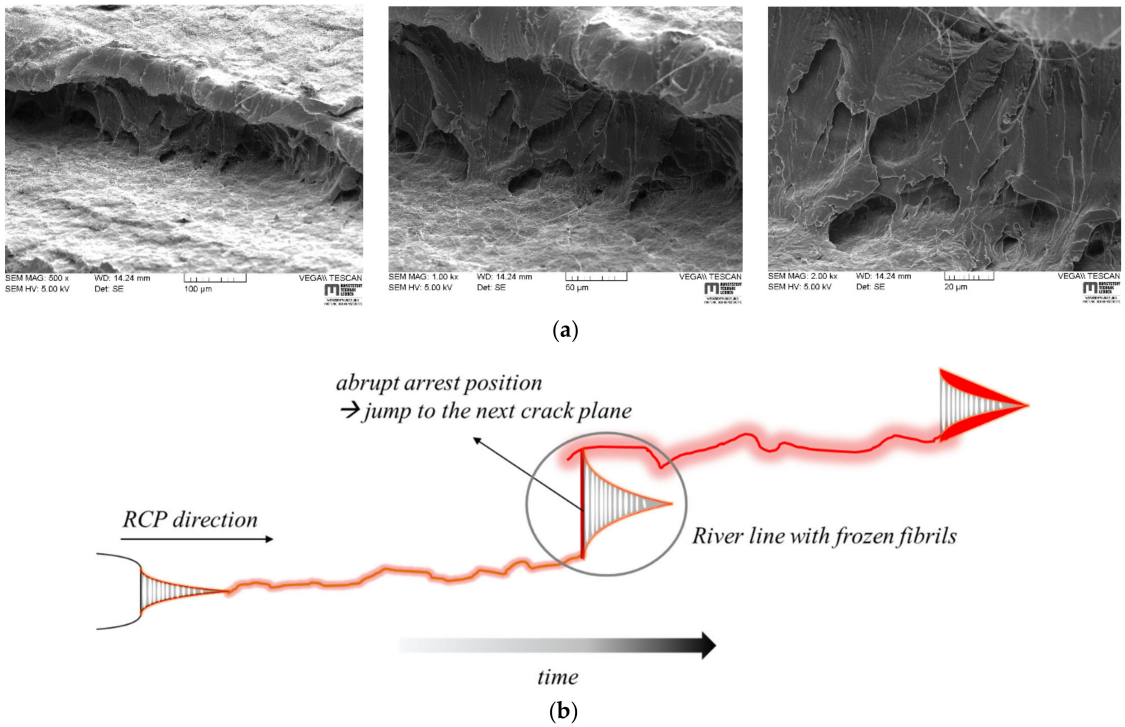

Figure 8. Fibrillar structures beneath river lines with increasing magnification (**a**) and schematic representation of how these structures could have evolved (**b**).

Another feature indicating the presence of high temperature localities during RCP might be seen in uniform-width, almost-straight lines fibrillar structures that could be observed on the high-magnification images of most PA12 grades (Figure 9). The length of this thin fibrils deviates from nano-meter to micro-meter scale, whereas the thickness remains essentially constant (about a few hundred nano-meters). At the current stage it is not clear how these structures were built and why they did not collapse back into the melt layer, if an adiabatic decohesion mechanism is true for RCP fractured PA12 grades (e.g., as thermoplastic fibers would do in the hot air stream from a hair-dryer). However, it is clear, that huge amounts of thermal energy are necessary to drain these very thin structures from a craze zone or the bulk during fracture. Additionally, perhaps if they were thicker they would contract back to the melt zone, because they would retain heat for long enough to do so, yet, due to their very thin nature solidification may occur very fast [34].

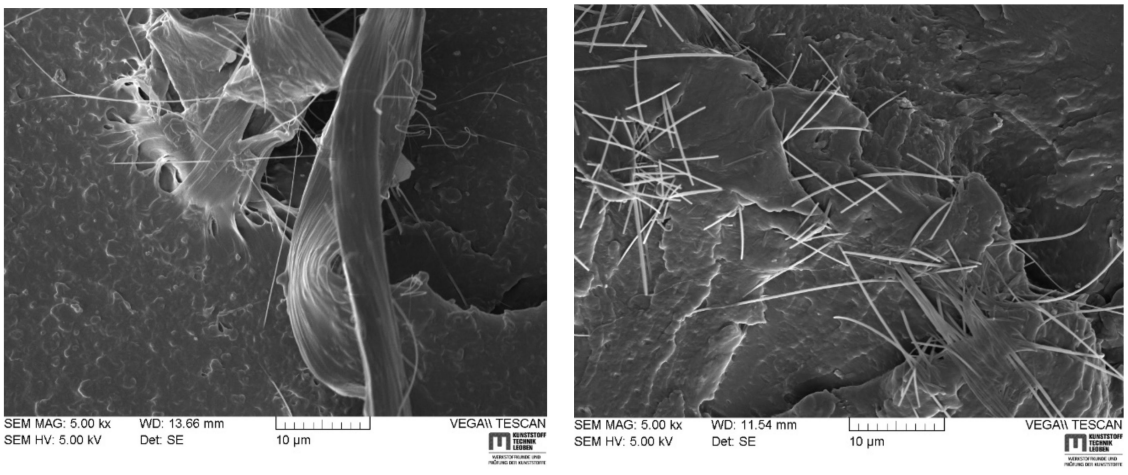

Figure 9. Characteristic macro—(left) and micro-fibrillar (right) structures found in all PA12 grades along the crack path after rapid fracture.

4. Conclusions and Outlook

This study has highlighted relevant structure-property relationships regarding the resistance against *Rapid Crack Propagation* (RCP) in morphologically different polyamide (PA) 12 grades. The RCP performance was measured using the *Small-Scale Steady State* (S4) test according to ISO 13477. An obvious improvement of the RCP resistance was observed with increasing molecular weight M_W, while the incorporation of inorganic pigments reduced the rapid fracture toughness of PA12. Furthermore, rubber-toughening of PA12 grades was also found to decrease the RCP resistance, due to underlying strain-rate effects. In contrast to the general believe that chain scission mechanism is governing physical processes on a molecular scale during RCP, fractographic analysis of S4 fractured pipe samples indicate the existence of high temperature, probably due to adiabatic conditions. In this regard the present work may be viewed as the first step to explain the complex relationship between rapid fracture performances of PA12 grades and underlying fracture mechanisms, such as thermo-mechanical chain disentanglement by means of adiabatic decohesion. Another key element of this research was the proposal of a novel evaluation concept of the S4 test results to improve the determination of critical temperature and pressure values on the basis of a significantly reduced amount of S4 tests.

Author Contributions: M.M.: Conceptualization, Methodology, Investigation, Data curation, Writing—original draft, Project administration. A.F.: Supervision, Writing—review & editing. J.H.: Resources, Funding acquisition, Writing—review & editing. F.A.: Supervision, Writing—review & editing. G.P.: Supervision, Writing—review & editing. All authors have read and agreed to the published version of the manuscript.

Funding: This research was funded by the Austrian Government and the State Governments of Styria and Upper Austria within the framework of the COMET-program of the Federal Ministry for Transport, Innovation and Technology (Austria) and Federal Ministry for Economy, Family and Youth (Austria).

Acknowledgments: Research work of this paper was performed at the Polymer Competence Center Leoben GmbH (PCCL, Austria) with contributions by Evonik Operations GmbH (Germany) and the Montanuniversitaet Leoben (Austria).

Conflicts of Interest: The authors declare no conflict of interest.

References

1. International Standards Organisation (ISO). *Thermoplastics Pipes for the Conveyance of Fluids—Determination of Resistance to Rapid Crack Propagation (RCP)—Small-Scale Steady-State Test (S4 Test)*; International Standards Organisation (ISO): Geneva, Switzerland, 2008.
2. Yayla, P. Rapid Crack Propagation in Polyethylene Gas Pipes. Ph.D. Thesis, Imperial College of Science, Technology and Medicine, London, UK, January 1991.
3. Argyrakis, C. Models for designing pipe-grade polyethylenes to resist rapid crack propagation, Ph.D. Thesis, Imperial College London, London, UK, March 2010.
4. Krishnaswamy, R.K.; Leevers, P.S.; Lamborn, M.J.; Refister, D.F.; Sukhadia, A.M. Rapid Crack Propagation (RCP) Failures in HDPE Pipes: Structure-Property Investigations. *Polym. Eng. Sci.* **2005**, *10*, 3152–3156. [CrossRef]
5. Perkins, W.G. Polymer toughness and impact resistance. *Polym. Eng. Sci.* **1999**, *39*, 2445–2460. [CrossRef]
6. Walker, I.; Collyer, A.A. Rubber toughening mechanisms in polymeric materials. In *Rubber Toughened Engineering Plastics*; Collyer, A.A., Ed.; Springer: The Netherlands, Dordrecht, 1994; pp. 29–56. [CrossRef]
7. Fond, C.; Schirrer, R. Influence of crack speed on fracture energy in amorphous and rubber toughened amorphous polymers. *Plast. Rubber Compos.* **2001**, *30*, 116–124. [CrossRef]
8. Fond, C.; Schirrer, R. Dynamic fracture surface energy values and branching instabilities during rapid crack propagation in rubber toughened PMMA. *Comptes Rendus de l'Académie des Sciences—Series IIB—Mechanics* **2001**, *329*, 195–200. [CrossRef]
9. Kopp, J.-B.; Schmittbuhl, J.; Noel, O.; Lin, J.; Fond, C. Fluctuations of the dynamic fracture energy values related to the amount of created fracture surface. *Eng. Fract. Mech.* **2014**, *126*, 178–189. [CrossRef]
10. Kopp, J.-B.; Fond, C.; Hochstetter, G. Rapid crack propagation in PA11: An application to pipe structure. *Eng. Fract. Mech.* **2018**, *202*, 445–457. [CrossRef]
11. Siviour, C.R.; Jordan, J.L. High Strain Rate Mechanics of Polymers: A Review. *J. Dyn. Behav. Mater.* **2016**, *2*, 15–32. [CrossRef]
12. Leevers, P.S.; Godart, M.-A. Adiabatic decohesion in a thermoplastic craze thickening at constant or increasing rate. *J. Mech. Phys. Solids* **2008**, *56*, 2149–2170. [CrossRef]

13. Buchar, J. The Effect of Strain Rate Sensitivity on Crack Initiation under Dynamic Loading, in Macro- and Micro-Mechanics of High Velocity Deformation and Fracture. In *IUTAM Symposium on MMMHVDF Tokyo, Japan, 12–15 August 1985*; Kawata, K., Shioiri, J., Eds.; Springer: Berlin/Heidelberg, Germany, 1987; pp. 231–241.
14. Aboushelib, M.N.; de Jager, N.; Kleverlaan, C.J.; Feilzer, A.J. The influence of pigments on the slow crack growth in dental zirconia. *Dent. Mater.* **2012**, *28*, 410–415. [CrossRef]
15. Lodeiro, M.J.; Tomlins, P.E.; Pearce, A. *The Influence of Pigments on the Mechanical Properties of High Density Polythylene (HDPE)*; NPL Report; NPL: Teddington, UK, 2000; CMMT(A)258.
16. Janostik, V.; Senkerik, V. Effect of Pigment Concentration on Mechanical Properties of Polycarbonate. *MATEC Web Conf.* **2017**, *125*, 2052. [CrossRef]
17. Kanu, R.; Chesebrough, M.; Spotts, T. The effects of some organic and inorganic pigments on the tensile and impact properties of injection-molded polypropylene. *J. Mod. Eng.* **2001**, *2*, 1.
18. Hull, D. *Fractography: Observing, Measuring and Interpreting Fracture Surface Topography*; Cambridge University Press: Cambridge, UK, 1999.
19. Moreno, L.; Leevers, P. Effect of axial surface scores on rapid crack propagation in polyethylene pipe. *Plast. Rubber Compos.* **2004**, *33*, 149–154. [CrossRef]
20. González-Velázquez, J.L. *Fractography and Failure Analysis*; Springer International Publishing: Cham, 2018.
21. Hayes, M.D.; Shah, A.R.; Edwards, D.B. *Fractography in Failure Analysis of Polymers*; William Andrew an imprint of Elsevier: Kidlington, Oxford, UK, 2015.
22. Donald, A.M.; Kramer, E.J. The competition between shear deformation and crazing in glassy polymers. *J. Mater. Sci.* **1982**, *17*, 1871–1879. [CrossRef]
23. Donald, A.M. The effect of temperature on crazing mechanisms in polystyrene. *J. Mater. Sci.* **1985**, *20*, 2630–2638. [CrossRef]
24. Plummer, C.J.G.; Kausch, H.H. Semicrystalline Polymers: Fracture Properties. In *Reference Module in Materials Science and Materials Engineering*; Elsevier: Amsterdam, The Netherlands, 2016.
25. Deblieck, R.A.; van Beek, D.; Remerie, K.; Ward, I.M. Failure mechanisms in polyolefines: The role of crazing, shear yielding and the entanglement network. *Polymer* **2011**, *52*, 2979–2990. [CrossRef]
26. Brown, N. A fundamental theory for slow crack growth in polyethylene. *Polymer* **1995**, *36*, 543–548. [CrossRef]
27. Pinter, G. Rißwachstumsverhalten von PE-HD unter statischer Belastung, Ph.D. Thesis, University of Leoben, Leoben, Austria, 1999.
28. Arbeiter, F.; Schrittesser, B.; Frank, A.; Berer, M.; Pinter, G. Cyclic tests on cracked round bars as a quick tool to assess the long term behaviour of thermoplastics and elastomers. *Polym. Test.* **2015**, *45*, 83–92. [CrossRef]
29. Frank, A.; Arbeiter, F.J.; Berger, I.J.; Hutař, P.; Náhlík, L.; Pinter, G. Fracture Mechanics Lifetime Prediction of Polyethylene Pipes. *J. Pipeline Syst. Eng. Pr.* **2019**, *10*, 04018030. [CrossRef]
30. Leevers, P.S. Impact and dynamic fracture of tough polymers by thermal decohesion in a Dugdale zone. *Int. J. Fract.* **1995**, *73*, 109–127. [CrossRef]
31. Leevers, P. Modelling Impact Fracture and RCP Resistance of Thermoplastics from Cohesive Properties. In Proceedings of the Society of Plastics Engineers 2004—Proceedings ANTEC, Chicago, IL, USA, 16–20 May 2004.
32. Leevers, P.; Morgan, R. Impact fracture of polyethylene: A non-linear-elastic thermal decohesion model. *Eng. Fract. Mech.* **1995**, *52*, 999–1014. [CrossRef]
33. Narayan, R.; Tandaiya, P.; Narasimhan, R.; Ramamurty, U. Wallner lines, crack velocity and mechanisms of crack nucleation and growth in a brittle bulk metallic glass. *Acta Mater.* **2014**, *80*, 407–420. [CrossRef]
34. Leevers, P.S.; (Former Researcher at Department of Mechanical Engineering at Imperial College London, London, UK); Messiha, M.; (Researcher at Polymer Competence Center Leoben GmbH, Leoben, Austria). Personal communication, 2020.

8.1.5 Publication 5

Bibliographic information:

Title:	**Mechanisms of rapid fracture in PA12 grades**
Authors:	Mario Messiha[a], Andreas Frank[a], Jan Heimink[b], Florian Arbeiter[c], Gerald Pinter[c]
Affiliation:	[a] PCCL GmbH, Leoben, Austria [b] Evonik Operations GmbH, Marl, Germany [c] Montanuniversitaet, Leoben, Austria
Processing status:	published
DOI:	https://doi.org/10.1016/j.tafmec.2021.103145

Relevant contributions to this publication:

Conceptualization:	Mario Messiha (100 %)
Methodology:	Mario Messiha (100 %)
Validation:	Mario Messiha (40 %), Jan Heimink (10 %), Florian Arbeiter (20 %), Gerald Pinter (20 %)
Investigation:	Mario Messiha (100 %)
Writing – Original Draft:	Mario Messiha (100 %)
Writing – Review & Editing:	Mario Messiha (40 %), Jan Heimink (10 %), Andreas Frank (10 %), Florian Arbeiter (20 %), Gerald Pinter (20 %)
Supervision:	Andreas Frank (20 %), Florian Arbeiter (30 %), Gerald Pinter (50 %)

Theoretical and Applied Fracture Mechanics 117 (2022) 103145

Contents lists available at ScienceDirect

Theoretical and Applied Fracture Mechanics

journal homepage: www.elsevier.com/locate/tafmec

Mechanisms of rapid fracture in PA12 grades

Mario Messiha [a], Andreas Frank [a], Jan Heimink [b], Florian Arbeiter [c,*], Gerald Pinter [c]

[a] PCCL GmbH, Leoben, Austria
[b] Evonik Operations GmbH, Marl, Germany
[c] Chair of Materials Science and Testing of Polymers, Montanuniversitaet Leoben, Austria

ARTICLE INFO

Keywords:
Dynamic fracture
Time–dependent material behavior
Rapid crack propagation
Fracture mechanics
Adiabatic decohesion

ABSTRACT

Evidence is presented for an adiabatic decohesion mechanism of Rapid Crack Propagation (RCP) in polyamide (PA) 12. RCP was induced in pipe specimens using the *Small–Scale Steady–State* (S4) test. Fractography revealed a surface of "flakes" attached to the bulk through highly fibrillated regions. A temperature rise recorded ahead of the propagating crack tip in combination with the observed fracture appearance indicates a thermally activated disentanglement fracture mechanism for PA12 pipe grades. Using mathematical formulations of the adiabatic decohesion model proposed by Leevers, strong correlation was found between S4 test results and a newly defined analytical ranking parameter R^{**}.

1. Introduction & background

Under certain conditions, tough polymers can sustain *Rapid Crack Propagation* (RCP). For gas- and water-pressurized pipe systems, their resistance to RCP is measured using the *Full–Scale* pipe test method – standardized as ISO 13478, which has become the gold standard for product qualification. Because each full-scale pipe test is expensive and time-consuming, a lab–scale *Small–Scale Steady–State* (S4) test was developed and standardized as ISO 13477. However, for the competitive development of new material formulations to improve specific properties, even an S4 test is too slow. Material developers need either a relatively simple batch test, or an accessible and reliable model for *virtual* RCP testing. To deliver either option, the underlying physical processes during RCP must be fundamentally understood.

Two fundamental mechanisms have been proposed for mechanism of rapid fracture in polymers. The first regards chain scission as the dominant failure mechanism [1–4], given that the time scale of RCP does not allow creep or chain disentanglement. The second considers chain disentanglement to be the dominant mechanism but, unlike slow crack growth [1,2,5–8], accelerated by adiabatic heating [9–12] and not only by mechanical creep and chain slipping against secondary forces (e.g. van der Waal, hydrogen bonds, etc.) of neighboring chains.

Leevers [9,10,12] developed a relatively simple analytical model – the *adiabatic* or *thermal decohesion* model, based on Dugdale's strip-yield model [9] – to estimate the RCP resistance of craze-forming semi-crystalline polymers. The model explains either crack initiation under impact or RCP under steady load. Highly oriented, inextensible craze fibrils are assumed to be drawn from the bulk material through a thin disentanglement layer which absorbs all of the fracture work. When adiabatic heating there has created and thickened a melt layer which liberates every extended chain passing through it, its strength becomes negligible and it separates to form the fracture surface.

At the crack tip, the cohesive zone starts to fail by whatever separation criterion limits the length l_{pl} or the height δ of the emerging plastic zone to a critical value. Hence, the craze must survive an applied load or grow in order to resist crack propagation. Two limiting cases in which craze zones are rapidly developed by adiabatic conditions are known [9,12]:

i. Rapid Crack Initiation (RCI) – under abrupt loads at high deformation rates, the plastic zone length and thickness grow, but the crack does not extend;
ii. RCP – at high propagation speeds of running cracks, the plastic zone geometry at the crack front remains essentially constant under adiabatic conditions.

In both cases, short–time decohesion is described by the introduction of a melt fracture mechanism grounded on adiabatic heating effects [11] that is capable of predicting the fracture initiation resistance $G_{Ic}(v)$ against high–speed impact loads v as well as the fracture resistance against RCP $G_{Id}(\dot{a})$, which is a function of the resulting crack speed $\dot{a}$. During RCI and subsequent RCP large amounts of energy are ultimately

* Corresponding author.
E-mail address: Mario.Messiha@pccl.at (M. Messiha).

https://doi.org/10.1016/j.tafmec.2021.103145
Received 13 October 2021; Accepted 26 October 2021
Available online 30 October 2021

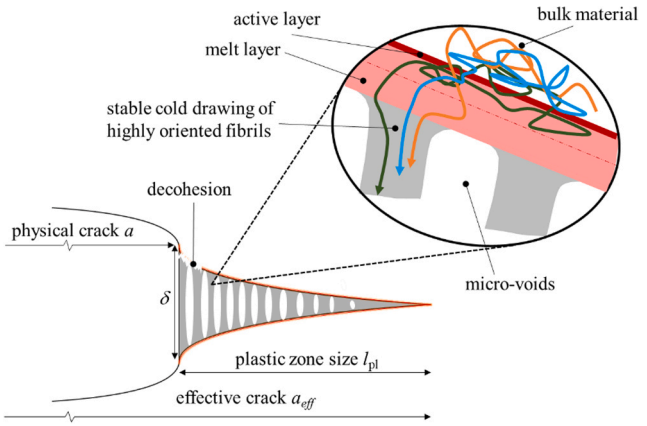

Fig. 1. The crack-tip craze in a polymer, modelled as a cohesive zone [according to 12].

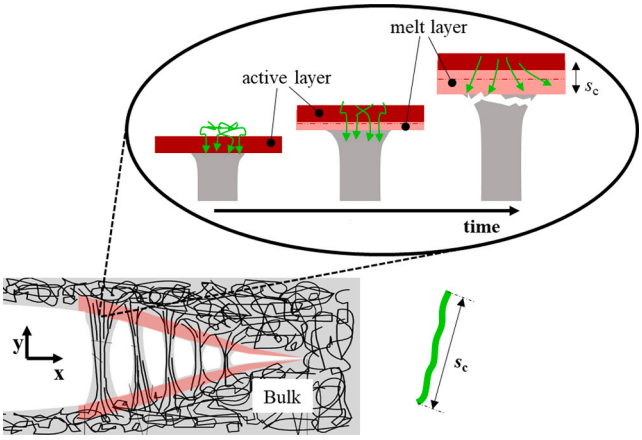

Fig. 2. Successive stages of decohesion at a craze-fibril root [11,14].

converted into heat. If the crack propagates at low speeds, the surrounding bulk material has sufficient time to conduct the generated heat away from the crack tip and the temperature stays almost constant. Due to the low thermal conductivity of polymers, however, a comparatively low crack propagation velocity is sufficient to obtain adiabatic conditions in front of the crack tip. In that context, Leevers [12] asserted the creation of a localized melt zone as a consequence of the heat, which is irreversibly generated at each cohesive zone surface by plastic work (compare to Fig. 1). The craze fibril extension is assumed to follow a *cold drawing* mechanism as proposed by Lauterwasser and Kramer [13]. Bridging polymer chains from the surrounding bulk material are pulled into the craze zone through a thin active layer at the craze-bulk interface. This active layer can be regarded as a hot spot, where local temperatures rise up to the melt point T_m due to adiabatic heating. It contains a mixture of polymer chains, which must be fully extended to give the craze strength, and others which are neither stretched, nor anchored. Once a chain transits the active layer, it pulls new bulk material along with it. Significant work is done to stretch, orient and fuse chains, that cross the active layer, into strong fibrillar structures. In doing so, more heat dissipates, which cannot be conducted away fast enough, heating up neighboring surfaces to the active layer. Eventually a successively growing melt zone of specific depth is left behind over a short time range (see Fig. 2). At the point where the melt layer thickness reaches a critical value s_c, at which the weight-average polymer chain becomes too short to bridge the growing gap between the bulk/active layer interface and the onset of the craze fibrils, it becomes mechanically unstable and the cohesive strength σ_c collapses instantaneously. In that manner, the energy needed to separate fibrils through the melt layer is much smaller than that needed to further expand the melt zone. This is why the separation mechanism is regarded to be a low–energy disentanglement of polymer chains, promoted by adiabatic heating, which overcomes competing conduction processes.

A real image of such fibrillar structures found in high–density polyethylene (PE–HD) during rapid fracture was captured by Hazra [15], as can be seen in Fig. 3. The large S–shaped ridge in Fig. 3a is believed to represent the torn boundary of a fracture surface "flake" where separation has switched from one melt layer to the other.

Based on the thermal decohesion theory, Leevers derived an approximation of a minimum resistance against RCP ($G_{Id,min}$) through which $G_{Id}(\dot{a})$ has to go through for any kind of semi–crystalline polymer [9]:

$$G_{Id,min} \approx s_w \rho \left[5c_p(T_m - T) + 2\Delta H_f\right] \quad (1)$$

Eq. (1) may be interpreted as follows:

- The longer the extended weight average chain , s_w, the thicker the melt zone can become before separation at one side of the cohesive surfaces occurs due to an insufficiency of oriented chains to span the gap and to provide any strength;
- an increase of the specific heat capacity ($c_p\uparrow$) means that the material can absorb more energy to increase its local temperature by 1 K, which subsequently results in more necessary energy to reach T_m at the active layer;
- a higher heat fusion enthalpy ($\Delta H_f\uparrow$) subsequently requires more energy to transform solid crystallites into melt state, where chains can move freely through the active layer into the craze zone.

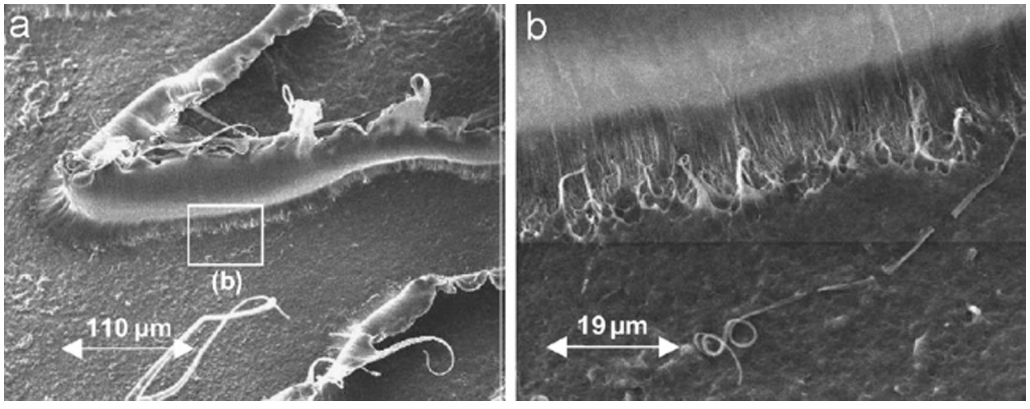

Fig. 3. Fibrillar structure found beneath a rapid fracture surface flake [10,15]. Reprinted from "Adiabatic decohesion in a thermoplastic craze thickening at constant or increasing rate", *Journal of the Mechanics and Physics of Solids*, vol. 56, no. 6, pp. 2149–2170, Copyright (2008) with permission from Elsevier.

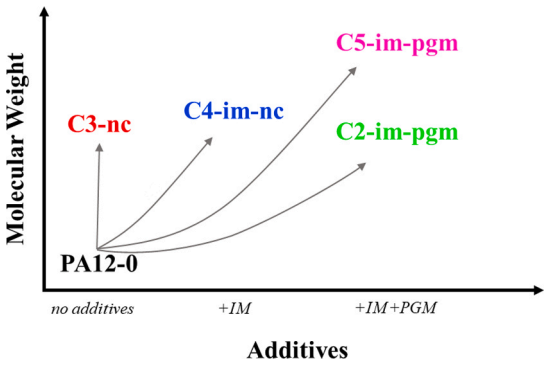

Fig. 4. Systematically developed series of unplasticized PA12 pipe grades.

The present work deals with the possibility of an adiabatic decohesion as dominating failure mechanism of PA12 grades during rapid crack extension. Based on that, an attempt is made to rank various PA12 grades according their fracture toughness expressed by $G_{Id,min}$, as well as the applied crack driving forces deduced from elasto–dynamic fracture mechanics theory. A detailed post–mortem examination of RCP fractured surfaces was done to find clear indications for thermally activated crack propagation (i.e. fibrillar structures).

2. Experimental

Five different grades that were provided by Evonik Operations GmbH, Marl (GER) were selected for this study (Fig. 4). All grades are part of a systematically manufactured series of unplasticized PA12 that differ primarily in their weight average chain length s_w and/or use of specific additives, such as an impact modifier (IM), an inorganic pigment (PGM), or the combination of both. Four of the five grades (coded with the letter "C") are highly viscous compounds developed on the basis of the material PA12–0. The number next to the letter "C" emphasizes the chain length (i.e. $s_{w,C5} > s_{w,C2}$; see also Table 1). All compounds are related to each other as indicated by Fig. 4: C3–nc can be viewed as a natural colored (nc) compound without any impact modification. Adding an IM to it yields to C4–im–nc, while a further coloration results in C2–im–pgm. Finally, C5–im–pgm can be viewed as a derivative of C2–im–pgm, which was modified to achieve a further extension of the average chain length.

Weight average molecular mass M_w was investigated by Size Exclusion Chromatography (SEC) and is expressed by the extended weight average chain length s_w. Samples, taken from extruded pipes of the given materials were dissolved in hexafluoroisopropanol (HFIP) and potassium–trifluoroacetate at room temperature. Thermal characterization was carried out in terms of Differential Scanning Calorimetry (DSC) on a Mettler-Toledo DSC 831 (Schwerzenbach, CH) system purged with 50 ml/min of nitrogen with a heating and cooling rate dT/dt of 10 K/min, to determine the glass transition (T_g) and melt temperature (T_m), as well as the degree of crystallinity (X_c) and melt fusion enthalpy (ΔH_m). Additionally, specific heat capacity (c_p) measurements were conducted over a temperature range of −70° C to 220 °C. For calculations of $G_{Id,min}$ by means of the adiabatic decohesion model, $\hat{c}_p$ values were averaged across the relevant temperature range ($T_m - T$) as proposed by Greenshield and Leevers [16]. Density (ρ) measurements according to ISO 1183-1 were accomplished using a balance of the type Mettler-Toledo AG 204 Delta Range according to Archimedes' principle. Three samples were used for thermal and physical characterization methods.

All grades were characterized via S4 testing and discussed in a previous work [17] in accordance to ISO 13477 as well as a modified evaluation concept of S4 results, to characterize abovementioned pipe grades with regard to their RCP resistance. To investigate governing failure mechanisms during RCP of PA12 grades, an in–dept fractographical analysis of S4 tested pipe segments at 0 °C was performed via a Scanning Electron Microscope (SEM) of the type Tescan Vega II (Tescan Brno, Brno, CZ). A high frame rate, infrared (IR) camera of the type Titanium SC7500 MB (FLIR Systems, Portland, USA) was additionally used to record temperature variations during S4 tests of C2–im–pgm. In order to account for the influences of material dependent dynamic crack driving forces during S4 testing, the dynamic Young's Modulus (E_d) and Rayleigh wave speed (c_R) was determined via ultrasonic measurements on a Consonic C3-KS device (Geotron–Elektronik, Pirna, DE). Three samples were used for characterizing selected grades at 0 °C. The impact plane stress plastic work dissipation was additionally determined by the aid of reversed Charpy tests according to [18] (supplementary information). Impact tests were conducted at an instrumented falling weight tower Zwick HIT230F system. A summary of relevant properties is provided in Table 1.

3. Results & discussion

Critical pressure ($p_{c,S4}$) and temperature ($T_{c,S4}$) values of all PA12 grades, as well as S4 results according to ISO 13477 were determined and discussed elsewhere [17]. The $p_{c,S4}$ results at 0 °C are summarised in Fig. 5.

Building upon previous studies [17], the possibility of adiabatic decohesion during RCP for PA12 pipe grades was revealed via SEM analysis of fractured pipe segments. Presupposing the validity of this observation a key objective of this work, was to relate the fracture

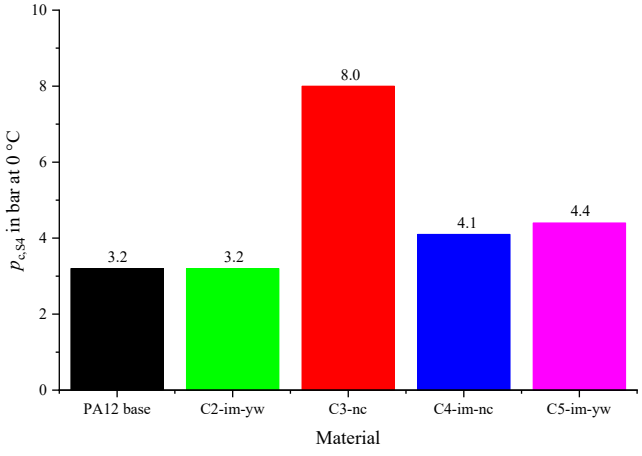

Fig. 5. Results of S4 test according ISO 13477.

Table 1
Basic characterization of selected PA12 pipe grades.

Material	IM	PGM	$\tilde{s}_w$ (μm)	X_c (%)	T_g (°C)	T_m (°C)	ΔH_m (J/g)	$\hat{c}_p$ (J/gK)	ρ (g/cm^3)	E_d (MPa)	c_R (m/s)
PA12-0	–	–	1.0	29	40	180	60	2.25	1.016	2644	901
C2impgm	+	+	1.2	22	44	180	47	2.57	1.008	2436	879
C3nc	–	–	1.4	20	37	177	43	2.21	1.015	2601	910
C4imnc	+	–	1.5	25	37	175	53	2.41	1.007	2352	864
C5impgm	+	+	1.6	21	40	175	44	2.32	1.009	2414	872

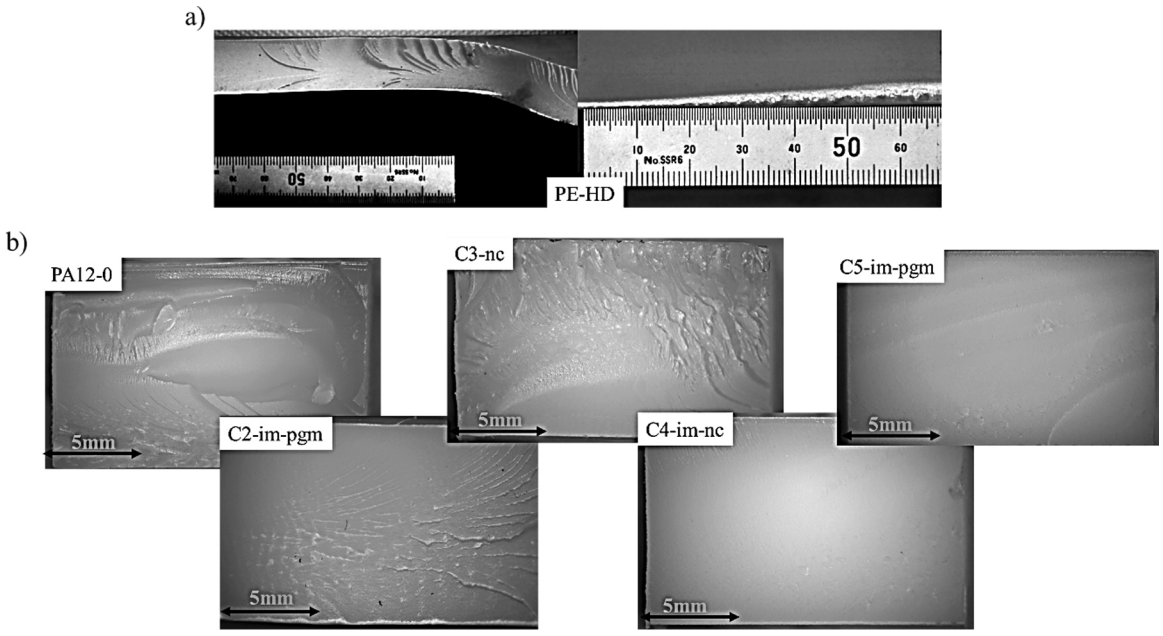

Fig. 6. Plane stress deformation zone on inner pipe wall side of an S4 fractured PE–HD pipe surface [20] (a); no distinctive shearing zones on PA12 fracture surface on the inner pipe wall side (b).

resistance obtained from the S4 material ranking to the calculated $G_{Id,min}$ resistance of the adiabatic decohesion model. At this point it must be clarified that for some polymers, such as PE–HD, the dynamic fracture toughness of a material $G_{Id}(\dot{a})$ was found to be a *composite fracture toughness* [19], consisting of a partial plane strain fracture toughness $G_{Id,1}(\dot{a})$ and a partial plane stress fracture toughness $G_{Id,2}(\dot{a})$. Although RCP fracture appearances seem to be profoundly brittle (mainly plane strain state), S4-fractured PE pipes showed a distinctive plastic deformation zone with shearing lips [20], indicating an obvious plane stress state (Fig. 6a). Thus, a composite crack resistance was formulated as [19]:

$$BG_{Id} = (B - 2\,s)G_{Id,1} + 2sG_{Id,2} \tag{2}$$

where B is the pipe wall thickness and s the thickness of the plane stress layer, which can be calculated by solving a corresponding equation as suggested by Moreno and Leevers [21]. Both fracture toughness values can be determined experimentally or by existing numerical or analytical models [1,3,12,13,15,19,34–36].

A similar distinctive plane stress shearing zone is hardly visible at the inner pipe wall side of PA12 grades (Fig. 6b) along the crack path of an S4 fractured pipe (except for the ultimate position of crack arrests, where increasing plasticity can lead the propagating crack to an end).

This observation is important, as it allows to reduce the relationship of $G_{Id}(\dot{a})$ from a composite fracture toughness to a dominating plane strain $G_{Id,1}(\dot{a})$ for PA12 pipe grades. An experimental measurement of $G_{Id,2}$ by means of reversed Charpy tests [18] for all grades showed that for a 10 mm thick pipe the dissipated plane stress fracture toughness $G_{Id,2}(\dot{a})$ ranged from 4% (for PA12–0) to a maximum of 16 % (for C4–im–nc) of the total composite fracture toughness of selected grades (see supplementary information). Hence, a reduction of $G_{Id}(\dot{a})$ to a dominating plane strain $G_{Id,1}(\dot{a})$ for PA12 materials seems viable.

Therefore, an attempt was made to characterize RCP resistances of all PA12 grades using only $G_{Id,min}$ of the adiabatic decohesion model (compare to Eq. (1)). Necessary input variables of individual grades (Table 1) were schematically plotted in Fig. 7a. A good correlation would be maintained if the shape of these radar plots shows a similar shape as obtained from the radar diagram of critical S4 pressures (Fig. 7c). Thus, a separate view of all variables does not deliver a reliable RCP ranking. A more appropriate ranking, on the other hand, is obtained when comparing $G_{Id,min}$ (Fig. 7b) to $p_{c,S4}$ (Fig. 7c) results. Though the shape of both plots is not identical, the highest fracture resistance is correctly predicted for C3–nc and C5–im–pgm, followed by C4–im–pgm and the lowest resistance for C2–im–pgm and PA12–0.

An exponential correlation exists between the calculated $G_{Id,min}$ and experimentally measured $p_{c,S4}$ as presented in Fig. 8. However, a sufficient ranking is particularly possible at the lower S4 pressure regime (up to approx. 4 bar) with regard to $G_{Id,min}$ values of PA12 pipe grades. Taking into account, that each parameter used for the determination of $G_{Id,min}$ (i.e. s_w, ρ, c_p, T_m, ΔH_f) exhibits a certain scatter range and that $p_{c,S4}$ values measured according ISO 13477 are based on single–point evaluations, a clear ranking with regard to higher critical S4 pressures, that is, between C5–im–pgm and C3–nc in Fig. 8, is barely possible.

To improve the ranking results with regard to RCP resistance of different pipe grades, a new method that additionally considers the material–dependent dynamic crack driving force $G_I(t)$ or $K_I(t)$ was developed. When testing PA12 pipe grades in an S4 test under identical conditions, it is often erroneously assumed, that the outcome of the test only depends on the dynamic fracture toughness $G_{Id}(t)$ or $K_{Id}(t)$ of the material. However, this assumption is not entirely true – different materials may experience different local loadings, although the applied loading situation is the same, as will be explained next.

Rapid loading of structures often causes a material's mechanical response to become a function of time. For a linear elastic material with Small Scale Yielding (SSY), the (quasi–) static crack driving force, expressed by K_I then becomes the time–dependent dynamic stress intensity factor $K_I(t)$. Based on the assumption that LEFM is still valid, inertial effects do not alter the singularity structure of stress fields near the tip of a stationary crack under dynamic loading, and the K concept can be used as given by Eq. (3) for Mode I:

$$\sigma_{ij} = \frac{K_I(t)}{\sqrt{2\pi r}} f_{ij}(\theta) \tag{3}$$

with $f_{ij}(\theta)$ being identical to the quasi–static angular correction functions.

In that context, a dynamic change in the state of stress – for example, due to impact or shock loading – causes a system to oscillate. This is illustrated by the dynamic formation of the instantaneous stress intensity field $K_I(t)$ at the crack tip of a stationary crack of length a_0,

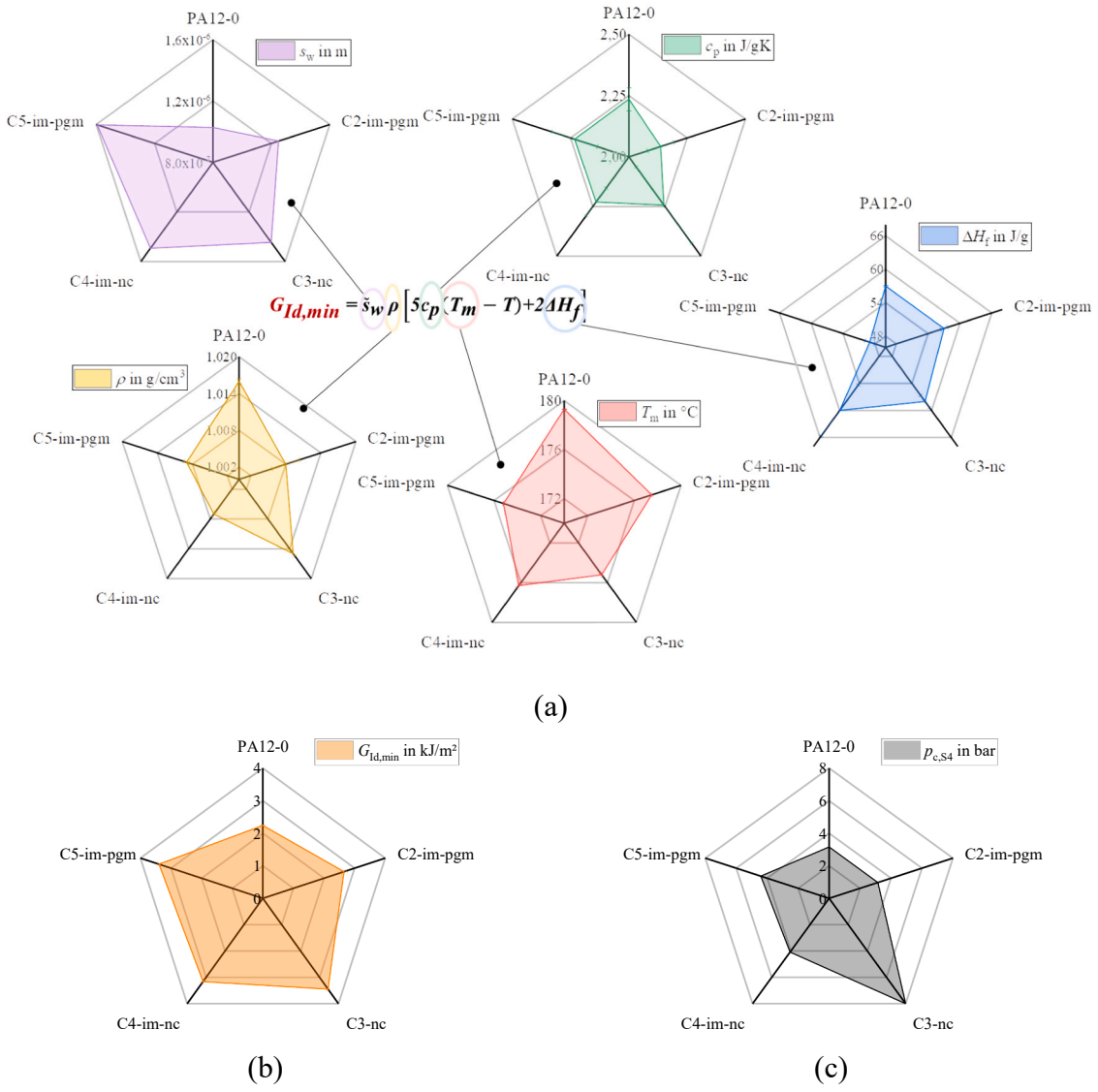

Fig. 7. Separate view of input variables (a) used for the calculation of $G_{Id,min}$ (b) of PA12 pipe grades according to the thermal decohesion principle [9,12], and critical pressure values obtained from S4 test (c).

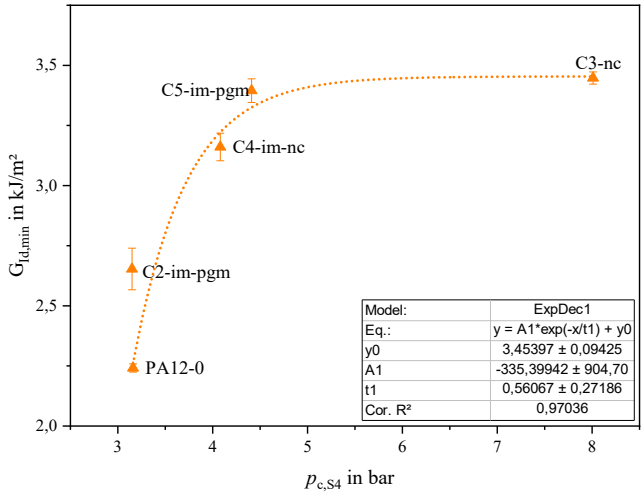

Fig. 8. Critical S4 pressure $p_{c,S4}$ vs. the minimum dynamic fracture toughness $G_{Id,min}$ of all PA12 pipe grades.

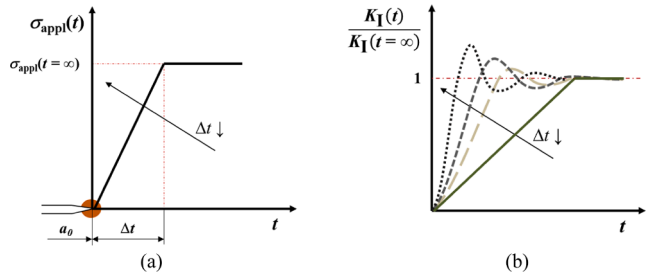

Fig. 9. Formation of the far–field stress (a) and the corresponding stress intensity field (b) during dynamic loading of a stationary crack, according [22].

without considering further boundary conditions (Fig. 9). As shown in Fig. 9a, a far-field stress σ_{appl} is applied to the crack over a finite time period Δt and then kept constant at $\sigma_{appl}(t = \infty)$. In the response function of the system, the build-up of $K_I(t)$ at the crack tip is determined by Δt (Fig. 9b): If Δt is long enough (quasi–static load rates), $K_I(t)$ builds up with a time delay and reaches a new equilibrium state $K_I(t = \infty)$, without serious changes of the amplitude – thus, these load cases are

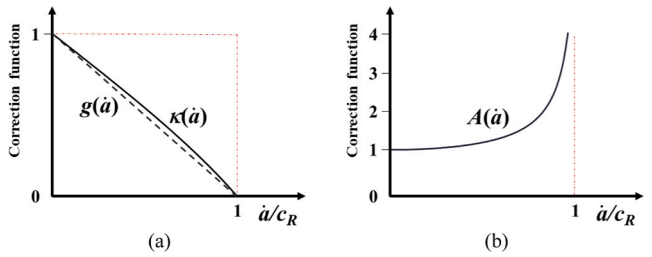

Fig. 10. Schematic representation of the universal correction functions relating $G_I(t)$ and $K_I(t)$ to G_I^{stat} and K_I^{stat}, respectively (a), as well as the correction function A(ȧ) to convert $G_I(t)$ into $K_I(t)$ and vice versa (b) over non–dimensional crack speed according [27].

regarded "time–independent". Yet, with strongly decreasing Δt (Fig. 9a) remarkable changes in amplitude and phase occur in the system response, until oscillations diminish and the stress intensity factor becomes identical for static and dynamic approaches (Fig. 9b). However, the resulting amplitude modulation is essential, since, compared to the static approach, the amplitude overshoot induces extremely high stress intensity factor peaks within a short period of time. This behavior is notably promoted by interactions of reflected stress waves that pass through the specimen constructively and destructively and interfere with one another, resulting in a highly complex time-dependent stress distribution. The instantaneous $K_I(t)$ is therefore controlled by the magnitude of the discrete stress waves that pass through the crack tip region at that particular moment in time. When these discrete waves are significant, it is nearly impossible to infer $K_I(t)$ from remote loads as in the quasi–static case. Hence, the shorter the time period Δt gets, which is reciprocally proportional to the v, the higher the degree of dynamic overshooting. A loading function of rectangular shape ($\Delta t \rightarrow 0$) creates the highest $K_I(t)$ overshoot values and takes the longest time to reach equilibrium state [22].

Based on mathematical simplifications formulated by Sih [23–26], Freund [27] and Maue [28], some closed–form solutions are available for a few number of dynamic fracture problems. Focusing on RCP, some investigators [24,27,29,30] have further formulated a simple elasto–dynamic relationship in order to approximate the general dynamic load case of a running crack on behalf of an equivalent static load

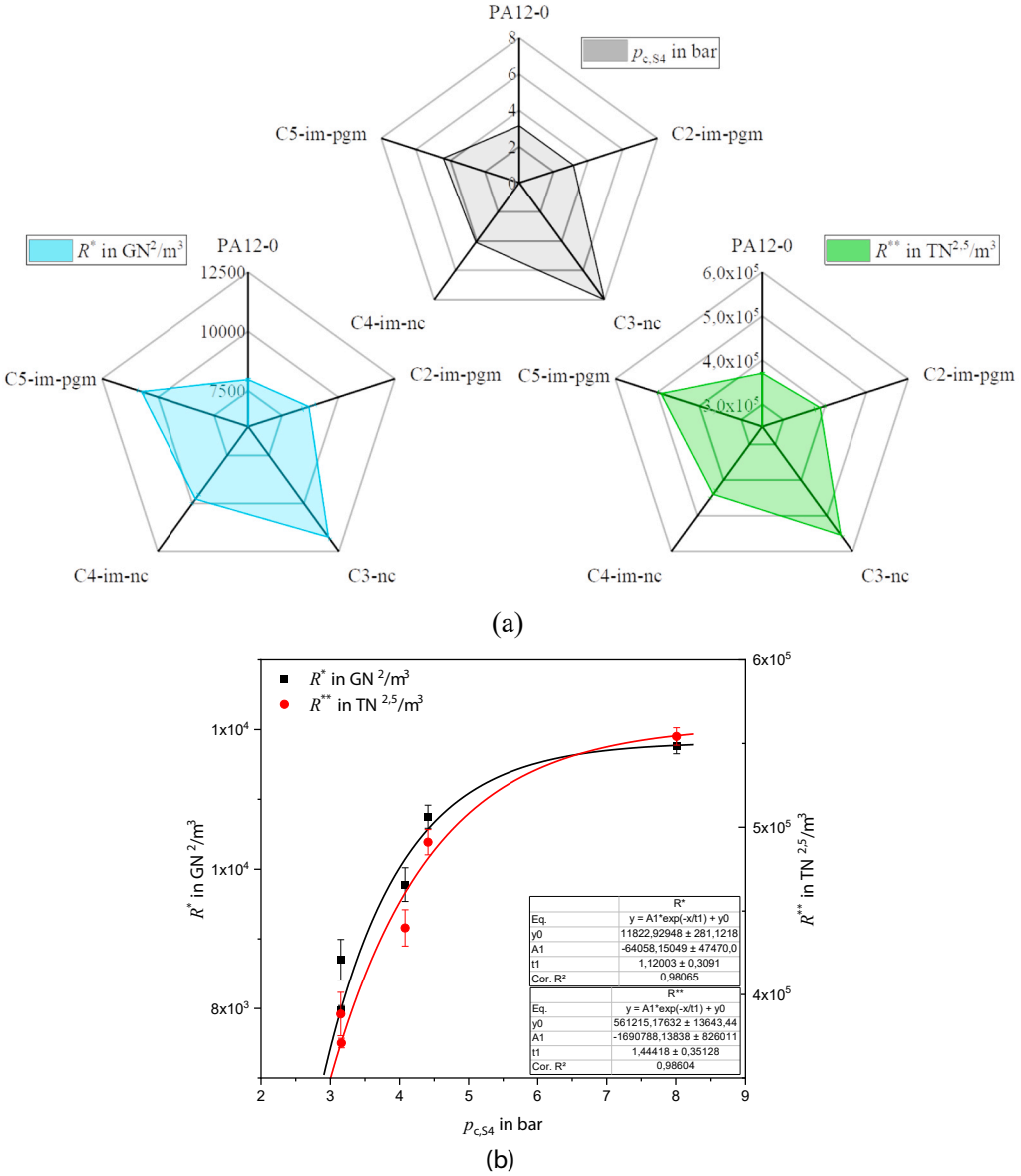

Fig. 11. Radar plots comparison of measured $p_{c,S4}$ and newly defined ranking parameters R^* and R^{**} (a). Exponential correlation between R^*, R^{**} and $p_{c,S4}$ (b).

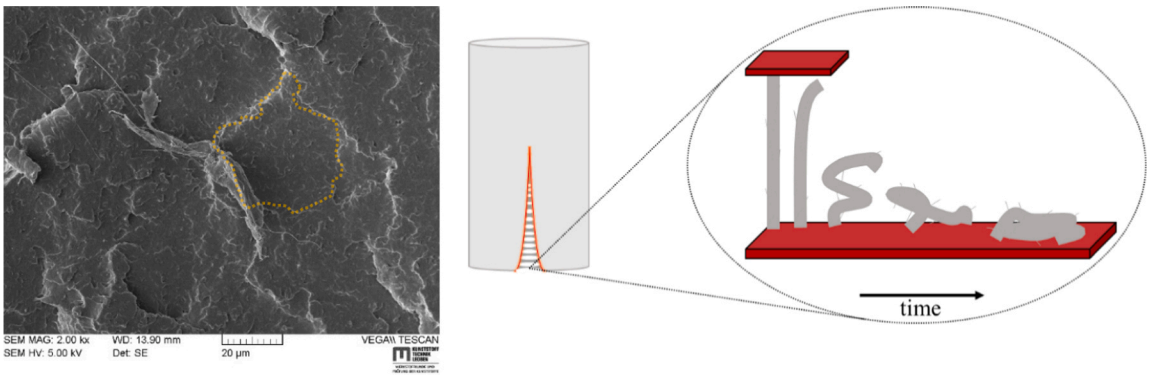

Fig. 12. Flake structures (a) on the fracture surface of C2–im–pgm as representative for all PA12 pipe grades, and schematic illustration of the creation of flat solidified flaky surfaces based on a single fibril (b) during RCP.

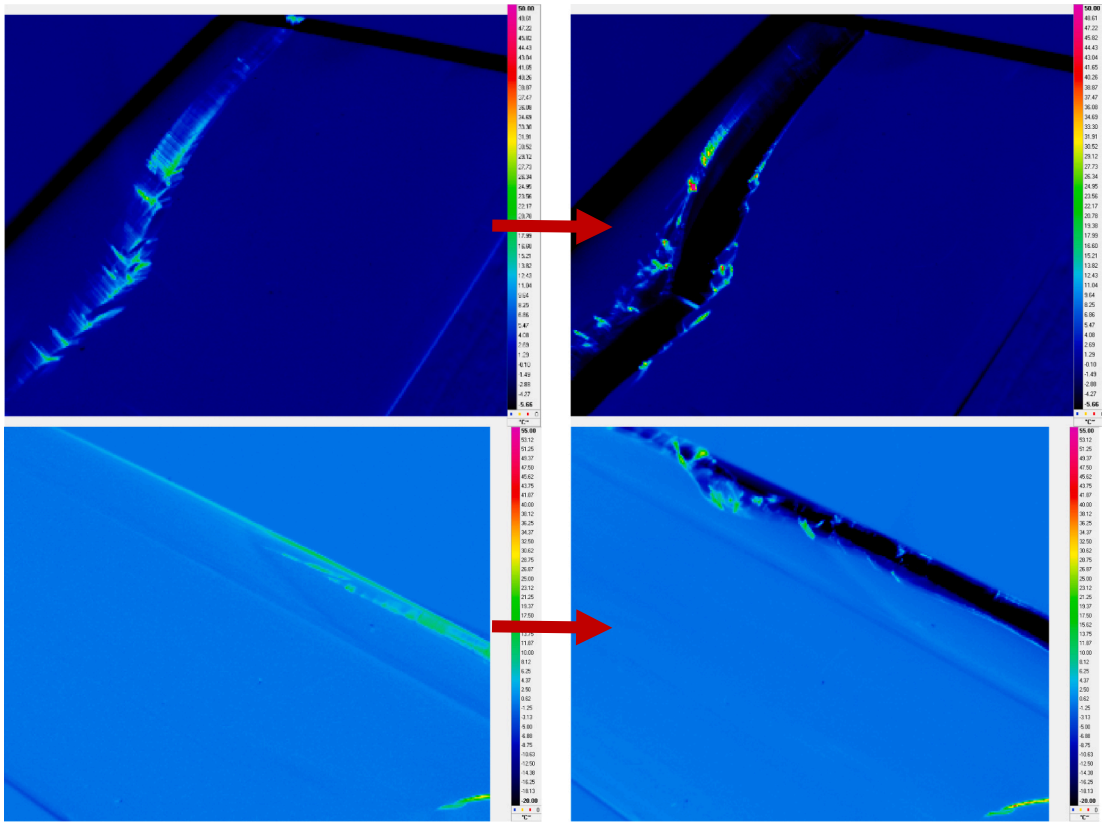

Fig. 13. Qualitative thermographic evaluation of RCP in two different S4 pipes of C2–im–pgm by stepwise image analysis (from left to right).

condition of a stationary crack using standard LEFM crack tip parameters [31]:

$$K_I(t) = \kappa(\dot{a}(t))K_I^{stat} \tag{4}$$

with

$$\kappa(\dot{a}(t)) \approx \left(1 - \frac{\dot{a}}{c_R}\right)\sqrt{1 - h\dot{a}} \tag{5}$$

and

$$h \approx \frac{2}{c_P}\left(\frac{c_S}{c_R}\right)^2\left(1 - \frac{c_S}{c_P}\right)^2 \tag{6}$$

In these equations K_I^{stat} (or simply K_I) is the static stress intensity factor and h a function of the elastic body and surface wave speeds with c_S and c_P as shear and pressure wave velocities, respectively. The term $\kappa(\dot{a}(t))$ denotes a universal correction function of the crack speed (compare to Fig. 10a) that equals 1 for $\dot{a} = 0$ and equals 0 for $\dot{a}$ approaching the Rayleigh speed. This can be explained on physical grounds, since no energy is left to do the work of fracture at the crack tip: it is all been spent accelerating the surrounding mass [22,32].

Analogously, the instantaneous energy release rate $G_I(t)$ can be described by:

$$G_I(t) = g(\dot{a}(t))G_I^{stat} \tag{7}$$

with

$$g(\dot{a}(t)) \approx 1 - \frac{\dot{a}}{c_R} \tag{8}$$

where G_I^{stat} (or simply G_I) is the energy release rate and $g\ (\dot{a}(t))$ a universal function of crack speed that equals 1 for $\dot{a} = 0$ and equals 0 for

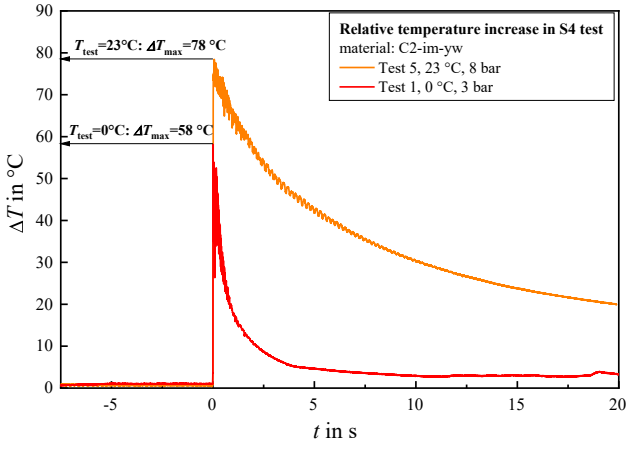

Fig. 14. Quantitative thermographic evaluation of RCP in an S4 tested C2–im–pgm pipe at different bulk temperatures and internal pressures.

$\dot{a}$ approaching the Rayleigh speed (see Fig. 10a). Following LEFM principles, a fundamental relation between $G_I(t)$ and $K_I(t)$ can be derived as follows:

$$G_I(t) = \frac{K_I(t)^2(1-\mu^2)}{E_d} A(\dot{a}) \tag{9}$$

for plane strain, with E_d as the dynamic Young's Modulus, μ as Poisson's number and the universal correction function $A(\dot{a})$ (see Fig. 10b) approximated by [27,33]:

$$A(\dot{a}) \approx \left[(1-h\dot{a})\left(1-\frac{\dot{a}}{c_R}\right)\right]^{-1} \tag{10}$$

According to this, the dynamic energy release rate is uniquely determined by the dynamic stress intensity factor and the crack propagation speed. It can be seen, that even for very low $K_I(t)$ values, $G_I(t)$ increases unrestrictedly, if $\dot{a}$ goes against the Rayleigh wave velocity c_R. Conversely, at a given $G_I(t)$, the stress intensity factor approaches zero for $\dot{a} \rightarrow c_R$. These simplified analytical solution for dynamic fracture problems are valid as long as the length of the crack propagation Δa is small compared to the specimen dimensions [33] (e.g. only initial stages of RCP in pressurized pipelines). It, therefore, justifies the neglect of interactions between the crack tip and reflected waves. If Δa increases significantly, the influence of reflected waves and the consequential crack driving force must be determined experimentally or numerically (i.e. PFRAC by O'Donoghue and Zhuang et al. [34–38], etc.). However, for the sake of simplicity this analytical approach will be considered for the finite medium (whole pipe under pressure) and used as correction factor, as will be shown in the following.

By relating the dynamic fracture toughness $G_{Id}(\dot{a})$ of a material to the acting crack driving force $G_I(\dot{a})$ using concepts of elasto–dynamic fracture mechanics (e.g. Eq. (3) to (10)), Eq. (11) can be deduced as:

$$\frac{G_{Id}(\dot{a})}{G_I(\dot{a})} = \frac{G_{Id}(\dot{a})E_d}{\left(K_I^{stat}\right)^2(1-\mu^2)g(\dot{a})} \tag{11}$$

Taking the possibility of a thermal decohesion mechanism in PA12 into account, $G_{Id}(\dot{a})$ reaches a minimum value $G_{Id,min}$ at a critical crack speed $\dot{a}_{crit}$ of approx. 30% of the material dependent reference speed c_0, which is defined as [11]:

$$c_0 \equiv 4.43\frac{E_d \rho \alpha c_p}{\beta \sigma_c^2 s_c}(T_m - T) \tag{12}$$

In that context, β is regarded as a material dependent fraction (i.e. 80–90% for most semi–crystalline polymers [19,39]) of the whole plastic work that dissipate as heat within the active layers of a thickness s_c, and σ_c the craze stress or cohesive strength, which is properly approximated by σ_{ys}. Substituting this critical crack speed $\dot{a}_{crit} \sim 0.3c_0$ into Eq. (11), a new ranking parameter R^* is proposed, which considers not only the fracture toughness $G_{Id}\left(\dot{a}_{crit}\right) = G_{Id,min}$ of a material, but also the influence of varying crack driving forces $G_I\left(\dot{a}_{crit}\right)$ at a given temperature between different grades that are identically loaded. Considering the right side of Eq. (13) it can be seen that R^* is defined to be only dependent on material parameters, while K_I^{stat} contains the actual material–independent part of the dynamic crack driving force:

$$R^* \equiv \frac{G_{Id}\left(\dot{a}_{crit}\right)}{G_I\left(\dot{a}_{crit}\right)}\left(K_I^{stat}\right)^2 \rightarrow R^* = \frac{G_{Id,min}E_d}{(1-\mu^2)\left(1-\frac{\dot{a}_{crit}}{c_R}\right)} \tag{13}$$

To overcome the difficulties of measuring and calculating c_R and $\dot{a}_{crit}$, respectively, a second ranking parameter R^{**} is established by substituting $G_I(\dot{a})$ of Eq. (11) with a numerical solution of the *maximum dynamic crack driving force* $G^d_{I,max}$ during RCP of a pressurized pipeline. This value is deduced from the mathematical model of Kanninen and O'Donoghue [38,40]:

$$G^d_{I,max} \equiv \frac{11.4p^{2.5}D\left(\frac{D}{t}-1\right)^2}{E_d^{1.5}} \tag{14}$$

Contrarily to R^*, R^{**} is only dependent on $G_{Id,min}$, E_d and μ at a given temperature:

$$R^{**} \equiv 11.4p^{2.5}D\left(\frac{D}{t}-1\right)^2\frac{G_{Id,min}}{G_{I,max}} \rightarrow R^{**} = \frac{G_{Id,min}E_d^{1.5}}{1-\mu^2} \tag{15}$$

Significant improvements of the ranking results could be achieved after determining R^* and R^{**} at $T = 0$ °C, in contrast to the initial fracture toughness parameter $G_{Id,min}$. Fig. 11a illustrates a radar plot of both new ranking parameters that are in high accordance with ranking results obtained from the S4 test. Exponential regression models with a corrected R^2 value of over 98 %, show the strength of relationship between R^* and R^{**} and the independent variable $p_{c,S4}$ (Fig. 11b). Because R^{**} is much easier to determine than R^* without worsening the ranking result, it is the recommended ranking parameter for a first assessment of the RCP resistance of newly developed pipe grades.

To back–up the reliability of R^{**} and thermal decohesion as dominating fracture mechanism, an additional high–resolution SEM investigation was conducted. Notably, each PA12 grade featured brighter, irregular boundary lines (see Fig. 12a). Many of these bright lines clearly delineate closed regions (highlighted in orange, Fig. 12a), which could be described as *flakes* and are commonly observed on RCP fracture surfaces [10,15]. Bearing the possibility of a thermal decohesion mechanism in mind, an explanatory hypothesis for these structures may be provided by Fig. 12b. As soon as fibrils detach from one of both melt layers of the craze zone at the craze/bulk interface, they lose their strength and stiffness due to the surrounding high temperature, and contract back to the hot ground (=one of both melt layers). Subsequently, solidification of the collapsed fibrils and the molten zones takes place, as soon as the temperature drops after a certain cooling time due to physical crack extension and associated thermal conduction processes. The white boundaries on the surface could then be regarded as the edges of single craze flakes, from which numerous fibrils (only simplified illustration in Fig. 12b based on single fibril) were initially drawn, before softening and returning back into the molten thermoplastic bed. Each fibril then would have started on one fracture surface and ended on the edge of the same flake on the complementary crack surface (except for those trapped within one half of a fractured pipe sample, e.g. beneath river lines; compare to [17]). It should also be noted that perhaps in theory there could be only one active melt layer on

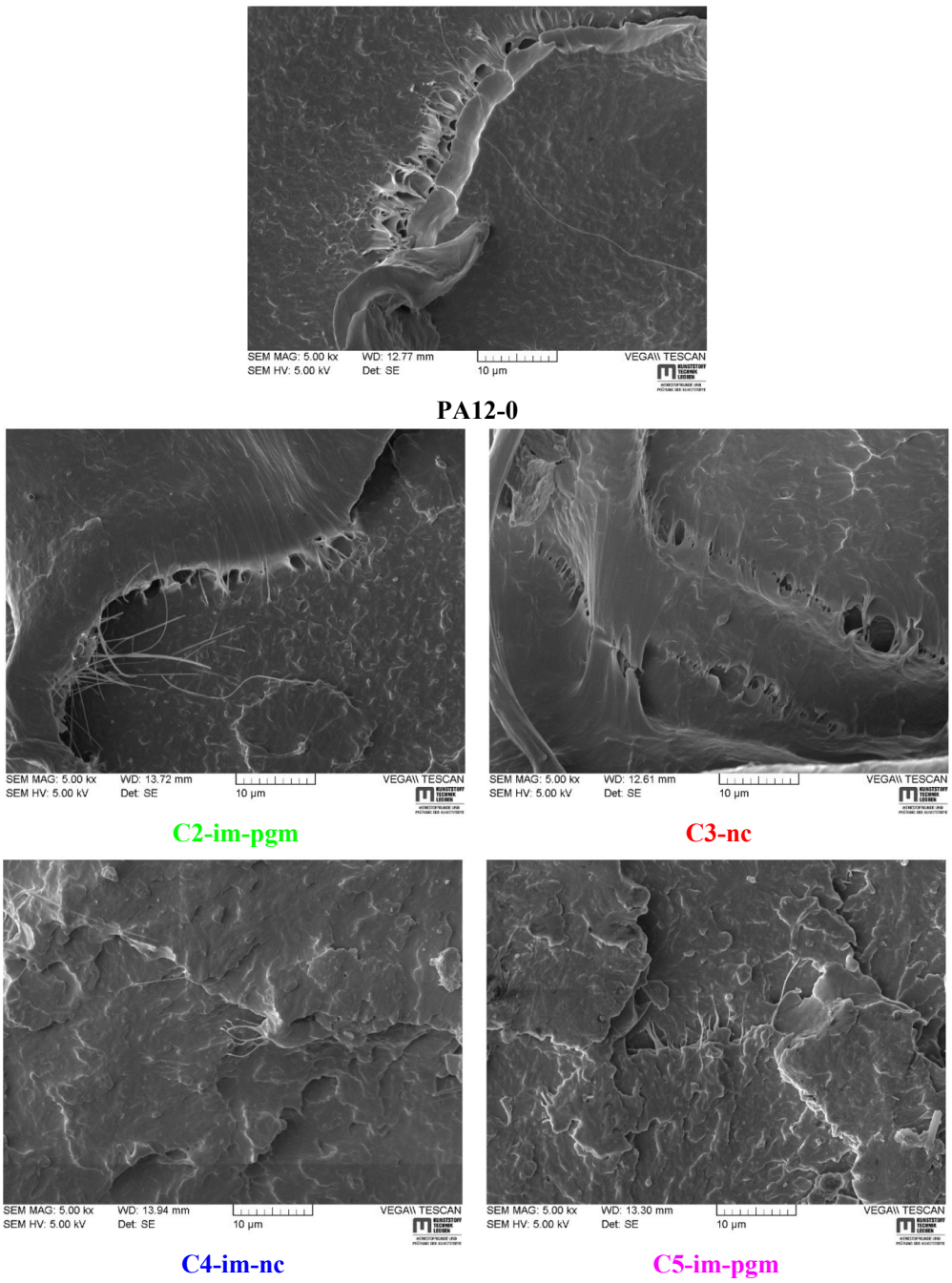

Fig. 15. High–magnification SEM images of fibrillar structures at the boundary lines of craze flakes observed on S4 tested PA12 pipe fragments.

one craze surface, as schematically illustrated in Fig. 12b. The fracture surfaces would then look identical, and almost featureless. But of course, a crystalline polymer is very heterogeneous at this scale, so that many different bifurcated crack planes of differently oriented fibrils interact and collapse at the same time, resulting in a randomly scattered mixture of flaky fracture surfaces, each formed by thermal decohesion within different active melt layers [41].

Another indication for a governing adiabatic decohesion mechanism was delivered by an in–situ thermographic analysis of rapid fracture processes in C2–im–pgm using an infra–red (IR) camera during S4 testing (Fig. 13). Unfortunately, the maximum image frequency was too low at reasonable resolutions (full frame rate up to 380 Hz), so that the crack front "jumped" from one image to the next, as crack propagation speeds were very high. Although there was no chance to capture the instantaneous crack tip temperature (Fig. 13, left), fractured surfaces showed localities of significantly higher temperatures compared to the actual bulk temperature (e.g. red spots in Fig. 13, right). A recorded increase of approx. 60 °C to 80 °C along the crack path is presented in Fig. 14 for two S4 tests at different test temperatures and internal pressure conditions. Even if no hot spots with temperatures around the melting point of the materials could be measured, thermographic results hint at a possible adiabatic heating process and support the idea of a thermal decohesion mechanism for PA12 pipe grades.

Finally, similar fibrillar micro–structures as reported by Hazra [15] and Leevers [10] (Fig. 3) could be found for nearly all grades at regions close to the edges of aforementioned craze flakes (see Fig. 15) within S4 fractured pipe samples. Fibrils are theoretically more likely to survive at the edges of flakes because of faster heat losses compared to middle area of the hot craze flakes. If it could be possible to somehow look underneath the observed flakes, at some point away from its edge no fibrils

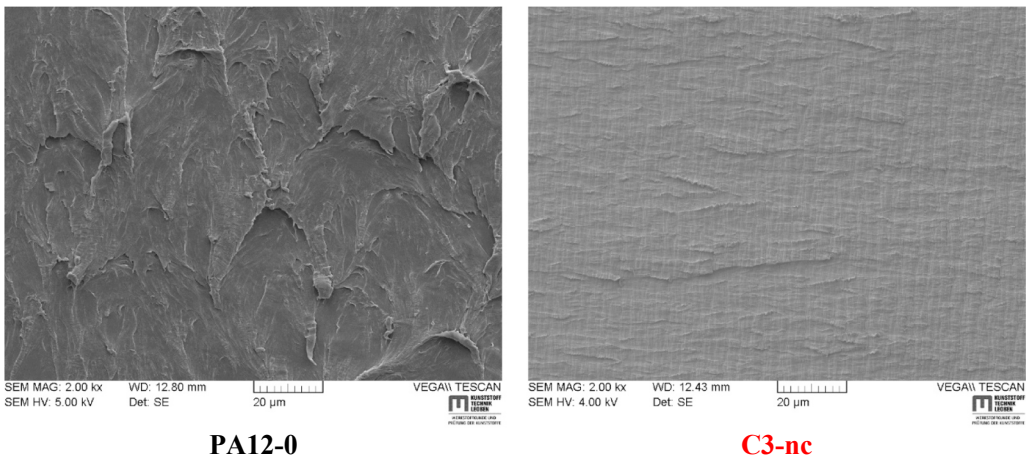

Fig. 16. Fracture images of PA12–0 and C3–nc tested at 24 MPa in the cyclic CRB test according ISO 18489.

would be found because they quickly contract back into the molten layer leaving behind this bumpy surface. Fortunately, images of Fig. 15 display a notable fibrillation for non–toughened grades, PA12–0 and C3–nc, respectively. Impact modified grades showed similar flake fibrils for C2–im–pgm, whereas micro–fibrils were not so easily found in C4–im–nc and C5–im–pgm. The length of fibrillar zones is about a few micro–meters, where high molecular weight compounds seem to portray smaller fibrillated areas than the low molecular weight PA12–0. It must be noted at this point that although it is difficult to locate these marks, it does not necessarily follow that thermal decohesion must be restricted to small local regions. Instead, the theory would rather predict very small amounts to no fibrils at all, as it would be more likely for them to contract back into the melt layer after decohesion before solidifying as observable highly–stretched structures.

The idea that RCP is predominated by adiacatic decohesion and not by chain scission mechanisms is further challenged by structural effects of the S4 test. Though this test allows to get as close as possible to the critical RCP conditions in service and seems very satisfactory to compare grades and obtain a critical pressure. It presents some “shortcomings” when concluding on the dynamic fracture behavior of a material. Kopp et al. [42] demonstrated that the energy release rate during dynamic propagation is mainly driven by the work of external forces in the case of a pipe under pressure. During S4 testing the applied pressure is assumed to be constant, however, this might not be the exact case when the crack propagates and decompression is occurring. Subsequently, the work of external forces may vary and therefore the crack velocity is not constant. In that context, it has been recently shown for PA11 [43] that the appearance of different fracture mechanisms would largely depend on the cracking regime and the characteristic time for polymer chains to react. It can be emphasized that at crack initiation and arrest zones (low crack speeds), it seems that the characteristic times for the appearance of adiabatic decohesion is possible in PA11. In the quasi-steady-state regime of rapid propagation (high crack speeds), however, it is much more localized and limited.

With this in mind, crack arrest and re-initiation by wave reflections are therefore common in an S4 test. And observed fibrillation in PA12 grades could be particularly argued after re-initiation of an arrested crack, while trans–passing the slow crack growth regime. Although this conclusion seems quite reasonable considering the structural effects of the S4 test, it would neither explain the remarkable increase of temperature observed in PA12, nor the highly correlating results based solely on thermal decohesion assumptions. Finally, it should be highlighted in Fig. 16 that during SCG characterization of selected pipe grades via cyclic CRB tests in previous studies (see [44,45]), some PA12 grades showed fibrillar structures (e.g. PA12–0), while others did not (e.g. C3–nc). Yet, both materials exhibit clear fibrils during RCP (Fig. 15) making it more difficult to attribute the fibrillation mechanism to slow crack extension mechanisms and not to thermal decohesion. In that sense, more detailed, systematic studies on the different cracking regimes and corresponding fracture mechanisms are needed.

4. Conclusion & outlook

Reliable accelerated material ranking with regard to *Rapid Crack Propagation* (RCP) resistances shall lead to an efficient material development of new plastic pipe grades without the necessity of expensive, experimental validations. Correspondingly, a novel ranking parameter R^{**} based on elasto–dynamic fracture mechanics concepts and the presupposition of a thermal decohesion as prime fracture mechanism during RCP of semi–crystalline plastics was proposed. Semi–analytical results of R^{**} were found to be in high accordance with the critical pressure values $p_{c,S4}$ obtained from a *Small–Scale Steady–State* (S4) test according ISO13477 of five different PA12 pipe grades. In contrast to the general believe that chain scission mechanism is governing physical processes on a molecular scale during rapid crack extension, an *in–situ* thermographic analysis during S4 tests backed up the existence of high temperatures, most likely due to adiabatic heating. Moreover, a post-mortem fractographic investigation revealed highly fibrillated structures on PA12 fracture surfaces indicating thermo–mechanical disentanglement processes on a molecular level. Still, more research would be beneficial to account for structural effects and corresponding cracking regimes of the S4 test as well as for different accompanying fracture mechanisms.

Declaration of Competing Interest

The authors declare that they have no known competing financial interests or personal relationships that could have appeared to influence the work reported in this paper.

Acknowledgement

The research work of this paper was performed at the Polymer Competence Center Leoben GmbH (PCCL, Austria) within the framework of the COMET-program (Grant Nr.: 879785), which is funded by the Federal Ministry for Transport, Innovation and Technology (Austria) and Federal Ministry for Economy, Family and Youth (Austria) with contributions by Evonik Operations GmbH (Germany) and the Montanuniversitaet Leoben (Austria). The PCCL is funded by the Austrian Government and the State Governments of Styria and Upper Austria. Special thanks go to Jutta Geier for a thorough fractographic analysis via SEM.

Appendix A. Supplementary material

Supplementary data to this article can be found online at https://doi.org/10.1016/j.tafmec.2021.103145.

References

[1] A.M. Donald, The effect of temperature on crazing mechanisms in polystyrene, J. Mater. Sci. 20 (7) (1985) 2630–2638.
[2] A.M. Donald, E.J. Kramer, The competition between shear deformation and crazing in glassy polymers, J. Mater. Sci. 17 (7) (1982) 1871–1879.
[3] R.A.C. Deblieck, D.J.M. van Beek, K. Remerie, I.M. Ward, Failure mechanisms in polyolefines: The role of crazing, shear yielding and the entanglement network, Polymer 52 (14) (2011) 2979–2990.
[4] C.J.G. Plummer, H.H. Kausch, "Semicrystalline Polymers: Fracture Properties," in: Reference Module in Materials Science and Materials Engineering, Elsevier, 2016.
[5] N. Brown, A fundamental theory for slow crack growth in polyethylene, Polymer 36 (3) (1995) 543–548.
[6] G. Pinter, Rißwachstumsverhalten von PE-HD unter statischer Belastung, Doctoral Dissertation, University of Leoben, 1999.
[7] F. Arbeiter, B. Schrittesser, A. Frank, M. Berer, G. Pinter, Cyclic tests on cracked round bars as a quick tool to assess the long term behaviour of thermoplastics and elastomers, Polym. Test. 45 (2015) 83–92.
[8] A. Frank, F.J. Arbeiter, I.J. Berger, P. Hutař, L. Náhlík, G. Pinter, Fracture mechanics lifetime prediction of polyethylene pipes, J. Pipeline Syst. Eng. Pract. 10 (1) (2019) 04018030, https://doi.org/10.1061/(ASCE)PS.1949-1204.0000356.
[9] P.S. Leevers, Impact and dynamic fracture of tough polymers by thermal decohesion in a Dugdale zone, Int. J. Fract. 73 (2) (1995) 109–127.
[10] P.S. Leevers, M.-A. Godart, Adiabatic decohesion in a thermoplastic craze thickening at constant or increasing rate, J. Mech. Phys. Solids 56 (6) (2008) 2149–2170.
[11] P. Leevers, "Modelling Impact Fracture and RCP Resistance of Thermoplastics from Cohesive Properties," in: Society of Plastics Engineers 2004 – Proceedings ANTEC.
[12] P.S. Leevers, R.E. Morgan, Impact fracture of polyethylene: A non-linear-elastic thermal decohesion model, Eng. Fract. Mech. 52 (6) (1995) 999–1014.
[13] B.D. Lauterwasser, E.J. Kramer, Microscopic mechanisms and mechanics of craze growth and fracture, Philos. Mag. A 39 (4) (1979) 469–495.
[14] J. Hertling, "Ausbreitungsgeschwindigkeit von instabilen Rissen in Polymeren bei tiefen Temperaturen," 1999.
[15] S. Hazra, Crazing and yielding of polyethylene under impact, University of London, 2000. PhD Thesis.
[16] C.J. Greenshields, P.S. Leevers, Rapid crack propagation in plastic water pipes: measurement of dynamic fracture resistance, Int. J. Fract. 79 (1) (1996) 85–95.
[17] M. Messiha, A. Frank, J. Heimink, F. Arbeiter, G. Pinter, Structure-property relationships of polyamide 12 grades exposed to rapid crack extension, Materials (Basel, Switzerland) 14 (19) (2021) 5899, https://doi.org/10.3390/ma14195899.
[18] P.S. Leevers, Plastics — Determination of Impact Plastic Work Dissipation — Reversed Charpy Test, Department of Mechanical Engineering, Imperial College London, 2004.
[19] C. Argyrakis, Models for designing pipe-grade polyethylenes to resist rapid crack propagation, Dissertation, Imperial College London, 2010.
[20] P. Yayla, Rapid Crack Propagation in Polyethylene Gas Pipes, Dissertation, Imperial College of Science, Technology and Medicine, 1991.
[21] P.S. Leevers, L. Moreno, Surface layer stiffness effects on fracture of polymer multilayers: a linear elastic model, Eng. Fract. Mech. 72 (6) (2005) 947–959.
[22] D. Gross, T. Seelig, Bruchmechanik: Mit einer Einführung in die Mikromechanik, Springer Vieweg, Berlin, Heidelberg, 2016.
[23] G.C. Sih (Ed.), Experimental evaluation of stress concentration and intensity factors, Springer Netherlands, Dordrecht, 1981.
[24] G.C. Sih, Dynamic crack problems — strain energy density fracture theory, in: G. C. Sih, G.C. Sih (Eds.), Mechanics of Fracture Initiation and Propagation: Surface and volume energy density applied as failure criterion, Springer, Netherlands, Dordrecht, 2012, pp. 99–125.
[25] G.C. Sih, J.F. Loeber, Wave propagation in an elastic solid with a line of discontinuity or finite crack, Q. Appl. Math. 27 (2) (1969) 193–213.
[26] G.C. Sih, G.T. Embley, R.S. Ravera, Impact response of a finite crack in plane extension, Int. J. Solids Struct. 8 (7) (1972) 977–993.
[27] L.B. Freund (Ed.), Dynamic Fracture Mechanics, Cambridge University Press, 1990.
[28] A.-W. Maue, Die Entspannungswelle bei plötzlichem Einschnitt eines gespannten elastischen Körpers, ZAMM - Zeitschrift für Angewandte Mathematik und Mechanik 34 (1-2) (1954) 1–12.
[29] L.B. Freund, Energy flux into the tip of an extending crack in an elastic solid, J. Elast. 2 (4) (1972) 341–349.
[30] L.B. Freund, R.J. Clifton, On the uniqueness of plane elastodynamic solutions for running cracks, J. Elast. 4 (4) (1974) 293–299.
[31] L.R.F. Rose, An approximate (Wiener-Hopf) kernel for dynamic crack problems in linear elasticity and viscoelasticity, Proc. R. Soc. Lond. A 349 (1659) (1976) 497–521.
[32] C.T. Sun, Z.-H. Jin, Special Topics, in: Fracture Mechanics, Elsevier, 2012, pp. 247–285.
[33] T.L. Anderson, Fracture Mechanics: Fundamentals and Applications, Fourth Edition, Chapman and Hall/CRC, Boca Raton, 2017.
[34] Z. Zhuo, P.E. O'Donoghue, Analysis model to simulate the cracked pipe buried in soil, Acta Mech. Sin. 14 (2) (1998) 147–156.
[35] Z. Zhuang, P.E. O'Donoghue, Determination of material fracture toughness by a computational/experimental approach for rapid crack propagation in PE pipe, Int. J. Fract. 101 (3) (2000) 251–268.
[36] Z. Zhuang, P.E. O'Donoghue, The recent development of analysis methodology for rapid crack propagation and arrest in gas pipelines, Int. J. Fract. 101 (3) (2000) 269–290.
[37] P.E. O'Donoghue, S.T. Green, M.F. Kanninen, P.K. Bowles, The development of a fluid/structure interaction model for flawed fluid containment boundaries with applications to gas transmission and distribution piping, Comput. Struct. 38 (5-6) (1991) 501–513.
[38] P.E. O'Donoghue, M.F. Kanninen, C.P. Leung, G. Demofonti, S. Venzi, The development and validation of a dynamic fracture propagation model for gas transmission pipelines, Int. J. Press. Vessels Pip. 70 (1) (1997) 11–25.
[39] Y.K. Godovsky (Ed.), Thermophysical Properties of Polymers, Springer Berlin Heidelberg, Berlin, Heidelberg, 1992.
[40] C. Lawrence, A proposed model for the periodic behaviour observed in the fast fracture failures seen in routine and full scale tests on plastic pipes, Polym. Test. 15 (2) (1996) 129–151.
[41] P.S. Leevers, Personal Communication, 2020.
[42] J.-B. Kopp, C. Fond, G. Hochstetter, Rapid crack propagation in PA11: An application to pipe structure, Eng. Fract. Mech. 202 (2018) 445–457.
[43] J.-B. Kopp, J. Girardot, Dynamic fracture in a semicrystalline biobased polymer: an analysis of the fracture surface, Int. J. Fract. 226 (1) (2020) 121–132.
[44] M. Messiha, B. Gerets, J. Heimink, A. Frank, F. Arbeiter, K. Engelsing, Slow crack growth resistance of modern PA-U12 grades measured by cyclic cracked round bar tests and strain hardening tests, Polym. Test. 86 (2020) 106468, https://doi.org/10.1016/j.polymertesting.2020.106468.
[45] M. Messiha, A. Frank, I. Berger, et al., Differences and similarities in fatigue failure mechanisms of PA12 pipe grades compared to modern PE pipe grades. Proceedings ANTEC, 2019.

8.2 Outside the framework of this thesis

1. Rueda, F.; Rull, N.; Quintana, C.; Torres, J. P.; Messiha, M.; Frank, A.; Arbeiter, F.; Frontini, P. M.; Pinter, G.: "Modelling Failure of Polymers: An Optimization Strategy Based on Genetic Algorithms and Instrumented Impact Tests", *Journal of Dynamic Behavior of Materials*, 2021.
2. Messiha, M.; Frank, A.; Koch, T.; Arbeiter, F.; Pinter, G.: "Effect of polyethylene and polypropylene cross-contamination on slow crack growth resistance", *International Journal of Polymer Analysis and Characterization*, pp. 1–18, 2020.
3. A. Frank, M. Messiha, T. Koch et al., "Correlation of the cyclic cracked round bar test and hydrostatic pressure test for unplasticized polyvinylchloride", *Polymer Testing*, vol. 95, p. 107125, 2021.

8.3 Conference contributions

1. M. Messiha, A. Frank, I. Berger, H. van Laak, J. Heimink, G. Pinter, F. Arbeiter, "Determination of the Slow Crack Growth resistance of PA12 pipe grades", in: Proceedings PPXIX, Las Vegas, Nevada, USA, 2018.
2. A. Frank, I. Berger, M. Messiha, C.-G. Ek, J.-M. Storheil, N. Schuler, F. Krause, S. Heeley, E. Mayrbäurl, Y.S. Deshmukh, P. Gabriëls, L. Niemöller, G. Pinter, T. Koch, F. Arbeiter, Slow crack growth resistance of non-virgin polymers, in: Proceedings PPXIX, Las Vegas, Nevada, USA, 2018.
3. M. Messiha, A. Frank, I. Berger, G. Pinter, F. Arbeiter, J. Heimink, H. van Laak, "Differences and similarities in fatigue failure mechanisms of PA12 pipe grades compared to modern PE pipe grades", in: Proceedings ANTEC, Detroit, US, 2019.
4. M. Messiha, B. Gerets, J. Heimink, A. Frank, F. Arbeiter, G. Pinter, "Investigating the influence of changes in molecular structure of polyamide 12 grades on the resistance against Slow Crack Growth", in: Proceedings PPXX, Amsterdam, NL, 2021.

9 SUPERVISED THESIS

1. J. Hinszica, “Accelerated prediction of the long-term strength behaviour of thermoplastic materials”. Master thesis, Montanuniversitaet, Leoben, 2020.
2. C. Waly, “Investigating novel concepts to characterize the resistance against rapid crack propagation of polyamide 12 pipe grades”. Master thesis, Montanuniversitaet, Leoben, 2021.
3. L. Schatz, “Investigating the plastic zone evolution of different PA12 grades via crack-freezing analysis”. Bachelor thesis, Montanuniversitaet, Leoben, 2021.